AD-A142 609 FATIGUE BEHAVIOR OF LONG AND SHORT CRACKS IN WROUGHT AND POWDER ALUMINUM..(U) CALIFORNIA UNIV BERKELEY DEPT OF MATERIALS SCIENCE AND MINERA.. R O RITCHIE MAY 84 1/3

UNCLASSIFIED UCB/RP/84/A1021 AFOSR-TR-84-0509 F/G 11/6 NL

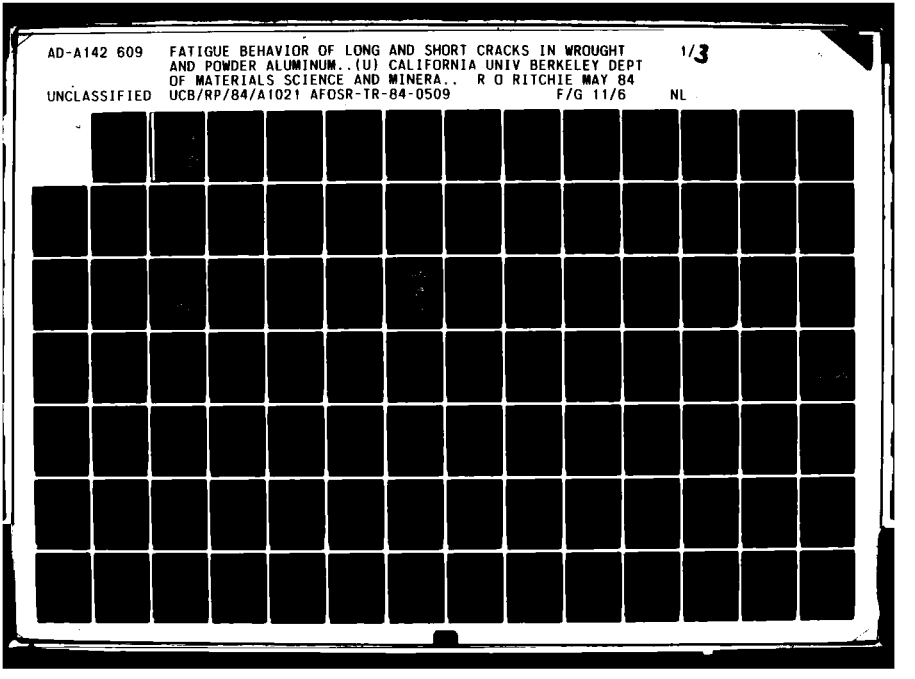

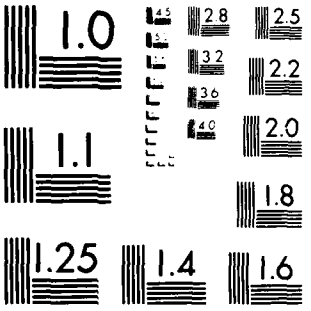

AFOSR-TR- 84-0509

Second Annual Report
to
U.S. Air Force Office of Scientific Research
on

FATIGUE BEHAVIOR OF LONG AND SHORT CRACKS IN WROUGHT AND POWDER ALUMINUM ALLOYS

Grant AFOSR-82-0181
for period 15 April 1983 to 14 April 1984

by
Robert O. Ritchie

May 1984

Report No. UCB/RP/84/A1021

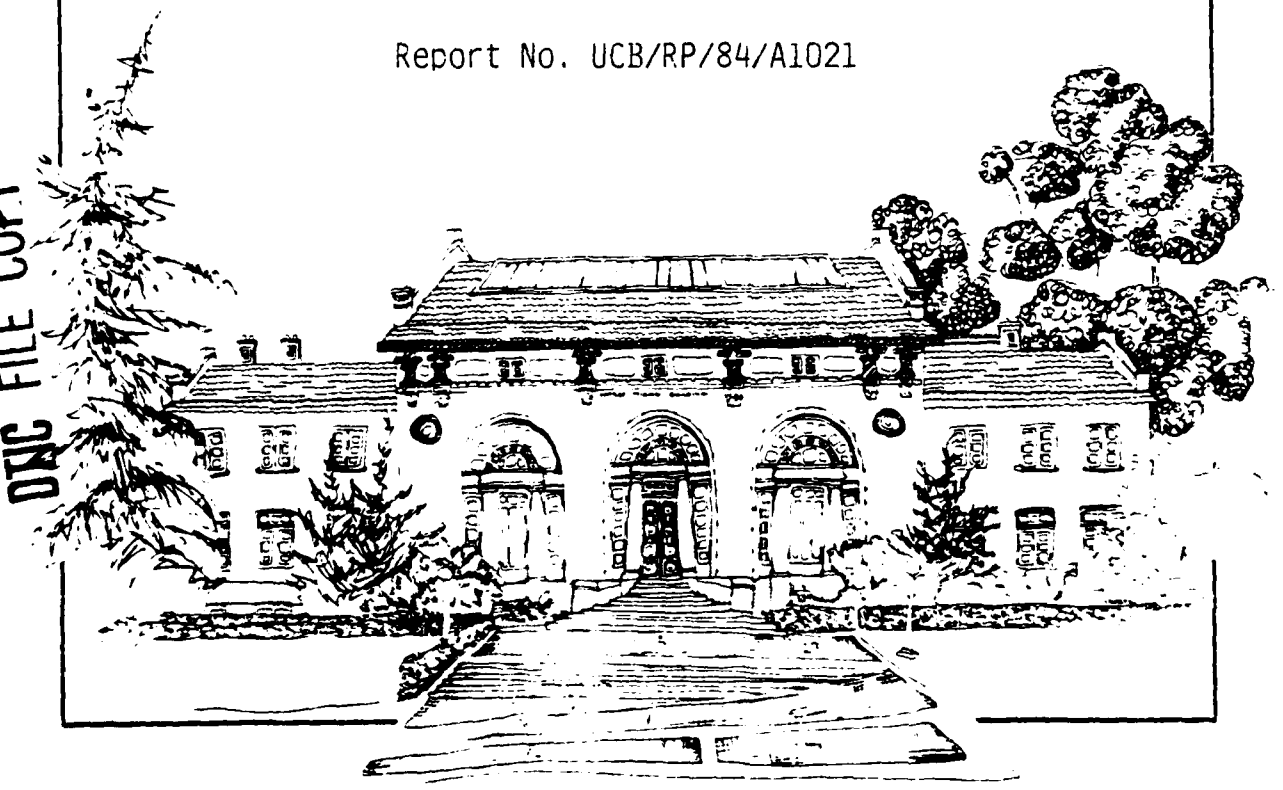

Department of Materials Science and Mineral Engineering
University of California, Berkeley, CA 94720

Unclassified

SECURITY CLASSIFICATION OF THIS PAGE (When Data Entered)

REPORT DOCUMENTATION PAGE		READ INSTRUCTIONS BEFORE COMPLETING FORM
1. REPORT NUMBER AFOSR-TR- 84-0509	2. GOVT ACCESSION NO.	3. RECIPIENT'S CATALOG NUMBER
4. TITLE (and Subtitle) FATIGUE BEHAVIOR OF LONG AND SHORT CRACKS IN WROUGHT AND POWDER ALUMINUM ALLOYS		5. TYPE OF REPORT & PERIOD COVERED Annual Report for period 15 April 1983-14 April 1984
		6. PERFORMING ORG. REPORT NUMBER UCB/RP/84/A1021
7. AUTHOR(s) Robert O. Ritchie		8. CONTRACT OR GRANT NUMBER(s) AFOSR-82-0181
9. PERFORMING ORGANIZATION NAME AND ADDRESS Robert O. Ritchie, Department of Materials Science and Mineral Engineering, University of California, Berkeley, CA 94720		10. PROGRAM ELEMENT, PROJECT, TASK AREA & WORK UNIT NUMBERS 2306/A1 61102F
11. CONTROLLING OFFICE NAME AND ADDRESS U.S. Air Force Office of Scientific Research, Bldg. 410, Bolling AFB, Washington, D.C. 20322, ATTN: Dr. Alan H. Rosenstein, AFOSR/NE		12. REPORT DATE May 1984
		13. NUMBER OF PAGES
14. MONITORING AGENCY NAME & ADDRESS (if different from Controlling Office) N/A		15. SECURITY CLASS. (of this report) Unclassified
		15a. DECLASSIFICATION/DOWNGRADING SCHEDULE N/A

A142 609

16. DISTRIBUTION STATEMENT (of this Report)

Approved for public release; distribution unlimited.

17. DISTRIBUTION STATEMENT (of the abstract entered in Block 20, if different from Report)

18. SUPPLEMENTARY NOTES

19. KEY WORDS (Continue on reverse side if necessary and identify by block number)

Fatigue
Defect-tolerant fatigue design
Fatigue in aluminum alloys
Fatigue behavior of long and short cracks
Fatigue cracks: Crack deflection and closure

20. ABSTRACT (Continue on reverse side if necessary and identify by block number)

The fatigue behavior of short cracks, which are small compared to the scale of the microstructure, small compared to the scale of local plasticity or simply physically small (i.e., $\sim$ 1 mm), must be considered as one of the major factors limiting the application of defect-tolerant fatigue design for airframe and engine components. Accordingly, the current program is aimed at identifying factors which govern the growth of such short cracks (in contrast to long cracks) in a series of commercial aluminum alloys, with specific reference to behavior at near-threshold levels (below $\sim 10^{-6}$ mm/cycle). In this second annual report

DD FORM 1 JAN 73 1473 EDITION OF 1 NOV 65 IS OBSOLETE

Unclassified

SECURITY CLASSIFICATION OF THIS PAGE (When Data Entered)

Block 20, Abstract (Cont.)

the status of the program is described in terms of i) an expanded review of the factors which lead to differences in long and short crack behavior, with particular regard to the role of crack closure mechanisms, ii) a description of experiments performed to characterize the role of microstructure in influencing the propagation of "long" cracks in I/M 7150 aluminum alloys, and iii) a description of experiments carried out to isolate the effects of crack closure on the propagation of both long and short cracks, and specifically to investigate the location of the closure responsible for the development of a threshold. It is concluded that mechanisms of crack closure are intimately linked with the existence of a threshold for long cracks, and the limitation of such closure in short cracks is primarily responsible for their "anomalous" growth rate and threshold behavior.

Report No. UCB/RP/84/A1021

Second Annual Report

to

U.S. Air Force Office of Scientific Research

on

FATIGUE BEHAVIOR OF LONG AND SHORT CRACKS IN WROUGHT AND POWDER ALUMINUM ALLOYS

Grant AFOSR-82-0181

for period 15 April 1983 to 14 April 1984

submitted to

U.S. Air Force Office of Scientific Research
Bldg. 410, Bolling Air Force Base
Washington, D.C. 20322
Attention: Dr. Alan H. Rosenstein

submitted by

Robert O. Ritchie
Professor of Metallurgy
Department of Materials Science
and Mineral Engineering
University of California
Berkeley, California 94720

May 1984

TABLE OF CONTENTS

FATIGUE BEHAVIOR OF LONG AND SHORT CRACKS IN WROUGHT AND POWDER ALUMINUM ALLOYS

R. O. Ritchie

(Grant No. AFOSR-82-0181)

FORWARD

This manuscript constitutes the Second Annual Report on Grant No. AFOSR-82-0181, administered by the U.S. Air Force Office of Scientific Research, with Dr. Alan H. Rosenstein as program manager. The work, covering the period April 15, 1983, through April 14, 1984, was performed under the direction of Dr. R. O. Ritchie, Professor of Metallurgy, University of California in Berkeley, with Drs. S. Suresh (now at Brown University) and W. Yu as Research Engineers, E. Zaiken as graduate student, and P. Donehoo as undergraduate student.

ABSTRACT

The fatigue behavior of short cracks, which are small compared to the scale of the microstructure, small compared to the scale of local plasticity or simply physically small (i.e., $\lesssim$ 1 mm), must be considered as one of the major factors limiting the application of defect-tolerant fatigue design for airframe and engine components. Accordingly, the current program is aimed at identifying factors which govern the growth of such short cracks (in contrast to long cracks) in a series of commercial aluminum alloys, with specific reference to behavior at near-threshold levels (below $\sim 10^{-6}$ mm/cycle). In this second annual report, the status of the program is described in terms of i) an expanded review of the factors which lead to differences in long and short crack behavior, with particular regard to the role of crack closure mechanisms, ii) a description of experiments performed to characterize the role of microstructure in influencing the propagation of "long" cracks in I/M 7150 aluminum alloys, and iii) a description of experiments carried out to isolate the effects of crack closure on the propagation of both long and short cracks, and specifically to investigate the location of the closure responsible for the development of a threshold. It is concluded that mechanisms of crack closure are intimately linked with the existence of a threshold for long cracks, and the limitation of such closure in short cracks is primarily responsible for their "anomalous" growth rate and threshold behavior.

1. INTRODUCTION

The objective of this program is to identify mechanical, microstructural and environmental factors governing the fatigue crack growth of long ($\gtrsim$ 25 mm) and short ($\lesssim$ 1 mm) cracks in commercial aluminum alloys with specific reference to behavior at ultralow, near-threshold growth rates below typically 10^{-6} mm/cycle. This report covers the second year of the program of research where attention has been focussed on i) compiling an extended review of the literature pertaining to general aspects and specifically the role of environment in influencing the propagation of short fatigue cracks, ii) defining the microstructural factors which contribute to crack closure in 7150 alloys and hence characterizing the near-threshold behavior of "long" cracks in this alloy, and iii) isolating the specific role of closure in influencing both long and short crack behavior and in particular to determine the location of the closure along the crack length which is primarily responsible for the development of a threshold.

2. REVIEW OF PREVIOUS RESEARCH

2.1 Introduction

Despite an increasing interest, both academically and technologically, in conventional long crack fatigue crack propagation, particularly at near-threshold levels (e.g., ref. 1), a major limitation in the application of such information to defect-tolerant design must be regarded as the problem of short flaws. By short flaws, it is implied that flaws are i) small compared with the scale of

microstructure, ii) small compared with the scale of local plasticity, or iii) simply physically small (i.e., $\lesssim$ 0.5 to 1 mm). Design codes at present attempt to predict the growth rates of in-service flaws based on data collected in the laboratory with specimens containing crack sizes of the order of 25 mm. In service, however, initial defects sizes are often far smaller than this. This leads to a potential for non-conservative defect-tolerant lifetime predictions since the vast majority of experimental observations[2-18] on the behavior of short cracks has shown that their growth rates are in excess of long cracks at the same nominal driving force (e.g., at the same stress intensity range ΔK) and furthermore that such short cracks can initiate and propagate at ΔK levels **below** the "long crack" fatigue threshold ΔK_{TH} (Fig. 2.1).

Due to the complexity and importance of this topic, an extensive literature review has been performed on all aspects of the propagation behavior of short fatigue cracks. This has been divided into two sections: the first covering all aspects of the problem and the second specific to the role of environmental factors. Since both reviews are currently in press,[19,20] only the abstracts are included here. The full texts can be found in the Appendix to this report.

2.2 The Propagation of Short Fatigue Cracks[19]

Fatigue crack propagation in engineering materials has been a topic of considerable research effort and extensive review articles over the past several years. The majority of such investigations have focussed on the behavior of "long" fatigue cracks, even though the characteristics associated with the extension of small flaws in metals

and alloys remain relatively unexplored, despite their unquestionable importance from an engineering standpoint. The mechanics and micromechanisms of the sub-critical growth of short fatigue cracks are examined and aspects of their propagation behavior contrasted with those of long cracks in terms of fracture mechanics, microstructure and environment. Cracks are defined as being short i) when their length is small compared to relevant microstructural dimensions (a continuum mechanics limitation, ii) when their length is small compared to the scale of local plasticity (a linear elastic fracture mechanics limitation), and iii) when they are merely physically small (e.g., < 0.5-1 mm). Since all three types of short flaws are known to propagate faster than (or at least at the same rate as) corresponding long fatigue cracks subjected to the same **nominal** driving force, current defect-tolerant fatigue design procedures which utilize long crack data can, in certain applications, result in non-conservative lifetime predictions. The characteristics of the short crack problem are critically reviewed in the light of the influences of local plasticity, microstructure, crack-tip environment, growth mechanisms, crack driving force, and the premature closure of the crack.

2.3 Environmental Effects Novel to the Propagation of Short Fatigue Cracks[20]

Crack size and opening morphology dominate the mechanical and chemical driving forces for fatigue propagation in embrittling environments. Similitude based on a crack tip field parameter is compromised, particularly for small cracks (< 5 mm) which grow up to several orders of magnitude faster than projected and below apparent

threshold conditions. Environment sensitive mechanical and chemical mechanisms which govern the growth of small cracks are reviewed. For the former the retarding effect of crack closure; originating from wake plasticity, surface roughness, deflection, corrosion debris or fluid pressure (Fig. 2.2); increases with increasing crack size particularly within the near threshold regime. Data for high strength steel in H_2 demonstrate the importance of such mechanisms, however, precise models of crack size dependencies and systematic closure measurements are lacking. Considering the chemical driving force, the embrittling activity of the occluded crack differs from that of the bulk environment, and is geometry dependent. The deleterious influence of small crack size is demonstrated experimentally for steels in aqueous chloride solutions, and related quantitatively to crack opening shape and size effects on diffusion, convective mixing and electrochemical reaction. Small crack size promotes hydrogen embrittlement due to enhanced hydrolytic acidification and reduced oxygen inhibition. Chemical crack size effects are material and environment specific; criteria defining limiting crack sizes and opening shapes for K or J-based similitude do not exist.

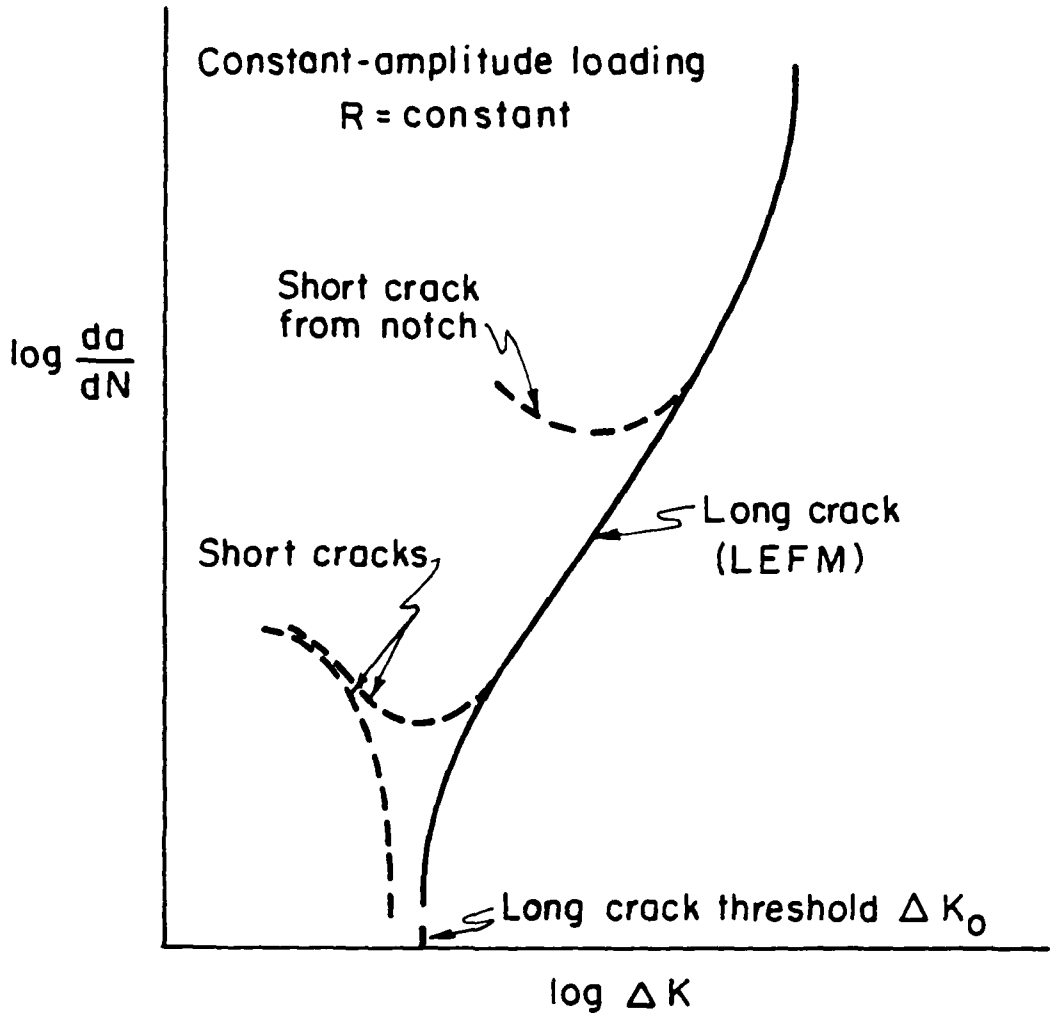

Fig. 2.1. Schematic representation of typical fatigue crack propagation rate da/dN data for long and short cracks as a function of the alternating stress intensity ΔK for constant amplitude loading with the load ratio R constant.

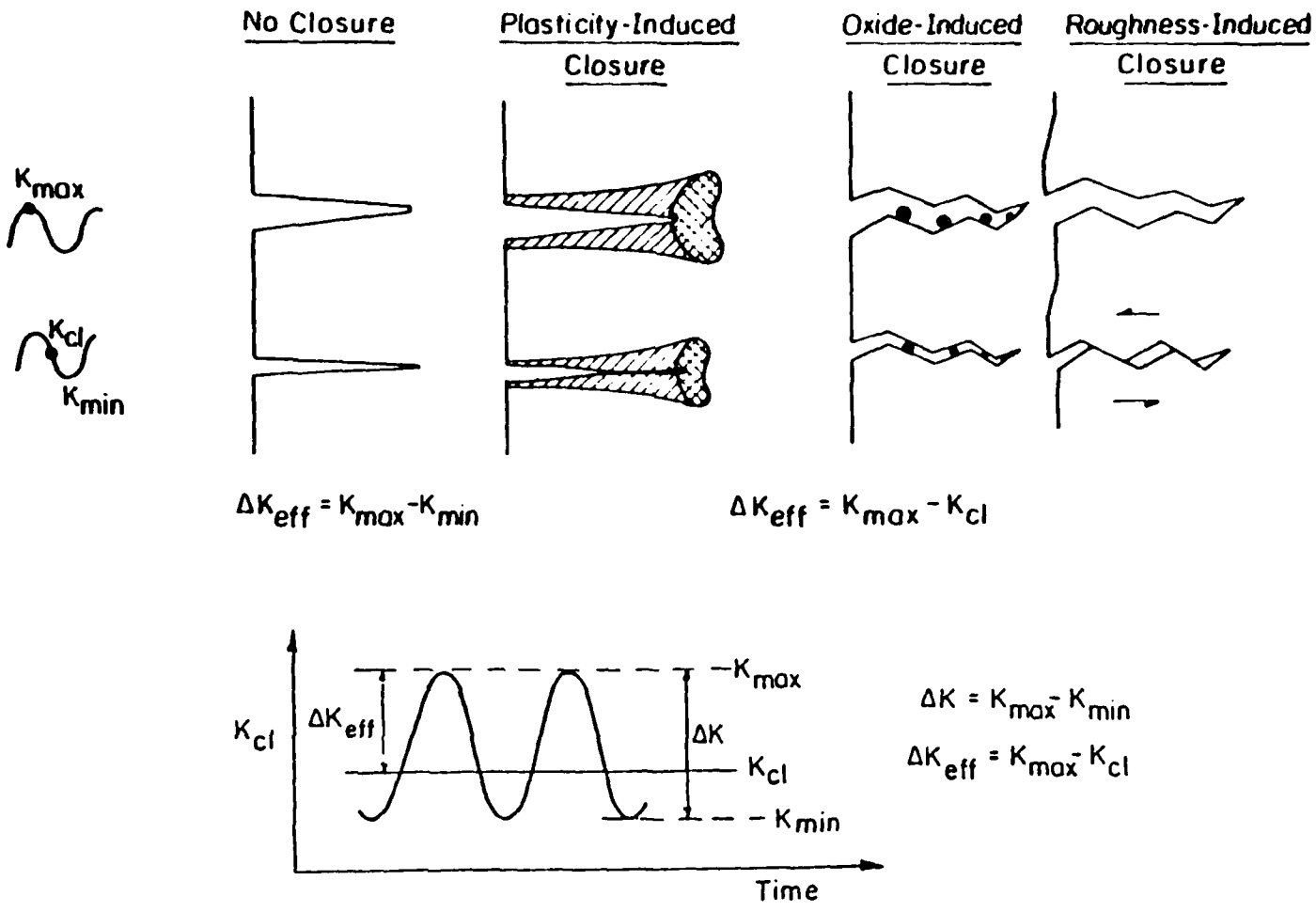

Fig. 2.2. Schematic illustration of primary mechanisms of fatigue crack closure and the nomenclature required in the definition of stress intensities representative of the fatigue cycle.

3. EXPERIMENTAL PROCEDURES AND MATERIALS

3.1 Materials

The following commercial wrought aluminum alloys, namely 7150, 2024 and 2124, were obtained from ALCOA in the solution treated, quenched and stretched (2%) conditions. In addition, a small 2024-T3 heat was acquired from Kaiser Aluminum Company. Nominal chemical compositions are shown below in Table 3.1.

Table 3.1: Nominal Chemical Compositions in wt% of Alloys

	Si	Fe	Cu	Mn	Mg	Cr	Zn	Ti	Zr	Al
2024	0.50	0.50	4.50	0.50	1.50	0.10	0.25	0.15	--	balance
2124	0.20	0.30	4.50	0.50	1.50	0.10	0.25	0.15	--	balance
7150	0.07	0.11	2.10	--	2.16	--	6.16	0.02	0.13	balance

Fatigue tests were performed on 6.4 mm thick compact C(T) test-pieces heat-treated to yield peak-aged (PA) microstructures and underaged (UA) and overaged (OA) microstructures at the same approximate yield strength. The rationale for this is that underaged (i.e., T3) structures are associated with deformation via planar slip due to the coherent nature of the hardening precipitates whereas overaged (i.e., T7) structures are associated with a more homogeneous wavy slip from incoherent particle hardening mechanisms.

3.2 Test Procedures

To obtain a comparison between long and short crack near-threshold behavior and to experimentally demonstrate that the anomalous behavior

of short cracks results from a lesser effect of closure in the wake of the crack tip, the "3-in-1" test specimen/procedure is being utilized, shown schematically in Fig. 3.1.

Starting with a conventional 1-T compact C(T) test-piece, 6.4 mm thick, long crack threshold tests are performed at 50 Hz using standard load shedding procedures to determine the near-threshold crack growth behavior and the value of the fatigue threshold range ΔK_o for long cracks[1] (A). To demonstrate the effect of closure in the wake of the crack tip, two procedures are then adopted for the long crack arrested at ΔK_o. In certain specimens material is machined away behind the crack tip to "remove" closure in the wake. This has been performed using a jeweler's saw to machine a 0.3 mm width cut. Conversely, closure is "removed" by applying a single compression overload. In either case, following such procedures, the subsequent growth of the formerly arrested long crack is monitored, under constant ΔK conditions, until closure has once again developed with increase in crack length to again cause arrest (B). The third stage of the test is then to carefully machine away the majority of the test-piece to leave a small crack in a strip of metal (C), which is then tested in three-point bend to investigate near- (and sub-) threshold short crack behavior (D).

Such procedures are often rather difficult to perform in practice due to difficulties in micro-machining and non-uniformity of crack fronts.

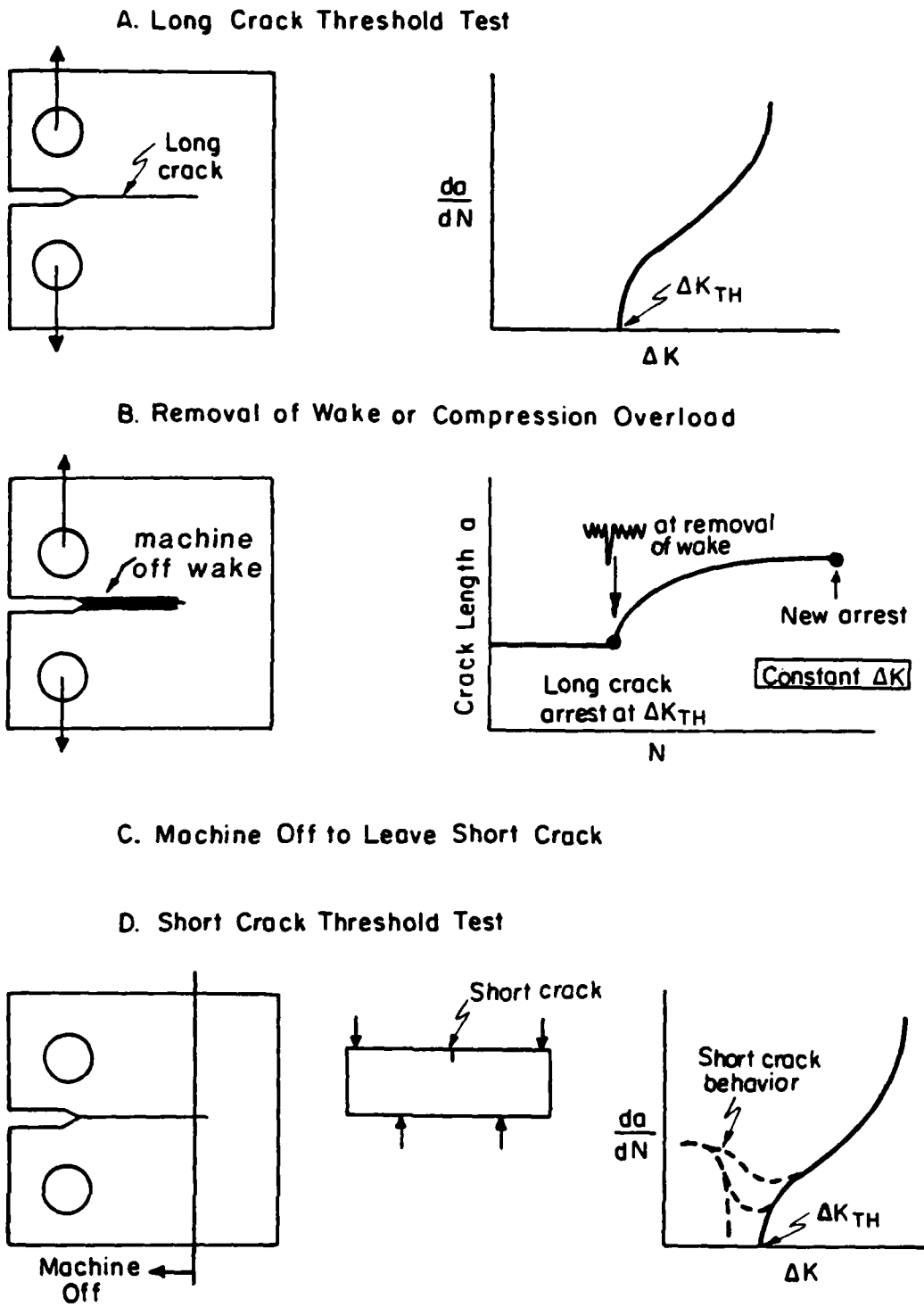

Fig. 3.1. Test geometries, procedures, and expected results for the "3-in-1" specimen developed to experimentally demonstrate the role of closure and the differences between long and short crack behavior.

4. LONG CRACK STUDIES IN 7150 ALUMINUM ALLOY

4.1 Introduction

Recent studies into the mechanics and mechanisms of fatigue have identified a prominant role of crack closure in influencing crack propagation behavior.[21-34] This is particularly apparent at low growth rates (i.e., below $\sim 10^{-6}$ mm/cycle) near the fatigue threshold stress intensity range for no crack growth, ΔK_{TH}. In this regime, the origin of such closure has been associated with mechanisms such as crack surface corrosion deposits,[24-26] irregular fracture morphologies coupled with crack tip shear displacements,[27-29] and fluid-induced pressure[35,36] in addition to conventional mechanisms relying on cyclic plasticity[21] (Fig. 2.1). The effect of the closure, which induces contact between mating fracture surfaces at positive stress intensities (K_{cl}) during the loading cycle, is to reduce the local driving force for crack advance from nominally applied levels, e.g., $\Delta K = K_{max} - K_{min}$, to some near-tip effective level, $\Delta K_{eff} = K_{max} - K_{cl}$,[21] where K_{max}, K_{min}, K_{cl} and ΔK are the maximum, minimum, closure and range of stress intensity, respectively.

Based largely on data in steels, effects of variable amplitude loading, frequency, load ratio, microstructure, environment and temperature have all been associated with closure phenomena (for review, see ref. 34). In non-ferrous alloys, however, comparatively less information exists. Elber[21] and Schmidt and Paris[22] first applied the concept of (plasticity-induced) closure to cyclic behavior in aluminum alloys, in an attempt to explain variable amplitude loading and load ratio effects in these alloys. Subsequent studies in this

system have focussed largely on effects of microstructure and environment.[31,37-42] Petit and Zeghoul[37] and Vasudévan and Suresh[38] identified a role of oxide-induced closure, although enhanced crack surface oxide films were only detected in overaged 7075 alloys and, unlike behavior in steels,[24-26] were not found to be consistent with lower growth rates. The more important mechanism in aluminum alloys appears to be associated with roughness-induced closure, where it has been suggested that the strongly crystallographic nature of crack paths,[43-46] particularly in underaged structures, promotes closure[39-42] and crack deflection,[41,57] and thus reduces near-threshold growth rates. Recently, these concepts of deflection and oxide/roughness-induced closure have been applied by Suresh et al.[41] to rationalize the microstructural effects of precipitation hardening on fatigue crack growth in 7075 alloys. The decreasing threshold ΔK_{TH} values with increasing aging treatment were attributed to a smaller influence of closure associated with less crystallographic crack paths although, aside from oxide thickness measurements, detailed crack closure measurements were not made.

In the present work, effects of microstructure during precipitation hardening are examined on fatigue crack propagation in a high purity 7150 alloy, for underaged, peak-aged and overaged conditions, in the light of quantitative measurements oxide film thickness, fracture surface roughness and closure stress intensity values. It is shown that near-threshold growth rates are slowest in underaged structures, consistent with the highest measured closure loads, and, similar to other aluminum alloy systems,[31,39,41,42]

consistent with the most deflected crack paths. No evidence of oxide-induced closure could be detected.

4.2 Experimental Procedures

Conventionally-cast I/M 7150 aluminum alloy was supplied by Alcoa with the composition shown in Table 4.1. The Al-Zn-Mg-Cu alloy, which is a high purity version of 7050 (i.e., lower Si and Fe), was received as 25 mm thick plate in the solution treated and 2% stretched (W51) condition. Samples for fatigue and tensile testing were machined from the center thickness location and tempered to produce underaged, peak-aged (T6) and overaged (T7) structures. The specific heat treatments and resulting room temperature uniaxial tensile properties are shown in Tables 4.2 and 4.3, respectively. The underaged and overaged heat treatments were designed to produce structures with approximately similar yield strength. Transmission electron micrographs of the three microstructures are shown in Fig. 4.1. Underaged structures are characterized by coherent GP zones roughly 4 to 8 nm in diameter, which on further aging are replaced by semi-coherent intermetallic η' precipitates ($MgZn_2$-$Mg(CuAl)_2$) in the peak-aged condition. In overaged structures, predominately incoherent η phase precipitates ($MgZn_2$ compounds) are found in both the matrix and grain boundaries (with small precipitate free zones of half width $\sim$30 nm), together with coarsened η' in the matrix. There is also evidence of small dispersoid particles (e.g., Al_3Zr) of less than 10 nm in diameter. Grains were somewhat elongated along the rolling direction with an approximate size of 15 by 5 μm.

Table 4.1

Nominal Chemical Compositions in wt.%

	Si	Fe	Cu	Mg	Zn	Ti	Zr	Al
7150	0.07	0.11	2.10	2.16	6.16	0.02	0.13	balance

Table 4.2

Heat Treatments Utilized for Tests on 7150 Alloy

Underaged	ST* + 1½ hr at 121°C
Peak-Aged (T6)	ST* + 100 hr at 121°C
Overaged (T7)	ST* + 24 hr at 121°C + 40 hr at 163°C

Table 4.3

Room Temperature Mechanical Properties of 7150 Alloy

	Yield Strength (MPa)	U.T.S. (MPa)	Elong.* (%)	Redn. Area (%)	Work Hardening Exponent
Underaged	371	485	6.8	12.1	0.055
Peak-Aged (T6)	404	480	6.0	10.3	0.046
Overaged (T7)	372	478	7.1	12.5	0.058

*On 32 mm gauge length

Fatigue crack growth tests were performed in controlled room temperature air (22°C, 45% relative humidity) on 6.4 mm thick compact C(T) test-pieces machined in the T-L orientation. Using D.C. electrical potential techniques to continuously monitor crack growth, tests were performed under load control at 50 Hz (sine wave) frequency with load ratios ($R = K_{min}/K_{max}$) of 0.10 and 0.75 using Instron electro-servo-hydraulic testing machines. Near-threshold crack propagation rates were determined under manual load shedding (decreasing ΔK) conditions, and checked under increasing ΔK conditions. The threshold ΔK_{TH} was defined as the highest ΔK level giving growth rates less than 10^{-8} mm/cycle.[1] The majority of tests were at least duplicated.

Macroscopic crack closure measurements to determine K_{cl} values were performed **in situ** with the back-face strain technique using two strain gauges to record strain both parallel and perpendicular to the loading axis (Fig. 4.2).[47] Mean closure loads were deduced from the point during the loading cycle where the resulting elastic compliance curves of load versus relative strain deviated from linearity. Crack surface corrosion deposits were measured with Scanning Auger Spectroscopy using Ar^+ sputtering techniques.[48] The excess oxide thickness, representing the excess material inside the crack, was computed with a Pilling-Bedworth ratio of 1.3 for Al_2O_3, assuming only thickness-direction growth and equal thicknesses on each face. The degree of fracture surface roughness was assessed from scanning electron and optical micrographs of the crack paths in terms of the ratio of total length of the crack to the projected length on the plane of maximum tensile stress.

4.3 Results

Growth Rate Behavior:

The variation in fatigue crack propagation rates (da/dN) with stress intensity range (ΔK) for 7150 in the underaged (UA), peak-aged (PA) and overaged (OA) conditions is shown in Fig. 4.3 for load ratios of 0.10 and 0.75. Although growth rates above $\sim 10^{-6}$ mm/cycle are similar at each load ratio for all three microstructures, at near-threshold levels it is evident that underaged structures show the highest fatigue resistance in terms of lowest growth rates and highest threshold ΔK_{TH} values. . Similar behavior has been reported for other aluminum alloys, including I/M 7075,[39,41,43,49,50] 7475,[42] and P/M 7091.[51] Compared to the underaged structure, threshold ΔK_{TH} values in the present results are roughly 15% and 28% lower in the peak-aged and overaged structures, respectively, at $R = 0.10$ (Table 4.4). Thresholds are similarly reduced with increased aging at R = 0.75, although the absolute magnitude of the differences in ΔK_{TH} values is much smaller.

Crack Closure Data:

Corresponding crack closure data, in terms of back-face strain measurements of K_{cl}/K_{max} as a function of ΔK, are shown in Fig. 4.4 for the three microstructures at both R = 0.10 and 0.75. Similar to behavior reported for steels[28,30,34,47] and other aluminum alloys[39,42,52] at low load ratios, the degree of crack closure increases sharply with decreasing ΔK level, approaching a maximum of K_{cl}/K_{max} close to unity at ΔK_{TH}. Although no evidence of closure could be detected experimentally in any microstructure at R = 0.75, at low load ratios underaged structures showed consistently the highest

Table 4.4

Threshold Data for 7150 Alloy at Load Ratios of 0.10 and 0.75

	Load Ratio (K_{min}/K_{max})	ΔK_{TH} (MPa$\sqrt{m}$)	ΔCTOD* (nm)	Maximum K_{cl}/K_{TH}*	Excess Oxide Thickness* (nm)	Degree of Roughness**
Underaged	0.10	3.05-3.31	100	0.88	3	1.26
	0.75	1.51	22	0	3	
Peak-Aged (T6)	0.10	2.44-2.94	65	0.85	3	1.21
	0.75	1.27	14	0	3	
Overaged (T7)	0.10	2.23-2.33	50	0.77	3	1.06
	0.75	1.16	13	0	3	

*Measured at the threshold, ΔK_{TH}.

**Ratio of total crack length to projected length on plane of maximum tensile stress.

closure levels. In fact, in keeping with this decrease in closure with increased aging, the threshold ΔK_{TH} similarly decreased.

Fractography:

Scanning electron micrographs of the fatigue fracture surfaces close to ΔK_{TH} (R = 0.10) in the three aging conditions are shown in Fig. 4.5. The fractography is transgranular in all cases with evidence of slip steps, ledges and facets. Such facets are particularly pronounced in the underaged structure and have an appearance characteristic of crystallographic fatigue surfaces.[16,43,53] The rougher or more tortuous nature of the crack path in the underaged structures can be seen more clearly in Fig. 4.6 where crack profiles are shown for the three conditions. In contrast to the zig-zag appearance of underaged fractures, crack paths in the overaged structures are predominately linear with far fewer crack deflections.

Associated Auger measurements of the extent of crack surface corrosion deposits are shown in Fig. 4.7. In marked contrast to behavior in lower strength steels,[26,48] there is no evidence in this present alloy of any pronounced oxide accumulation within the crack even at threshold levels. Oxide films were similar at all aging conditions and at both load ratios, with a measured thickness of the order of 3 nm which is comparable with the limiting thickness of naturally-occurring oxides in this alloy. Such results are similar to those reported for underaged and peak-aged 7075 alloys, but in contrast to those reported for overaged 7075 where excess oxide thicknesses approached 100 nm at ΔK_{TH} (R = 0.33).[41] As listed in Table 4.4, the excess oxide film thicknesses in 7150 are small compared to computed

values of the cyclic crack tip opening displacements (ΔCTOD) indicating that, for this alloy tested in room air environments, the contribution from oxide-induced crack closure is likely to be minimal.

4.4 Discussion

Similar to other aluminum alloy systems,[31,38-46] the present results on a high purity I/M 7150 alloy indicate clearly that underaged microstructures have superior near-threshold fatigue crack propagation resistance to overaged and peak-aged microstructures. This is seen in terms of lower growth rates below $\sim 10^{-6}$ mm/cycle and higher threshold ΔK_{TH} values at both low and high load ratios, although the magnitude of the effect is diminished at R = 0.75 (Fig. 4.3). The higher thresholds in the underaged structures are consistent with an increased magnitude in crack closure (Fig. 4.4), faceted and crystallographic fracture surfaces (Fig. 4.5) and more tortuous crack paths (Fig. 4.6), compared to the smoother, more linear (undeflected) crack morphology in overaged structures. Data indicating this trend of lower thresholds with decreasing K_{cl}/K_{max} values and decreasing degrees of fracture surface roughness for increased aging are listed in Table 4.4.

In keeping with current notions on the role of crack closure,[34] this trend, which has been similarly rationalized in 7075[39,41] and 7475[42] alloys, is to be expected. Similar to behavior in dual phase steels[47,54] and certain titanium and aluminum alloys,[27,55-57] the generation of a tortuous crack path, either by crack deflection at harder phases[47,54-56] or in the present case by crystallographic deflection at grain boundaries, can lead to slower fatigue crack growth rates through a reduction in local crack driving force. This results

from three major factors: i) lower effective da/dN due to a longer path length of the crack, ii) lower effective stress intensities at the crack tip due to crack deflection from the plane of maximum tensile stress,[57] and iii) lower effective ranges of stress intensity at the crack tip due to the resulting production of increased crack closure due to asperity contact behind the crack tip.[27-29] Since the thicknesses of crack surface oxide films are so small compared to ΔCTOD values, it would appear that the major contribution to this closure in the present alloy originates from the roughness-induced mechanism[27-29] (Fig. 2.1), aided by the rough out-of-plane crack morphologies and the crack tip shear displacements[58] which result. These effects are far less pronounced in the overaged structures where crack paths are far more linear (Fig. 4.6) such that crack growth rates are increased. Furthermore, at the high load ratios, these differences between the underaged and overaged microstructures are expected to be reduced because the role of crack closure will be diminished with the larger crack opening displacements (Fig. 4.4).

This argument is consistent with previous explanations based solely on microstructural factors.[44] In underaged precipitation hardening systems, where the mode of alloy hardening is primarily the shearing of small coherent precipitates, the resulting heterogeneous deformation (i.e., coarse planar slip) promotes a crystallographic crack path. Because slip is occurring on fewer slip systems, the degree of slip reversibility is greater and hence the crack tip damage per cycle is less. Conversely, in overaged systems where the mode of hardening is now Orowan bypassing of larger, semicoherent or incoherent, non-shearable precipitates, the resulting homogeneous

deformation (i.e., wavy slip) generates a far more planar fracture surface due to the larger number of finer slip steps. This leads to greater slip irreversibility and more crack tip damage per cycle. Furthermore, as noted by Zedalis et al.,[31] the larger precipitate free zones in overaged 7000 series aluminum alloys, arising from the growth of incoherent grain boundary precipitates, must contribute somewhat to the lower fatigue resistance in these microstructures.

Finally, it is interesting to note that the microstructures which show superior fatigue crack growth resistance at near-threshold levels do not necessarily retain such resistance at higher growth rates.[59,60] For example, although the effect is not apparent in 7150 (Fig. 4.3), underaged microstructures in many aluminum alloys show faster growth rates above $\sim 10^{-6}$ mm/cycle, and slower growth rates close to ΔK_{TH}, compared to overaged structures. Such observations tend to support explanations based on crack closure since at higher growth rates with associated larger crack tip opening displacements, the effect of closure mechanisms relying on asperity contact (i.e., roughness-induced) would be reduced. Conversely, where crack closure and deflection mechanisms are important, e.g., for transient crack growth behavior under variable amplitude loading conditions, underaged structures clearly show the longest post-overload retardations and the highest general resistance to crack growth.[60] However, these planar slip characteristics of coherent particle precipitation hardened systems, which are so important in generating **superior fatigue** crack growth resistance through inhomogeneous deformation, rough crystallographic crack paths and enhanced closure and deflection, can lead simultaneously to **inferior** crack initiation **toughness** from a

greater tendency for strain localization. This is particularly evident in aluminum-lithium alloys where the increased coherency between lithium-containing intermetallics and the matrix can result in exceptionally good fatigue crack propagation resistance,[61] through enhanced crack path tortuosity,[62] yet at the same time can produce extremely low fracture toughness values.[63]

4.5 Concluding Summary

Similar to behavior in other high strength precipitation hardened aluminum alloy systems, the fatigue crack growth resistance of high purity 7150 alloy is decreased, specifically at near-threshold levels, with increasing aging treatment. The trend of increased growth rates and decreased threshold ΔK_{TH} values with increased aging is found to be consistent with lower measured levels of crack closure and a decreasing tortuosity in crack path. For the current tests on 7150 in controlled moist room air, where the contribution to crack closure from corrosion product formation is found to be negligible, the superior fatigue crack growth resistance of the underaged microstructures is thus attributed to greater slip reversibility and to enhanced (roughness-induced) crack closure and deflection from the more tortuous crack paths, factors which result from the non-homogeneous, planar slip characteristics of deformation in alloy systems hardened by coherent, shearable precipitates.

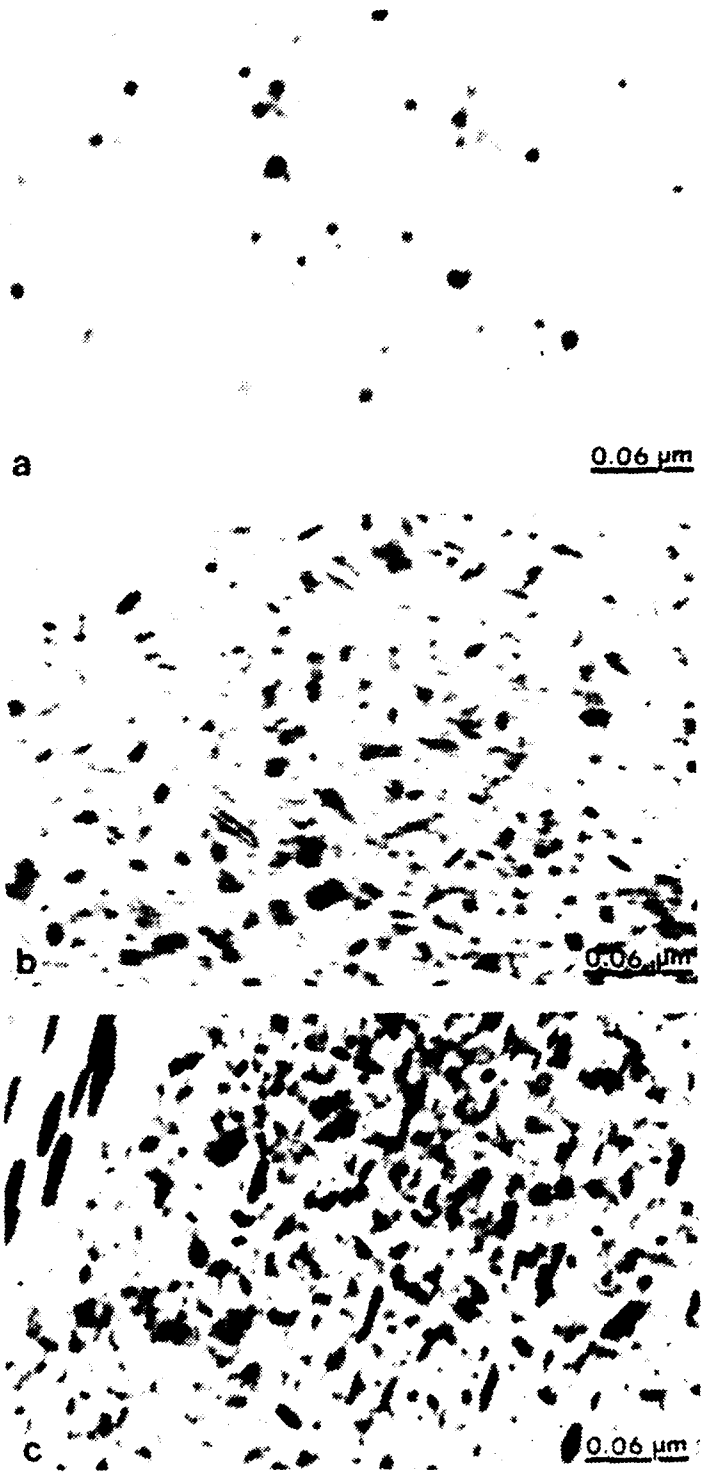

Fig. 4.1. Transmission electron micrographs of a) underaged, b) peak-aged (T6) and c) overaged (T7) I/M 7150 aluminum alloy.

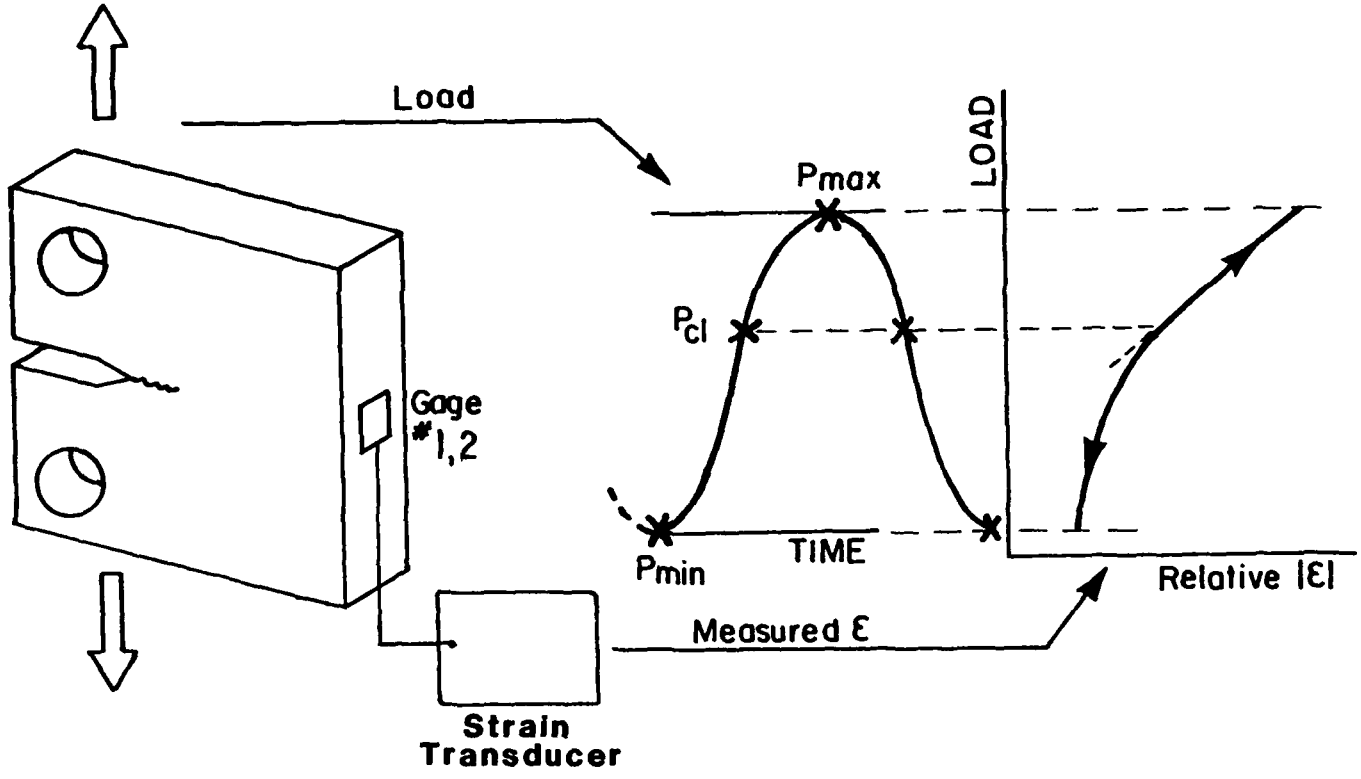

Fig. 4.2. Schematic illustration of the back-face strain technique used to estimate closure stress intensity K_{cl} values. P_{max}, P_{min} and P_{cl} are the maximum, minimum and closure loads, respectively.

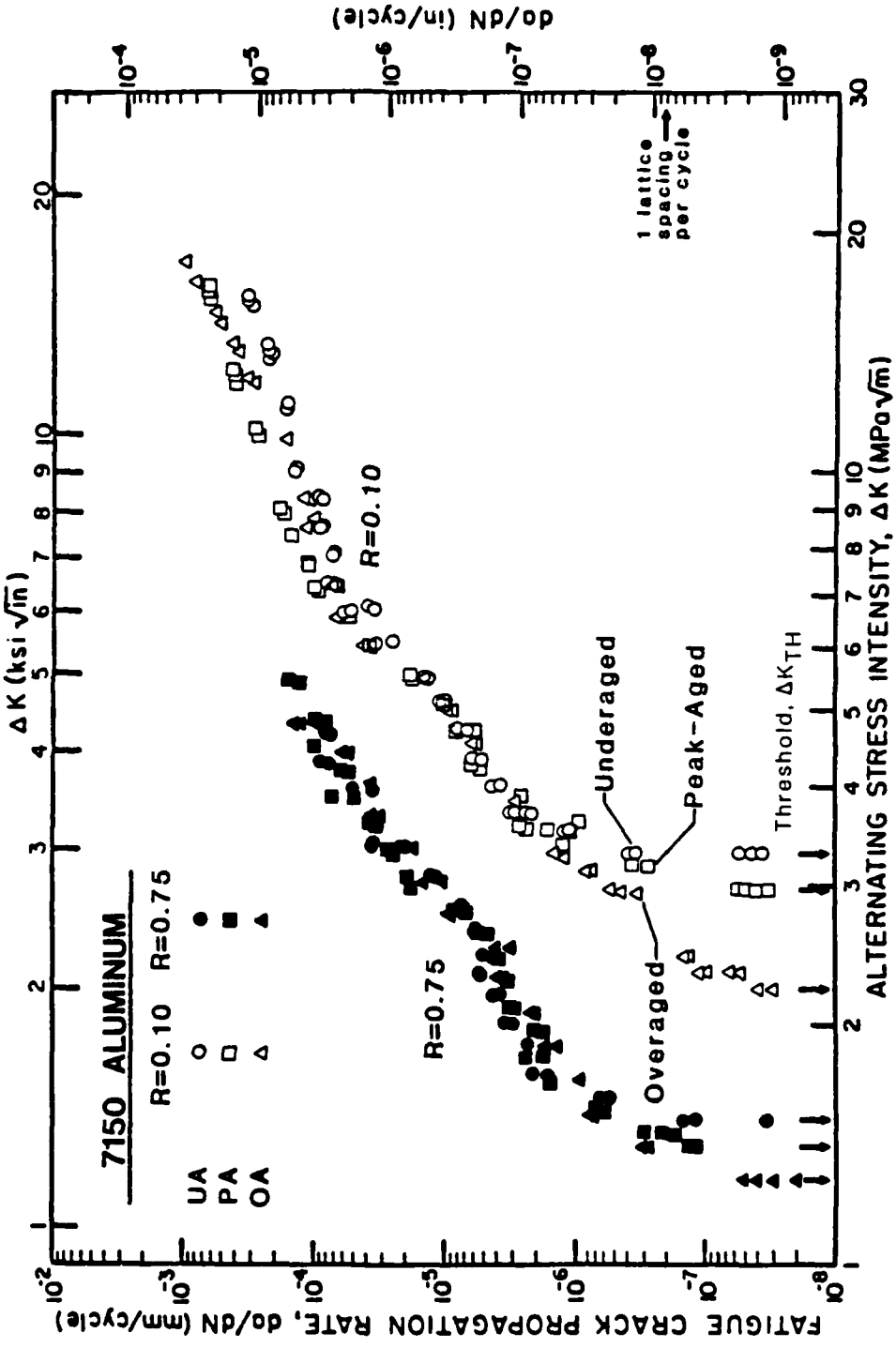

Fig. 4.3. Variation in fatigue crack growth rate (da/dN) as a function of stress intensity range (ΔK) for I/M 7150 aluminum alloy tested at R = 0.10 and 0.75 in controlled moist air. Data are shown for underaged, peak-aged (T6) and overaged (T7) microstructures.

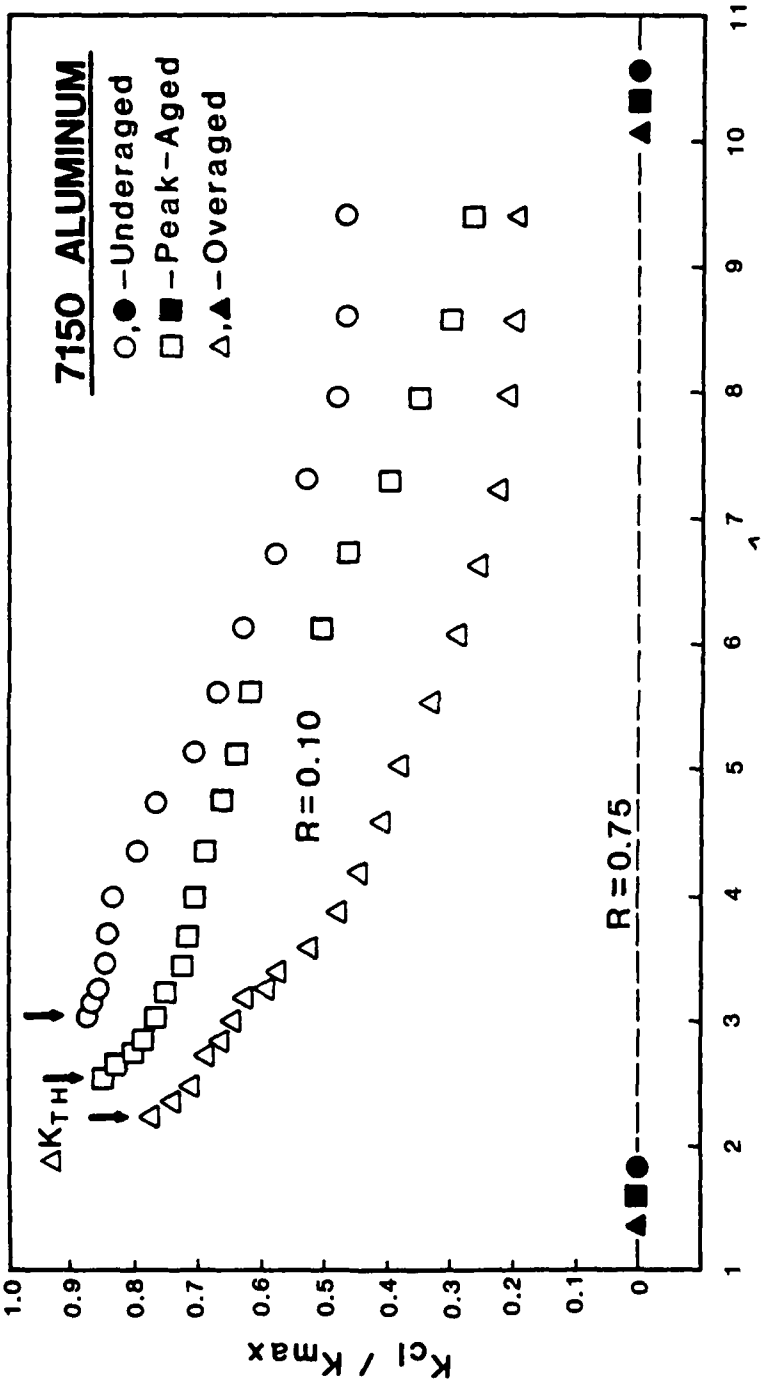

Fig. 4.4. Variation in crack closure, in terms of the ratio of closure to maximum stress intensity, K_{cl}/K_{max}, as a function of ΔK, for underaged, peak-aged (T6) and overaged (T7) 7150 alloy at R = 0.10 and 0.75.

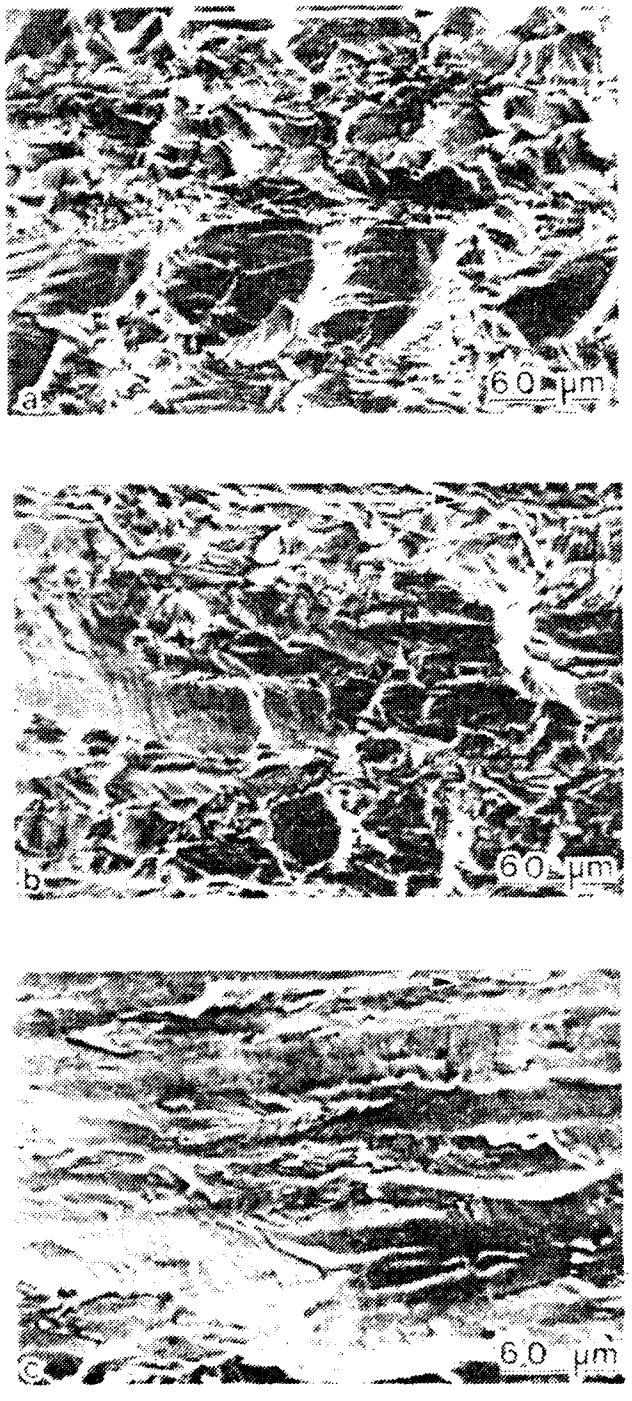

Fig. 4.5. Scanning electron micrographs of fatigue fracture surfaces close to ΔK_{TH} (R = 0.10) in I/M 7150 aluminum alloy, showing the morphology in a) underaged, b) peak-aged (T6) and c) overaged (T7) microstructures.

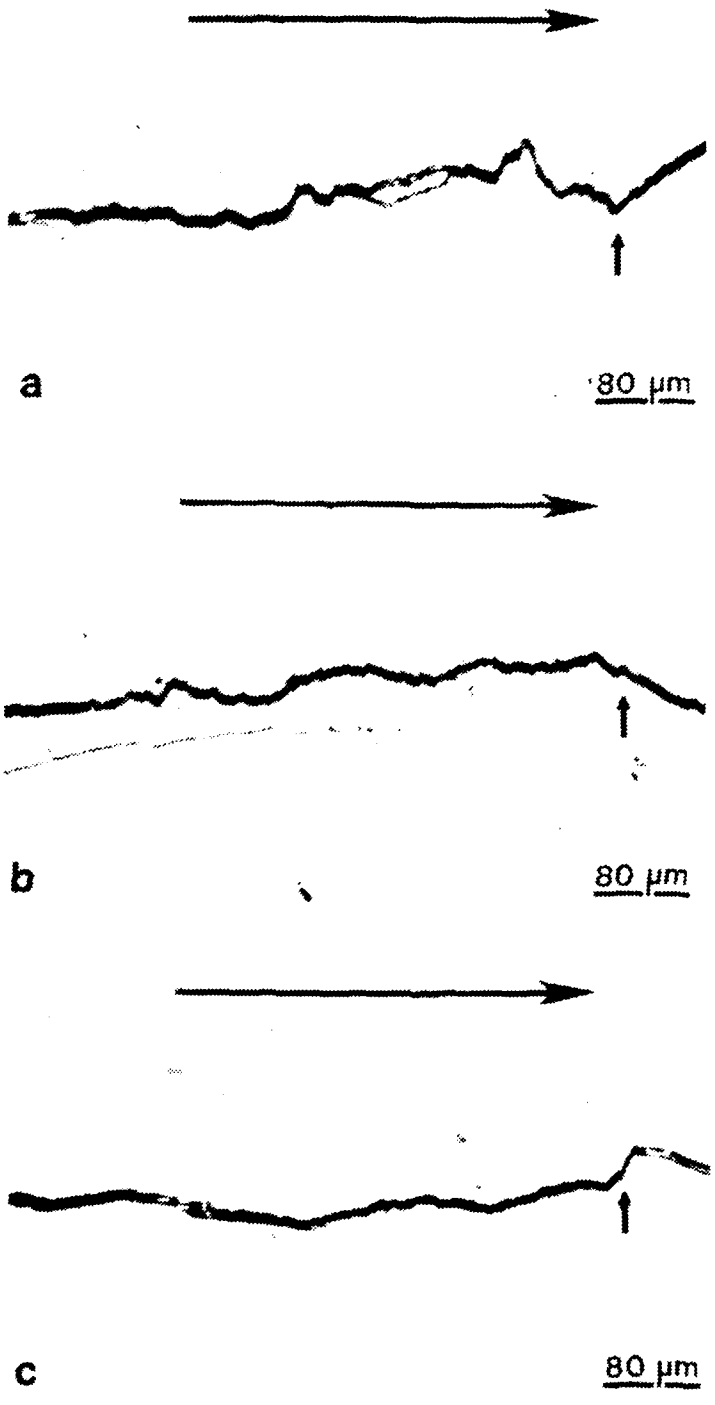

Fig. 4.6. Crack path morphology of near-threshold fatigue cracks in I/M 7150 aluminum alloy in the a) underaged, b) peak-aged (T6) and c) overaged (T7) conditions.

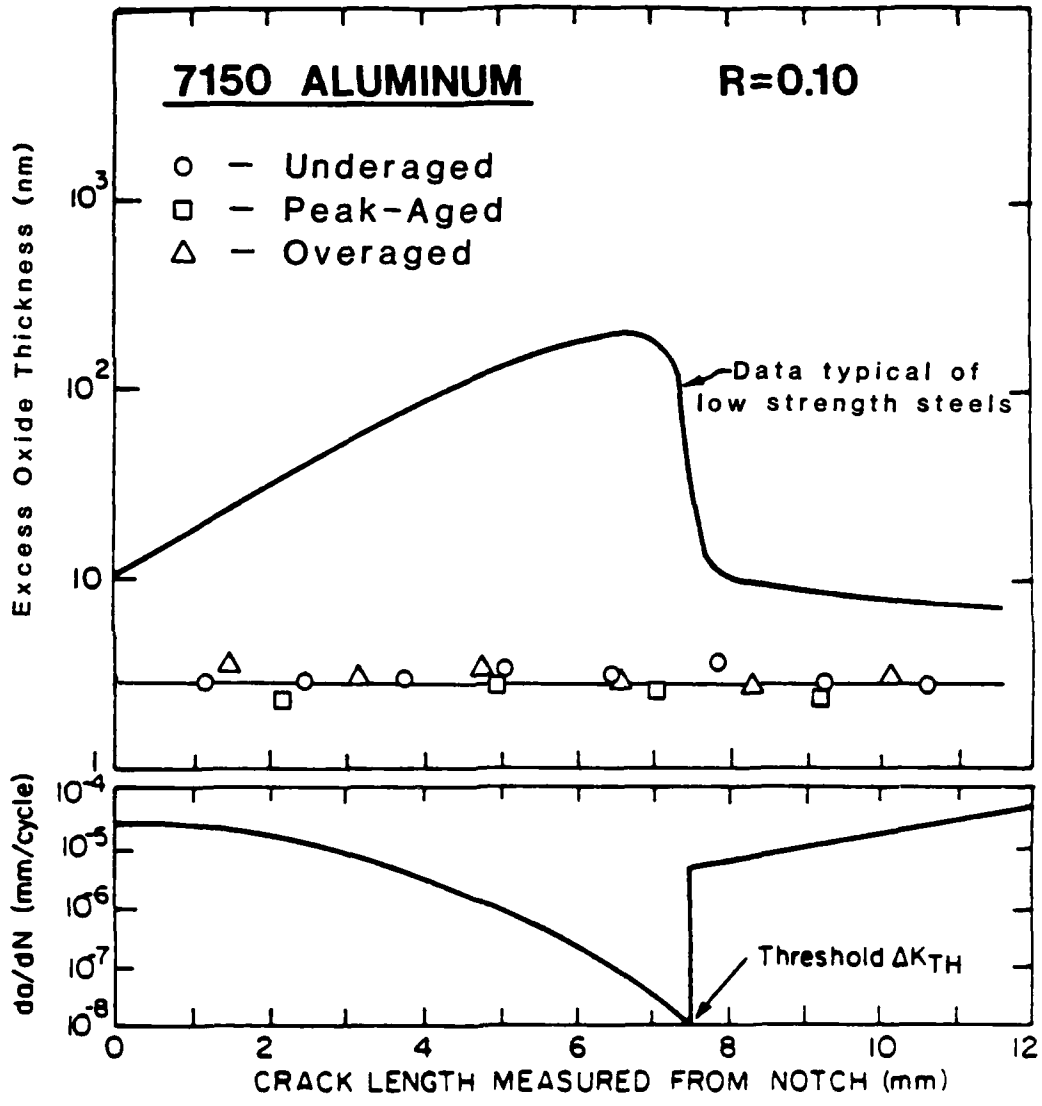

Fig. 4.7. Scanning Auger spectroscopic measurements of excess crack surface oxide deposits as a function of fatigue crack length and growth rate (da/dN). Data points, for I/M 7150 aluminum alloy in the underaged (UA), peak-aged (PA) and overaged (OA) microstructures are compared with prior data[26] on lower strength steels at low load ratios.

5. LOCATION OF CRACK CLOSURE AND THE THRESHOLD CONDITION IN 7150 ALUMINUM ALLOYS

5.1 Introduction

Recent studies on the propagation of fatigue cracks at ultralow growth rates (i.e., typically approaching lattice dimensions per cycle) have suggested that the existence of a fatigue threshold, representing a stress intensity range ΔK_{TH} below which cracks appear dormant, is intimately associated with the development of crack closure in the wake of the crack tip (e.g., refs. 23-34). Observations, that short cracks (small compared to microstructural size-scales or the extent of local plasticity) can propagate below this threshold,[2-20] are consistent with this notion since by definition short cracks possess a limited wake and are thus less likely to be influenced by closure to the same degree as long cracks (e.g., refs. 13 and 19).

Such closure, which results from interference between mating fracture surfaces, acts to reduce the local driving force from the nominal level, based on global measurements of applied loads and crack size, e.g., $\Delta K = K_{max} - K_{min}$, to some effective near-tip level, e.g., $\Delta K_{eff} = K_{max} - K_{cl}$, where K_{cl} is the stress intensity at first contact of the crack surfaces during unloading.[21] The origin of such closure has been related to several mechanisms,[34] including cyclic plasticity,[21] the wedging action of insoluble corrosion products[24-26] or irregular fracture surface morphologies coupled with inelastic crack tip shear displacements,[27-29] fluid-induced pressure inside the crack[35,36] and metallurgical phase transformations[34] (Fig. 2.1).

Despite a good phenominalogical description of closure, the significance of where the actual fracture surface contact develops in relation to the crack tip is still poorly understood. Recent studies[32] in powder metallurgy X-7090-T6 aluminum alloys, where material left in the wake of a crack at threshold was removed by electro-discharge machining, indicated that closure well behind the crack tip was relatively unimportant compared to near-tip closure (i.e., within 1 mm of the tip), which was considered to contribute most to the development of a threshold level. In another study[64] in nickel-based superalloys (Waspaloy), however, where a **single** 0.31 mm diameter hole was drilled a short distance (within 0.31 mm) behind the tip of a threshold crack, the degree of closure was reported to be not significantly affected.

The aim of this study is to substantiate whether near-tip crack closure is most responsible for the development of a threshold by specifically monitoring the closure stress intensity, K_{cl}, during the progressive (on load) removal of material in the wake of an arrested crack at ΔK_{TH}.

5.2 Experimental Procedures

Tests were performed on commercial high purity 7150 alloy plate, of composition shown in Table 4.1, heat-treated to the peak-aged (T6) condition (Fig. 4.1b). Heat treatment schedules and room temperature mechanical properties are listed in Tables 4.2 and 4.3, respectively.

Fatigue crack growth rates were monitored, using D.C. electrical potential techniques, on 6.4 mm thick compact C(T) test-pieces machined in the T-L orientation. Using conventional manual load-shedding to approach the threshold,[1] tests were performed under load control at 50

Hz (sine wave) with a load ratio ($R = K_{min}/K_{max}$) of 0.1 in controlled room air (22°C, 45% relative humidity).

Macroscopic crack closure measurements were made with the back-face strain technique using two strain gauges to record strain both parallel and perpendicular to the loading axis (Fig. 4.2). Mean closure loads, deduced from the point during the fatigue cycle at which the resulting elastic compliance curves, of load versus relative strain, deviated from linearity, were utilized to compute stress intensities at closure, K_{cl}.[47]

5.3 Results and Discussion

The variation in fatigue crack propagation rates with stress intensity range ΔK, for 7150-T6 aluminum alloy over the range 10^{-8} to 10^{-3} mm/cycle, is shown in Fig. 5.1 from the load shedding data at R = 0.1, and indicates a long crack threshold of $\Delta K_{TH} \approx 2.6$ MPa$\sqrt{m}$. Corresponding closure measurements, presented in Fig. 4.4 as the ratio of closure to maximum stress intensity, K_{cl}/K_{max}, as a function of ΔK, show a progressively increasing influence of closure as the threshold is approached, with $K_{cl}/K_{max} \rightarrow 1$ as $\Delta K \rightarrow \Delta K_{TH}$.

To determine the location of the closure most significant to the development of this threshold, material in the wake of the crack tip was progressively removed, in steps of roughly 1 mm, from cracks arrested at ΔK_{TH}, whilst the specimen was maintained at mean load. Material was removed to within 0.5 mm of the tip using a fine jeweler's saw on cracks typically of a total length (including notch) of the order of 25 mm (Fig. 3.1). The width of the saw cut was approximately 0.3 mm. At each stage of the removal, with the remaining fatigue crack

varying from an initial 8 mm to 0.5 mm, closure measurements were made to determine K_{cl} using a threshold loading cycle. The results, in terms of the ratio K_{cl}/K_{max} as a function of the remaining fatigue crack length, $\tilde{a}$, are shown in Fig. 5.2 and indicate the distribution of closure along the crack length. It is apparent that, although the extent of closure is fairly evenly distributed over the majority of the crack length, more than 40% of the closure is developed within a region 0.5 mm of the crack tip. For example, at ΔK_{TH}, the arrested fatigue crack, of length $\tilde{a} \approx 8$ mm, has a closure stress intensity of $K_{cl} \approx 2.5$ MPa$\sqrt{m}$ ($\Delta K_{eff} \approx 0.4$ MPa$\sqrt{m}$) at the nominal threshold of $\Delta K_{TH} = 2.6$ MPa$\sqrt{m}$ ($R = 0.1$). After removal of 7.5 mm of wake, however, K_{cl} is reduced to 1.1 MPa$\sqrt{m}$ ($\Delta K_{eff} \approx 1.8$ MPa$\sqrt{m}$) such that the remaining closure is confined within the very near tip region.

The effect of this removal of closure can be best appreciated by immediate re-cycling of the previously arrested crack following wake removal ($\tilde{a} = 0.5$ mm) under the same constant $\Delta K = \Delta K_{TH}$ conditions, i.e., similar to experiments in ref. 32. Even though nominal ΔK levels do <u>not</u> exceed the threshold, crack growth re-commences consistent with the local increase in ΔK_{eff} (Fig. 5.1). In essence, the crack behaves as an effective "short" crack. As shown in Fig. 5.3, after an initial acceleration subsequent growth rates reach a plateau, but do not completely re-arrest. This is presumably due to experimental difficulties in maintaining constant ΔK cycling precisely at the threshold level of 2.6 MPa$\sqrt{m}$, in a region where growth rates are extremely dependent upon ΔK (Fig. 5.1).

Parallel studies on mechanisms of fatigue crack growth in this alloy suggest that such crack closure can originate from several

sources (Section 4). Oxide-induced closure, however, does not appear to be a major factor as Auger studies on broken fracture surfaces reveal only uniformly thin oxide films, small compared to crack tip opening displacements (i.e., less than 3 nm thick even close to ΔK_{TH}, Fig. 4.7). Due to the irregular nature of the crack path (Fig. 4.6), however, roughness-induced crack closure would seem to provide a more potent contribution, although this effect is less pronounced than in underaged structures where the greater planarity of slip promotes greater crack deflection and hence more closure (Section 4).

5.4 Concluding Remarks

The present experiments on ingot aluminum alloys provide further confirmation that the development of a threshold for the growth of "long" fatigue cracks is primarily associated with a reduction in local crack driving force due to crack closure in the wake of the crack tip. Moreover, based on studies of the change in K_{cl} during progressive removal of the wake at threshold levels, it appears that, although such closure is fairly evenly distributed over most of the crack length, more than 40% of the closure is confined to the near-tip region; in the present case within 0.5 mm of the crack tip.

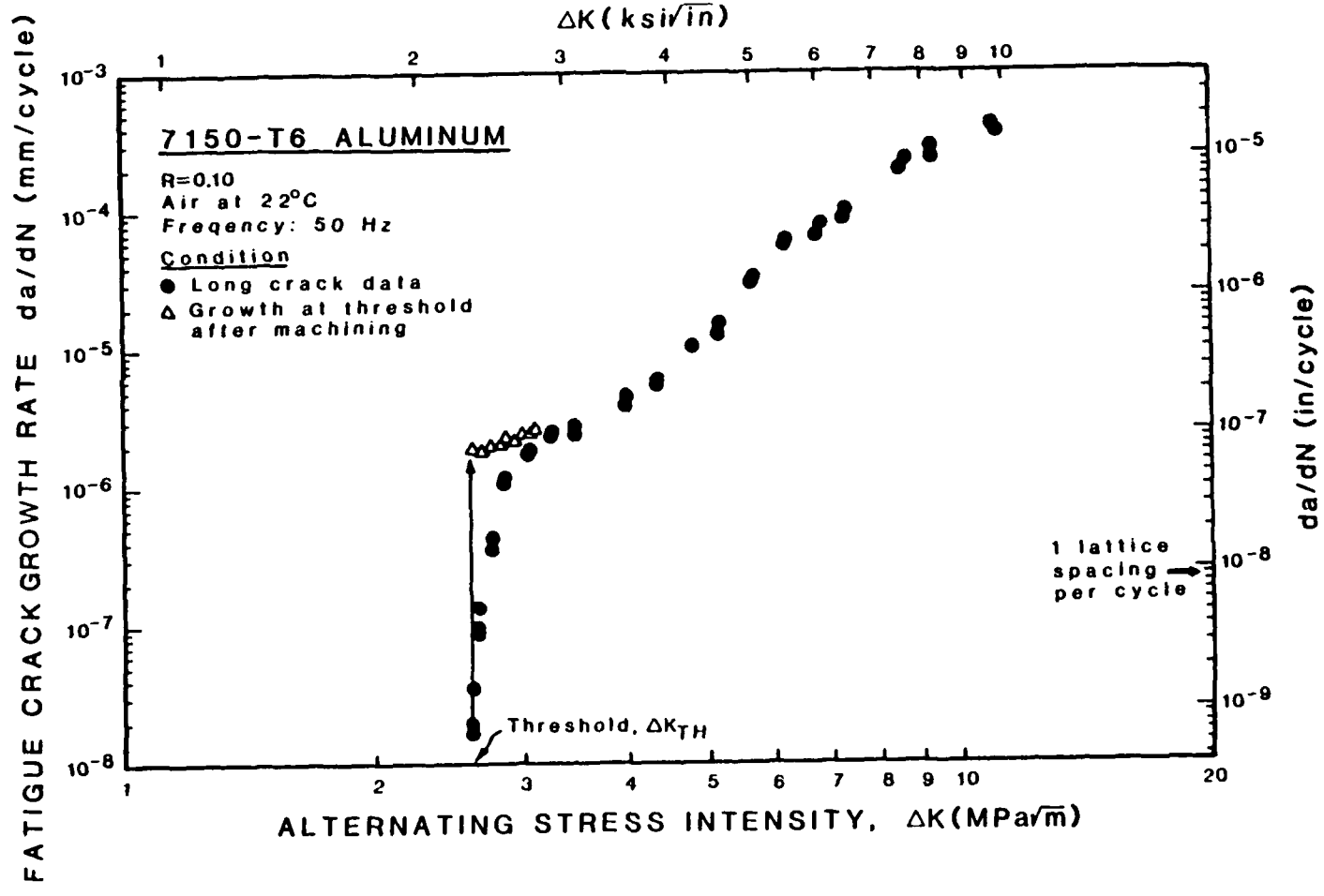

Fig. 5.1. Variation in fatigue crack propagation rate (da/dN) with stress intensity range (ΔK) for 7150-T6 aluminum alloy in room air at a load ratio of R = 0.10. Open triangles refer to the behavior of the previously arrested crack at the threshold ΔK_{TH} immediately following removal of the wake to within 0.5 mm of the crack tip.

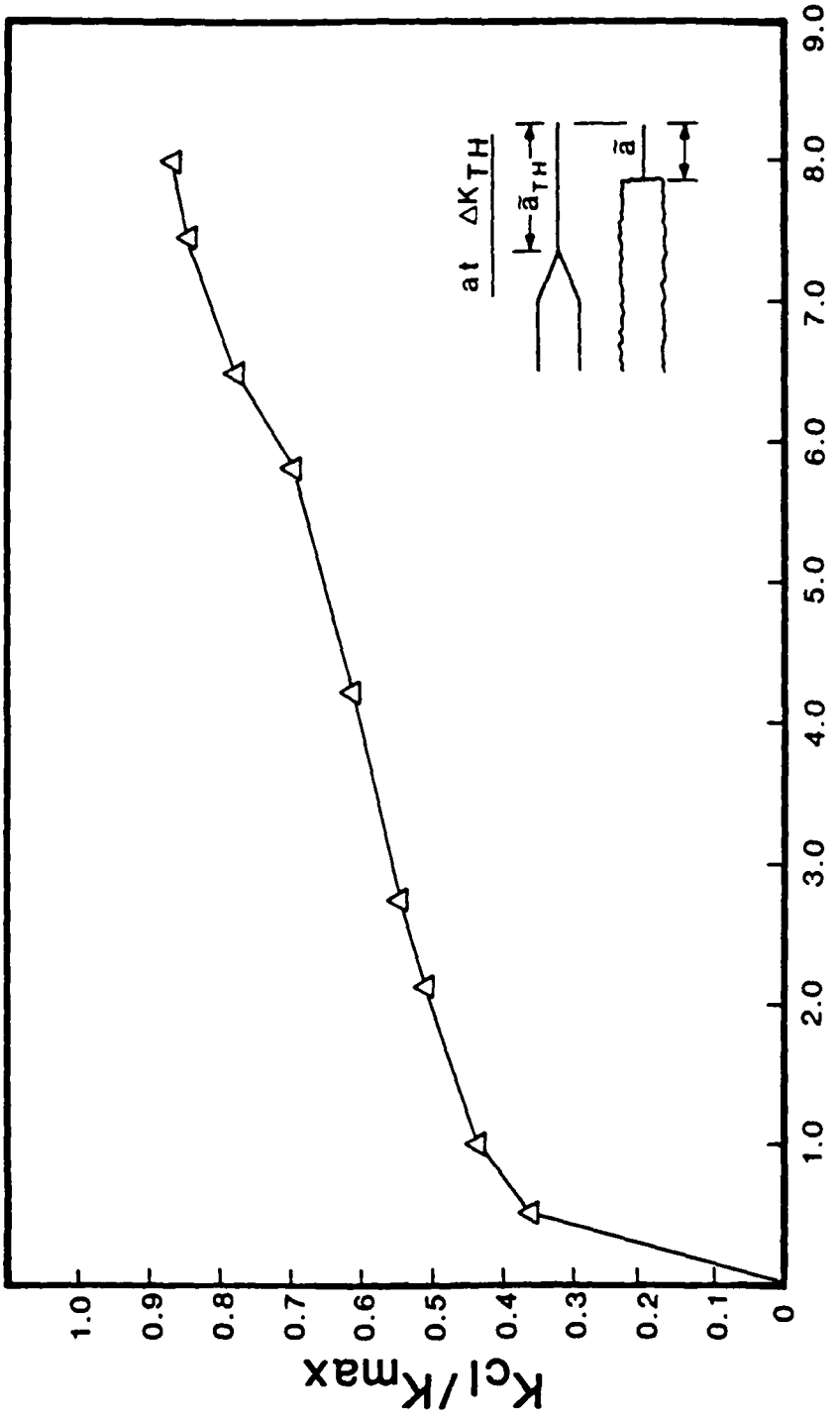

Fig. 5.2. Variation in crack closure in 7150-T6, measured in terms of K_{Cl}/K_{max}, for an arrested fatigue crack at ΔK_{TH} ($R = 0.10$) as a function of remaining fatigue crack length, ã, during progressive machining away of material in the wake of the crack tip.

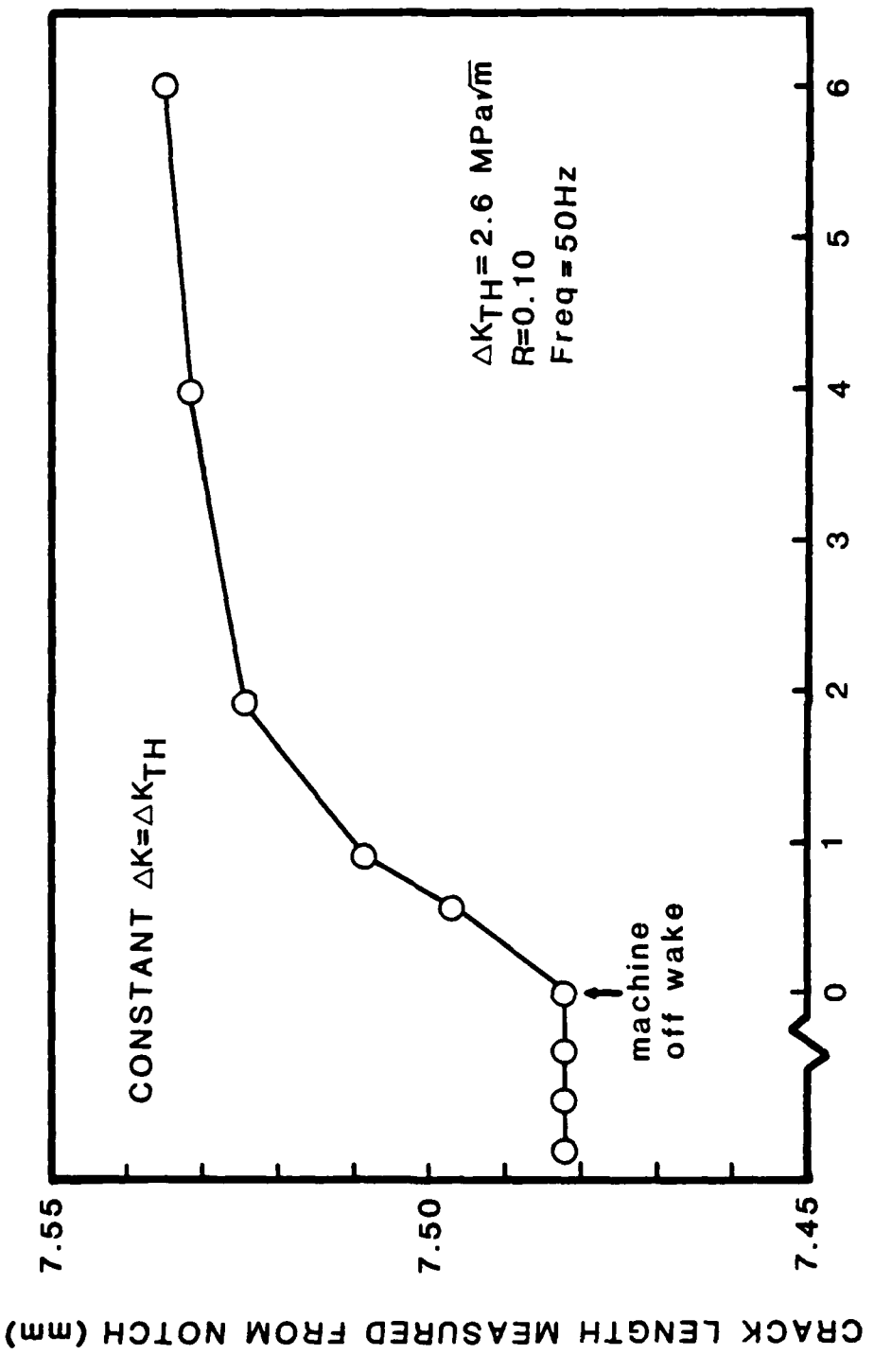

Fig. 5.3. Fatigue crack growth behavior, in terms of crack length versus number of cycles, in 7150-T6 aluminum at the threshold ΔK_{TH} (R = 0.10), before and after removal of the material in the wake of the crack tip (remaining $\tilde{a}$ = 0.5 mm). Effect is also shown in terms of da/dN vs. ΔK by the open triangles in Fig. 5.1.

6. BRIEF SUMMARY OF FUTURE WORK

During the coming year, studies to locate the principal site of crack closure in relation to the crack tip (as described in Section 5), will be extended to the under- and overaged tempers in the 7150 alloy, where the origin and extent of closure is distinctly different. In addition, tests on the third stage of the 3-in-1 test-piece, namely to determine actual short crack threshold values, will be completed on all three microstructures in this alloy. We also plan to initiate similar fatigue testing programs in the two 2000 series alloys, namely 2024 and the high purity 2124. Of particular interest for investigation is the observation[31] in 7000 series alloys that high purity alloys have **lower** near-threshold crack growth resistance than their lower purity equivalents. Finally, we have initiated a program using center-cracked plate specimens to examine the role of periodic compression overload cycles in influencing ΔK_{TH} values and near-threshold growth rates in 7150 alloy. Based on limited observations[65] in 2024-T3, such periodic compression overloads appear to severely reduce thresholds and to increase growth rates. Our intent is to document the magnitude of the effect in 7000 series alloys and decern whether it results from a reduction in closure due to a flattening of asperities during the compressive portion of the cycle. Moreover, by comparison of the constant amplitude fatigue data from the center-cracked specimens with that already obtained from compact C(T) geometries (described in Section 4), we intend to investigate reports[66,67] of a specimen geometry effect on crack closure and hence near-threshold crack growth

behavior, which if verified would have far-reaching consequences on the measurement and application of crack propagation data.

7. ACKNOWLEDGEMENTS

The work was supported by the U.S. Air Force Office of Scientific Research under Grant No. AFOSR-82-0181, with Dr. Alan H. Rosenstein as program manager. Thanks are due to Dr. Rosenstein for helpful discussions, and to the Aluminum Company of America, specifically Drs. R. J. Bucci, R. R. Sawtell and J. T. Staley, and Kaiser Aluminum Company, specifically Dr. J. A. Moskovitz, for provision of materials. Particular thanks are due to the Alcoa Foundation for their interest and support of this program.

8. REFERENCES

1. R. O. Ritchie: International Metals Reviews, 1979, vol. 20, p. 205.

2. M. E. Fine and R. O. Ritchie: in Fatigue and Microstructure, p. 245, American Society for Metals, Metals Park, OH, 1979.

3. S. J. Hudak: J. Eng. Matls. Tech., Trans. ASME Series H, 1981, vol. 103, p. 26.

4. S. Pearson: Eng. Fract. Mech., 1975, vol. 7, p. 235.

5. H. Kitagawa and S. Takahashi: Proc. 2nd Intl. Conf. on Mech. Beh. of Materials, p. 627, American Society for Metals, Metals Park, OH, 1976.

6. Y. H. Kim, T. Mura and M. E. Fine: Eng. Fract. Mech., 1978, vol. 11, p. 1697.

7. N. E. Dowling: ASTM Spec. Tech Publ. 637, 1978, p. 97.

8. M. H. El Haddad, N. E. Dowling, T. H. Topper and K. N. Smith: Int. J. Fract., 1980, vol. 16, p. 15.

9. R. A. Smith and K. J. Miller: Int. J. Mech. Sci., 1977, vol. 19, p. 11.

10. W. L. Morris: Met. Trans. A, 1980, vol. 11A, p. 1117.

11. B. N. Leis and T. P. Forte: ASTM Spec. Tech. Publ. 743, 1982, p. 100.

12. S. Usami and S. Shida: Fat. Eng. Matls. Struct., 1979, vol. 1, p. 471.

13. K. Tanaka and Y. Nakai: Fat. Eng. Matls. Struct., 1983, vol. 5, p. 315.

14. G. P. Sheldon, T. S. Cook, T. W. Jones and J. Lankford: Fat. Eng. Matls. Struct., 1981, vol. 3, p. 219.

15. R. P. Gangloff: Res. Mech. Letters, 1981, vol. 1, p. 299.

16. J. F. McCarver and R. O. Ritchie: Mater. Sci. Eng., 1982, vol. 55, p. 63.

17. J. Lankford: Fat. Eng. Matls. Struct., 1982, vol. 5, p. 223.

18. J. L. Breat, F. Mudry and A. Pineau: Fat. Eng. Matls. Struct., 1983, vol. 6, p. 349.

19. S. Suresh and R. O. Ritchie: International Metals Reviews, 1984, vol. 25, in press.

20. R. P. Gangloff and R. O. Ritchie: in Fundamentals of Deformation and Fracture, Proc. Eshelby Memorial Symp., B. A. Bilby and K. J. Miller, eds., Cambridge University Press, U.K., 1984, in press.

21. W. Elber: ASTM Spec. Tech. Publ. 486, 1981, p. 230.

22. R. A. Schmidt and P. C. Paris: ASTM Spec. Tech. Publ. 536, 1973, p. 79.

23. P. C. Paris, R. J. Bucci, E. T. Wessel, W. G. Clark and T. R. Mager: ASTM Spec. Tech. Publ. 513, 1972, p. 141.

24. R. O. Ritchie, S. Suresh and C. M. Moss: J. Eng. Matls. Tech., 1980, vol. 102, p. 293.

25. A. T. Stewart: Eng. Fract. Mech., 1980, vol. 13, p. 463.

26. S. Suresh, G. F. Zamiski and R. O. Ritchie: Met. Trans. A, 1981, vol. 12A, p. 1435.

27. N. Walker and C. J. Beevers: Fat. Eng. Matls. Struct., 1979, vol. 1, p. 135.

28. K. Minakawa and A. J. McEvily: Scripta Met., 1981, vol. 15, p. 937.

29. S. Suresh and R. O. Ritchie: Met. Trans. A, 1982, vol. 13A, p. 1627.

30. P. K. Liaw, T. R. Leax, R. S. Williams and M. G. Peck: Met. Trans. A, 1982, vol. 13A, p. 1607.

31. M. Zedalis, L. Filler and M. E. Fine: Scripta Met., 1982, vol. 16, p. 471.

32. K. Minakawa, J. C. Newman and A. J. McEvily: Fat. Eng. Matls. Struct., 1983, vol. 6, p. 359.

33. W. W. Gerberich, W. Yu and K. Esaklul: Met. Trans. A, 1984, vol. 15A, p. 875.

34. S. Suresh and R. O. Ritchie: in Fatigue Crack Growth Threshold: Concepts, D. L. Davidson and S. Suresh, eds., TMS-AIME, Warrendale, PA, 1984.

35. K. Endo, T. Okada, K. Komai and M. Kiyota: Bull. JSME, 1972, vol. 15, p. 1316.

36. J. L. Tzou, S. Suresh and R. O. Ritchie: Acta Met., 1984, vol. 32, in press.

37. J. Petit and A. Zeghoul: in Fatigue Thresholds, p. 563, J. Backlund, A. Blom and C. J. Beevers, eds., EMAS Ltd., U.K., vol. 1, 1982.

38. A. K. Vasudévan and S. Suresh: Met. Trans. A, 1982, vol. 13A, p. 2271.

39. M. C. Lafarie-Frenot and C. Gasc: Fat. Eng. Matls. Struct., 1983, vol. 6, p. 329.

40. J. Petit: in Fatigue Crack Growth Threshold: Concepts, D. L. Davidson and S. Suresh, eds., TMS-AIME, Warrendale, PA, 1984.

41. S. Suresh, A. K. Vasudévan and P. E. Bretz: Met. Trans. A, 1984, vol. 15A, p. 369.

42. R. D. Carter, E. W. Lee, E. A. Starke and C. J. Beevers: Met. Trans. A, 1984, vol. 15A, p. 555.

43. G. G. Garrett and J. F. Knott: Acta Met., 1975, vol. 23, p. 841.

44. E. Hornbogen and K. H. Zum Gahr: Acta Met., 1976, vol. 24, p. 581.

45. J. Lindgkeit, A. Gysler and G. Lütjering: Met. Trans. A, 1981, vol. 12A, p. 1613.

46. F. S. Lin and E. A. Starke: in Hydrogen in Metals, p. 485, A. Thompson and I. M. Bernstein, eds., TMS-AIME, Warrendale, PA, 1981.

47. V. B. Dutta, S. Suresh and R. O. Ritchie: Met. Trans. A, 1984, vol. 15A, in press.

48. S. Suresh, D. M. Parks and R. O. Ritchie: in Fatigue Thresholds, p. 391, J. Bäcklund, A. Blom and C. J. Beevers, eds., EMAS Ltd., U.K., vol. 1, 1982.

49. J. Petit, P. Renaud and P. Violan: in Proc. 14th European Conf. on Fracture, p. 426, Leoben, EMAS Ltd., U.K., 1982.

50. K. Schulte, H. Nowack and K. H. Trautmann: Z. Werkstofftech, 1980, vol. 11, p. 287.

51. M. Zedalis and M. E. Fine: Scripta Met., 1982, vol. 16, p. 1411.

52. R. J. Asaro, L. Hermann and J. M. Baik: Met. Trans. A, 1981, vol. 12A, p. 1133.

53. M. Gell and G. R. Leverant: Acta Met., 1968, vol. 16, p. 553.

54. K. Minakawa, Y. Matsuo and A. J. McEvily: Met. Trans. A, 1982, vol. 13A, p. 439.

55. G. R. Yoder, L. A. Cooley and T. W. Crooker: Met. Trans. A, 1977, vol. 8A, p. 1737.

56. G. R. Yoder, L. A. Cooley and T. W. Crooker: Met. Trans. A, 1978, vol. 9A, p. 1413.

57. S. Suresh: Met. Trans. A, 1983, vol. 14A, p. 2375.

58. D. L. Davidson: Fat. Eng. Matls. Struct., 1981, vol. 3, p. 229.

59. R. J. Bucci, A. B. Thakker, T. H. Saunders, R. R. Sawtell and J. T. Staley: ASTM Spec. Tech. Publ. 714, 1980, p. 41.

60. S. Suresh and A. K. Vasudévan: in Fatigue Crack Growth Threshold: Concepts, D. L. Davidson and S. Suresh, eds., TMS-AIME, Warrendale, PA, 1984.

61. E. J. Coyne, T. H. Saunders and E. A. Starke: in Aluminum-Lithium Alloys, p. 293, T. H. Saunders and E. A. Starke, eds., TMS-AIME, Warrendale, PA, 1981.

62. A. K. Vasudévan, P. E. Bretz, A. C. Miller and S. Suresh: Mater. Sci. Eng., 1984, vol. 62, in press.

63. E. S. Balmuth and R. Schmidt: in Aluminum-Lithium Alloys, p. 69, T. H. Saunders and E. A. Starke, eds., TMS-AIME, Warrendale, PA, 1981.

64. T. V. Duggan: in Fatigue Thresholds, p. 809, J. Bäcklund, A. Blom and C. J. Beevers, eds., EMAS Ltd., Warley, U.K., vol. 2, 1982.

65. P. Au, T. H. Topper and M. H. El Haddad: in Behavior of Short Cracks in Airframe Components, p. 11.1, AGARD Conf. Proc. No. 328, AGARD, France, 1983.

66. J. C. Radon: in Fatigue Thresholds, p. 113, J. Bäcklund, A. Blom and C. J. Beevers, eds., EMAS Ltd., Warley, U.K., vol. 1, 1982.

67. J. L. Horng and M. E. Fine: in Fatigue Crack Growth Threshold: Concepts, D. L. Davidson and S. Suresh, eds., TMS-AIME, Warrendale, PA, 1984.

9. PROGRAM ORGANIZATION AND PERSONNEL

The work described was performed in the Department of Materials Science and Mineral Engineering, University of California in Berkeley, under the supervision of Professor R. O. Ritchie, aided by a research engineer, a graduate student research assistant (for M.Eng. degree) and an undergraduate research helper. The individual personnel are listed below:

i) Professor R. O. Ritchie, Principal Investigator (Department of Materials Science and Mineral Engineering)

ii) Dr. S. Suresh, Assistant Research Engineer (until 6/83) (now with Division of Engineering, Brown University)

iii) Dr. W. Yu, Post-Graduate Research Engineer (after 7/83) (Department of Materials Science and Mineral Engineering)

iv) E. Zaiken, Graduate Student Research Assistant (Department of Mechanical Engineering)

v) P. Donehoo, Undergraduate Engineering Aide (Department of Materials Science and Mineral Engineering)

10. PUBLICATIONS

1983

i) R. O. Ritchie and S. Suresh: "The Fracture Mechanics Similitude Concept: Questions Concerning its Application to the Behavior of Short Fatigue Cracks," Materials Science and Engineering, 1983, vol. 57, pp. L27-L30.

ii) R. O. Ritchie and S. Suresh: "Mechanics and Physics of the Growth of Small Cracks," in Behavior of Short Cracks in Airframe Components, AGARD, vol. CP328, pp. 1.1-1.14, North Atlantic Treaty Organization, AGARD, France, 1983.

iii) S. Suresh: "Crack Deflection: Implications for the Growth of Long and Short Cracks," Metallurgical Transactions A, 1983, vol. 14A, pp. 2375-2385.

1984

iv) S. Suresh and R. O. Ritchie: "Propagation of Short Fatigue Cracks," International Metals Reviews, 1984, vol. 25, in press.

v) R. P. Gangloff and R. O. Ritchie: "Environmental Effects Novel to the Propagation of Short Fatigue Cracks," in Fundamentals of Deformation and Fracture, Proc. Eshelby Memorial Symp., B. A. Bilby and K. J. Miller, eds., Cambridge University Press, 1984.

vi) E. Zaiken and R. O. Ritchie: "On the Location of Crack Closure and the Threshold Condition for Fatigue Crack Growth," submitted to Scripta Metallurgica, April 1984.

In Preparation

vii) E. Zaiken and R. O. Ritchie: "Effects of Microstructure on Fatigue Crack Propagation and Crack Closure Behavior in 7150 Aluminum Alloy," to be submitted to Materials Science and Engineering, May 1984.

viii) E. Zaiken and R. O. Ritchie: "The Development and Location of Crack Closure at the Fatigue Threshold in 7150 Aluminum Alloys: Role of Aging Treatment/Microstructure," to be submitted to Metallurgical Transactions A, May 1984.

11. DISTRIBUTION LIST

AFOSR/NE
ATTN: Dr. A. H. Rosenstein
Bldg. #410
Bolling AFB
Washington, D.C. 20332

AFWAL/MLLM
ATTN: Branch Chief
Wright-Patterson AFB, Ohio 45433

AFWAL/MLLS
ATTN: Branch Chief
Wright-Patterson AFB, Ohio 45433

AFWAL/MLLN
ATTN: Branch Chief
Wright-Patterson AFB, Ohio 45433

Dr. Hugh R. Gray
NASA Lewis Research Center
Materials & Structures Division
21000 Brookpark Rd.
Cleveland, Ohio 44135

Drs. R. J. Bucci, R. R. Sawtell and J. T. Staley
Alcoa Technical Center
Alcoa Laboratories
Alcoa Center, PA 15069

APPENDIX

THE PROPAGATION OF SHORT FATIGUE CRACKS

S. Suresh and R. O. Ritchie

June 1983

Report No. UCB/RP/83/1014

Department of Materials Science and Mineral Engineering
University of California, Berkeley

Review

Report No. UCB/RP/83/1014

THE PROPAGATION OF SHORT FATIGUE CRACKS

S. Suresh*

Division of Engineering, Brown University,
Providence, Rhode Island 02912, U.S.A.

and

R. O. Ritchie

Materials and Molecular Research Division, Lawrence Berkeley Laboratory
and Department of Materials Science and Mineral Engineering,
University of California, Berkeley, California 94720, U.S.A.

June 1983

Accepted for Publication in International Metals Reviews

*Formerly with the Department of Materials Science and Mineral Engineering, University of California, Berkeley, California, U.S.A.

THE PROPAGATION OF SHORT FATIGUE CRACKS

S. Suresh and R. O. Ritchie

ABSTRACT

Fatigue-crack propagation in engineering materials has been a topic of considerable research effort and extensive review articles over the past several years. The majority of such investigations have focussed on the behavior of "long" fatigue cracks, even though the characteristics associated with the extension of small flaws in metals and alloys remain relatively unexplored,despite their unquestionable importance from an engineering standpoint. In this review, the mechanics and micromechanisms of the sub-critical growth of short fatigue cracks are examined and aspects of their propagation behavior contrasted with those of long cracks in terms of fracture mechanics, microstructure and environment. Cracks are defined as being short i) when their length is small compared to relevant microstructural dimensions (a continuum mechanics limitation), ii) when their length is small compared to the scale of local plasticity (a linear elastic fracture mechanics limitation), and iii) when they are merely physically small (e.g., < 0.5-1 mm). Since all three types of short flaws are known to propagate faster than (or at least at the same rate as) corresponding long fatigue cracks subjected to the same *nominal* driving force, current defect-tolerant fatigue design procedures which

---

S. Suresh, BTech, MS, ScD, is Assistant Professor, Division of Engineering, Brown University, Providence, Rhode Island 02912, U.S.A.
R. O. Ritchie, MA, PhD, MIM, CEng, is Professor, Department of Materials Science and Mineral Engineering and Lawrence Berkeley Laboratory, University of California, Berkeley, CA 94720, U.S.A. Professor Suresh was formerly with the University of California, Berkeley.

utilize long crack data can, in certain applications, result in non-conservative lifetime predictions. The characteristics of the short crack problem are critically reviewed in the light of the influences of local plasticity, microstructure, crack-tip environment, growth mechanisms, crack driving force, and the premature closure of the crack.

LIST OF SYMBOLS

a	= crack length
a_o	= constant characteristic of material/material condition in expression of ΔK, equation (23)
A	= constant in cyclic constitutive law
Δa	= increment of crack extension
b	= sum of the crack length a and the blocked slip band zone w_o, equation (18)
B	= test piece thickness
c	= depth of edge notch or half length of internal notch
$\bar{c}$	= half the width of a surface micro-crack
C	= experimentally-determined scaling constant, equation (2)
CTOD	= crack tip opening displacement
ΔCTOD	= cyclic crack tip opening displacement
d	= proportionality factor dependent upon yield strain ε_o and work hardening exponent, n, equation (13)
d_o	= maximum thickness of the excess oxide layer
da/dN	= fatigue-crack propagation rate per cycle
d_g	= grain size
E	= elastic (Young's) modulus
E'	= symbol denoting the effective value of Young's modulus under different loading conditions
e	= nominal crack length difference between a fatigue crack of length a in an unnotched specimen and an equivalent fatigue crack of length ℓ growing from a notch
f	= a function of stress intensity factor range, ΔK and load ratio, R, equation (15)
f_{ij}	= a dimensionless function of the polar angle measured from the crack plane θ, equation (2)

f'_{ij}, f''_{ij} = universal functions of the polar angle measured from the crack plane, θ, and the work hardening exponent, n, equation (10)

G = strain energy release rate

J = scalar amplitude of crack tip stress and strain field under non-linear elastic conditions

ΔJ = cyclic component of J

k_f = fatigue-strength reduction factor

k_t = theoretical elastic stress concentration factor

k_σ, k_ε = stress and strain concentration factors

K_1, K_2 = local Mode I and Mode II stress intensity factors for a non-linear crack

K_I = stress intensity factor in Mode I loading

K_{Ic} = stress intensity at final failure (plane strain fracture toughness)

K_{cl} = closure stress intensity factor

K_c^m, K_{II}^m = critical and Mode II values, respectively, of the microscopic stress intensity at the tip of the slip band

K_ℓ = limiting stress intensity for a long crack emanating from a notch

K_{max}, K_{min} = maximum and minimum stress intensities during cycle

K_s = limiting stress intensity for a short crack emanating from a notch

K_o = long crack threshold stress intensity factor

K_{TH} = threshold stress intensity factor

ΔK = nominal stress intensity factor range ($K_{max} - K_{min}$)

ΔK_{eff} = effective stress intensity factor range ($K_{max} - K_{cl}$)

ΔK_{eq} = equivalent stress intensity range for a short crack

ΔK_i = initial stress intensity range

ΔK_o = long crack threshold stress intensity factor range

ΔK_{TH} = threshold stress intensity factor range

ΔK_ε = pseudo-elastic-plastic strain intensity range

ℓ = length of a crack growing from a notch

ℓ_o = transition size of a crack growing from a notch

m = exponent in Paris power law, equation (2)

m' = exponent in the power law for elastic-plastic fatigue crack growth, equation (12)

n, n' = monotonic and cyclic work hardening exponents, respectively

N = number of cycles

N_i = number of cycles to initiate a macro-crack

N_p = number of cycles to propagate a macro-crack sub-critically until final failure

P_{cl}, P_{max}, P_{min} = closure, maximum and minimum loads, respectively, during the fatigue cycle

q = a fraction of the elastic strain with values between 0.5 and 1, equation (21)

Q = a dimensionless function of geometry, equation (8)

r = radial distance from the crack tip

r_{max}, r_Δ = maximum and cyclic plastic zone sizes

r_y = plastic zone size

r_Δ^F = cyclic plastic zone size at the fatigue limit

R = load or stress ratio (K_{min}/K_{max})

R_ε = ratio of minimum to maximum strain

s = half of the distance between the location of thickest oxide layer and the crack tip

S = compliance of the micro-crack in the completely opened state

1. INTRODUCTION

Fatigue fractures account for the vast majority of in-service failures in most engineering structures and components, either as a result of pure mechanical loading or in conjunction with sliding and friction between surfaces (fretting-fatigue), rolling contact between surfaces (rolling contact fatigue), aggressive environments (environmentally-assisted or corrosion fatigue) or elevated temperatures (creep-fatigue). Such progressive fracture of materials by incipient growth of flaws under cyclically-varying stresses, termed fatigue, can be categorized into the following discrete yet related phenomena involving i) initial cyclic damage in the form of cyclic hardening or softening, ii) creation of initial microscopic flaws (micro-crack initiation), iii) coalescence of these micro-cracks to form an initial "fatal" flaw (micro-crack growth), iv) subsequent macroscopic propagation of this flaw (macro-crack growth), and v) final catastrophic failure or instability. In engineering terms, the first three stages, involving cyclic deformation and micro-crack initiation and growth, are generally embodied into the single classification of (macro-) crack initiation, implying the formation of an "engineering-size" detectable crack (e.g., of the order of several grain diameters in length). Thus, in such terms, the total fatigue life (N) can be defined as the number of cycles both to initiate a (macro-) crack (N_i) and to propagate it subcritically until final failure (N_p), i.e.,

$$N = N_i + N_p \quad . \tag{1}$$

From the perspective of fatigue design, where data from laboratory-sized specimens are utilized to predict the lifetime of more complex components in service (Fig. 1), this distinction between initiation and propagation lives can be critical. Conventional fatigue design approaches, on the one hand, classically involve the use of S-N curves, representing the *total life* resulting from a given stress, or strain, amplitude, suitably adjusted to take into account effects of mean stress (using, for example, Goodman diagrams), effective stress concentrations at notches (using fatigue-strength reduction factors or local strain analysis), variable-amplitude loading (using the Palmgren-Miner cumulative-damage law or rainflow counting methods), multiaxial stresses, environmental effects, and so forth (for summary, see ref. 1). Although based on total life, this approach, which is in widespread use particularly in the automotive industry, essentially represents design against *crack initiation*, since near the fatigue limit, especially in smooth specimens, the major portion of the lifetime is spent in the formation of an engineering-size crack. In life prediction procedures, such S-N or low cycle fatigue (LCF) testing might simulate the initiation and early growth of the fatigue crack within the fully plastic region of the strain field at some stress concentrator (Fig. 1) [2].

For safety-critical structures, especially with welded and riveted components, on the other hand, there has been a growing awareness that the presence of defects in a material below certain size must be assumed and taken into account at the design stage. Under such circumstances, the integrity of a structure will depend upon the lifetime spent in crack propagation, and since the crack initiation stage will be small,

the use of conventional S-N total life analyses may lead to dangerous *overestimates* of life. Such considerations have led to the adoption of so-called *defect-tolerant approach*, where the fatigue lifetime is assessed in terms of the time, or number of cycles, to *propagate* the largest undetected crack to failure [3]. Here the initial crack size is estimated using non-destructive evaluation or proof tests whereas the final crack size is defined in terms of the fracture toughness (K_{Ic}), limit load or some allowable strain criteria. This approach, which is used exclusively for certain applications in the nuclear and aerospace industries, for example, relies on integration of a crack growth expression, representing a fracture mechanics characterization of relevant fatigue-crack propagation data suitably modified to account for mean stress effects (e.g., using the Forman equation), variable-amplitude loading (e.g., using the Wheeler or Willenborg models), environmental effects, and so forth, as required (for summary, see ref. 4). Such crack growth expressions are generally based on the original Paris power law relationship, i.e., of the form:

$$\frac{da}{dN} = C\,\Delta K^{m} \quad , \tag{2}$$

where C and m are experimentally determined scaling constants, da/dN the crack growth increment per cycle and ΔK the alternating stress intensity factor given by the difference between the maximum and minimum stress intensities in the fatigue cycle ($\Delta K = K_{max} - K_{min}$) [5]. Eq. 2 in its simplest form provides a reasonable description of growth rate behavior in the so-called intermediate range of growth rates, typically between 10^{-6} and 10^{-3} mm/cycle. However, it *underestimates* propagation rates at higher ΔK levels as final instability is approached (e.g., when

$K_{max} \rightarrow K_{Ic}$), and *overestimates* propagation rates at lower ΔK levels approaching the so-called long crack fatigue threshold stress intensity range ΔK_o, below which *long* cracks remain dormant or grow at experimentally undetectable rates [6]. Since the crack initiation life is generally taken to be zero, such defect-tolerant life predictions are assumed to be inherently *conservative*, and, with reference to Fig. 1, to simulate the macroscopic growth of the fatigue crack. In its most widely used form, i.e., relying on linear elastic fracture mechanics (LEFM), the latter approach would imply crack growth outside the notch strain field where the size-scale of the crack tip plastic zone is small compared to the crack length, i.e., the propagation of a long crack under nominally elastic conditions [5,6].

Current practice in the determination of the relevant crack growth "law"* for a particular material under a particular set of conditions for a given application is to utilize the existing data-base of laboratory-determined fatigue-crack propagation results, characterized in terms of the linear elastic stress intensity range ΔK. However, the majority of these data have been determined from test-piece geometries containing crack sizes of the order of 25 mm or so, whereas many defects encountered in service are far smaller than this, particularly in turbine disc and blade applications, for example. In the relatively few instances where the fatigue behavior of such short cracks has been experimentally studied (for earlier reviews, see refs. 7-12), it has been found, almost without

*Although often termed "laws," such crack growth relationships are invariably totally empirical in nature and are derived simply by fitting mathematical equations, of the form of Eq. (2), to sets of experimental data.

exception, that, at the same nominal driving force, the growth rates of short cracks are greater than (or at least equal to) the corresponding growth rates of long cracks (see schematic illustration in Fig. 2). This implies a breakdown in the similitude concept generally assumed in fracture mechanics, as described in Section 2.3. Furthermore, it suggests that the use of existing long crack data for defect-tolerant lifetime calculations in components, where the growth of short flaws represents a large proportion of the life, has the potential for seriously non-conservative life predictions.

There are several factors which constitute a definition of a short* crack [12], namely i) cracks which are of a length comparable to the scale of microstructure (e.g., of the order of the grain size), ii) cracks which are of a length comparable to the scale of local plasticity (e.g., small cracks embedded in the plastic zone of a notch or of a length comparable with their own crack tip plastic zones, i.e., typically $\leq 10^{-2}$ mm in ultrahigh strength materials to $\leq$ 0.1-1 mm in low strength materials), and iii) cracks which are simply physically-small (e.g., $\leq$ 0.5-1 mm).** Most investigations to date have focussed on the first two factors which represent, respectively, a continuum mechanics limitation and an LEFM limitation to current analyses. Here, presumably with an appropriate micro- or macro-mechanics characterization of crack advance, a correspondence between long and short crack growth rate data should be achieved. However, physically-short flaws, which are "long" in terms of continuum and LEFM analyses, have also been shown to propagate at rates

---

*A distinction is sometimes made between small cracks, which are small in all dimensions, and short cracks, which are small in all but one (presumably the width) dimension, although such definitions are not considered in the present review.

**Such physically-small flaws are sometimes referred to as "chemically-small" where environmental effects are dominant [11].

faster than corresponding long cracks at the same nominal driving force [e.g., 11,12]. This may reflect basic differences in the physical micro-mechanisms associated with the extension of long and short flaws. Thus, physically-short cracks represent a limitation in the similitude concept of fracture mechanics.

In the present article, we review the existing experimental information and accompanying interpretations on the growth of short fatigue cracks in engineering materials. In the interests of brevity, we devote little space to a review of the literature on "conventional" crack initiation and "long" crack growth, topics which have been given ample coverage in refs. 4-7. We have, however, made a concerted effort to review *all* the currently available information on short cracks. Since this is a rapidly increasing field we may have inadvertantly missed certain references and we regret these omissions. Our intent is to discuss, both from engineering and mechanistic viewpoints, situations where short crack growth behavior may differ from that of long cracks, in terms of i) appropriate fracture mechanics characterization and ii) the physics and mechanisms involved in crack advance. In the former case, the short crack problem is treated principally in terms of elastic-plastic fracture mechanics (EPFM) analyses which incorporate the effects of local crack tip plasticity and the strain fields at notches, whereas in the latter case behavioral differences are examined in terms of the role of crack size and shape, microstructure, environment, crack closure and crack extension mechanisms. We begin, however, with a brief summary of the fracture mechanics procedures used to characterize fatigue-crack propagation for both long and short flaws.

2. FRACTURE MECHANICS CHARACTERIZATION OF FATIGUE-CRACK GROWTH

2.1 Linear Elastic Fracture Mechanics (LEFM)

The essential features of fracture mechanics used to correlate cyclic crack advance begin with characterizing the stress and deformation fields, local to the region at the crack tip. This is achieved principally through asymptotic continuum mechanics analyses where the functional form of the local singular field is determined within a scalar amplitude factor whose magnitude is calculated from a complete analysis of the applied loading and geometry. For the linear elastic behavior of a nominally stationary crack subjected to tensile (Mode I) opening, the *local* crack tip stresses (σ_{ij}) can be characterized in terms of the K_I singular field [13,14]:

$$\sigma_{ij}(r,\theta) = \frac{K_I}{\sqrt{2\pi r}} f_{ij}(\theta) + O(r^{\frac{1}{2}}) + \ldots$$

$$\rightarrow \frac{K_I}{\sqrt{2\pi r}} f_{ij}(\theta) \qquad \text{as } r \rightarrow 0 \ , \qquad (3)$$

where K_I is the Mode I stress intensity factor, r the distance ahead of the tip, θ the polar angle measured from the crack plane, and f_{ij} a dimensionless function of θ. Similar expressions exist for cracks subjected to pure shear (Mode II) and anti-plane strain (Mode III). Provided this asymptotic field can be considered to "dominate" the local crack tip vicinity over a region which is large compared to the scale of microstructural deformation and fracture events involved, the scalar amplitude factor K_I can be considered as a single, configuration-independent parameter which uniquely and autonomously characterizes the local stress field ahead of a linear elastic crack and can be used as a correlator of crack extension.

For cracks subjected to cyclically varying loads, K_I must be defined at the extremes of the cycle, such that a maximum and a minimum stress intensity, K_{max} and K_{min}, respectively, for a particular crack length a, can be computed. According to the original analysis of Paris and co-workers [15], the crack growth increment per cycle in fatigue (da/dN) can be described in terms of a power law function (Eq. 2) of the range of K_I, given by the stress intensity range ΔK. It is important to note here that such asymptotic continuum mechanics characterization does not necessitate detailed quantitative microscopic models to be known for the individual fracture events, and thus the analysis is independent of the specific micro-mechanism of crack advance.

One of the principal limitations of this approach, specifically the criterion that K_I is a valid description of the crack tip field, is that a state of small-scale yielding must exist. From Eq. 3, it is apparent that as r tends to zero, stresses become infinite at the tip. In reality, however, such stresses are limited by local crack tip yielding, which occurs over a region ahead of the crack tip known as the plastic zone size r_y. Calculations of the extent of this region vary depending upon the mode of applied loading and the geometry of the body [16], but a rough estimate for r_y for a monotonically-loaded crack can be taken as:

$$r_y \approx \frac{1}{2\pi}\left(\frac{K_I}{\sigma_0}\right)^2 \quad , \tag{4}$$

where σ_0 is the yield strength of the material. Provided this extent of local plasticity is small compared with the extent of the K_I-field, which itself is small compared to the overall dimensions of the body (including the crack length), the plastic zone can be considered as merely a small

perturbation in the linear elastic field and K_I crack tip dominance can be preserved. In general, this situation, known as *small-scale yielding*, exists where the plastic zone size from Eq. 4 is at most one fifteenth of the in-plane dimensions of crack length (a) and remaining ligament depth (b).

The local yielding ahead of fatigue cracks is somewhat more complex due to the presence of reversed plasticity. However, following the analysis of Rice [17] for a cyclically-stressed elastic-perfectly plastic solid, plastic superposition of loading and unloading stress distributions can be used to compute the extent of plastic zones ahead of a fatigue crack. On loading to K_{max}, a monotonic or maximum plastic zone is formed at the crack tip of dimension (from Eq. 4):

$$r_{max} \approx \frac{1}{2\pi}\left(\frac{K_{max}}{\sigma_0}\right)^2 \quad . \tag{5}$$

However, on unloading from K_{max} to K_{min}, superposing an elastic unloading distribution of maximum extent $-2\sigma_0$ results in a region ahead of the crack tip where residual compressive stresses, of magnitude $-\sigma_0$, will exist. This region is known as the cyclic plastic zone size r_Δ and is approximately one fourth of the size of the monotonic zone, i.e.:

$$r_\Delta \approx \frac{1}{2\pi}\left(\frac{\Delta K}{2\sigma_0}\right)^2 \quad , \tag{6}$$

where, strictly speaking, σ_0 is now the cyclic yield strength. Once again, the correlation of K_I to crack extension by fatigue will be a valid approach provided small-scale yielding conditions apply, namely r_{max} small compared to the in-plane dimensions.

The numerical values of the stress intensity factors at the crack tip, i.e., K_I, ΔK, etc., remain undetermined from the asymptotic analyses, yet can be computed fro the overall geometry and applied loading conditions. In fact, solutions for K_I applicable to a wide variety of situations are now tabulated in handbooks [18-20]. A useful example of such K_I solutions, which is particularly relevant to the short crack problem, is that of a crack (length ℓ) growing from a notch (length 2c) (Fig. 3) [21]. Assuming a circular hole in an infinite plate under a remotely applied tensile stress σ^∞, the limiting analytical K_I solution for a short crack emanating from the notch is given as:

$$K_s = 1.12\, k_t \sigma^\infty \sqrt{\pi \ell} \quad , \tag{7}$$

where k_t is the theoretical elastic stress concentration factor (equal to 3 in this case) and 1.12 is the free surface correction factor. However, when the crack becomes long, the limiting stress intensity is obtained by idealizing the geometry so that the notch becomes part of a long crack of dimension $a = c + \ell$, such that:

$$K_\ell = Q\sigma^\infty \sqrt{\pi \ell} \quad , \tag{8}$$

where Q is a dimensionless function of geometry, such as a finite width correction factor. The numerically-determined K_I solution for any crack emanating from a notch, shown by the dashed line in Fig. 3, can be seen to be given by these short and long crack limiting cases. As shown by Dowling [21], the transition crack size ℓ_o, which can be interpreted as the extent of the local notch field, can then be obtained by combining Eqs. 7 and 8 as:

$$\ell_o = \frac{c}{(1.12\ k_t/Q)^2 + 1} \quad . \tag{9}$$

Values of ℓ_o are generally a small fraction of the notch root radius ρ, and for moderate to sharp notches generally fall in the range $\rho/20$ to $\rho/4$. Dowling [21] has further noted that $k_t\sigma^\infty$ values only 20-30% above σ_0 are sufficient to generate a notch tip plastic zone which engulfs the small crack region ℓ_o and thus, for small cracks at notches, LEFM analysis will often be suspect.

2.2 Elastic-Plastic Fracture Mechanics (EPFM)

The above example serves to illustrate one aspect of the short crack problem where the crack length is comparable with the notch tip plastic zone size. A similar situation, where small-scale yielding conditions may not apply, is when the plastic zone at the tip of the fatigue crack itself is comparable with the crack length, i.e., when $a \sim r_y$. Since the use of K_I singular fields is no longer appropriate in such instances, alternative asymptotic analyses have been developed to define the crack tip stress and strain fields in the presence of more extensive local plasticity (for recent review, see ref. 22). Based on the deformation theory of plasticity (i.e., non-linear elasticity), the asymptotic form of these local fields, for non-linear elastic power-hardening solids of constitutive law $\sigma \propto \varepsilon_p^n$, is given by the Hutchinson, Rice and Rosengren (HRR) singularity as [23,24]:

$$\sigma_{ij}(r,\theta) \rightarrow \left(\frac{E'\ J}{\sigma_0^{\,2}\ r}\right)^{n/n+1} \sigma_0\ f'_{ij}(\theta,n) \quad ,$$

and

$$\varepsilon_{ij}(r,\theta) \rightarrow \left(\frac{E' J}{\sigma_0^2 r}\right)^{1/n+1} f''_{ij}(\theta,n) \quad , \quad \text{as } r \rightarrow 0 \ , \quad (10)$$

where n is the work hardening exponent, E' the appropriate elastic modulus (= E for plane stress or $E/(1 - \nu^2)$ for plane strain) and f'_{ij}, f''_{ij} are universal functions of their arguments depending upon whether plane stress or plane strain is assumed. The amplitude of this field is the so-called J-integral [25], and analogous to K_I, J uniquely and autonomously characterizes the crack tip field under elastic-plastic conditions *provided some degree of strain hardening exists*. Further, for small-scale yielding, J can be directly related to the strain energy release rate G, and hence K_I, i.e.,

$$J = G = K_I^2/E' \qquad \text{(linear elastic)} \quad . \qquad (11)$$

Despite difficulties in the precise meaning of J as applied to a description of crack growth of cyclically-stressed (non-stationary) cracks, Dowling and co-workers [26,27] proposed a power-law correlation of fatigue crack growth rates under elastic-plastic conditions to the range of J, i.e.,

$$\frac{da}{dN} \propto \Delta J^{m'} \quad . \qquad (12)$$

Provided such analysis is fundamentally justified, the use of ΔJ does present a first approach to characterize the growth of short cracks which are comparable in size to the extent of local yielding. However, as alluded to above, the validity of the ΔJ approach is often questioned since it appears to contradict a basic assumption in the definition of J that stress is proportional to the *current* plastic strain [25]. This

follows because J is defined from the deformation theory of plasticity which does not allow for the elastic unloading and non-proportional loading effects which accompany crack advance [28]. By recognizing, however, that constitutive laws for *cyclic* plasticity (i.e., the cyclic stress-strain curve) can be considered in terms of *stable* hysteresis loops, and that such loops can be mathematically shifted to a common origin after each reversal, the criterion of stress proportional to current plastic strain can be effectively satisfied for cyclic loading [29,22].

An alternative treatment of elastic-plastic fatigue-crack growth, which is not subject to such restrictions required by non-linear elasticity, is to utilize the concept of crack tip opening displacement (CTOD). From Eq. 10, it is apparent that the opening of the crack faces at $r \to 0$ varies as $r^{n/n+1}$, such that this separation can be used to define the CTOD (δ_t) as the opening where 45° lines emanating back from the crack tip intercept the crack faces, i.e., for proportional loading:

$$\delta_t = d(\varepsilon_o, n) \frac{J}{\sigma_0^2} \qquad \text{(elastic-plastic)} \ ,$$

$$\propto \frac{K_I^2}{\sigma_0 E'} \qquad \text{(linear elastic)} \ , \qquad (13)$$

where d is a proportionality factor ($\sim$ 0.3 to 1) dependent upon the yield strain ε_o, the work hardening exponent n, and whether plane stress or plane strain is assumed [30]. Since δ_t, like J, can be taken as a measure of the intensity of the elastic-plastic crack tip fields, it is feasible to correlate rates of fatigue crack growth to the range of δ_t, i.e., the cyclic crack tip opening displacement (ΔCTOD), as

$$\frac{da}{dN} \propto \Delta CTOD \qquad \text{(elastic-plastic)} \ ,$$

$$\propto \frac{\Delta K_I^2}{2\sigma_0 E'} \qquad \text{(linear elastic)} \ . \qquad (14)$$

Approaches based on J and δ_t are basically equivalent for proportional loading, and are of course valid under both elastic-plastic and linear elastic conditions. Therefore, they are generally applicable to a continuum description of the growth rate behavior of cracks considered small because their size is comparable with the scale of local plasticity. For such short cracks, the use of elastic-plastic, rather than linear elastic, fracture mechanics may thus be expected, at least in part, to normalize differences in behavior between long and short flaws. However, the short crack problem is not *simply* a breakdown in the application of linear elastic fracture mechanics since the use of elastic-plastic analyses cannot totally normalize differences between short and long cracks. Although elastic-plastic analysis is certainly important, differences in behavior of long and short flaws can also be attributed to microstructural, environmental and closure effects. Thus the short crack problem relates to a breakdown, not simply in LEFM, but in the fracture mechanics similitude concept.

2.3 The Similitude Concept

The application of fracture mechanics to the propagation of fatigue cracks is based on the premise that the governing parameter, such as the stress intensity factor K_I or the J-integral, used for the correlation of growth rates, fully describes the stress and deformation fields in the vicinity of the crack tip. In addition, it is implicitly assumed that

the concept of *similitude* is valid. The latter concept implies that, for two different sized cracks (Fig. 4) subjected to equal stress intensity values (under small-scale yielding) in a given material/microstructure/environment system, crack tip plastic zones will be equal in size and the stress and strain distributions along the borders of these zones (ahead of the crack) will be identical. Accordingly, equal amounts of crack extension (Δa) will be expected. For a cyclic load denoted by K_{max} and K_{min}, this dictates that:

$$\Delta a = \frac{da}{dN} = f(K_{max},K_{min}) = f(\Delta K,R) \quad , \tag{15}$$

for each cycle N, where the stress intensity range $\Delta K = K_{max} - K_{min}$ and the load ratio $R = K_{min}/K_{max}$. However, this concept of similitude becomes violated i) when crack sizes approach local microstructural dimensions, ii) when crack sizes are comparable with the extent of local plasticity for non-stationary flaws, iii) when through-thickness out-of-plane stresses (which are independent of K_I) are different, iv) when crack extension mechanisms are different, v) when extensive fatigue-crack closure is observed, and vi) when external environments significantly influence crack growth, to name but a few [10,12,31,32]. The majority of these mechanisms are specific to the short crack problem and thus contribute to differences between the growth rate behavior of long and short cracks at nominally identical driving forces. They are discussed below in terms of local plasticity, microstructural and environmental factors. In general, however, their effect on the breakdown of the similitude concept for short cracks is that they influence (to varying degrees dependent upon crack length, for example) the local

driving force (i.e., the characterizing parameter K_I or J effectively experienced in the near-tip region). It is this "near-tip" parameter that governs crack advance, and not the "nominal" value of this parameter computed globally by conventional analyses of externally applied loads and macroscopic crack length measurements. In only a few instances have the relationships between the near-tip and nominal driving forces been quantified, indicating that the methodology for a global fracture mechanics analysis of short crack growth has yet to be developed.

3. EXPERIMENTAL TECHNIQUES

Experimental measurement of the crack propagation and threshold behavior of small fatigue flaws can be subject to many complex problems associated with reproducibility and scatter. This is particularly true since the approach to date has been largely to adapt procedures originally designed for long crack measurements.

Several experimental techniques are currently available for monitoring the growth rates of such long fatigue cracks [e.g., refs. 33-34]. These include i) optical techniques (i.e., with the naked eye, travelling microscopes or using high speed cameras), ii) electrical resistance or potential methods using either d.c. or a.c. currents, iii) compliance techniques using mouth opening (clip) or back-face strain gauges, iv) acoustic emission, v) ultrasonics and vi) eddy current methods, with the first three being the most widely used in practice. For long cracks, growth rates above typically 10^{-6} mm/cycle are obtained generally with such techniques at constant cyclic load levels (i.e., increasing ΔK with increasing crack length) [34]. At near-threshold levels, on the other hand, crack growth rates ($da/dN \leq 10^{-6}$ mm/cycle) and threshold ΔK_o values for long cracks are normally measured using the so-called load-shedding (decreasing ΔK) method [e.g., ref. 6]. This procedure involves continual reductions in ΔK (starting from an intermediate ΔK value) of not more than 10% and, at each ΔK level, the growth of the crack over an increment of crack length of at least four times the maximum plastic zone size generated at the previous higher ΔK level. This load reduction scheme is repeated until the threshold ΔK_o for no detectable (long) crack advance is reached. Such procedures [6], typically used to monitor the

growth and arrest of long fatigue cracks, pose extreme difficulties when adopted for short crack measurements. Firstly, one faces the problem of estimating the depth of a short crack, emanating from a surface, from its width. This requires an empirical calibration and/or an educated guess. Also, with load-shedding procedures to approach the threshold, the crack is continually growing such that it may cease to be "short" by the time the threshold is reached. Moreover, the initiation stage of a "major" short crack may involve the link-up of several flaws (e.g., from cracked inclusions) at different locations on the sample. While low magnification optical techniques are not easily amenable to detect the presence, and to monitor the growth, of short cracks while the fatigue test is in progress, other crack length measuring methods such as the potential or compliance techniques may not have the required resolution and reproducibility to characterize the growth of (part-through) short flaws of complex geometry. In addition to the difficulties associated with the limitations of the crack monitoring device, the growth of a short crack can be a strong function of *local* microstructural characteristics and environment, for example [7-12]. This aspect of short crack advance can lead to poor reproducibility between duplicate tests.

Since, in general, load-shedding procedures are difficult to utilize, there is always the question as to whether short crack behavior should be studied from an artificial or naturally-occurring crack. Obtaining artificial notches where the material immediately ahead of the notch is undamaged is particularly difficult, yet of vital importance since this is where the short crack growth must be studied. Machined notches have the problem of residual stresses, whereas notches or starter cracks

introduced using electro-discharge machining will have a locally melted zone at the tip. Subsequent annealing cannot be guaranteed to remove such damage without drastically changing the microstructure under test. As reviewed below, certain procedures have been utilized whereby long cracks are grown and then material in the wake machined off to leave a short flaw. Reproducibility is a major problem here, as is crack shape, since any amount of non-uniformity or "bowing" in the original long crack will introduce irregular short cracks. However, one very successful method for rapidly initiating short cracks without significant damage, specific to aluminum alloys, has been to embrittle the sample surface, prior to fatigue, using small ink drops at well separated locations [36]. Although the precise mechanism involving some environmentally-influenced fatigue process in this case is unknown, short cracks have been found to initiate extremely rapidly using this method.

3.1 Initiation and Growth Measurements of Short Cracks

Optical Techniques

Crack monitoring techniques using visual methods have probably been the most widely used procedures to date. For example, following procedures originally utilized by Barsom and McNicol [37] for crack initiation studies, Fine and co-workers [38-39] have used a long working distance metallurgical microscope for visual and photographic observations of crack initiation and micro-crack growth in wide single edge-notched samples of steels and aluminum alloys. The microscope was mounted on an x-y micrometer base for positioning and measuring crack length. A camera attachment was available for photographic recording of the progressive changes in the surface of the specimens from cyclic loading.

Morris and co-workers [40-49] used tapered flexural and hourglass-shaped fatigue samples to monitor micro-cracks in aluminum and titanium alloys. Cracks were initiated on the specimen surface using various techniques including starter notches and marking with felt-tip pens. Crack propagation rates were estimated by monitoring crack size at regular intervals during the test by transferring the specimen to a scanning electron microscope (SEM). The specimens were loaded in the SEM to estimate the micro-crack-tip opening displacement at the maximum load. For example, an empirical calibration equation was obtained, for 2219-T851 aluminum alloy, from several measurements on surface micro-cracks to estimate their depth a, from a knowledge of their width 2c. The following expression was obtained [47]:

$$a/2c = 0.362 + 25.01[\delta(\sigma_{max})/2c - 0.015] \quad , \qquad (16)$$

where $\delta(\sigma_{max})$ is the crack tip opening displacement at the maximum stress, σ_{max}.

Optical techniques have also been used to study short flaws at elevated temperatures. For example, Sheldon et al. [50] designed a long working distance microscope to monitor *in situ* the growth of short and long cracks in nickel-base superalloys at temperatures as high as 650°C. Cracks were initiated at high stress intensities at ambient temperature, whereupon the load was successively reduced until the approximate room temperature long crack threshold values were reached. Once load shedding was complete, the specimen was machined and polished into a configuration such that only 0.06-0.16 mm long crack was left in the test panel. The cross section of the specimen was a

parallelogram containing the crack at one acute corner. It was claimed [50] that the taper allows a better definition of the crack front location, and that the crack in the taper interacted with only a small amount of material along its front. This was considered representative of a naturally occurring small crack.

Replication Techniques

One of the most widely used techniques for monitoring the initiation and growth of small flaws has been the replication method. For example, Dowling [51,52] used cellulose acetate surface replicas for short crack growth measurements during low cycle fatigue tests on smooth axial specimens in A533B steel. Tests were interrupted periodically for replicating with $\sim$ 0.1 mm tape, softened with acetone to gain an impression of the specimen surface. Propagation rates (da/dN) of such surface flaws (of length 0.25 to 1.75 mm) were characterized in terms of elastic-plastic fracture mechanics, specifically involving ΔJ. Procedures for calculating J values from the loading portion of the fatigue cycle are summarized in Fig. 5 and involve the following approximations [51]: i) surface flaws were assumed to have depths, a, one half of their surface lengths, 2c, ii) ranges of stress and plastic strain, obtained from stable cyclic hysteresis loops, were used to quantify ΔJ, iii) the value of ΔJ for such semi-circular surface crack geometries was given by:

$$\Delta J \simeq 3.2\ \Delta W_e a + 5.0\ \Delta W_p a \quad , \tag{17}$$

where ΔW_e and ΔW_p are the elastic and plastic components of the remote strain energy density range values (Fig. 5), and iv) the scaling constants in Eq. 17, which incorporate specimen geometry and flaw shape correction factors, were derived from equivalent *linear elastic* solutions.

In the general sense, there are problems with using either optical or replication techniques in that they are difficult to utilize in hostile environments such as in corrosive solutions or at elevated temperatures. More importantly, they give information only on the surface length of the flaw and therefore assumptions must be made to estimate internal crack profiles.

Electrical Potential Techniques

Electrical potential techniques have also been developed for short crack studies. For example, Gangloff used the technique to quantify the formation and sub-critical propagation of small cracks emanating from artificial surface defects [11,53,54]. Flaws were introduced along a chord of an hourglass type (low cycle fatigue) specimen (at the minimum diameter) by either conventional grinding or electrospark discharge machining. Continuous crack depth information, obtained from d.c. electrical potential measurements through an analytical calibration model [53], was found to agree reasonably well with the corresponding values measured optically. The calibration model used was claimed to account for crack shape as well as depth variations for the elliptical surface flaws utilized in the experiments. This technique is particularly suitable for physically-short cracks, i.e., of a size 0.5 to 1 mm, and thus has been effective in gaining information of short fatigue-crack growth in higher strength materials. Furthermore, since it is a remote monitoring technique, it can be utilized even in aggressive environments.

Other Techniques

Several other techniques have been proposed for detection and monitoring of small flaws, and although many are still in the development

stage they show excellent promise for measurements in the micron to millimeter range. For example, Nelson and co-workers [55] have utilized a method of surface acoustic wave monitoring to quantify the depth and crack closure characteristics of microscopic surface fatigue cracks. Using acoustic measurements of the reflection coefficient of Rayleigh waves incident on the crack, coupled with optical measurements of surface crack length, these authors were able to claim good accuracy over a range of crack aspects ratios for depths between 50 and 150 μm [55]. Several electrochemical methods have also been proposed for early detection of microscopic fatigue damage, notably by Baxter [56]. Accuracies of 10 μm have been reported for detection of small fatigue cracks in both steels and aluminum alloys through identification of locations where such cracks rupture the surface oxide film. Such rupture sites are imaged using photoelectron microscopy and more recently through measurement of the reanodization current or with the aid of an iodine-containing gel [56].

3.2 Measurements of Short Crack Thresholds

The load-shedding procedure commonly used to obtain the threshold for no detectable propagation, ΔK_o, for long cracks is not readily applicable in the case of short cracks (of a size scale smaller than the local plastic zone or the characteristic microstructural dimension) because of the need to reduce the load to threshold levels over a considerable distance of crack growth. However, the procedure can be used for physically-short cracks (i.e., of sizes 0.1 to 0.8 mm) in ultrahigh strength materials where both the scale of local plasticity and grain size is smaller than the crack depth and load-shedding procedures can be

sufficiently rapid to enable the near-threshold region to be approached over small increments of crack advance [e.g., 57].

Wiltshire and Knott [58] utilized two types of short crack preparation techniques to obtain "through-thickness" and "thumb-nail" cracks in a study to investigate the effect of crack length on the fracture toughness values. Such procedures seem appealing to evaluate the growth and thresholds for short flaws. For the case of through-thickness cracks in maraging steels, a long crack was first produced by fatiguing single-edge-notch bend specimens, as shown in Fig. 6a, with the sample in the solution annealed condition. Short through-thickness cracks were then obtained by grinding away the upper surface, and the samples subsequently aged to develop full strength. Similar procedures were used to produce short "thumb-nail" shaped cracks, as outlined in Fig. 6b. The two top corners of a bend specimen were machined away to leave a ridge in the center. A slot was introduced in the ridge and the specimen fatigue pre-cracked in bending. The fatigue crack was found to propagate down the ridge as a straight fronted crack and then into the bulk of the specimen in a semi-elliptical shape, which was controlled by observing its length on the pre-polished shoulders. Finally, the ridge was removed to leave a semi-elliptical surface crack in the remaining rectangular section, as shown in Fig. 6b.

Such procedures have been used to produce through-thickness and part-through thickness short cracks to measure the thresholds for short crack arrest [59-62]. Usami and Shida [59], for example, utilized this technique to measure fatigue thresholds in a range of steels for crack sizes between 0.1 and 0.3 mm. McCarver and Ritchie [60] used similar

procedures to monitor the thresholds for physically-short flaws in a wrought nickel-base superalloy, René 95. In the latter two cases, fatigue pre-cracking was performed under cyclic compressive loads on bend specimens. This technique results in growth and arrest of the pre-crack to a predictable depth which is a function of the plastic zone size computed from the compressive loads. Such compression gives rise to residual tensile stresses which apparently act as the driving force for crack growth.* Following pre-cracking and machining away of the majority of the crack, the samples were annealed in an attempt to minimize possible damage in the vicinity of the short crack tip. McCarver and Ritchie [60] subsequently measured short crack thresholds with such specimens using a procedure analogous to defining a fatigue limit in unnotched specimens. Samples were cycled at different initial stress intensity ranges (ΔK_i) and the short crack threshold defined in terms of the largest value of ΔK_i which did not cause failure (or any evidence of crack growth) in 10^8 cycles (Fig. 7).

*Recent studies of crack initiation under compression by Suresh [63] in a wide range of alloys have revealed that cracks arrest at a length approximately equal to the cyclic plastic zone size in compression. However, at high cyclic compressive loads, it is found that crack arrest can occur at critical lengths independent of applied loads, apparently due to the development of closure behind the crack tip [63].

3.3 Measurements of the Closure of Short Cracks

The techniques presently available to monitor routinely the premature closure of long fatigue cracks are generally not amenable to the problem of short cracks whose growth involves considerable geometrical changes, irreproducibility and scatter, and demands far superior resolution in measurements. Measurement of closure in long fatigue cracks has been achieved using visual techniques, compliance techniques, electrical resistance or potential methods, acoustic emission and ultrasonics [e.g., refs. 33, 34]. Most of these techniques do not seem appealing for the case of short cracks because of their insufficient resolution, insensitivity to short crack shape and geometry as well as irreproducibility.

Early studies of crack closure for short cracks were carried out by Morris and Buck [41], who examined a compliance technique to determine the closure load for surface micro-cracks, of up to one grain size, produced in triangular shaped specimens of aluminum alloys subjected to fully reversed loading. Scanning electron microscopy was then used to measure the compliance of surface micro-cracks. A "home-made" fixture incorporated in the electron microscope was utilized to apply known loads to the samples *in situ*. A high resolution micrograph of the crack was obtained at different load (stress) levels, from which the crack opening δ was inferred. Fig. 8 shows a typical compliance curve for a micro-crack obtained for the 2219-T851 aluminum alloy. Morris and Buck [41] defined the following parameters to characterize crack closure: $\delta(o)$, the crack opening displacement at zero load, σ_{cl}/σ_{max}, the closure stress ratio taken to be the value of σ/σ_{max} at the inflection point in the stress-displacement curve, and $S = \Delta\delta/\Delta(\sigma/\sigma_{max})$ measured for $\sigma > \sigma_{cl}$, where S is

a measure of the compliance of the micro-crack in the completely opened state.

Compliance techniques were also used by Tanaka and Nakai [61,64] for measuring crack closure levels in their study to examine the growth of short cracks emanating from notched center-cracked specimens of a structural low-carbon steel. Here, the hysteresis loop of load versus crack opening displacement at the center of the crack was recorded intermittently during the test, and the point of crack opening was determined as the inflection point of compliance, magnified by a circuit subtracting the elastic compliance from the loading curve.

Recently, procedures have been developed to monitor the fatigue crack growth behavior of short cracks, using stereo-imaging techniques and *in situ* analyses in the scanning electron microscope [65,66]. Such methods enable direct observations of the crack opening (Mode I) and sliding (Mode II) displacements as a function of load for both short and long cracks subjected to cyclic loads within the electron microscope.

4. RESULTS ON SHORT FATIGUE-CRACK GROWTH

4.1 Microstructural Effects

The first definition of a short fatigue crack involves flaws which are of a size comparable to the scale of characteristic microstructural features. Fig. 9 shows a micrograph of such a typical surface microcrack initiated at a β phase (Cu_2FeAl_7) intermetallic in 2219-T851 aluminum alloy taken from the work of Morris and co-workers [45]. Several recent experimental studies [7-12,37-49,67-76] on the initiation and growth of cracks in a wide range of materials have revealed that such short cracks, initiated near regions of surface roughening caused by the to and fro motion of dislocations or at inclusions and grain boundaries, propagate at rates which are different from those of equivalent long cracks, when characterized in terms of conventional fracture mechanics concepts. For example, it was first shown by Pearson [68] in precipitation hardened aluminum alloys that cracks, of a size comparable to the average grain diameter, grew several times faster than long cracks at nominally identical alternating stress intensity values (Fig. 10). Other studies in mild steels [69] (Fig. 11), silicon iron [70] (Fig. 12) and peak aged 7075 aluminum alloy [71] (Fig. 13), for example, clearly reveal this lack of correspondence between long and microscopically-short crack data. The results of Lankford [71,72], among others [39,49, 69-74], however, have shown that there is generally a consistent trend to this variation between long and short crack growth rates. This trend is depicted clearly in Fig. 14 for 7075-T6 aluminum alloy where long and microscopically-short (i.e., of a size comparable with grain diameter) crack growth rates are plotted as a function of the linear elastic stress

intensity range [71]. It is apparent from this figure that the growth rates associated with the short cracks are up to two orders of magnitude faster than those of the long cracks, and further that such accelerated short crack advance occurs at stress intensity ranges well below the long crack fatigue threshold stress intensity range (ΔK_o) [71]. The initially higher growth rates of the short cracks can be seen to decelerate progressively (and even arrest in certain cases) before merging with the long crack data at stress intensities close to ΔK_o, similar to observations reported elsewhere by Morris and co-workers [42-46], Kung et al. [39], Tanaka et al. [70,75,76], Taylor and Knott [73] and others. The progressively *decreasing* growth rates of the short cracks, *below* the long crack threshold, is intriguing since in terms of conventional analyses one would imagine the nominal driving force for crack advance, such as ΔK, to increase with increasing crack length (e.g., in Eqs. 7 and 8) thereby leading to progressively *increasing* growth rates. However, microscopically-short crack behavior has been rationalized in terms of a deceleration of short crack growth through crack closure effects, in general, and through interactions with microstructural features, particularly grain boundaries [12,42-47,69-76]. For example, specific observations of grain boundaries acting as an impedence to short crack growth have been reported for aluminum alloys [42-46,71,72], nickel-base superalloys [50], tempered martensitic high strength steels [78] and lower strength mild steels [75,76]. Using arguments based on microplasticity and crack closure effects, Morris and co-workers [44-49] have modelled the process in terms of two factors, namely a cessation of propagation into a neighboring grain until a sizeable plastic zone is

developed, and a retardation in growth rates due to an elevated crack closure stress. Tanaka et al. [76,79,80] similarly considered the impeded growth of microstructurally-short cracks in terms of the pinning of slip bands, emanating from the crack tip, by the next grain boundary. The results of Lankford [71] in Fig. 14 indicate that the crack growth rate minimum appears to correspond to a crack length roughly equal to the smallest grain dimension (i.e., $a \sim d_g$). Further, the extent, or depth, of the deceleration "well," shown in this figure, appeared to be determined by the degree of micro-plasticity involved in the crack traversing the boundary. For example, when the orientation between the grain containing the crack and the neighboring grain was similar, little deceleration in growth rates at the boundary was seen to occur. Thus a consensus from these studies is that despite their accelerated propagation rates compared to long crack data, short cracks are apparently impeded by the presence of grain boundaries, which in general would be unlikely to affect significantly the local propagation rates of long cracks. Analyses to predict the extent of reductions in the *effective* driving force for various degrees of such short crack deflections at grain boundaries have recently been reported by Suresh [81]. It is the authors' opinion that the interaction of short flaws with microstructural features, which leads to the apparent progressive deceleration of short cracks below ΔK_o for long cracks, results principally from crack deflection [81] and associated crack closure [12,61] mechanisms. The specific evidence for this will be discussed in Section 5.

From such experimental studies, it is readily apparent that threshold stresses, or stress intensities, associated with long and short cracks are likely to be very different. Conventional fracture mechanics

arguments imply that the threshold stress intensity range (ΔK_{TH}) for a particular material should be independent of crack length (i.e., ΔK_{TH} = ΔK_o (the long crack threshold) = constant). Kitagawa and Takahashi [82], however, first showed that below a critical crack size, the threshold ΔK_{TH} for short cracks actually decreased with decreasing crack length, where the threshold *stress* $\Delta\sigma_{TH}$ approached that of the smooth bar fatigue limit $\Delta\sigma_e$ at very short crack lengths (e.g., Fig. 15). Typical experimental data showing this decay in the threshold stress intensity range ΔK_{TH} at short crack lengths, are shown in Fig. 16, taken from the results of Romaniv et al. [69] on annealed mild steel, 0.45% C austenitic steel and an Al-Zn-Mg alloy. Several workers have claimed that the critical crack size (below which ΔK_{TH} is no longer constant with crack size) is dependent upon microstructural and mechanical factors [8-10,12, 47,64,69-76,80-83]. It has even been suggested, for example, that this critical crack length above which LEFM is applicable is simply ten times the characteristic microstructural dimension [83]! However, from continuum arguments, an estimate of this crack size can be obtained in terms of $1/\pi(\Delta K_o/\Delta\sigma_e)^2$, where both ΔK_o and $\Delta\sigma_e$ are corrected for a common load ratio. Values of this dimension, which effectively represent the limiting crack size for valid LEFM analysis (see Section 2), typically range from 1-10 μm in ultrahigh strength materials (i.e., $\sigma_o \sim 2000$ MPa) to 0.1-1 mm in low strength materials (i.e., $\sigma_o \sim 200$ MPa) [12].

Based on such experimental results, it is generally concluded that the threshold condition for no growth for long cracks is one of a constant *stress intensity*, i.e., ΔK_o, whereas the threshold condition for short cracks is one of a constant *stress*, i.e., the fatigue limit $\Delta\sigma_e$ or

endurance strength. Such a premise has been shown consistent with the modelling studies of Tanaka et al. [76] where the threshold for short crack propagation is governed by whether the crack tip slip bands are blocked, or can traverse the grain boundary to an adjacent grain. This threshold condition of whether the slip band is blocked or not, which is denoted in Fig. 17 in terms of a critical value of the microscopic stress intensity K_c^m at the tip of the band, yields expressions for the fatigue threshold stress σ_{TH} and stress intensity K_{TH} of:

$$\sigma_{TH} = \frac{K_c^m}{\sqrt{\pi b}} + (2/\pi)\,\sigma_{fr}^* \cos^{-1}(a/b) \quad , \tag{18a}$$

$$K_{TH} = \sigma_{TH}\sqrt{\pi a} = K_c^m\sqrt{a/b} + 2\sqrt{a/\pi}\,\sigma_{fr}^* \cos^{-1}(a/b) \quad . \tag{18b}$$

Here, for the slip band coplanar to the crack plane in the two dimensional representation of Fig. 17, b is the crack length a plus the blocked slip band zone w_o and σ_{fr}^* is the frictional stress for dislocation motion in the band. The long crack threshold stress intensity K_o thus follows from Eq. (18b) by taking the limit of K_{TH} when $w_o \ll a$, i.e.,

$$K_o = K_c^m + 2\sqrt{2/\pi}\,\sigma_{fr}^*\sqrt{w_o} \quad , \tag{19}$$

whereas the short crack threshold stress, i.e., the fatigue limit σ_e, follows from Eq. (18a) at a = 0, i.e.,

$$\sigma_e = \sigma_{fr}^* + K_c^m/\sqrt{\pi w_o} \quad . \tag{20}$$

Since at the fatigue limit, the slip band can be considered to be constrained within a single grain, w_o can be assumed to be approximately half the grain size d_g. The interesting aspect of the blocked slip band

model is the prediction (Eqs. 19 and 20) that the long crack threshold K_o is increased with increasing grain size whereas the short crack threshold, or fatigue limit σ_e, is decreased [76]. Such predictions are borne out by experiment and highlight the fact that metallurgical factors which may improve resistance to the growth of long cracks (i.e., raise ΔK_o) may simultaneously lower resistance to the initiation and growth of small cracks (i.e., lower $\Delta\sigma_e$) [77]. This effect is particularly pronounced in ferrous alloys, as shown in Fig. 18 where increasing the tempering temperature to decrease strength level in an ultrahigh strength silicon-modified 4340 steel (300-M) *lowers* the long crack threshold ΔK_o yet *raises* the fatigue limit $\Delta\sigma_e$ [6]. A second example shown in Fig. 19 is from the work of Usami and Shida [59] where they compare threshold behavior, as a function of surface roughness (to simulate crack size), of cast iron (σ_o = 113 MPa) with maraging steel (σ_o = 1906 MPa). It is quite clear from this work [59] that the substantially higher strength maraging steel, whilst having a far superior fatigue resistance at short crack sizes (below 0.1 to 1 mm), is actually inferior to cast iron from the viewpoint of long crack threshold behavior.

4.2 Local Plasticity Effects

The second definition of a short crack involves flaws which are of a size comparable to the scale of local plasticity such as the crack tip plastic zone generated by the flaw itself (near-tip plasticity), or the strain field of a notch or a larger stress concentration which may encompass the flaw in the vicinity of the notch (notch-field plasticity). We now examine, in turn, these two categories of local plasticity effects.

Near-Tip Plasticity Effects

Whilst elastic-plastic fracture mechanics analyses seem more appealing for the characterization of short flaws comparable in size to the extent of *self-induced* near-tip plasticity, a comparison of their behavior with equivalent long cracks using LEFM analyses (i.e., at the same nominal ΔK) shows that the short cracks grow much faster [8-10,12, 47,84]. Part of the reason for such apparently anamolous results lies not in any physical difference between long and short crack behavior but more with the inappropriate use of linear elastic analyses. This was shown particularly clearly by Dowling [51] who monitored the growth of small surface cracks in smooth bar specimens of A533B nuclear pressure vessel steel subjected to fully-reversed strain cycling. By analyzing the growth rates (da/dN) in terms of ΔJ, where J values were computed from the stress-strain hysteresis loops (described in Eq. 17 and Fig. 5), a closer correspondence was found between long and short crack behavior (Fig. 20). Analogous approaches to the short crack problem have been suggested in terms of the pseudo-elastic-plastic strain intensity range (ΔK_ε) [85-87] or equivalent stress intensity range (ΔK_{eq}) [87], given in terms of a crack length a, elastic modulus E, and representative strain range $\Delta\varepsilon$ as:

$$\Delta K_\varepsilon = \Delta\varepsilon\sqrt{\pi a} = (q\Delta\varepsilon_e + \Delta\varepsilon_p)\sqrt{\pi a} \quad , \tag{21}$$

$$\Delta K_{eq} = Q\, E\Delta\varepsilon\sqrt{\pi a} \quad , \tag{22}$$

where $\Delta\varepsilon$ is expressed as the sum of the plastic strain range ($\Delta\varepsilon_p$) plus some fraction of the elastic strain ($q\Delta\varepsilon_e$), where $0.5 < q < 1$, and Q is the compliance function based on equivalent *linear elastic* K_I solution

for the particular loading geometry in question. Recently, Starkey and Skelton [88] have shown that the ΔJ and ΔK_{eq} approaches are essentially the same up to high plastic strains, and good correlations have been found between long and short crack data at both room and elevated temperatures by expressing the crack growth data in terms of $\sqrt{E\Delta J}$ or ΔK_{eq}.

Although analyses of short crack behavior in terms of elastic-plastic constitutive laws seem necessary in many cases, even with the more appropriate characterization afforded by such fracture mechanics, it is still often apparent that short cracks propagate at somewhat faster rates (Fig. 20). In order to account for this further "breakdown" in continuum mechanics characterization, El Haddad and co-workers [9,84,89,90] have proposed an empirical approach based on the notion of an intrinsic crack length parameter, a_o. These authors re-defined the stress intensity factor in terms of the physical crack length plus a_o, such that the stress intensity range which characterizes the growth of fatigue cracks, independent of crack length, is given by:

$$\Delta K = Q\Delta\sigma^{\infty}\sqrt{\pi(a + a_o)} \quad , \tag{23}$$

where Q is the usual geometry factor [84]. The "material-dependent constant" a_o was estimated from the limiting conditions of crack length where the nominal stress $\Delta\sigma^{\infty}$ approaches the fatigue limit $\Delta\sigma_e$ when $a \to 0$ and where $\Delta K = \Delta K_o$, i.e.,

$$a_o \approx \frac{1}{\pi}\left(\frac{\Delta K_o}{\Delta\sigma_e}\right)^2 \quad . \tag{24}$$

The value of the intrinsic crack size a_o can be seen to be equivalent to the critical crack size above which ΔK_{TH} becomes constant at the long crack threshold stress intensity ΔK_o in Figs. 15 and 18. In other words, a_o is an indication of the smallest crack size that can be characterized at the threshold in terms of LEFM. This intrinsic crack size approach has been claimed to be a special case of Tanaka and co-workers' blocked slip band model [76] discussed above, where the friction stress σ^*_{fr} in Eq. (19) is taken to be zero. Although somewhat physically unrealistic, by consideration of $\sigma^*_{fr} = 0$ in Eq. (18), $K_o = K_c^m$ and $a_o = w_o$ such that [76]:

$$\sigma_{TH} = \frac{K_o}{\sqrt{\pi(a + a_o)}} \quad , \tag{25}$$

or

$$K_{TH} = \frac{K_o \sqrt{a}}{\sqrt{a + a_o}} \quad , \tag{26}$$

which is identical to the expressions derived by El Haddad et al. [84]. Through the use of Eqs. (25)-(26), a_o has been used essentially as a fitting parameter to reproduce the variation of $\Delta\sigma_{TH}$ with crack length (i.e., in Fig. 18). Furthermore, by recomputing both ΔJ and ΔK to include the a_o term, El Haddad et al. [91] have reanalyzed the short crack data of Dowling [51], shown in Fig. 20, and claimed a closer correspondence between long and short crack results. This intrinsic or "fictitious" crack size approach has also been utilized to characterize the situation of a short crack emanating from a notch [64,91]. This is discussed in the following section.

Although such intrinsic crack length arguments seem to rationalize successfully many apparent anomalies between the growth rate kinetics of

AD-A142 609 FATIGUE BEHAVIOR OF LONG AND SHORT CRACKS IN WROUGHT AND POWDER ALUMINUM..(U) CALIFORNIA UNIV BERKELEY DEPT OF MATERIALS SCIENCE AND MINERA.. R O RITCHIE MAY 84

2/3

UNCLASSIFIED UCB/RP/84/A1021 AFOSR-TR-84-0509 F/G 11/6 NL

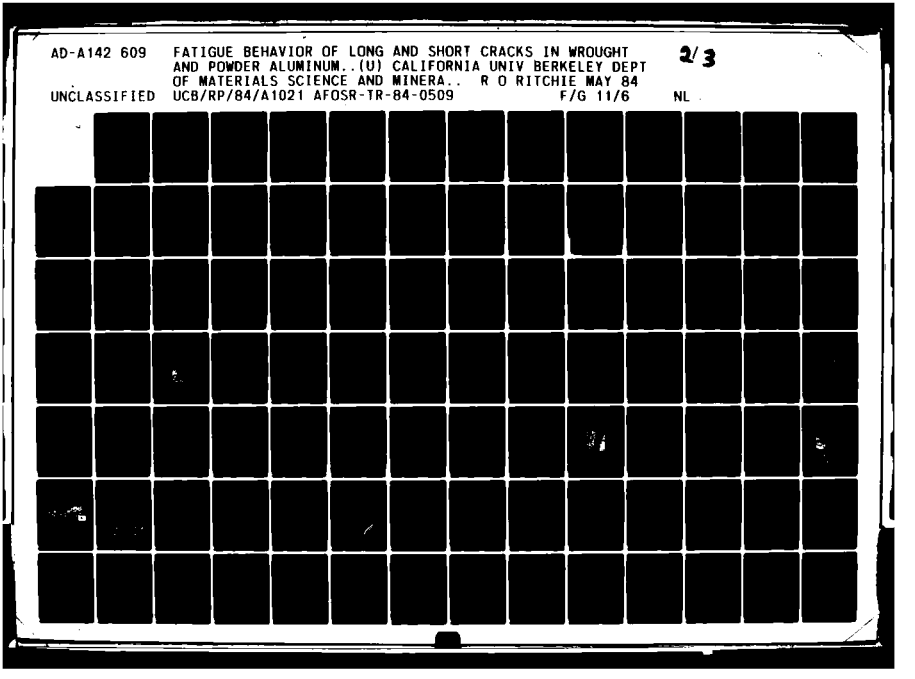

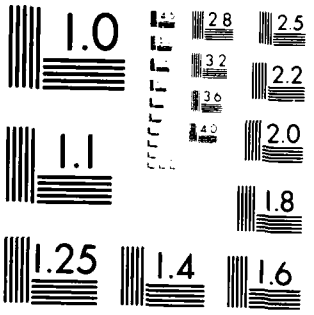

long and short cracks limited by conventional LEFM analyses, the approach is totally empirical as there is no currently available physical interpretation for the parameter a_o. There is also no convincing correlation between a_o and any characteristic microstructural dimension.

A somewhat different approach to rationalizing the behavior of long and short cracks, specifically with respect to the threshold condition, was presented by Usami and co-workers [59,92-94]. To replace the notion that the threshold condition for short cracks is one of a constant stress, compared to one of a constant stress intensity range for long cracks, these authors proposed a single criterion that the cyclic plastic zone dimension (r_Δ) at the fatigue limit is a material constant [59,92-94]. Using the Dugdale solution to approximate this plastic zone size at the fatigue limit (r_Δ^F) for $R \geq 0$, in terms of the yield stress σ_o and crack size a, i.e.,

$$r_\Delta^F = a[\sec(\pi\Delta\sigma_{TH}/4\sigma_o) - 1] \quad , \tag{27}$$

this approach, specifically using Eq. (27), was shown to reproduce the form of the $\Delta\sigma_{TH}$ versus crack size curves shown in Figs. 15, 18 and 19. Similar to the intrinsic crack size approach, this model can again be considered as a special case of the blocked slip band model (Eqs. 18-20) by setting $K_c^m = 0$ [76]. By developing similar expressions for negative R ratios, Usami and Shida [59] have also claimed to rationalize effects of stress ratio and yield strength on short crack behavior. However, experimental confirmation of the constancy of r_Δ^F at the threshold for long and short cracks and the validity of the Dugdale solutions for the plastic zone size in this instance have yet to be obtained.

Notch-Field Plasticity Effects

Local plasticity also plays an important role in influencing the initiation and growth of flaws emanating from notches, where the cracks are defined as being short because their size is comparable to the extent of the strain field of the notch-tip plastic zone (Fig. 21).

Stress analyses and failure predictions for notched components have traditionally involved the use of theoretical elastic stress concentration factors (k_t) or, where plasticity is considered, using procedures such as those developed by Neuber [95]. For example, the well-known Neuber rule suggests that the elastic stress concentration factor k_t, under conditions of plastic deformation, is approximately given by the geometric mean of the stress and strain concentration factors, k_σ and k_ε respectively, such that [95]:

$$k_t = \sqrt{k_\sigma k_\varepsilon} \quad . \tag{28}$$

For elastic conditions, Eq. (28) reduces to:

$$k_t = \frac{\sqrt{\sigma \varepsilon E}}{\sigma^\infty} \quad , \tag{29}$$

where σ and ε are the local stress and strain at the notch surface, respectively, σ^∞ is the nominally applied stress and E is the elastic modulus.

Although elastic stress concentration factors are sometimes used in fatigue for conservative design in the presence of notches, k_t is generally replaced by k_f, the fatigue-strength reduction factor. k_f can be considered as the effective stress concentration under fatigue loading conditions and is defined for finite life as:

$$k_f = \frac{\text{unnotched bar endurance limit}}{\text{notched bar endurance limit}} \leq k_t \quad . \tag{30}$$

Values of k_f approach the theoretical k_t values for larger sized notches and in higher strength materials, with the degree of agreement measured in terms of the so-called notch-sensitivity index defined as $(k_f - 1)/(k_t - 1)$. Although values of k_t are well tabulated in handbooks [e.g., 96], the determination of k_f values generally involves experimental measurements or empirical predictions, such as the Peterson equation for ferrous-based wrought alloys [97]:

$$k_f \approx 1 + \frac{(k_t - 1)}{(1 + \alpha/\rho)} \quad , \tag{31}$$

where ρ is the notch root radius and α is an empirical constant dependent upon material strength and ductility. Typical values for α generally range from 0.01 for annealed steels to 0.001 for highly hardened steels [1]. Since such empirical equations are only available for steels, to avoid always measuring k_f experimentally, Morrow and co-workers [e.g., refs. 1, 98,99] have recently developed the so-called local strain approach which is essentially a modification of the Neuber rule for cyclic loading. The k_f values suggested by Morrow and co-workers [98] are determined from:

$$k_f = \sqrt{k_\sigma k_\varepsilon} \qquad \text{(plastic)} \quad , \tag{32a}$$

$$= \frac{\sqrt{\Delta\sigma\Delta\varepsilon E}}{\Delta\sigma^\infty} \qquad \text{(elastic)} \quad , \tag{32b}$$

where $\Delta\sigma^\infty$, $\Delta\sigma$ and $\Delta\varepsilon$ are the ranges of the nominal stress, local stress and local strain, respectively. To compute k_f values, Eq. (32b), which is the equation of a rectangular hyperbola ($\Delta\sigma\Delta\varepsilon$ = constant), must be

solved simultaneously with the cyclic constitutive law, which similarly relates cyclic stresses to cyclic strains.

Fracture mechanics analyses, incorporating both analytical and numerical procedures (e.g., Eqs. 7 and 8) have also been utilized by many authors to treat the problem of notches in fatigue. In particular, Barsom and McNicol [37], Smith and Miller [100], Dowling [21,101], Kitagawa et al. [102], Lukăš and Klesnil [103], El Haddad et al. [91,104, 105] and Tanaka and co-workers [64], have all attempted to characterize the growth of small flaws which are either fully or partially submerged in a notch-tip plastic zone. Although not concerned specifically with the *growth* of short cracks, Barsom and McNicol [37] proposed the concept of a fatigue-crack initiation threshold ($\Delta K/\sqrt{\rho}$) which is assumed to be a material constant for the initiation of "engineering-sized" cracks from notches of varying root radii ρ (Fig. 22). Using the usual definition of the stress concentration factor (k_t), however, the concept of an initiation threshold $\Delta K/\sqrt{\rho}$ is really the notched bar fatigue limit $\Delta\sigma_e\ k_t$ expressed in fracture mechanics terms [7]. Smith and Miller [100], on the other hand, assumed that the fatigue crack of length a growing in an unnotched specimen can be equated to a fatigue crack of length ℓ growing from a notch, when both have the same instantaneous velocity under identical conditions of bulk applied stresses. They further suggested that the contribution e (= a - ℓ) to a crack of length ℓ growing from an edge notch of depth c and root radius ρ can be expressed as [100]:

$$e = 7.691\ \ell\sqrt{c/\rho} \quad , \tag{33}$$

and that the extent of the notch field is equal to $0.13\sqrt{c\rho}$. This estimate of the notch field size appears to be less accurate for fairly sharp

notches and is in disagreement with the predictions of Dowling [21] in this regime (Eq. 9).

An interesting aspect of crack growth from notches is that, after growing a short distance, cracks can arrest completely and become so-called non-propagating cracks (NPC), as first demonstrated by Phillips and Frost et al. [106-108]. Many subsequent studies [64,89,91,100,103, 109-111] have confirmed the existence of such NPC's although a precise understanding of the mechanisms for their occurrence is still lacking. Stress-strain/life analyses, however, have revealed that NPC's only form at sharp notches above the critical stress concentration factor k_t [e.g., 100,109,111]. This is illustrated in Fig. 23 where the long life fatigue strengths (i.e., fatigue limits) are plotted as a function of k_t. It is apparent from this figure that the threshold stress for crack initiation, i.e., the unnotched fatigue limit $\Delta\sigma_e$ divided by k_f or k_t, is less than the stress to cause complete failure above the critical k_t for NPC's.

Fracture mechanics analyses of the plasticity of the notch field suggest that the condition for non-propagation involves either the long crack threshold stress intensity ΔK_o applied to the short crack [94], or a threshold strain intensity factor incorporating an intrinsic crack length (a_o) term [89]. As discussed below, the above models fail to explain *physically* why NPC's occur since the mere presence of a notch plastic zone does not obviously give rise to a driving force for crack growth which goes through a minimum.

Whether short cracks emanating from notches arrest or not, their growth compared to conventional long crack LEFM data is generally non-unique and significantly faster when characterized in terms of ΔK or K_{max}. An example of this behavior is shown in Fig. 24 from the work of

Leis and Forte [110] where growth rates are plotted for cracks, 250 μm or smaller in length, propagating from notches of varying k_t, and are compared to long crack behavior of an AISI 1015 mild steel. Hammouda and Miller [109] have analyzed such behavior in terms of notch plasticity theory and argue that the total plastic shear displacement, which is taken as the sum of the shear displacement arising from (notch) bulk plasticity and that due to the local crack-tip plastic zone for LEFM controlled growth, determines the growth kinetics of such short cracks. Where the crack is completely submerged in the notch-tip plastic zone (Fig. 21), bulk plasticity conditions dominate behavior. Here it is argued that the growth rates of the short cracks will progressively decrease until they arrest or merge with the long crack LEFM curve where behavior is dominated by local plasticity conditions within the crack tip plastic zone (Fig. 25). Several continuum mechanics explanations for such observations of decreasing growth rates of short cracks within the notch-tip plastic zone have been claimed based on the above total plastic shear displacement argument [109], on elastic-plastic J-based analyses incorporating the a_0 concept [89] and on the concept that the reversed plastic zone size is a material concept (independent on crack length) [94]. The physical reasons for such behavior, however, are difficult to comprehend, particularly since a striking similarity exists between Fig. 25 and Fig. 14. In the latter case the progressive deceleration in short crack growth rates was reported *in the absence of a notch* and attributed to impeded growth at grain boundaries [71]. With this in mind, we must conclude that the precise mechanism for the occurrence of decelerated short crack growth and NPC's is currently unclear but we do recognize that factors such as notch-tip plasticity,

micro-plasticity, grain boundary blocking of slip bands, cessation of growth, crystallographic reorientation and deflection at grain boundaries, and crack closure all may play a significant role. In this regard, it has been claimed that since small cracks are capable of propagating below the long crack threshold ΔK_o value, they may propagate for some distance until the combination of their size and local stress cause them to arrest at or below the ΔK_o value [8]. Although this is a convenient statement to rationalize the behavior schematically illustrated in Figs. 14 and 25, physically based mechanistic interpretations of such behavior do not follow from conventional elastic or elastic-plastic notch analyses. However, recent studies have suggested that the most general explanation, which seems readily amenable to the physical interpretation of this behavior, involves the phenomenon of fatigue-crack closure, and the variation of such closure with crack length [12,61]. This is now discussed in detail in the following sections.

4.3 Environmental and Closure Effects

The third definition of a short crack, and perhaps the most ominous from a design viewpoint, is the physically-short flaw where the crack is long compared to both the scale of microstructure and the scale of local plasticity, yet simply physically small, i.e., typically less than 0.5-1 mm in length. Since both continuum mechanics and LEFM characterizations of the behavior of such flaws would be expected to be valid, it is perhaps surprising to find that under certain circumstances [11,48,49, 54,60] even physically-short cracks show growth rates in excess of those of long cracks under conditions of a nominally identical driving force (i.e., at the same ΔK). This realization represents a significant

breakdown in the similitude argument engrained in fracture mechanics analyses of sub-critical crack growth and has been attributed primarily to two basic factors [32].

The first of these pertains to the phenomenon of crack closure where, due to interference and physical contact between mating fracture surfaces in the *wake* of the crack tip, the crack can be effectively closed at positive loads during the fatigue cycle. Since the crack cannot propagate whilst it remains closed, the net effect of closure is to reduce the nominal stress intensity range (ΔK), computed as $K_{max} - K_{min}$ from applied loads and crack length measurements, to some lower effective value (ΔK_{eff}) actually experienced at the crack tip, i.e., $\Delta K_{eff} = K_{max} - K_{cl}$, where K_{cl} is the stress intensity at closure ($\geq K_{min}$) [112]. Closure can arise from a number of sources, such as the constraint of surrounding elastic material on the residual stretch in material elements previously plastically-strained at the tip (plasticity-induced closure) [112], the presence of corrosion debris within the crack (oxide-induced closure [113-116], and the contact at discrete points between faceted or rough fracture surfaces where significant inelastic Mode II crack tip displacements are present (roughness-induced closure) [116-120]. These mechanisms of crack closure are schematically illustrated in Fig. 26 [119].

Plasticity-induced closure, as first defined by Elber [112] based on compliance measurements on fatigue cracks in aluminum alloys at high stress intensity ranges, is generally considered to play a dominant role under plane stress conditions and is thus presumed to be of less importance at near-threshold levels where mostly plane strain conditions exist. For the latter case, the major contribution to the closure effect on fatigue-crack growth is known to result from oxide deposits within the crack and from

the premature contact between the fracture surface asperities. Based on simple geometric modelling studies, Suresh and Ritchie [120-122] have proposed the following relationships for such closure:

$$\left(\frac{K_{cl}}{K_{max}}\right)_{oxide} \approx \sqrt{\frac{d_o^2\,\beta}{\pi s\,\delta_{max}\,\varepsilon}} \quad , \tag{34}$$

and

$$\left(\frac{K_{cl}}{K_{max}}\right)_{roughness} \approx \sqrt{\frac{2\gamma x}{1 + 2\gamma x}} \quad , \tag{35}$$

where d_o is the maximum thickness of the excess oxide deposit located distance 2s from the crack tip, δ_{max} is the maximum crack tip opening displacement (Mode I), x is the ratio of Mode II to Mode I crack tip displacements, ε_o is the yield strain (σ_o/E), γ is a non-dimensional roughness factor given by the ratio of the height to width of a fracture surface asperity and β is a constant of numerical value $\sim$ 1/32.

Extensive studies on the behavior of long cracks particularly at near-threshold stress intensity levels have revealed that such closure mechanisms are dominant in giving rise to the respective roles of load ratio [114-116,123], yield strength [116,124,125], grain size [116,120], environment [114-116,121,122,125], and variable amplitude cycling [126-128] and even to the very existence of a threshold for no long crack growth [116,121,125,129]. However, such microscopic closure mechanisms are also particularly relevant to short crack behavior simply because their action predominates in the *wake* of the crack tip. Since small cracks, by definition, have only a limited wake, it is to be expected that the effect of crack closure will be different for long and short cracks, and specifically, the short crack is likely to be subjected to a smaller

influence of closure. Evidence for the extent of crack closure being a function of crack size has been reported by Morris et al. [48] for the growth of short flaws in titanium alloys. Here, by monitoring the surface crack opening displacement (at zero load) for crack sizes ranging from 50 to 500 μm (Fig. 27), these authors concluded that for cracks less than approximately 160 μm in length, the extent of crack closure, particularly that induced by roughness, decreased with decreasing crack length. A further influence of roughness-induced closure was inferred in the work of McCarver and Ritchie [60] on the crystallographic growth of long and physically-short fatigue cracks in René 95 nickel-base superalloy. In this latter study, threshold ΔK_{TH} values for short cracks ($a \sim 0.01$-0.20 μm) at low mean stresses ($R = 0.1$) were found to be 60% smaller than for long cracks ($a \sim 25$ mm), yet at high mean stresses ($R = 0.7$) where closure effects were minimal, this difference was not apparent. More recently, Tanaka and Nakai [61] used compliance techniques to measure the extent of crack closure for small cracks emanating from notches in low carbon steel and found a marked reduction in closure at short crack lengths. In fact, when analyzed in terms of ΔK_{eff} (Fig. 28), based on the closure measurements taken, these authors claimed that the anomalous (sub-threshold) behavior of short cracks (as shown in Figs. 14 and 25) could be brought into direct correspondence with conventional long crack data (see Section 5). Thus, at equivalent nominal ΔK levels, physically-short flaws may be expected to propagate faster (and show lower thresholds) than corresponding long flaws simply due to a smaller influence of closure producing larger effective stress intensity ranges at the crack tip. Specific mechanisms for this effect are discussed in more detail in the following section.

A second factor which may also produce accelerated growth rates for short cracks, however, can be associated with chemical and electrochemical effects and is relevant to the growth of physically-short flaws in aggressive environments [11,53,54,57,130]. Experiments by Gangloff [11,54] on high strength AISI 4130 steels tested in NaCl solution revealed corrosion fatigue crack propagation rates of short cracks (0.1-0.8 mm) to be up to two orders of magnitude faster than corresponding rates of long cracks (25-60 mm) at the same ΔK level, although behavior in inert atmospheres was essentially similar (Fig. 29). A comple[illegible]nder-standing of this phenomenon is as yet lacking but preliminary [illegible]alyses indicated that the effect could be attributed to differences [illegible]e local crack tip environments in the long and short flaws, principally resulting from different electrochemically-active surface-to-volume ratios of the cracks and from the influence of crack length on the solution renewal rate in the crack tip region [11,54,57].

5. DISCUSSION

From the preceding review of experimental results, it is apparent that short fatigue cracks may present difficulties in fatigue design simply because their growth behavior is somewhat unpredictable when based on current (long crack) analyses and methodologies (e.g., using long crack LEFM data). It is also apparent that the latter procedures are liable to yield non-conservative predictions of lifetimes for components containing short flaws because, at the same nominal driving force, the short crack invariably propagates at a faster rate than the corresponding long crack. This problem of lack of similitude from long and short crack behavior can be considered to arise from a number of reasons, such as i) inappropriate fracture mechanics characterization of tne crack driving force for short cracks subjected to near-tip and notch-field plasticity effects, ii) local microstructural features which, on the average, do not substantially alter the growth of macro-cracks but can interact strongly with small cracks because of their relatively significant and comparable size-scales, iii) lack of similitude associated with crack extension mechanisms, vi) crack closure effects, and vii) differences in the local crack tip environments. We now examine each of these factors in turn.

Questions concerning the inappropriate use of linear elastic fracture mechanics to characterize the extension of short cracks have been central to the short crack problem [e.g., 7-10,12,131,132]. In fact, it has often been claimed that the short crack problem occurs simply when LEFM analyses become invalid [131], although it is now clear that this is an over-simplification. Conventional LEFM

approaches can be inappropriate for short cracks even under nominally elastic conditions since the use of the linear elastic singularity to characterize the local stresses on the basis of K_I (i.e., Eq. (3)) invariably involves neglecting all terms of higher order than $r^{-\frac{1}{2}}$ [133,134]. However, when $a \sim r_y$, such higher order terms can have an appreciable effect and therefore should be considered when comparing long and short crack behavior [133,134]. It is also well recognized that one of the major reasons for the breakdown in LEFM analyses for short cracks is the presence of excessive plasticity over distances comparable with the crack size in the vicinity of the crack tip. This problem has been partly resolved by the use of elastic-plastic fracture mechanics through the J-integral or CTOD-based methodologies, as evidenced by the results of Dowling [51] in Fig. 20. It is now apparent that much earlier data indicating differences in long and short crack behavior can be traced back to the fact that growth rates were compared at equivalent ΔK values, and that the use of this LEFM parameter did not provide an adequate characterization of the stress and strain fields at the tip of the short crack where $a \sim r_y$. However, for the case of short cracks emanating from notches, where initial growth is occurring within the plastic zone of the notch (Fig. 21), a continuum mechanics description of the behavior is less clear. Certainly there is experimental evidence that such short cracks can propagate below the long crack threshold at progressively decreasing growth rates (Fig. 25) and even arrest to form non-propagating cracks [106-110], but such behavior has also been shown in the absence of a notch and attributed alternatively to microstructural factors (Fig. 14) [71]. Certainly no

linear elastic analysis of the case of a notch plus short crack [e.g., refs. 21, 100] has demonstrated that the crack driving force (e.g., K_I) goes through a minimum, as the crack extends from the notch, to rationalize such behavior, and to our knowledge there is no formal elastic-plastic analysis available which similarly predicts the appropriate variation in crack driving force (without incorporation of crack closure effects [12,64,135]). Whilst we cannot ignore the experimental data showing anamolous short crack growth at notches, in the absence of a complete continuum mechanics analysis we must conclude that part of the reason for the differing growth rate behavior of the short cracks in this instance may similarly result from the interaction of the short flaw with microstructural features and principally from the role of crack closure.

With respect to microstructural features, it is generally accepted that the presence of microscopic discontinuities such as grain boundaries, hard second phases, or inclusions play a somewhat minimal role in influencing the growth of long fatigue cracks [6] (at least over the range of growth rates below $\sim 10^{-3}$ mm/cycle), because behavior is governed primarily by average bulk properties [10]. However, this clearly will not be the case for small micro-cracks whose length will be comparable to the size of these microstructural features. For example, for micro-cracks contained within a single grain, cyclic slip will be strongly influenced by the crystal orientation and the proximity of the grain boundary, resulting in locally non-polar crack extension [49,71-74]. There is now a large body of evidence that shows that the growth of small cracks is impeded by the presence of grain boundaries (e.g., Fig. 30) by such mechanisms as the blocking of slip bands [76] or

containment of the plastic zone [49] within the grain, reorientation and re-initiation of the crack as it traverses the boundary [49,71], and simply cessation of growth at the boundary [49]. The latter effect has also been demonstrated for the presence of harder second phases, where in duplex ferritic-martensitic steels, micro-cracks were observed to initiate and grow in the softer ferrite only to arrest when they encountered the harder martensite [136]. Many of these effects can be explained by considering the mechanics of crack deflection.

Based on the theoretical analysis of Bilby et al. [137] and Cotterell and Rice [138], recent studies by Suresh [81] have shown that alternative approaches to such previous interpretations of crack tip-grain boundary interactions can be developed by considering the role of crack deflection in influencing the propagation of short fatigue cracks. For a short crack, the low restraint on cyclic slip promotes a predominantly crystallographic mode of failure. When a crack tip reaches a grain boundary, it tends to reorient itself in the adjacent grain to advance by the single shear mechanism and can be considerably deflected by the grain boundary. This phenomenon is schematically illustrated in Fig. 31. The extent of deflection at the grain boundary is a function of the relative orientations of the most favorable slip systems in the adjoining crystals. For an *elastic* crack initially inclined at the angle θ_o to the Mode I growth plane and deflected at the first grain boundary by an angle θ_1 (Fig. 31), approximate estimates of the *local* stress intensity factors yield [81]:

$$\frac{K_1}{K_I} = \cos^2\theta_o \cos^3\left(\frac{\theta_1}{2}\right) + 3 \sin\theta_o \cos\theta_o \sin\left(\frac{\theta_1}{2}\right) \cos^2\left(\frac{\theta_1}{2}\right), \quad (36)$$

$$\frac{K_2}{K_I} = \cos^2\theta_o \sin(\frac{\theta_1}{2}) \cos^2(\frac{\theta_1}{2}) - \sin\theta_o \cos\theta_o \cos(\frac{\theta_1}{2})\left[1 - 3 \sin^2(\frac{\theta_1}{2})\right] \quad . \qquad (37)$$

Here, K_1 and K_2 are the near-tip Mode I and Mode II stress intensity factors, respectively, immediately following deflection at the grain boundary, whereas K_I is the nominal Mode I (far-field) value. For a typical short crack emanating from the surface at an angle of $\theta_o \approx 45°$ and deflected at the grain boundary by $\theta_1 \approx 90°$, the above equations result in $K_1 \approx 0.7\ K_I$ and $K_2 \approx 0.35\ K_I$. The effective driving force for coplanar growth can then be approximated to be the square root of the sum of the squares of K_1 and K_2, such that $\Delta K_{eff} \approx 0.78\ \Delta K_I$. Thus consideration of crack deflection processes alone can account for a significant reduction in driving force during crack tip-grain boundary interactions when the mechanics of short crack advance is characterized by linear elastic fracture mechanics. It has been postulated [81] that if the extent of deflection at the grain boundary is large, the *effective* cyclic stresses may be reduced to a value smaller than the true threshold for short crack advance (e.g., fatigue endurance limit) such that complete crack arrest will result (denoted by curve A in Fig. 32). If the effective cyclic stresses following deflection are above such threshold values, no crack arrest occurs (as denoted by curve B in Fig. 32) and only a temporary deceleration in growth rates would be noticed. Although the numerical predictions of the deflection models can be subject to considerable uncertainties when used to characterize the mechanics of short cracks in metals and alloys, the mechanisms underlying crack deflection processes [81] have been shown to offer a

physically-appealing rationale not only for the role of microstructure in influencing short crack advance, but also for several fatigue characteristics of long cracks under constant [81] and variable amplitude [81,126-128] loading conditions.

In addition to causing a reduction in the effective driving force, crack deflection mechanisms could play a major role in enhancing closure [81,120]. For example, the irreversibility of slip steps and surface oxidation can lead to nonuniform tensile opening and shear displacements of short cracks [12,81]. Given the presence of serrated fracture surfaces and Mode II crack tip displacements due to deflection, such nonuniformities in crack opening and sliding, in reality, result in premature asperity contact leading to roughness-induced closure (Figs. 26 and 31). (An ideally elastic crack may not result in any roughness-induced closure irrespective of the extent of deflection.) Experimental measurements of crack closure by Morris and co-workers [47-49] do indeed show that even short cracks (spanning only a few grain diameters) can close above the minimum load of the fatigue cycle (Fig. 27).

A further factor which may contribute to differences in the behavior of long and short cracks is the question of crack shape [10]. Even long cracks, which encompass many grains, are known to possess certain irregularities in their geometry (*on a microscale level*) due to local interactions with microstructural features [10], yet, at a given ΔK, the overall growth behavior would be expected to be similar. However, on comparing a macro-crack and a micro-crack contained within a few grains, this similarity would seem questionable. Moreover, the early stages of fatigue damage often involve the initiation of several

micro-cracks such that the subsequent growth of a particular small flaw is likely to be strongly influenced by the presence of other micro-cracks [37-40].

Differences in the behavior of long and short cracks may also result from the fact that, at the same nominal ΔK, the crack extension mechanisms may be radically different. As pointed out by Schijve [10], the restraint of the elastic surrounding on a small crack near a free surface is very different from that experienced at the tip of a long crack inside the material. For a small grain-sized crack, cyclic slip along the system with the highest critical resolved shear stress results in Mode II + Mode I slip band cracking akin to Forsyth's Stage I mechanism [139]. For the long crack, however, which spans many grains, maintaining such slip-band cracking in a single direction in each grain is incompatible with a coherent crack front. The resulting increased restraint on cyclic plasticity will tend to activate further slip-systems leading to a non-crystallographic mode of crack advance by alternating or simultaneous shear, commonly referred to as striation growth (Forsyth's Stage II) [139]. At near-threshold levels where the extent of local plasticity can be small enough to be contained within a single grain, even long cracks propagate via this single shear mechanism with the orientation of the slip-band cracking changing at each grain boundary and leading to a faceted or zig-zag crack path morphology (Fig. 34) [117-120]. The occurrence of this shear mode of crack extension, together with the development of a faceted fracture surface, has major implications with respect to the magnitude of crack closure effects [116-120], which further may lead to differences in long and short crack behavior (Figs. 26 and 31).

The origin of the differences in fatigue characteristics resulting from crack closure arises basically from two sources. First, since closure results from the constraint of surrounding *elastic* material on the plastic encave surrounding the crack, the contribution from closure on a small crack at high stress amplitudes in a fully plastic specimen would be far less than on a larger crack at lower stress amplitudes in an elastic-plastic or nominally elastic specimen at the same (nominal) driving force. However, more importantly, differences between the role of closure in influencing long and short cracks result from the fact that such closure effects predominate in the *wake* of the crack tip. Since short cracks, by definition, possess a limited wake, it is to be expected that in general such cracks will be subjected to less closure. Thus, at the same *nominal* driving force, short cracks may experience a larger *effective* value compared to the equivalent long crack. As outlined in Section 4, this can arise from two sources. Firstly, with respect to plasticity-induced closure, plastic deformation in the wake of the crack has to build up before it can be effective in reducing ΔK_{eff} [112]. From analogous studies of the role of dilatant inelasticity (generated by phase transformations) on reducing the effective stress intensity at the crack tip in ceramics [140], it has been found that the full effect of this closure is only felt when the transformed zone extends a distance into the wake of the crack of the order of five times its forward extent. Although this analysis has not been completed for plastic deformation in metals, it is to be expected that the role of the compressive stresses in the plastic zone encompassing the wake of the crack would be limited for small cracks of a length comparable to the

forward extent of this zone (i.e., for $a \sim r_y$). It is believed [12,64, 133] that this is one of the major reasons (at least from the perspective of continuum mechanics) for non-propagating cracks and why microstructurally-short cracks and cracks emanating from notches can propagate below the long crack threshold ΔK_o (Figs. 14 and 25). Essentially they can initiate and grow at nominal stress intensities below ΔK_o due to the absence of closure effects, but, as they increase in length, the build-up of permanent residual plastic strains in their wake promotes a contribution from crack closure, which progressively decreases the effective ΔK experienced at the crack tip resulting in a progressive reduction in crack growth rate and sometimes complete arrest.

This notion, which relates the anomalous behavior of short cracks below the long crack threshold regime and in the strain field of notches (e.g., Fig. 1) primarily to a decrease in crack closure effects at small crack sizes [12,64,135], has recently been substantiated by both numerical [135] and experimental [64] studies. Newman [135] has demonstrated that by incorporating plasticity-induced closure into finite-element computational models for fatigue-crack propagation, the progressively decreasing growth rates of short cracks emanating from notches could be predicted in good agreement with experimental data on lower strength steel (Fig. 33). Furthermore, Tanaka and Nakai [64] monitored the growth of similar short cracks in notched specimens of low strength steel at both R = 0 and 0.4 whilst simultaneously measuring the extent of crack closure. Their data, which show the characteristic decreasing growth rate behavior at short crack sizes when plotted in the

usual way in terms of a nominal ΔK, can be seen to coincide with the long crack data and to fall on a single smooth curve when reanalyzed in terms of ΔK_{eff} incorporating the experimental K_{cl} measurements (Fig. 28).

An analogous situation can arise due to the contribution from roughness-induced crack closure promoted by rough, irregular fracture surfaces, particularly where the crack extension mechanism involves a strong single shear (Mode II + Mode I) component [118-120]. Since a crack of zero length can have no fracture surface and hence no roughness-induced closure, it is to be expected that the development of such closure will be a strong function of crack size [47-49,120,133], as demonstrated by the experimental data of Morris et al. [48] in Fig. 27. A lower bound estimate for the transition crack size below which roughness-induced closure will be ineffective (at near-threshold levels) can be appreciated from Figs. 31 and 34 [120]. The long crack, which encompasses several grains, will at near-threshold levels have developed a faceted morphology and, due to incompatibility between mating crack surfaces from the Mode II crack tip displacements, will be subjected to roughness-induced closure in the manner depicted in Fig. 26. The short crack, however, will be unable to develop such closure whilst its length remains less than a grain diameter since it will not have changed direction at a grain boundary and accordingly will not have formed a faceted morphology, despite extension via the same single shear mechanism.

In general, since the majority of results showing differences in long and short crack growth rates have been observed at low stress intensity ranges, and since the fatigue-crack propagation behavior of

long cracks in this near-threshold regime is known to be strongly influenced by crack closure effects, it seems most likely that the major reason for the faster growth of short cracks and the fact that they can propagate below the long crack threshold ΔK_o is associated with a decreasing role of closure at decreasing crack sizes. The recent studies of Potter [141] on the behavior of short flaws under variable amplitude loading are consistent with this notion, since the crack growth transients (i.e., accelerations and retardations) normally observed following overloads and spectrum loading sequences, which have been attributed, at least in part to closure mechanisms [e.g., 112], were largely absent for short flaws. In this regard it would be useful to compare short crack data with data for long cracks *at high load ratios*, since closure effects are minimal here even for long cracks. Where this has been done, i.e., for crystallographic near-threshold fatigue in nickel-base alloys [60], the threshold for short cracks, despite being 60% smaller than the long crack threshold at R = 0.1, was approximately equal to the long crack threshold at R = 0.7.

Finally, large differences in the behavior of long and short cracks can arise at stress intensities well outside the threshold regime due to environmental factors [11,54,130]. As shown in Fig. 29, the results of Gangloff [11,54] have demonstrated that corrosion fatigue crack growth rates of physically-short cracks in AISI 4130 steel tested in aqueous NaCl solution can be 1-2 orders of magnitude faster than the corresponding growth rates of long cracks at the same ΔK value. This unique environmentally-assisted behavior of short cracks was attributed to differing local crack tip environments as a function of crack size.

Specifically, the local concentration of the embrittling species within the crack was reasoned to depend on the surface to volume ratio of the crack, on the diffusive and convective transport of the embrittling medium to the crack tip, and on the distribution and coverage of active sites for electrochemical reaction, all processes sensitive to crack depth, opening displacement and crack surface morphology [54,57]. Analogous, yet less spectacular, environmental crack size effects may also arise in gaseous environments or due to internally-charged hydrogen where, for example, the presence of hydrogen may induce an intergranular fracture mode. The rough fracture surfaces promoted by this failure mechanism would lead to roughness-induced closure which again acts to influence primarily the long crack behavior of reducing ΔK_{eff} [e.g., 142].

These examples of the differences in behavior of fatigue cracks of varying size are a clear indication of where the fracture mechanics similitude concept can break down. The stress intensity, although adequately characterizing the mechanical driving force for crack extension, cannot account for the chemical activity of the crack-tip environment, or the *local* interaction of the crack with microstructural features. Since these factors, together with the development of crack closure, are a strong function of crack size, it is actually unreasonable to expect identical crack growth behavior for long and short cracks. Thus, in the absence of the similitude relationship, the analysis and utilization of laboratory fatigue-crack propagation data to predict the performance of in-service components, where short cracks are present, becomes an extremely complex task; a task which immediately demands a major effort in fatigue research from both researchers and practicing engineers alike.

6. CONCLUDING REMARKS

The problem of short cracks must now be recognized as one of the most important and challenging topics currently faced by researchers in fatigue. Not only is it a comparatively unexplored area academically, but it also raises doubts in the universal application of fracture mechanics to the characterization of sub-critical flaw growth and accordingly has the potential, from an engineering viewpoint, for creating unreliable, non-conservative defect-tolerant lifetime predictions. It is an area that, in fact, represents an interface between the fracture mechanics methodologies dealing specifically with the macroscopic growth of fatigue cracks and the classical engineering mechanics methodologies dealing with total life and engineering concepts of (macro-) crack initiation (as depicted in Fig. 1). As discussed in the Introduction, the latter process of macro-crack initiation is simply the growth of short flaws (micro-cracks). We have not, however, explicitly treated in this paper the process of the *initiation* of short flaws (i.e., micro-crack initiation), which has been the subject of several recent reviews [e.g., 143,144,7]. Suffice to say that such micro-cracks tend to initiate at constituent particles (i.e., inclusions and intermetallics, as shown in Fig. 9) in commercial materials [e.g., 39,41,145] whereas in pure metals and alloys their initiation is often associated with emerging planar slip bands called persistent slip bands (PSB's) [e.g., 143,144,146,147]. In fcc metals, such micro-cracks appear to initiate with a crystallographic Stage I mechanism along the PSB, as shown in Fig. 35 from high resolution transmission electron microscopy studies on copper [148], although the

specific mechanisms of initiation and their relation to the PSB's varies markedly from material to material [144].

In the current paper, we have attempted to provide a critical overview of recent experimental studies on the *growth* of small fatigue cracks, and specifically, to outline the mechanical, metallurgical and environmental reasons, as to why the behavior of such cracks should differ from the behavior of long cracks. Our intent was not to present a formal analysis of each of these factors, since in most cases such an analysis simply does not exist, but rather to review thoroughly the many inter-disciplinary factors which may be relevant to the short crack problem. We conclude that behavioral differences between the short and long flaw are to be expected, and such differences can arise from a number of distinct phenomena, namely: i) inadequate characterization of the mechanics of crack-tip stress and deformation fields of short cracks, including the neglect of higher order terms for the elastic singularity and the presence of extensive local crack-tip plasticity, ii) notch-tip stress and deformation field effects (for cracks emanating from notches), iii) interaction, including deflection, of short cracks with microstructural features, e.g., grain boundaries, inclusions, second phases, etc., of dimensions comparable in size with the crack length, iv) differences in crack shape and geometry, v) differences in crack extension mechanisms, vi) differences in the contribution from crack closure mechanisms with crack length, and finally vii) differences in the local crack-tip environments. Each of these factors represents a formidable challenge in fatigue research, because of the complex nature of both experimental and theoretical studies, yet their importance

is undeniable to rationalizing the anomalous behavior of short flaws. It is without doubt that this problem will assume even greater significance in the future since, with improvements in the science and practice of non-destructive testing (NDT), the projected lifetime of a fatigue flaw in the short crack regime will become an increasingly larger proportion of the total life.

7. ACKNOWLEDGEMENTS

The work was performed under Grant No. AFOSR-82-0181 from the U.S. Air Force Office of Scientific Research to the University of California in Berkeley. The authors wish to thank Dr. A. H. Rosenstein of AFOSR for his support and encouragement, Drs. W. L. Morris and J. Lankford for kindly supplying original micrographs, and Madeleine Penton for her help in preparing the manuscript. This review is an expanded version of a paper presented at the 55th Specialists Meeting of the AGARD Structural Materials Panel in Toronto, Canada, during September 1982.

REFERENCES

1. M. R. Mitchell: 'Fatigue and Microstructure,' 385; 1979, American Society for Metals, Metals Park, OH.

2. L. F. Coffin: 'Fatigue and Microstructure,' 1; 1979, American Society for Metals, Metals Park, OH.

3. J. E. Campbell, W. E. Berry, and C. E. Feddersen: 'Damage Tolerant Design Handbook,' 1972, Metals and Ceramics Info. Center, Battelle Columbus Laboratories, OH.

4. S. T. Rolfe and J. M. Barsom: 'Fracture and Fatigue Control in Structures: Applications of Fracture Mechanics,' 1977, Prentice-Hall, Inc., New Jersey.

5. H. H. Johnson and P. C. Paris: Eng. Fract. Mech., 1968, 1, 3.

6. R. O. Ritchie: Int. Metals Reviews, 1979, 20, 205.

7. M. E. Fine and R. O. Ritchie: 'Fatigue and Microstructure,' 245; 1979, American Society for Metals, Metals Park, OH.

8. S. J. Hudak: J. Eng. Mater. Technol., (Trans. ASME, H), 1981, 103, 26.

9. M. H. El Haddad, T. H. Topper, and B. Mukherjee: J. Test. Eval., 1981, 9, 65.

10. J. Schijve: 'Fatigue Thresholds' (eds. J. Bäcklund, A. Blom and C. J. Beevers), Vol. 2, 881; 1982, EMAS Ltd., Warley, U.K.

11. R. P. Gangloff: 'Advances in Crack Length Measurement' (ed. C. J. Beevers), 1983, in press, EMAS Ltd., Warley, U.K.

12. R. O. Ritchie and S. Suresh: 'Behavior of Short Cracks in Airframe Components,' Proc. 55th Specialists Meeting of AGARD Structural and Materials Panel, 1983, in press, Advisory Group for Aeronautical Research and Development, France.

13. M. L. Williams: J. Appl. Mech. (Trans. ASME), 1957, 24, 109.

14. G. R. Irwin: J. Appl. Mech. (Trans. ASME), 1957, 24.

15. P. C. Paris and F. Erdogan: J. Basic Eng. (Trans. ASME, D), 1963, 85, 528.

16. J. R. Rice: 'Fracture: An Advanced Treatise' (ed. H. Liebowitz), Vol. 2, 191; 1968, Academic Press, New York, NY.

17. J. R. Rice: 'Fatigue Crack Propagation,' ASTM STP 415, 247; 1967, American Society for Testing and Materials, Philadelphia, PA.

18. H. Tada, P. C. Paris, and G. R. Irwin: 'The Stress Analysis of Cracks Handbook,' 1973, Del Research Corp., Hellertown, PA.

19. G. C. Sih: 'Handbook of Stress Intensity Factors,' 1973, Lehigh University, Bethlehem, PA.

20. D. P. Rooke and D. J. Cartwright: 'Compendium of Stress Intensity Factors,' 1975, Her Majesty's Stationary Office, London, U.K.

21. N. E. Dowling: Fat. Eng. Mat. Struct., 1979, 2, 129.

22. R. O. Ritchie: J. Eng. Mater. Technol. (Trans. ASME, H), 1983, 105, 1.

23. J. W. Hutchinson: J. Mech. Phys. Solids, 1968, 16, 13.

24. J. R. Rice and G. R. Rosengren: J. Mech. Phys. Solids, 1968, 16, 1.

25. J. R. Rice: J. Appl. Mech. (Trans. ASME), 1968, 35, 379.

26. N. E. Dowling: 'Cracks and Fracture,' ASTM STP 601, 19; 1976, American Society for Testing and Materials, Philadelphia, PA.

27. N. E. Dowling and J. A. Begley: 'Mechanics of Crack Growth,' ASTM STP 590, 82; 1976, American Society for Testing and Materials, Philadelphia, PA.

28. J. W. Hutchinson and P. C. Paris: 'Elastic-Plastic Fracture,' ASTM STP 668, 37; 1979, American Society for Testing and Materials, Philadelphia, PA.

29. D. M. Parks: unpublished work, Yale University, New Haven, 1978.

30. C. F. Shih: J. Mech. Phys. Solids, 1981, 29, 305.

31. D. Broek and B. N. Leis: 'Materials, Experimentation and Design in Fatigue' (eds. F. Sherratt and J. B. Sturgeon), 129; 1981, Westbury House, Guildfard, U.K.

32. R. O. Ritchie and S. Suresh: Mater. Sci. Eng., 1983, 57, L27.

33. C. J. Beevers, ed.: 'The Measurement of Crack Length and Shape During Fracture and Fatigue,' 1980, EMAS Ltd., Warley, U.K.

34. C. J. Beevers, ed.: 'Advances in Crack Length Measurement,' 1983, in press, EMAS Ltd., Warley, U.K.

35. 'ASTM Standard E647-83 on Test Method for Constant-Load-Amplitude Fatigue Crack Growth Rates above 10^{-8} m/cycle,' Annual Book of ASTM Standards, Section 3, 710; 1983, American Society for Testing and Materials, Philadelphia, PA.

36. W. L. Morris, M. R. James, and O. Buck: 'Nondestructive Evaluation-Microstructural Characterization and Reliability Strategies' (eds. O. Buck and S. M. Wolf), 387; 1981, TMS-AIME, Warrendale, PA.

37. J. M. Barsom and R. C. McNicol: 'Fracture Toughness and Slow Stable Cracking,' ASTM STP 559, 1983; 1974, American Society for Testing and Materials, Philadelphia, PA.

38. Y. H. Kim, T. Mura, and M. E. Fine: Met. Trans. A, 1978, 9A, 1679.

39. C. Y. Kung and M. E. Fine: Met. Trans. A, 1979, 10A, 603.

40. W. L. Morris: Met. Trans. A, 1977, 8A, 589.

41. W. L. Morris and O. Buck: Met. Trans. A, 1977, 8A, 597.

42. W. L. Morris: Met. Trans. A, 1978, 9A, 1345.

43. R. Chang, W. L. Morris, and O. Buck: Scripta Met., 1979, 13, 191.

44. W. L. Morris: Met. Trans. A, 1979, 10A, 5.

45. W. L. Morris: Private communication, 1983, Rockwell International Science Center, Thousand Oaks, CA.

46. W. L. Morris: Met. Trans. A, 1980, 11A, 1117.

47. W. L. Morris, M. R. James, and O. Buck: Met. Trans. A, 1981, 12A, 57.

48. M. R. James and W. L. Morris: Met. Trans. A, 1983, 14A, 153.

49. W. L. Morris, M. R. James, and O. Buck: Eng. Fract. Mech., 1983, 18, 871.

50. G. P. Sheldon, T. S. Cook, T. W. Jones, and J. Lankford: Fat. Eng. Mat. Struct., 1981, 3, 219.

51. N. E. Dowling: 'Cycle Stress-Strain and Plastic Deformation Aspects of Fatigue Crack Growth,' ASTM STP 637, 97; 1977, American Society for Testing and Materials, Philadelphia, PA.

52. N. E. Dowling: Proc. ASME 4th Nat. Congress in Pressure Vessel and Piping Technology, Portland, OR, 1983, American Society for Mechanical Engineers, New York.

53. R. P. Gangloff: General Electric Co. Report No. 79CRD267, Jan. 1980.

54. R. P. Gangloff: Res. Mechanica Letters, 1981, 1, 299.

55. M. T. Resch, D. V. Nelson, J. C. Shyne, and G. S. Kino: 'Advances in Crack Length Measurement' (ed. C. J. Beevers), 1983, in press, EMAS Ltd., Warley, U.K.

56. W. Baxter: Int. J. Fatigue, 1983, 5, 37.

57. R. P. Gangloff: 'Localized Crack Chemistry and Mechanics in Environment Assisted Cracking' (ed. R. P. Gangloff), 1983, The Metallurgical Society of AIME, Warrendale, PA.

58. B. Wiltshire and J. F. Knott: Int. J. Fract., 1980, 16, R21.

59. S. Usami and S. Shida: Fat. Eng. Mat. Struct., 1979, 1, 471.

60. J. F. McCarver and R. O. Ritchie: Mater. Sci. Eng., 1982, 55, 63.

61. K. Tanaka and Y. Nakai: Fat. Eng. Mat. Struct., 1983, 6, in press.

62. J. Byrne and T. V. Duggan: 'Fatigue Thresholds' (eds. J. Bäcklund, A. Blom, and C. J. Beevers), Vol. 2, 753; 1982, EMAS Ltd., Warley, U.K.

63. S. Suresh: Fat. Eng. Mat. Struct., 1983, to be submitted.

64. K. Tanaka and Y. Nakai: J. Eng. Mater. Technol. (Trans. ASME, H), 1983, 105, in press.

65. J. Lankford and D. L. Davidson: Acta Met., 1983, 31, in press.

66. J. Lankford and D. L. Davidson: Fat. Eng. Mat. Struct., 1983, 6, 241.

67. F. Guiu, R. Dulniak, and B. C. Edwards: Fat. Eng. Mat. Struct., 1982, 5, 311.

68. S. Pearson: Eng. Fract. Mech., 1975, 7, 235.

69. O. N. Romaniv, V. N. Siminkovich, and A. N. Tkach: 'Fatigue Thresholds' (eds. J. Bäcklund, A. F. Blom, and C. J. Beevers), Vol. 2, 799; 1982, EMAS Ltd., Warley, U.K.

70. K. Tanaka, M. Hojo, and Y. Nakai: 'Quantitative Measurement of Fatigue Damage,' ASTM STP, 1983, American Society for Testing and Materials, Philadelphia, PA, in press.

71. J. Lankford: Fat. Eng. Mat. Struct., 1982, 5, 233.

72. J. Lankford: Fat. Eng. Mat. Struct., 1983, 6, 15.

73. D. Taylor and J. F. Knott: Fat. Eng. Mat. Struct., 1981, 4, 147.

74. C. W. Brown and M. A. Hicks: Fat. Eng. Mat. Struct., 1983, 6, 67.

75. Y. Nakai and K. Tanaka: 'Proceedings of 23rd Japan Congress on Materials Research,' 106; 1980.

76. K. Tanaka, Y. Nakai, and M. Yamashita: Int. J. Fract., 1981, 17, 519.

77. R. O. Ritchie: J. Eng. Mater. Technol. (Trans. ASME, H), 1977, 99, 195.

78. J. Lankford: Eng. Fract. Mech., 1977, 9, 617.

79. S. Taira, K. Tanaka, and M. Hoshina: 'Fatigue Mechanisms,' ASTM STP 675, 135; 1979, American Society for Testing and Materials, Philadelphia, PA.

80. S. Taira, K. Tanaka, and Y. Nakai: Mech. Res. Comm., 1978, 5, 375.

81. S. Suresh: Met. Trans. A, 1983, 14A, 2375.

82. H. Kitagawa and S. Takahashi: 'Proceedings 2nd Intl. Conf. on Mech. Beh. of Materials,' 627; 1976, Boston, MA.

83. D. Taylor: Fat. Eng. Mat. Struct., 1982, 5, 305.

84. M. H. El Haddad, K. N. Smith, and T. H. Topper: J. Eng. Mater. Technol. (Trans. ASME, H), 1979, 101, 42.

85. R. C. Boettner, C. Laird, and A. J. McEvily: Trans. AIME, 1965, 233, 379.

86. H. D. Solomon: J. Materials, 1972, 7, 299.

87. J. R. Haigh and R. P. Skelton: Mater. Sci. Eng., 1978, 36, 133.

88. M. S. Starkey and R. P. Skelton: Fat. Eng. Mat. Struct., 1982, 5, 329.

89. M. H. El Haddad, T. H. Topper, and K. N. Smith: Eng. Fract. Mech., 1979, 11, 573.

90. M. H. El Haddad, T. H. Topper, and K. N. Smith: J. Test. Eval., 1980, 8, 301.

91. M. H. El Haddad, N. E. Dowling, T. H. Topper, and K. N. Smith: Int. J. Fract., 1980, 16, 15.

92. H. Ohuchida, A. Nishioka, and S. Usami: 'Proc. 3rd Int. Conf. on Fract.,' Vol. 5, V-443/A; 1973, München, Germany.

93. H. Ohuchida, S. Usami, and A. Nishioka: Bull. Japan Soc. Mech. Engrs., 1975, 18, 1185.

94. S. Usami: 'Fatigue Thresholds' (eds. J. Bäcklund, A. Blom, and C. J. Beevers), Vol. 1, 205; 1982, EMAS Ltd., Warley, U.K.

95. H. Neuber: J. Appl. Mech. (Trans. ASME, H), 1961, 28, 544.

96. R. E. Peterson: 'Stress Concentration Factors,' 1974, Wiley-Interscience, New York.

97. R. E. Peterson: 'Metal Fatigue' (eds. G. Sines and J. L. Waisman), 293; 1959, McGraw Hill, New York.

98. T. H. Topper, R. M. Wetzel, and J. Morrow: J. Metals, 1969, 4, 200.

99. N. E. Dowling, W. R. Brose, and W. K. Wilson: 'Fatigue Under Complex Loading - Analysis and Experiments,' 55; 1977, Society of Automotive Engineers, Inc., Warrendale, PA.

100. R. A. Smith and K. J. Miller: Int. J. Mech. Sci., 1977, 19, 11.

101. N. E. Dowling: 'Fracture Mechanics,' ASTM STP 677, 247; 1979, American Society for Testing and Materials, Philadelphia, PA.

102. H. Kitagawa: 'Fatigue Thresholds' (eds. J. Bäcklund, A. F. Blom, and C. J. Beevers), Vol. 2, 1051; 1982, EMAS Ltd., Warley, U.K.

103. P. Lukáš and M. Klesnil: Mater. Sci. Eng., 1978, 34, 61.

104. M. H. El Haddad, K. N. Smith, and T. H. Topper: 'Fracture Mechanics,' ASTM STP 677, 274; 1979, American Society for Testing and Materials, Philadelphia, PA.

105. T. H. Topper and M. H. El Haddad: 'Fatigue Thresholds' (eds. J. Bäcklund, A. Blom, and C. J. Beevers), Vol. 2, 777; 1982, EMAS Ltd., Warley, U.K.

106. C. E. Phillips: 'Proc. Colloquium on Fatigue,' 210; 1955, IUTUM, Stockholm; 1956, Springer, Berlin.

107. N. E. Frost: J. Mech. Eng. Sci., 1960, 2, 109.

108. N. E. Frost and D. S. Dugdale: J. Mech. Phys. Solids, 1957, 5, 182.

109. M. M. Hammouda and K. J. Miller: 'Elastic-Plastic Fracture,' ASTM STP 668, 703; 1979, American Society for Testing and Materials, Philadelphia, PA.

110. B. N. Leis and T. P. Forte: 'Fracture Mechanics,' ASTM STP 743, 100; 1982, American Society for Testing and Materials, Philadelphia, PA.

111. N. E. Frost, K. J. Marsh, and L. P. Pook: 'Metal Fatigue,' 1974, Clarenden Press, Oxford.

112. W. Elber: 'Damage Tolerance in Aircraft Structures,' ASTM STP 486, 230; 1971, American Society for Testing and Materials, Philadelphia, PA.

113. K. Endo, K. Komai, and Y. Matsuda: Memo. Faculty Eng., Kyoto Univ., 1969, 31, 25.

114. R. O. Ritchie, S. Suresh, and C. M. Moss: J. Eng. Mater. Technol. (Trans. ASME, H), 1980, 102, 293.

115. A. T. Stewart: Eng. Fract. Mech., 1980, 13, 463.

116. S. Suresh, G. F. Zamiski, and R. O. Ritchie: Met. Trans. A, 1981, 12A, 1435.

117. N. Walker and C. J. Beevers: Fat. Eng. Mat. Struct., 1979, 1, 135.

118. K. Minakawa and A. J. McEvily: Scripta Met., 1981, 15, 633.

119. R. O. Ritchie and S. Suresh: Met. Trans. A, 1982, 13A, 937.

120. S. Suresh and R. O. Ritchie: Met. Trans. A, 1982, 13A, 1627.

121. S. Suresh, D. M. Parks, and R. O. Ritchie: 'Fatigue Thresholds' (eds. J. Bäcklund, A. F. Blom, and C. J. Beevers), Vol. 1, 391; 1982, EMAS Ltd., Warley, U.K.

122. S. Suresh and R. O. Ritchie: Scripta Met., 1983, 17, 575.

123. R. A. Schmidt and P. C. Paris: 'Progress in Flaw Growth and Fracture Toughness Testing,' ASTM STP 536, 79; 1973, American Society for Testing and Materials, Philadelphia, PA.

124. R. O. Ritchie, S. Suresh, and P. K. Liaw: 'Ultrasonic Fatigue' (eds. J. M. Wells, O. Buck, L. D. Roth, and J. K. Tien), 433; 1982, The Metallurgical Society of AIME, Warrendale, PA.

125. S. Suresh and R. O. Ritchie: 'Concepts of Fatigue Crack Growth Thresholds' (eds. D. L. Davidson and S. Suresh), 1983, The Metallurgical Society of AIME, Warrendale, PA.

126. S. Suresh: Scripta Met., 1982, 16, 995.

127. S. Suresh: Eng. Fract. Mech., 1983, 18, 577.

128. S. Suresh and A. K. Vasudévan: 'Concepts of Fatigue Crack Growth Thresholds' (eds. D. L. Davidson and S. Suresh), 1983, The Metallurgical Society of AIME, Warrendale, PA.

129. R. J. Cooke, P. E. Irving, G. S. Booth, and C. J. Beevers: Eng. Fract. Mech., 1975, 7, 69.

130. B. F. Jones: J. Mater. Sci., 1982, 17, 499.

131. K. J. Miller: Fat. Eng. Mat. Struct., 1982, 5, 223.

132. W. T. Chiang and K. J. Miller: Fat. Eng. Mat. Struct., 1982, 5, 249.

133. A. Talug and K. Reifsnider: 'Cyclic Stress-Strain and Plastic Deformation Aspects of Fatigue Crack Growth,' ASTM STP 637, 81; 1977, American Society for Testing and Materials, Philadelphia, PA.

134. R. J. Allen and J. C. Sinclair: Fat. Eng. Mat. Struct., 1982, 5, 343.

135. J. C. Newman, Jr.: 'Behavior of Short Cracks in Airframe Components,' Proc. 55th Specialists Meeting of AGARD Structural and Materials Panel, 1983, in press, Advisory Group for Aeronautical Research and Development, France.

136. T. Kunio and K. Yamada: 'Fatigue Mechanisms,' ASTM STP 675, 342; 1979, American Society for Testing and Materials, Philadelphia, PA.

137. B. A. Bilby, C. E. Cardew and I. C. Howard: Fracture 1977 (ed. D. M. R. Taplin), Vol. 3, 197; 1977, Pergamon Press, New York.

138. B. Cotterell and J. R. Rice: Int. J. Fract., 1980, 16, 155.

139. P. J. E. Forsyth: 'Crack Propagation,' Proc. Symp., Cranfield College of Aeronautics, 76; 1962, Cranfield Press, Cranfield, U.K.

140. R. M. McMeeking and A. G. Evans: J. Amer. Cer. Soc., 1982, 65, 242.

141. J. M. Potter: 'Behavior of Short Cracks in Airframe Components,' Proc. 55th Specialists Meeting of AGARD Structural and Materials Panel, 1983, in press, Advisory Group for Aeronautical Research and Development, France.

142. K. A. Esaklul, A. G. Wright, and W. W. Gerberich: Scripta Met., 1983, 17, in press.

143. C. Laird: 'Fatigue and Microstructure,' 149; 1979, American Society for Metals, Metals Park, OH.

144. H. Mughrabi: 'Strength of Metals and Alloys,' Proc. 5th Int. Conf. (eds. P. Haasen, V. Gerold, and G. Kostotz), Vol. 3; 1979, Pergamon Press, New York.

145. G. Lütjering, H. Doker, and D. Munz: 'The Microstructure and Design of Alloys,' Proc. 3rd Int. Conf., Vol. 2, 427; 1973, Institute of Metals/Iron and Steel Institute, London, U.K.

146. P. Neumann: Z. Metallk., 1967, 58, 780.

147. J. G. Antonopoulos, L. M. Brown, and A. T. Winter: Phil. Mag., 1976, 34, 549.

148. K. Katagiri, A. Omura, K. Koyanagi, J. Awatani, T. Shiraishi, and H. Kaneshiro: Met. Trans. A, 1977, 8A, 1769.

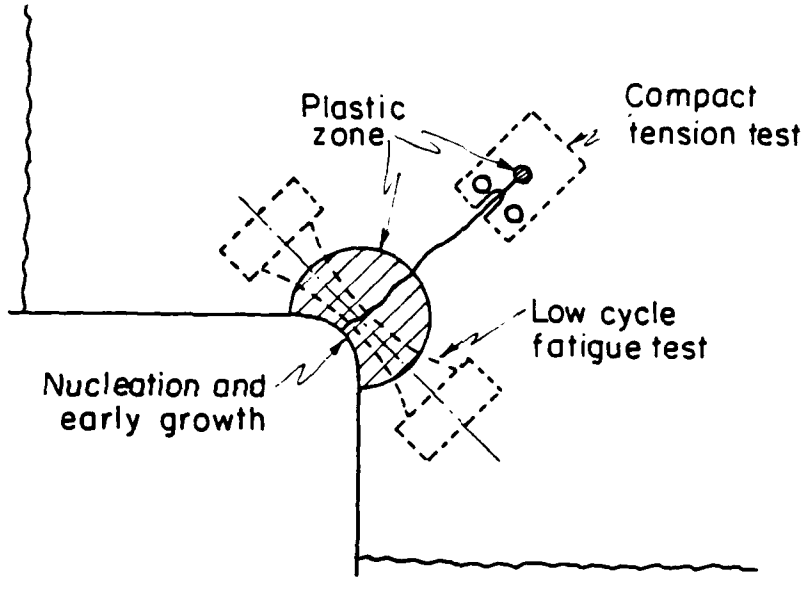

XBL 836-10184

1. Schematic showing the various stages of fatigue in engineering components and typical tests to evaluate fatigue life in the laboratory (after Ref. 2).

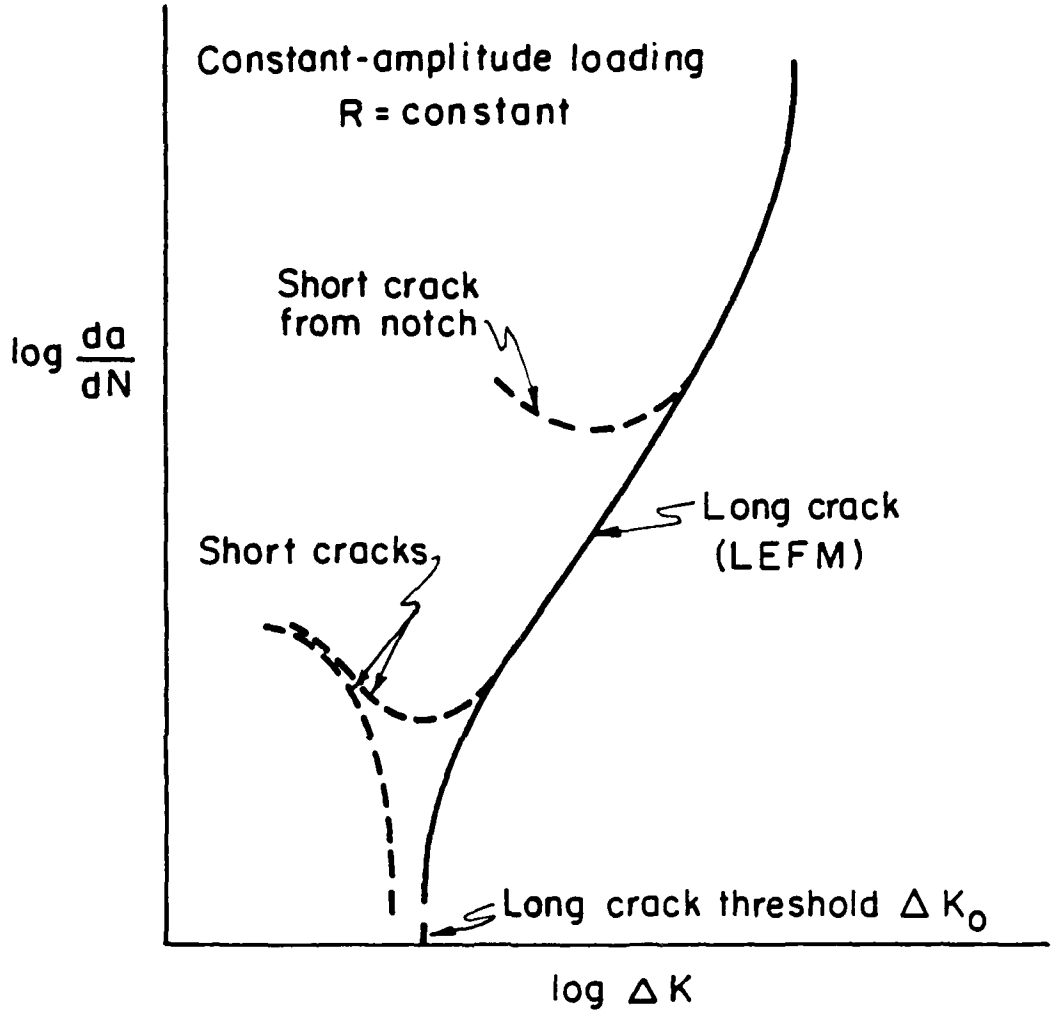

XBL 835-9687

2. Schematic representation of typical fatigue crack propagation rate (da/dN) data for long and short cracks as a function of the stress intensity factor range (ΔK).

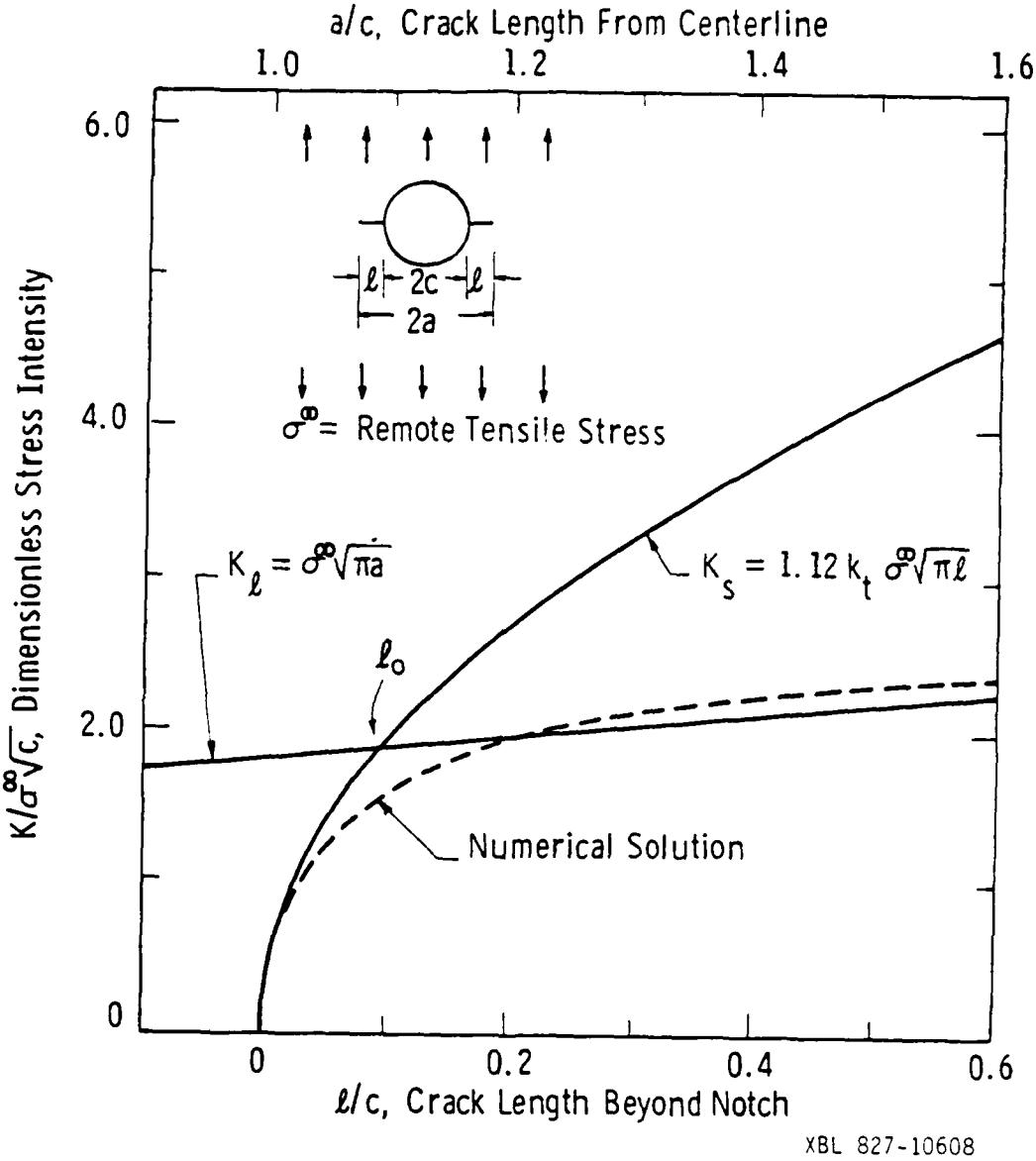

3. Linear elastic K_I solutions for a crack, of length ℓ, emanating from a circular notch, of radius c, in an infinite plate subjected to a remotely applied uniaxial tensile stress σ. Short (K_s) and long (K_ℓ) crack limiting solutions and numerical solutions are shown (after Ref. 21).

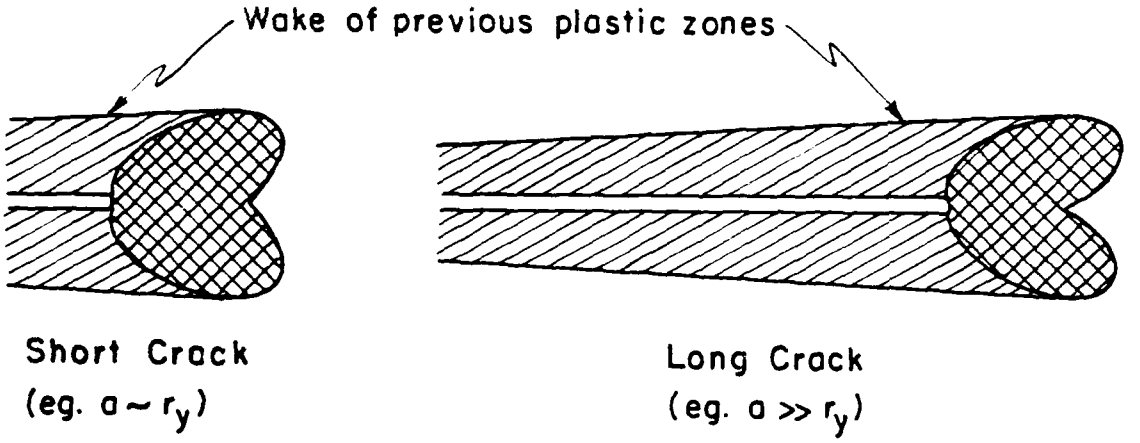

XBL 836-10185

4. Schematic representation of the similitude concept, which implies that cracks of differing length (a) subjected to the same *nominal* driving force (e.g., ΔK) have equal plastic zone sizes r_y ahead of the crack and will, therefore, advance by equal increments Δa per cycle: (a) short crack ($a \approx r_y$); (b) long crack ($a >> r_y$).

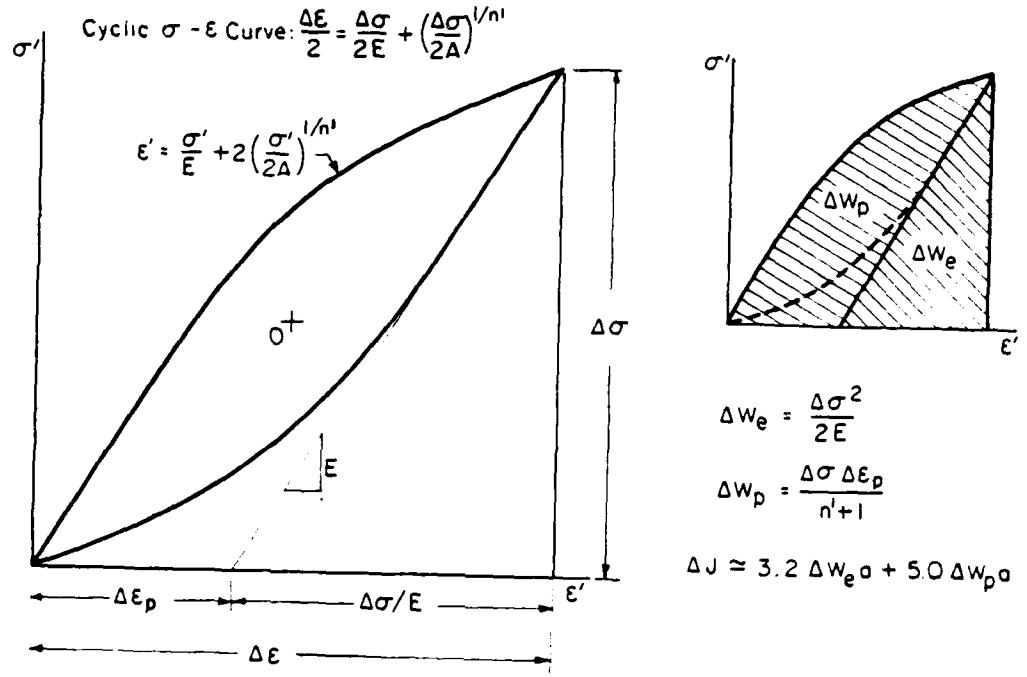

XBL 836-10304

5. Procedure to estimate ΔJ, from stress-strain hysteresis loops, for the growth of small cracks during low cycle fatigue of smooth axial specimens (after Ref. 51).

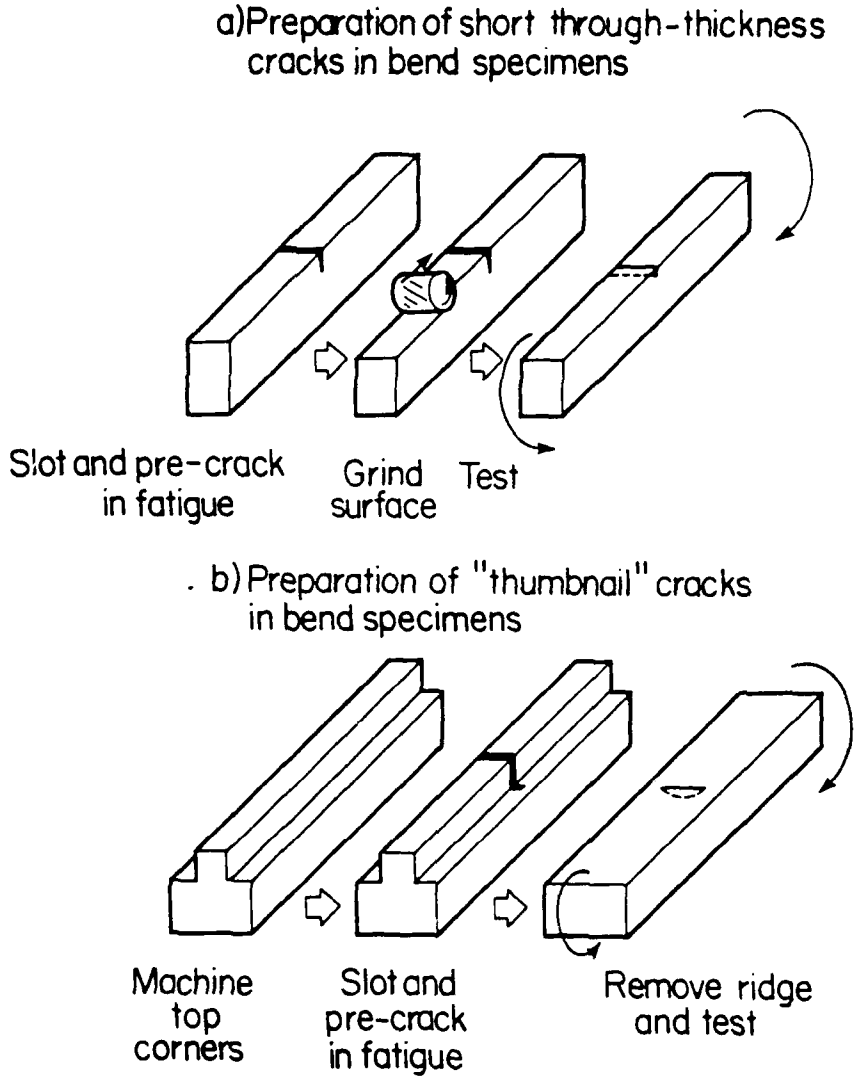

6. Preparation techniques to obtain "through-thickness" and 'thumbnail" short cracks (after Ref. 58).

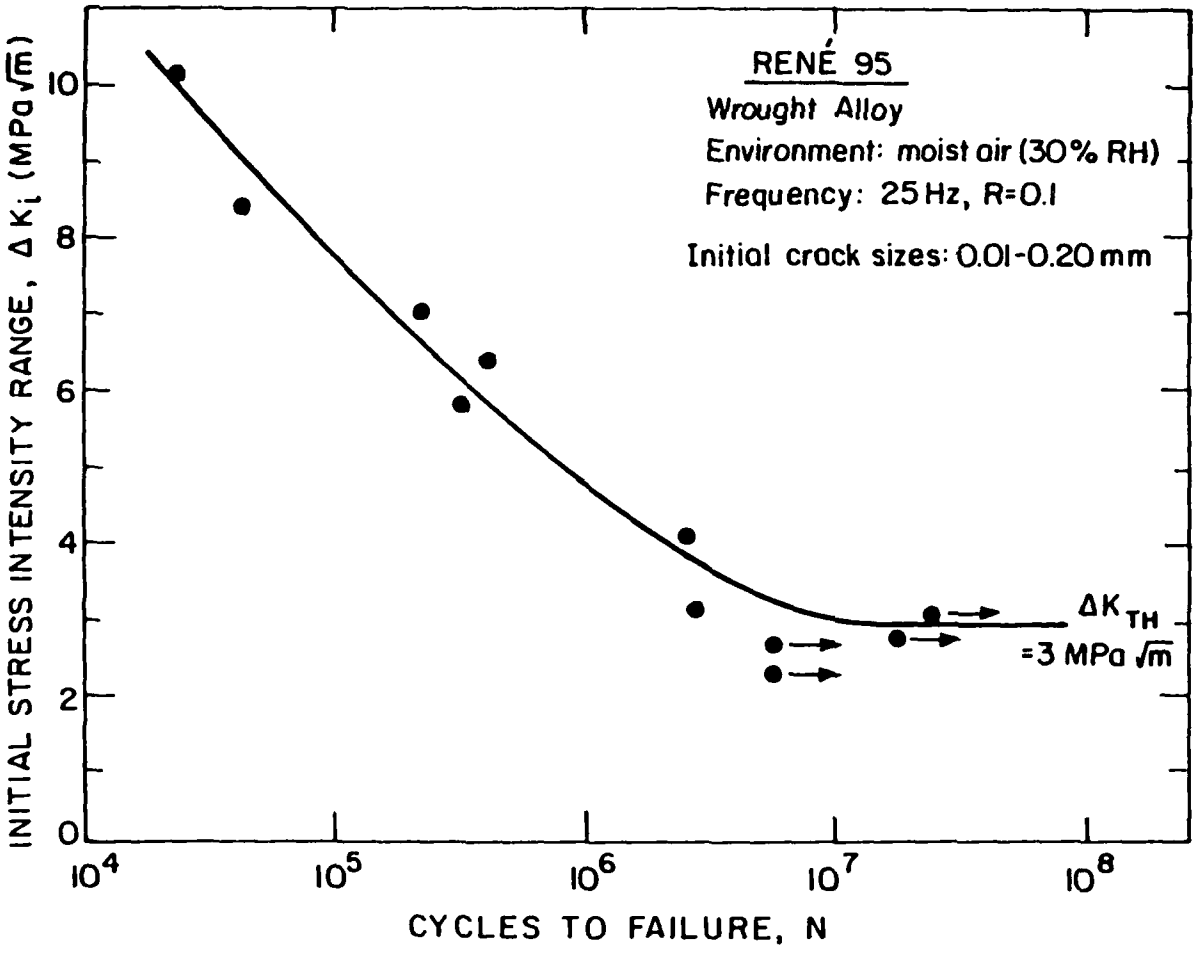

7. Variation of the initial stress intensity ΔK_i with the number N of cycles to failure for physically short cracks in wrought René 95 (σ_o = 1400 MPa), showing the definition of threshold ΔK_{TH} for 0.01-0.2 mm cracks, fatigue-tested in a moist air environment at a frequency of 25 Hz and R = 0.1 (after Ref. 60).

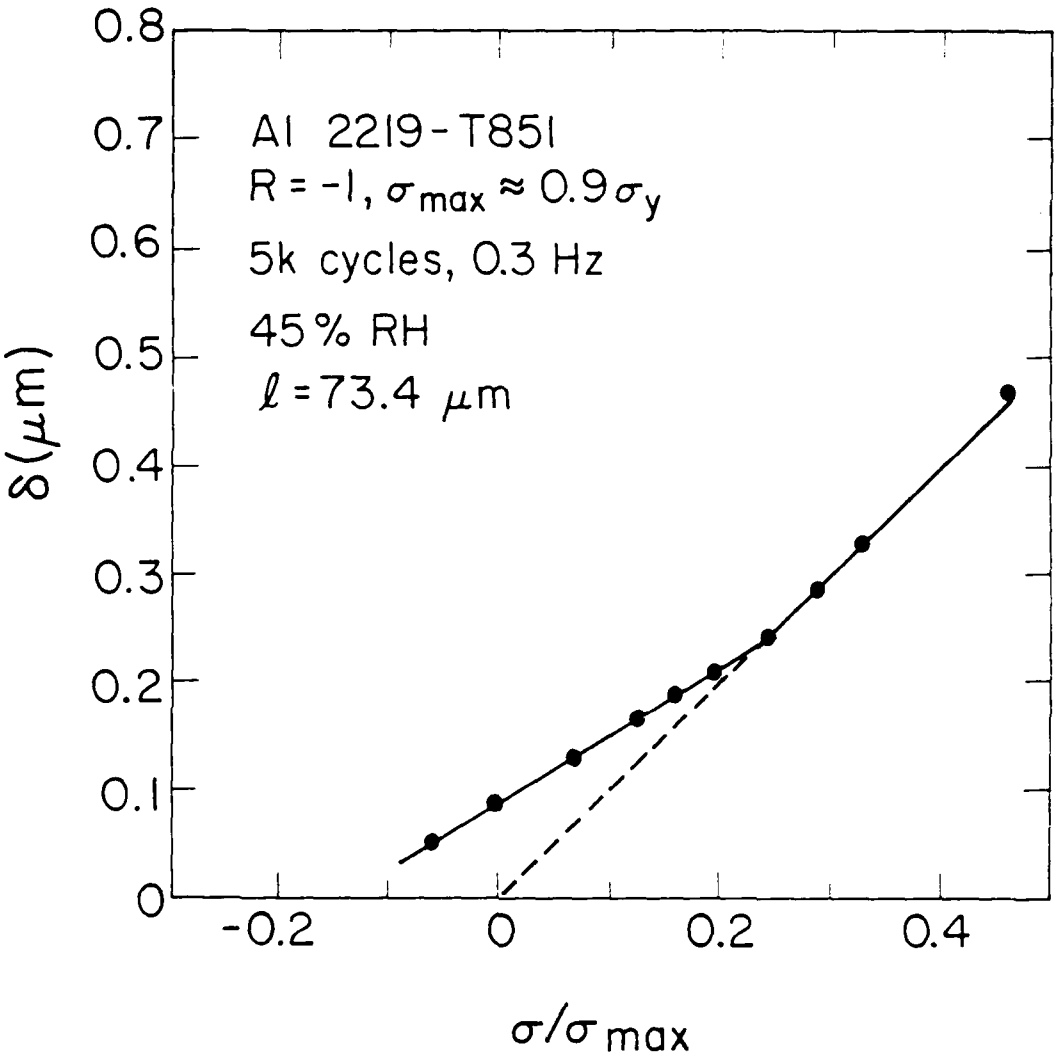

XBL 836-2662

8. Typical micro-crack compliance curve for 2219-T851 aluminum alloy; δ is the opening across the micro-crack and σ/σ_{max}, the fraction of maximum load applied during fatigue (after Ref. 41).

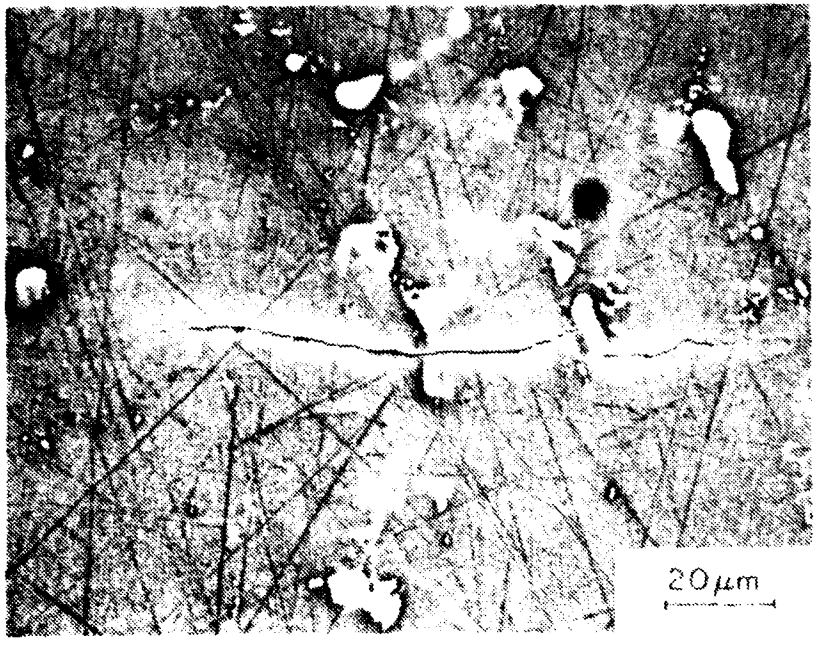

9. Appearance of a typical surface micro-crack initiated at a β phase (Cu_2FeAl_7) intermetallic in 2219-T851 aluminum alloy fatigue-tested in humid air (after Ref. 45).

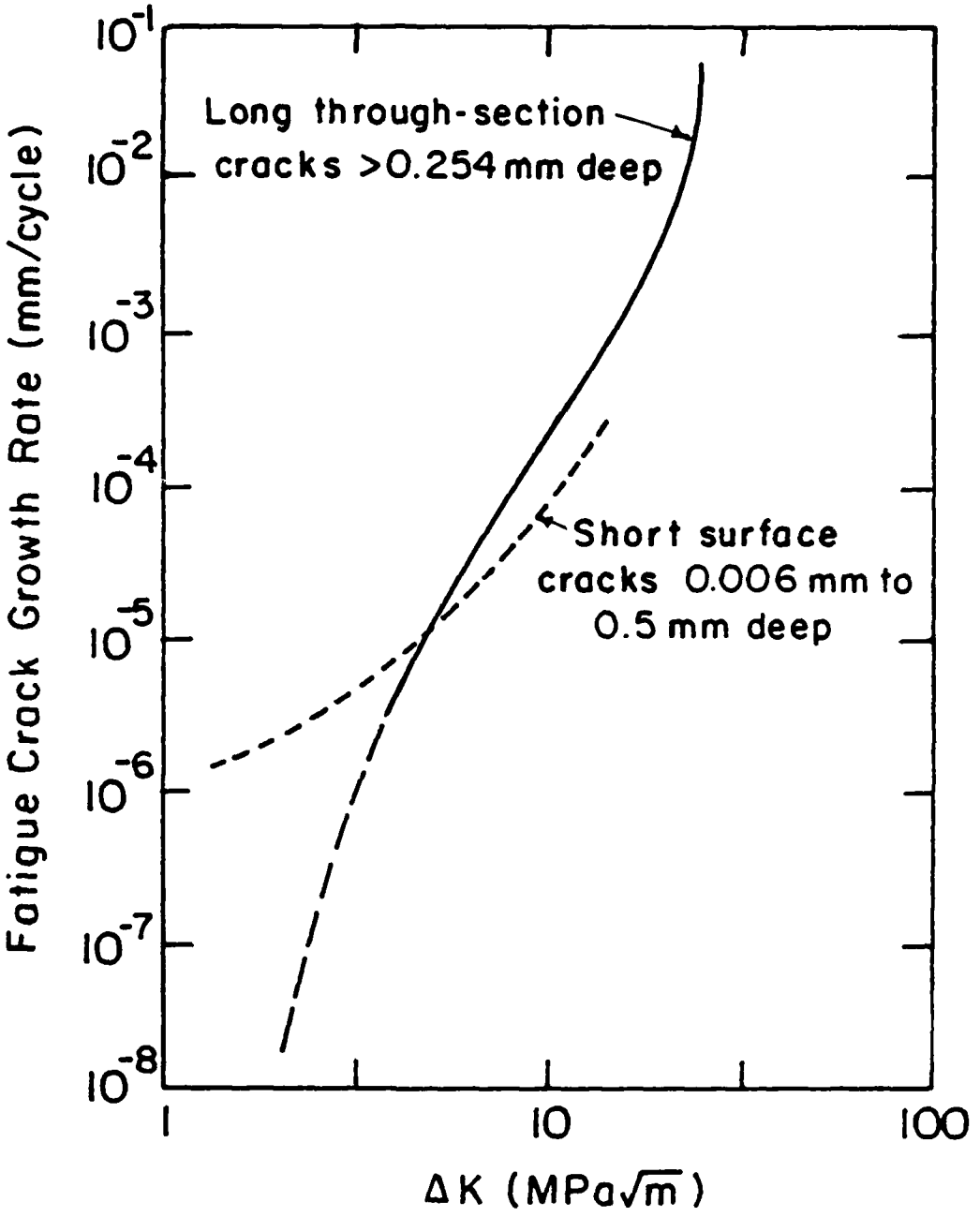

10. Variation of short and long crack fatigue crack propagation rates (da/dN) as a function of stress intensity factor range (ΔK) for precipitation hardened aluminum alloys (after Ref. 68).

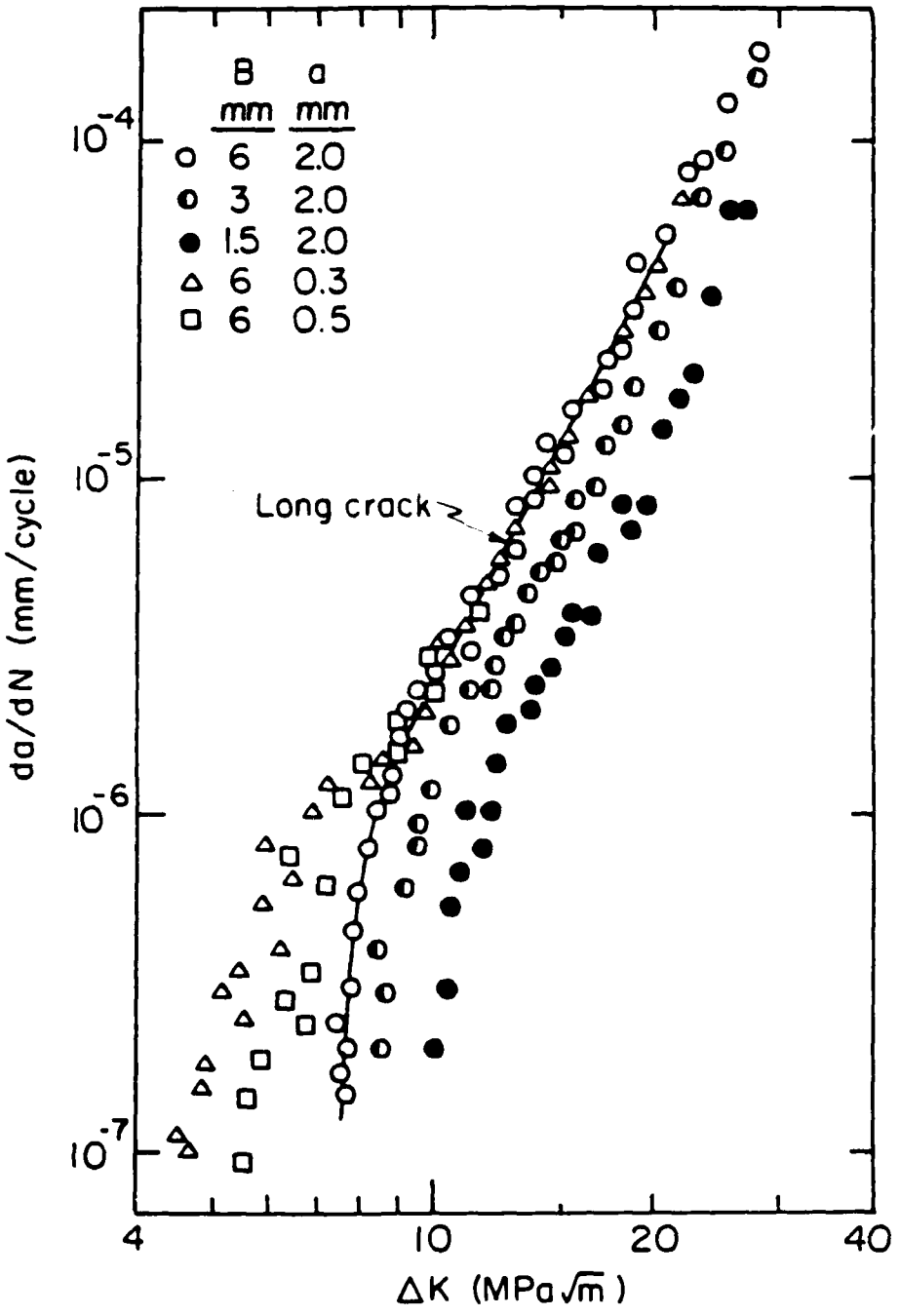

XBL 836-10300

11. Variation of short and long crack fatigue crack propagation rates (da/dN) as a function of stress intensity factor range (ΔK) for 0.035%C mild steel of yield strength σ_0 = 242 MPa (after Ref. 69).

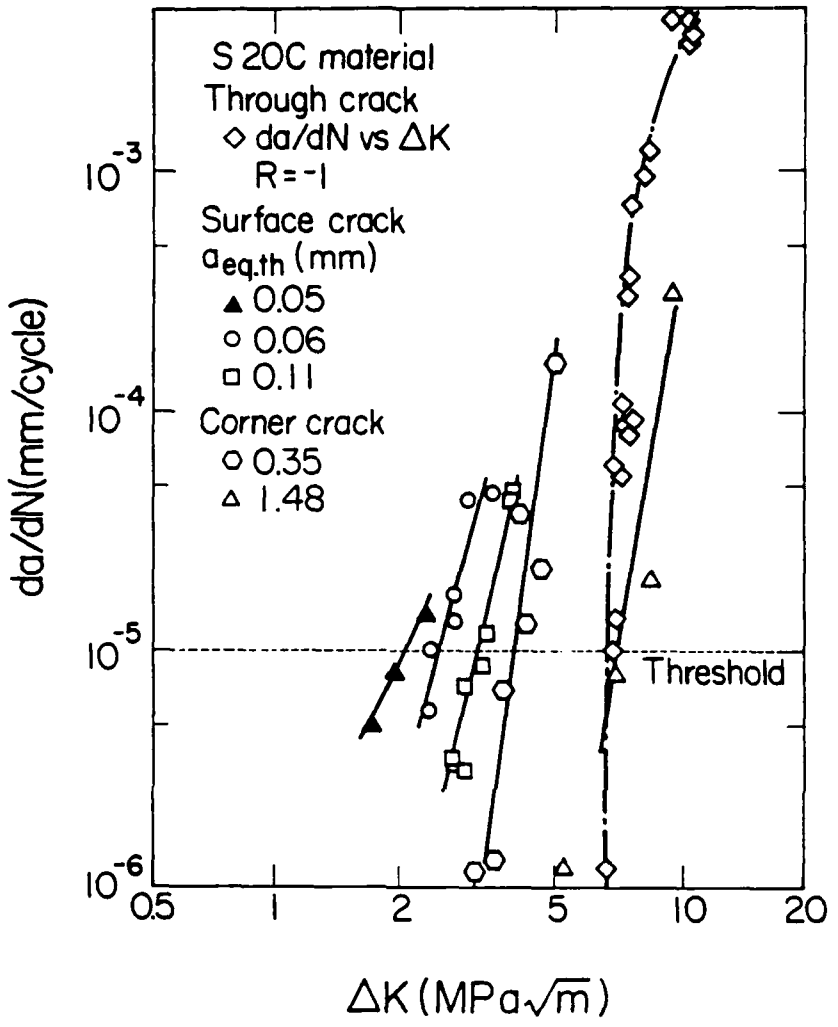

12. Variation of short and long crack fatigue crack propagation rates (da/dN) as a function of stress intensity factor range (ΔK) for a 3% Si iron of yield strength 431 MPa (after Ref. 70).

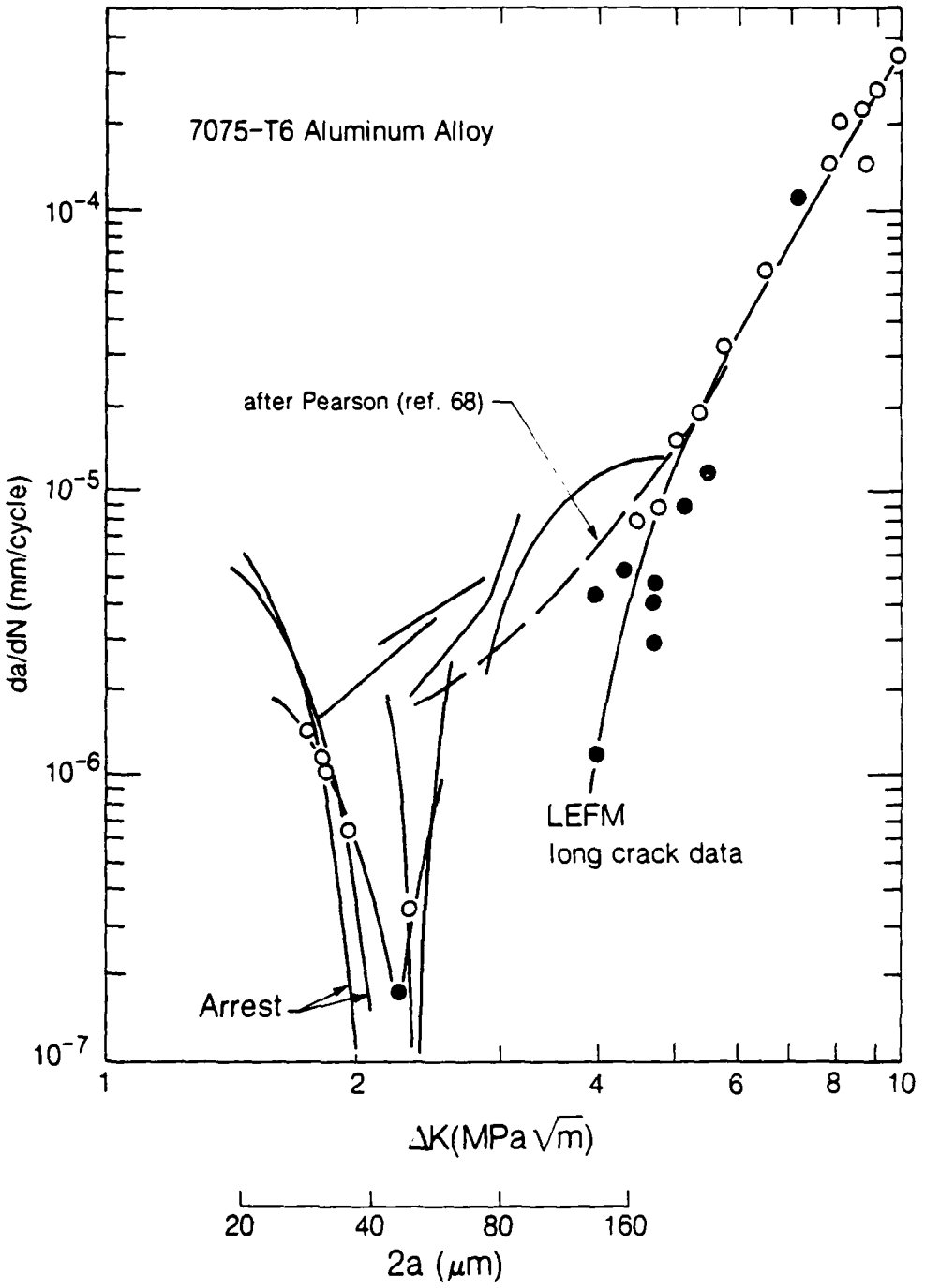

XBL835-913

13. Variation of short and long crack fatigue crack propagation rates (da/dN) as a function of stress intensity factor range (ΔK) for peak aged Al-Zn-Mg alloy (7075-T6) of yield strength σ_0 = 515 MPa (after Ref. 71).

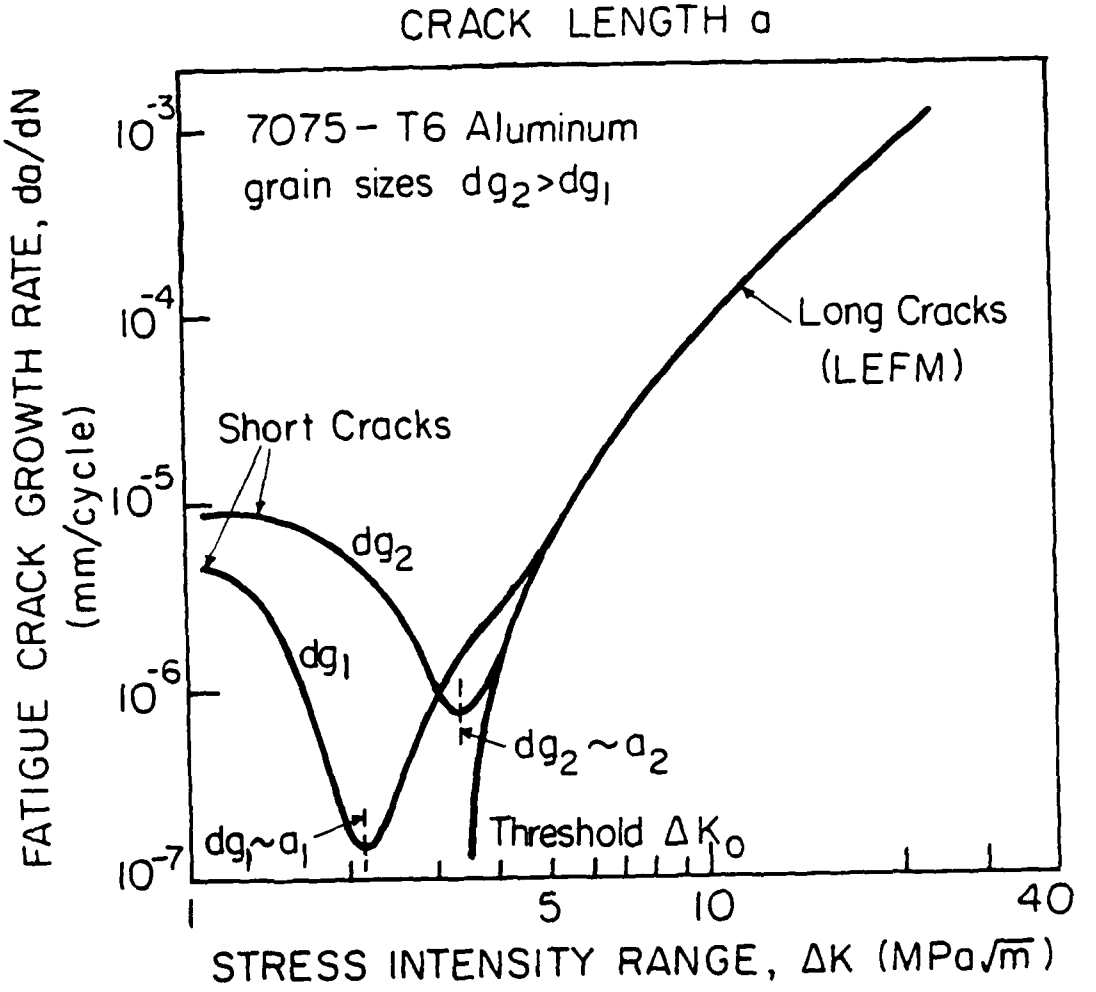

XBL 828-6266

14. Effect of grain size (d_g) on the growth of microstructurally-short and long cracks in 7075-T6 aluminum alloy (σ_o = 515 MPa). Microcracks grow below the long crack threshold ΔK_o and further, for the two grain sizes ($d_{g_2} > d_{g_1}$), show growth rate minima approximately where crack length $a \sim$ grain size d_g (after Ref. 71).

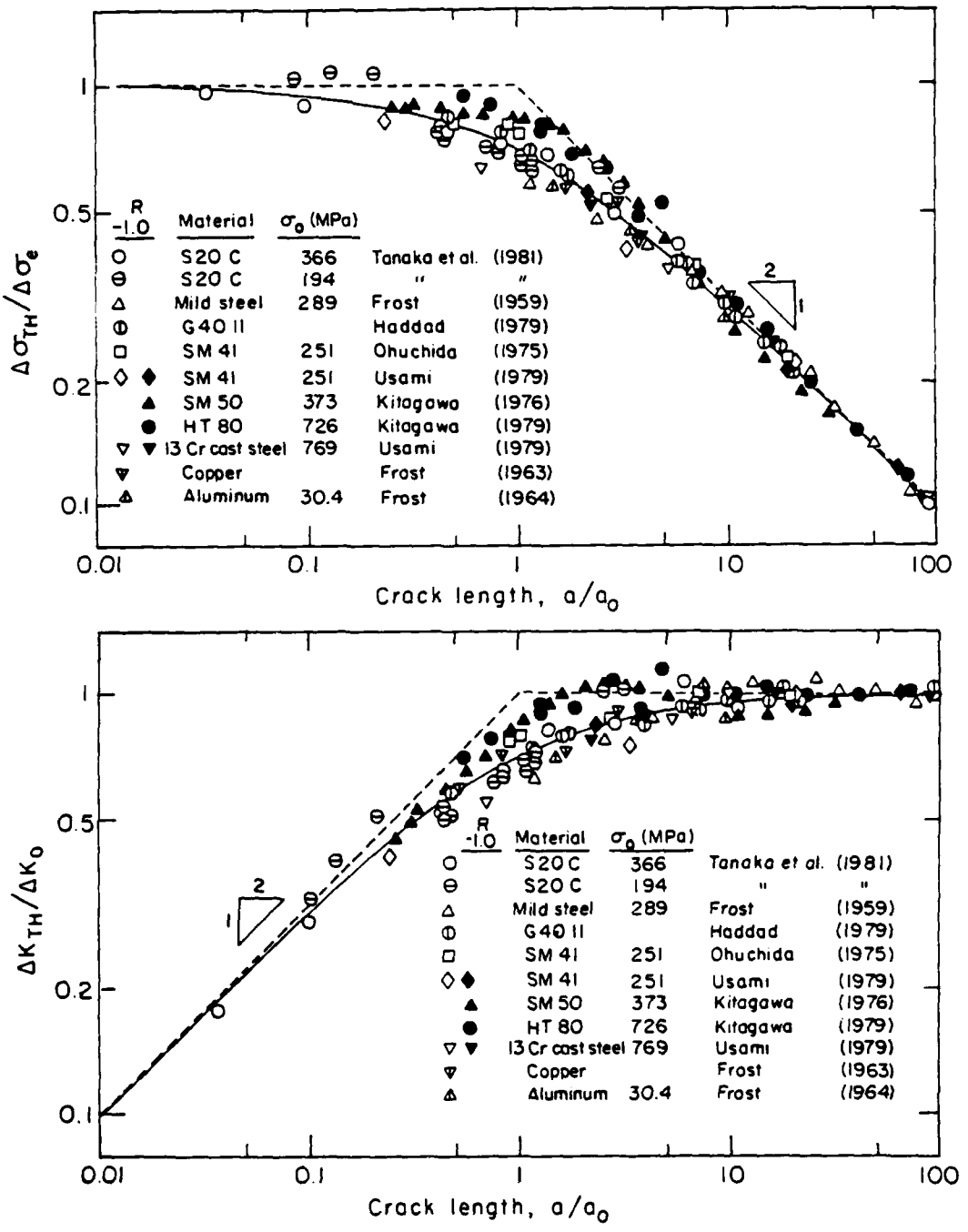

XBL 828-10818

15. Variation of threshold stress ($\Delta\sigma_{TH}$), normalized with respect to the smooth bar fatigue limit ($\Delta\sigma_e$), and threshold stress intensity range (ΔK_{TH}), normalized with respect to the long crack threshold (ΔK_o), with crack length (a), normalized with respect to the intrinsic crack length ($a_o = 1/\pi[\Delta K_o/\Delta\sigma_e]^2$) (after Ref. 76).

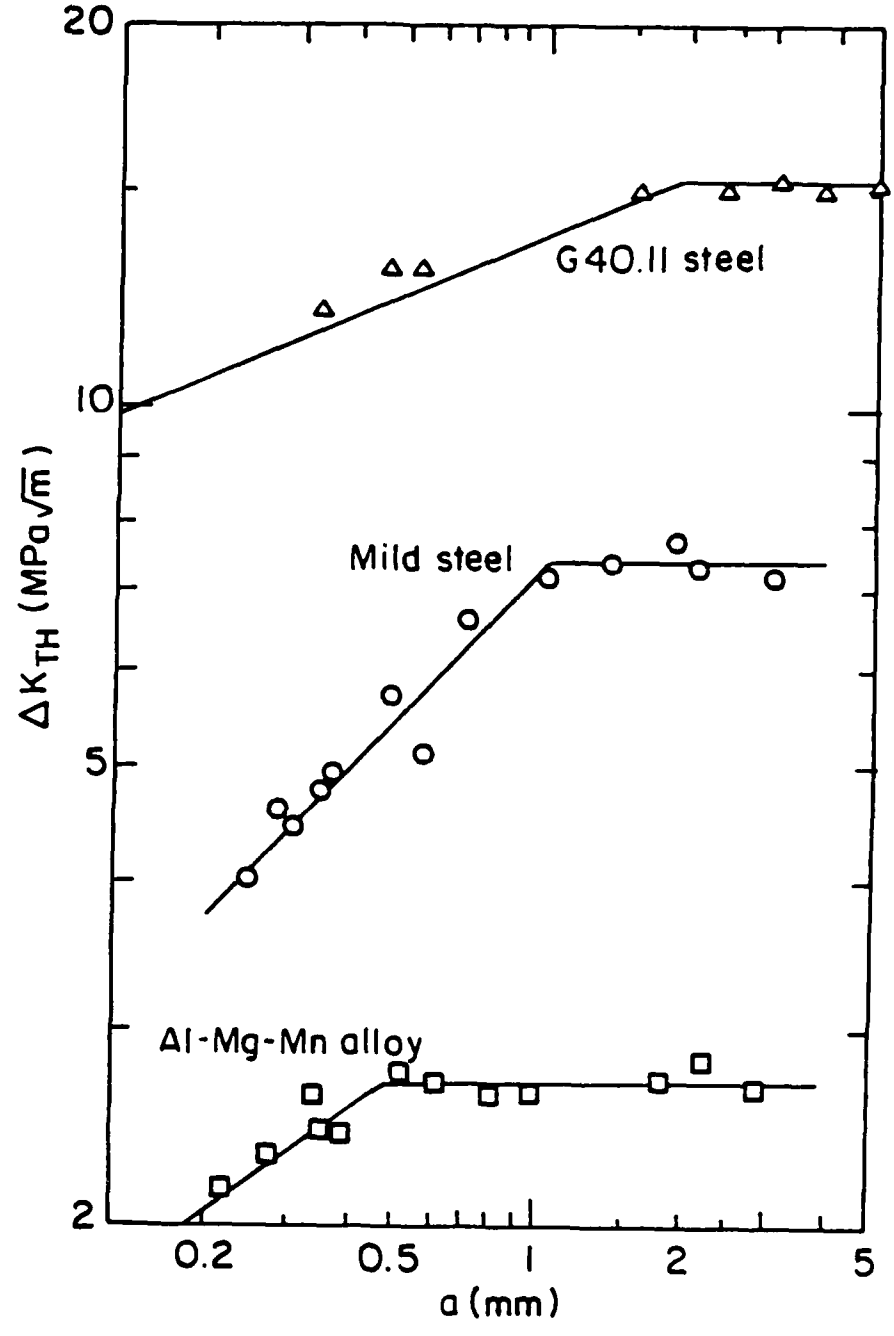

XBL 836-10302

16. Variation of threshold stress intensity range (ΔK_{TH}) with short crack length (a) in an austenitic 0.45% C (G40.11) steel (σ_o = 550 MPa), a 0.035% C mild steel (σ_o = 242 MPa) and an Al-Zn-Mg alloy (σ_o = 180 MPa) (after Ref. 69).

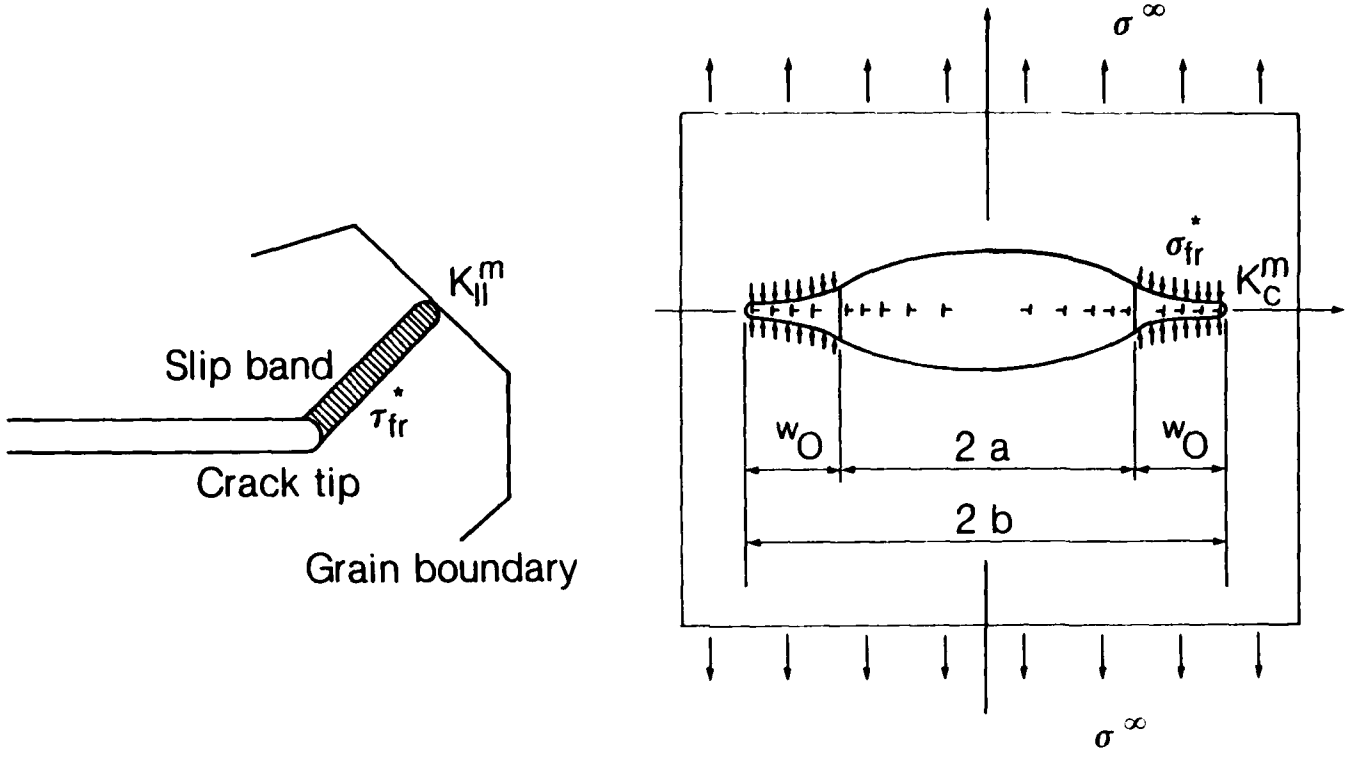

XBL 835-916

17. Schematic illustration of the model of a crack-tip slip band blocked by grain boundary (after Ref. 76); a) crack-tip slip band blocked by grain boundary and b) coplanar slip band emanating from the tip of isolated crack.

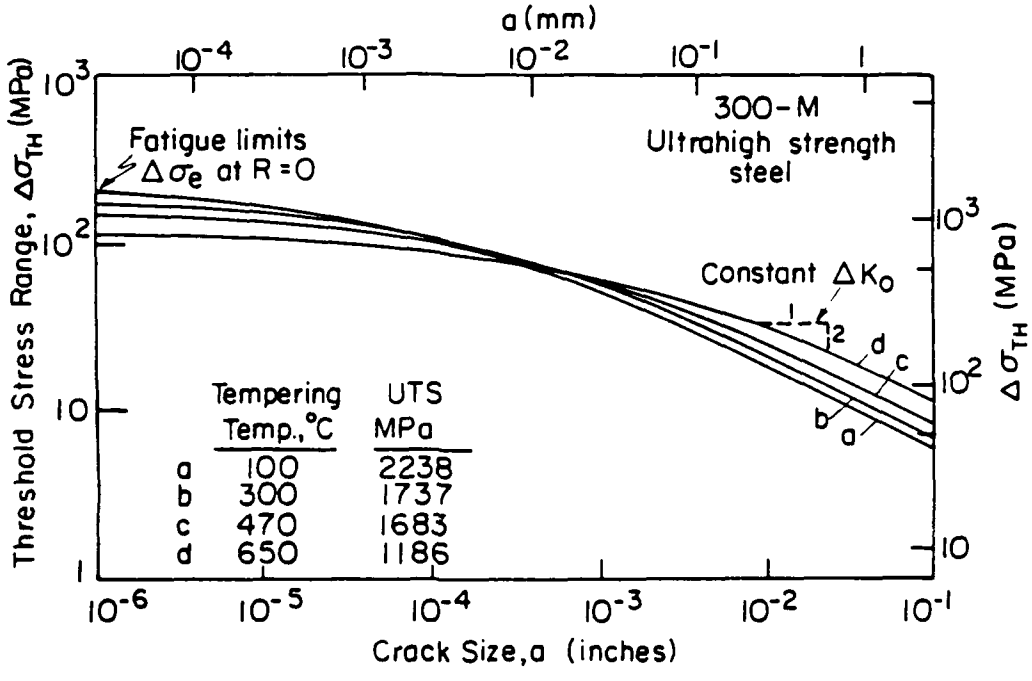

18. Predicted variation of threshold stress $\Delta\sigma_{TH}$ at R = 0 with crack size (a) based on data for 300-M ultrahigh-strength steel (Si-modified AISI 4340), oil quenched and tempered between 100° and 650°C to vary tensile strength (1186 to 2338 MPa) (after Ref. 6).

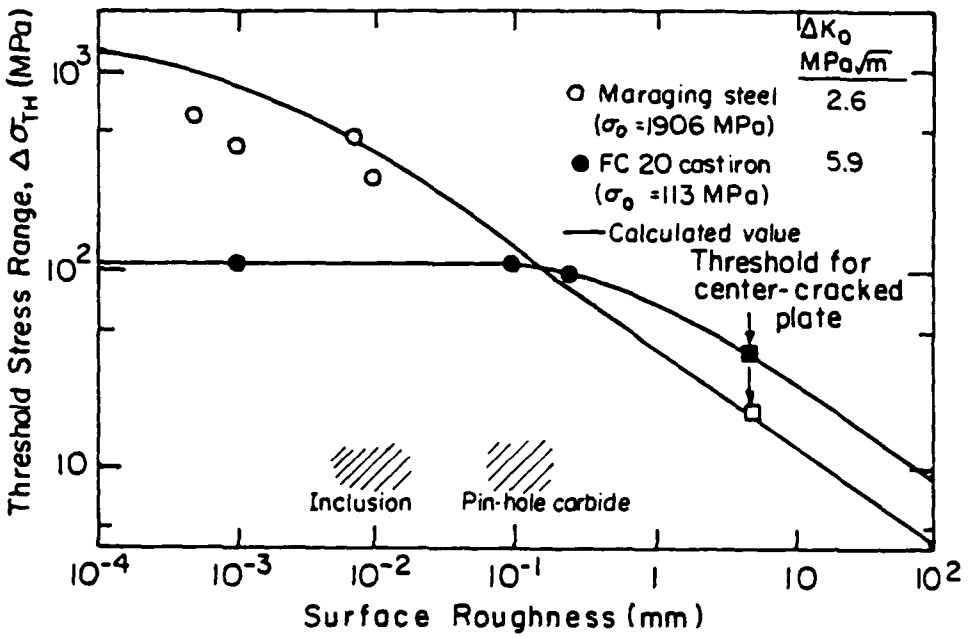

XBL 836-10301

19. A comparison of the threshold behavior between cast iron (σ_0 = 113 MPa) and maraging steel (σ_0 = 1906 MPa), as a function of surface roughness (to simulate crack size) (after Ref. 59).

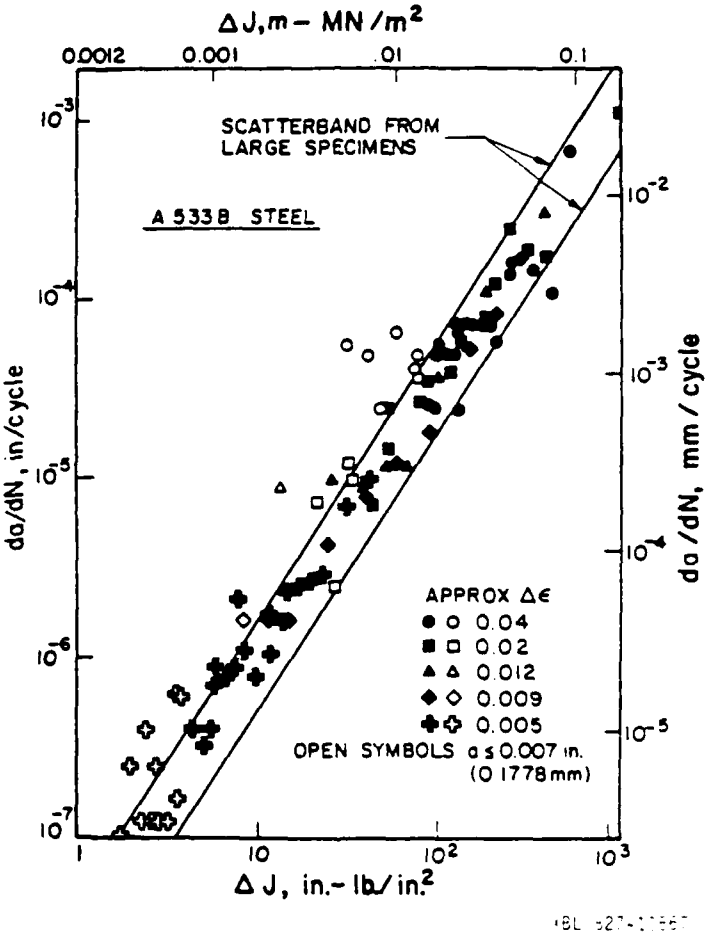

20. Variation of fatigue crack growth rates (da/dN) for long ($a \geq 25$ mm) and short ($a \leq 0.18$ mm) cracks in A533B steel ($\sigma_0 = 480$ MPa) under plastic loading, where the data are analyzed in terms of ΔJ (after Ref. 51).

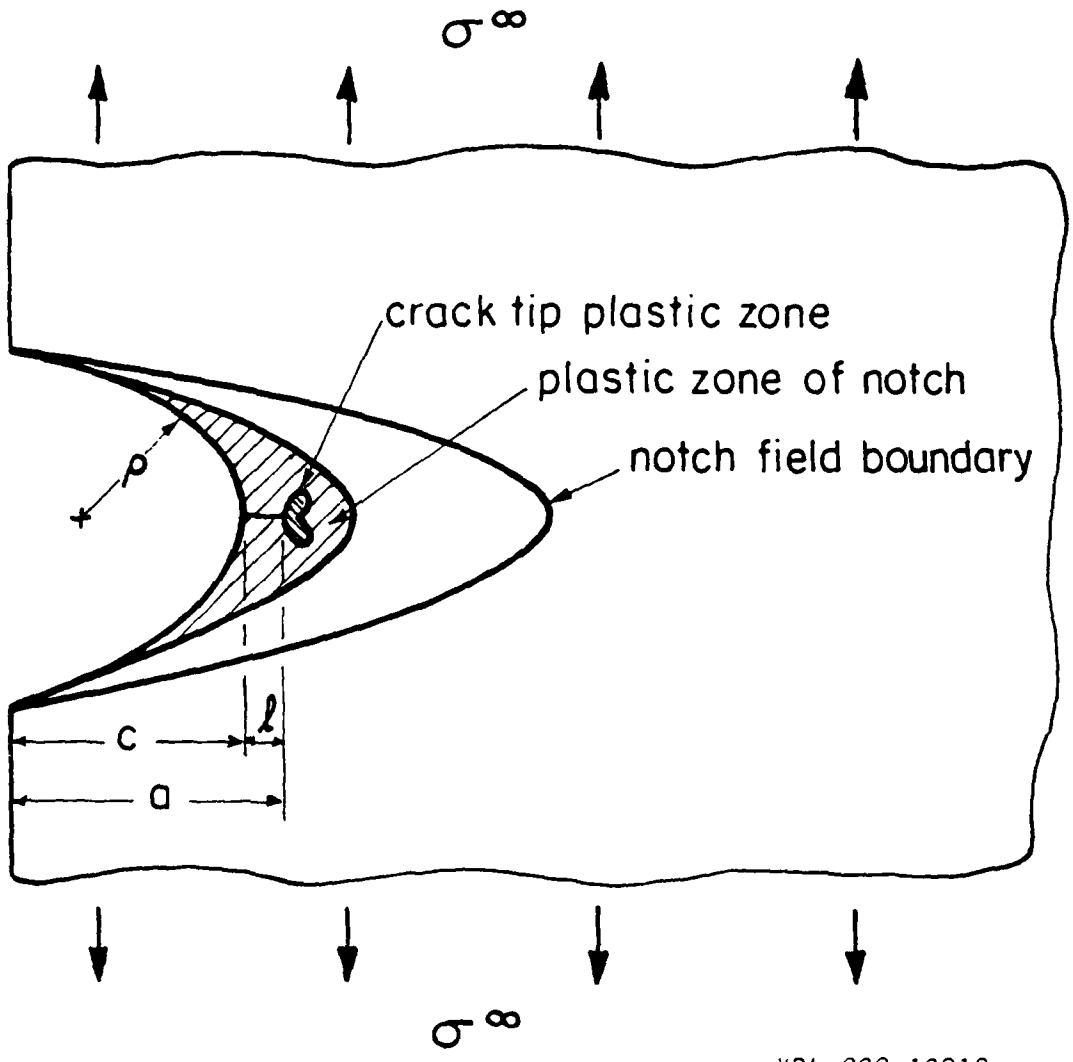

XBL 828-10819

21. Schematic illustration of crack-tip and notch-tip plastic strain fields associated with the growth of a short crack, of length ℓ, emanating from a notch, of depth c, and root radius ρ (after Ref. 109).

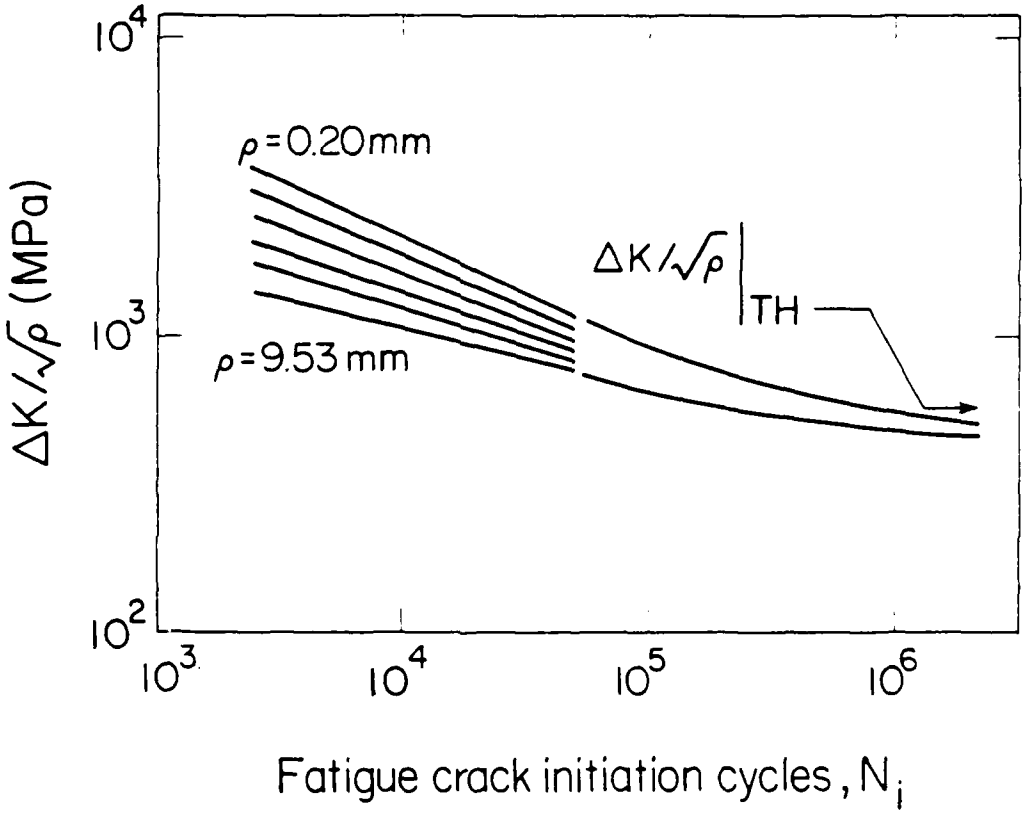

XBL 836-2689

22. Correlation of the fatigue life based on the initiation of an engineering-sized crack with the so-called fatigue crack initiation threshold ($\Delta K/\sqrt{\rho}$), based on results on an HY-130 steel (σ_o = 1000 MPa) tested in double-edge-notched specimens of root radius ρ varying from 0.2 to 9.5 mm (after Ref. 37).

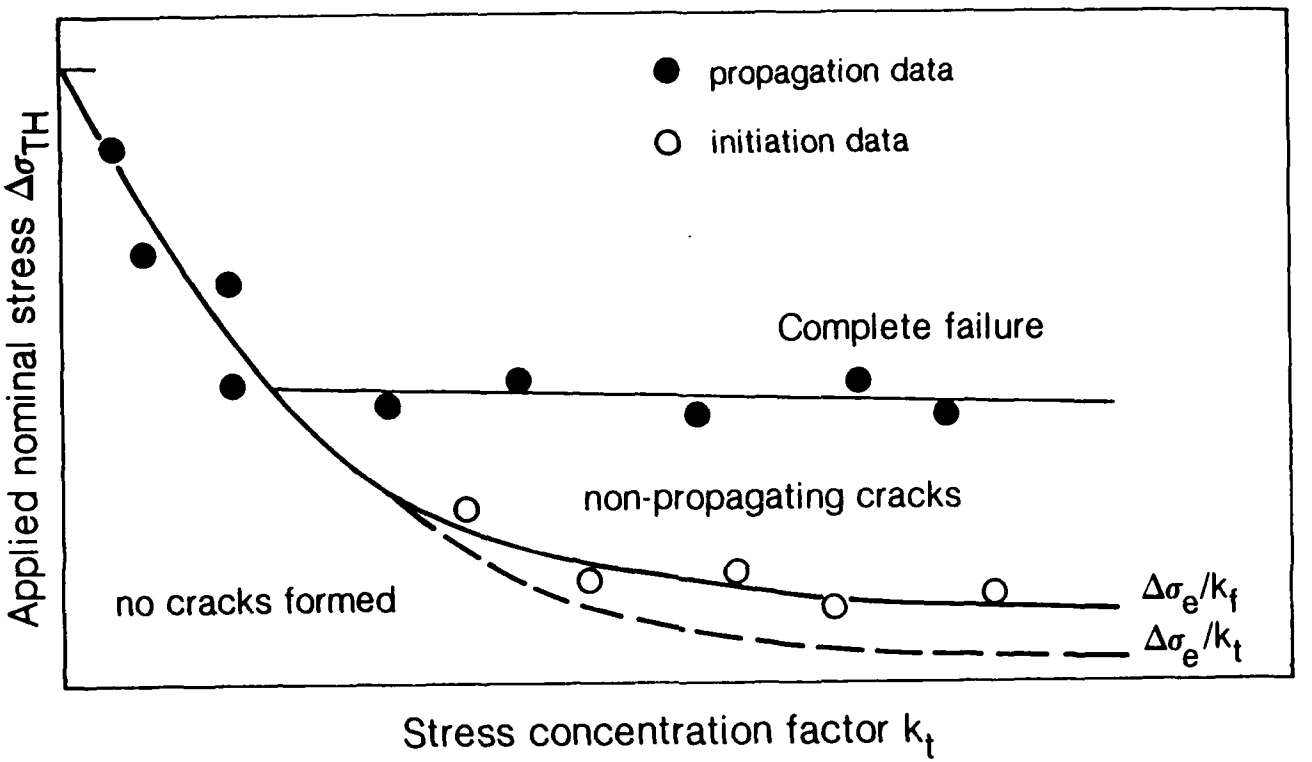

XBL 835-915

23. Variation of threshold stress for crack initiation, i.e., the unnotched fatigue limit $\Delta\sigma_e$ divided by k_f or k_t, as a function of k_t (after Ref. 111).

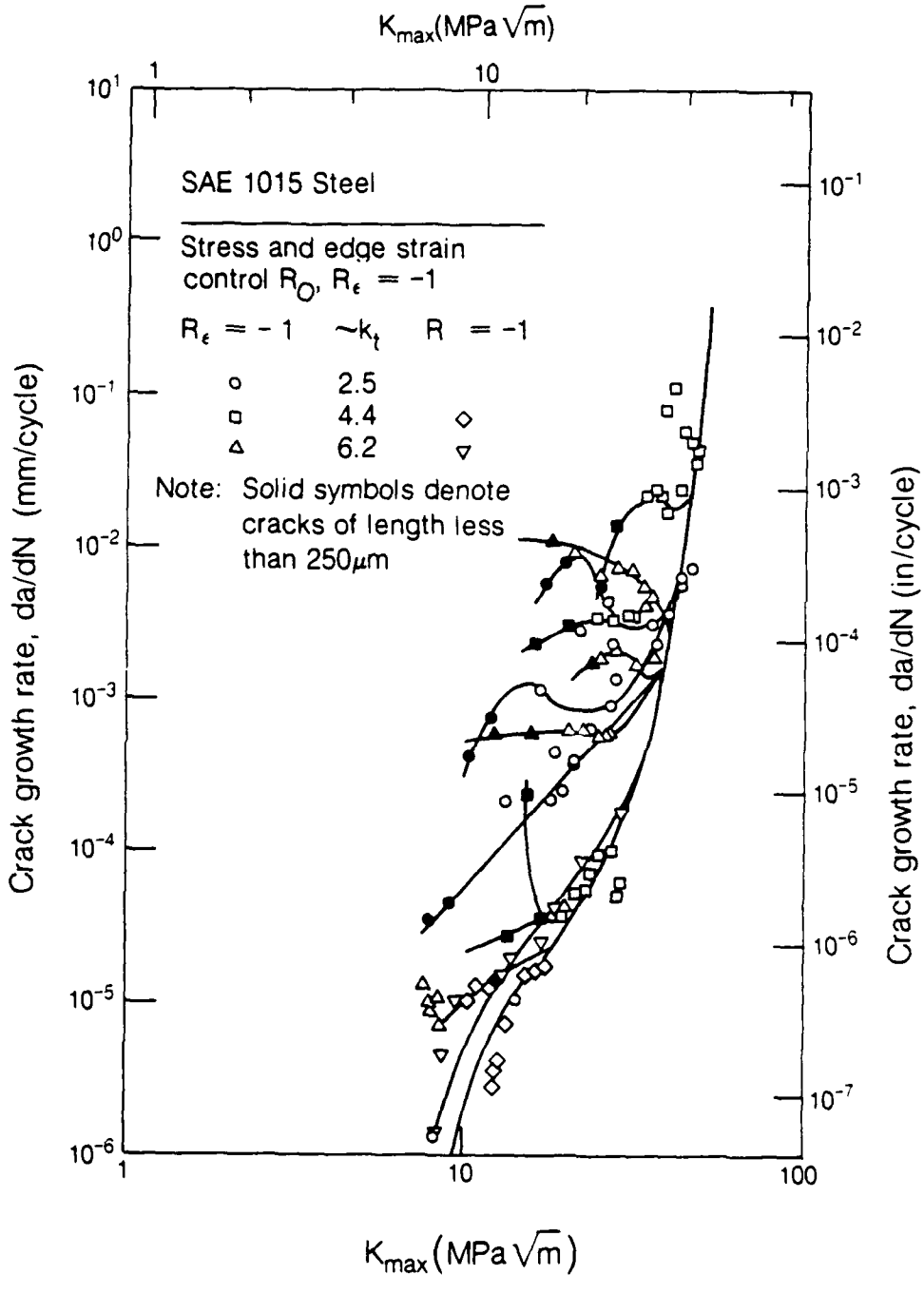

XBL835-912

24. Variation of the propagation rate (da/dN) of cracks emanating from notches as a function of the maximum stress intensity factor (K_{max}) in 0.15% C mild steel. k_t is the theoretical elastic stress concentration factor, R the stress ratio and R_ϵ the edge strain ratio (after Ref. 110).

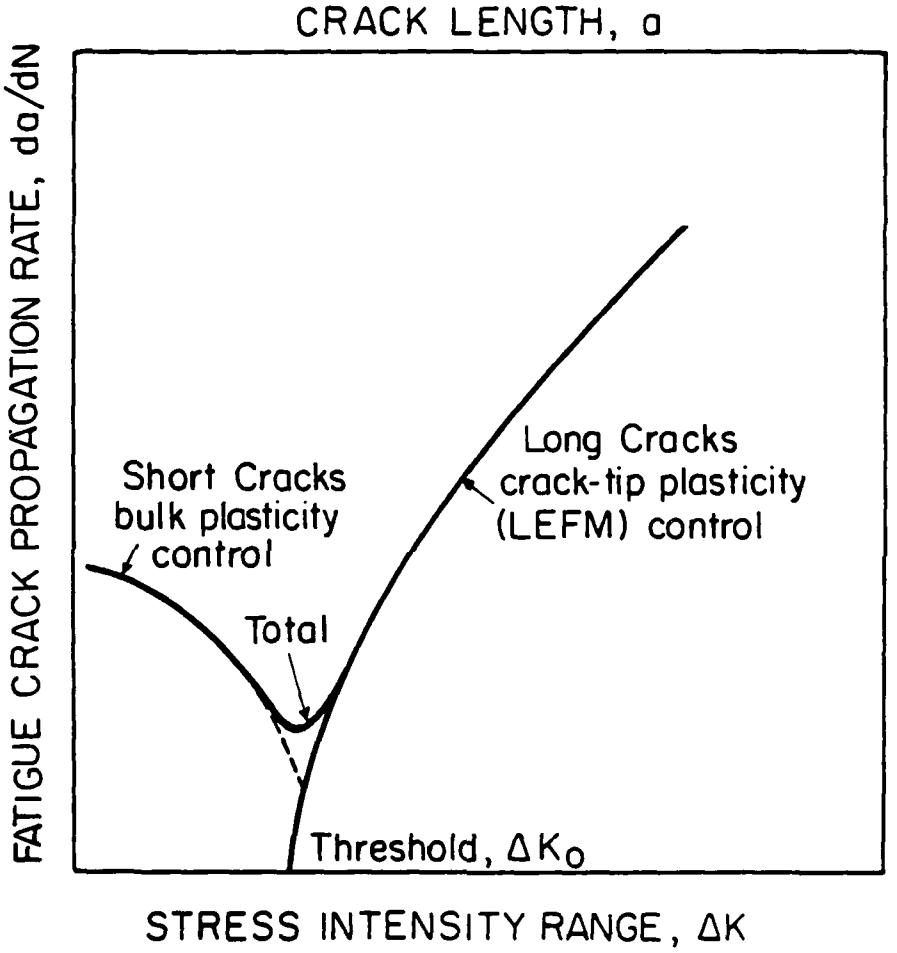

XBL 828-6268

25. Schematic illustration of the elastic-plastic and linear elastic characterization of the kinetics of crack growth for a short crack propagating from a notch, as shown in Fig. 16 (after Ref. 109).

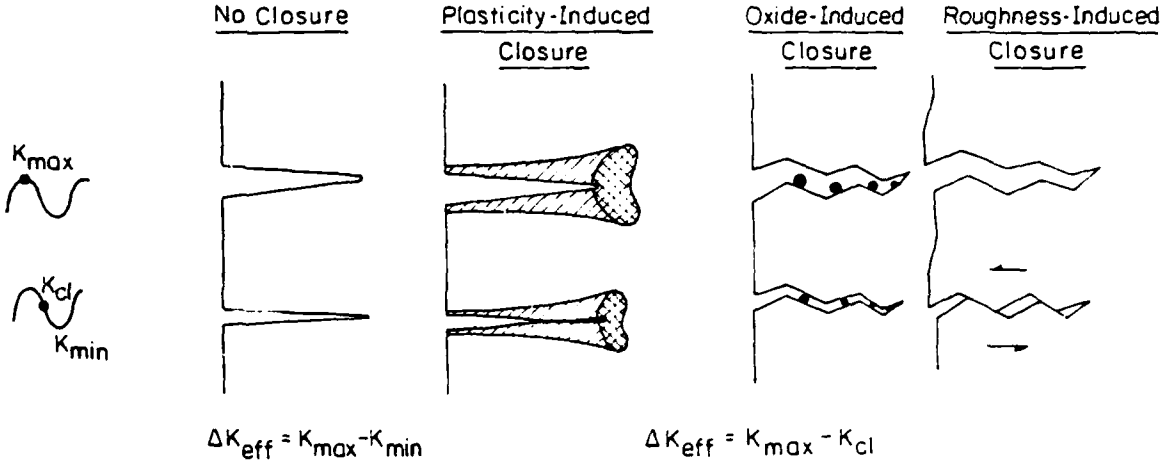

26. Schematic illustration of the mechanisms of fatigue crack closure induced by cyclic plasticity, corrosion deposits and rough fracture morphology. ΔK_{eff} is the effective stress intensity range, defined by $K_{max} - K_{cl}$, where K_{cl} is the stress intensity at which the two fracture surfaces come into contact ($K_{cl} \geq K_{min}$) (after Ref. 119).

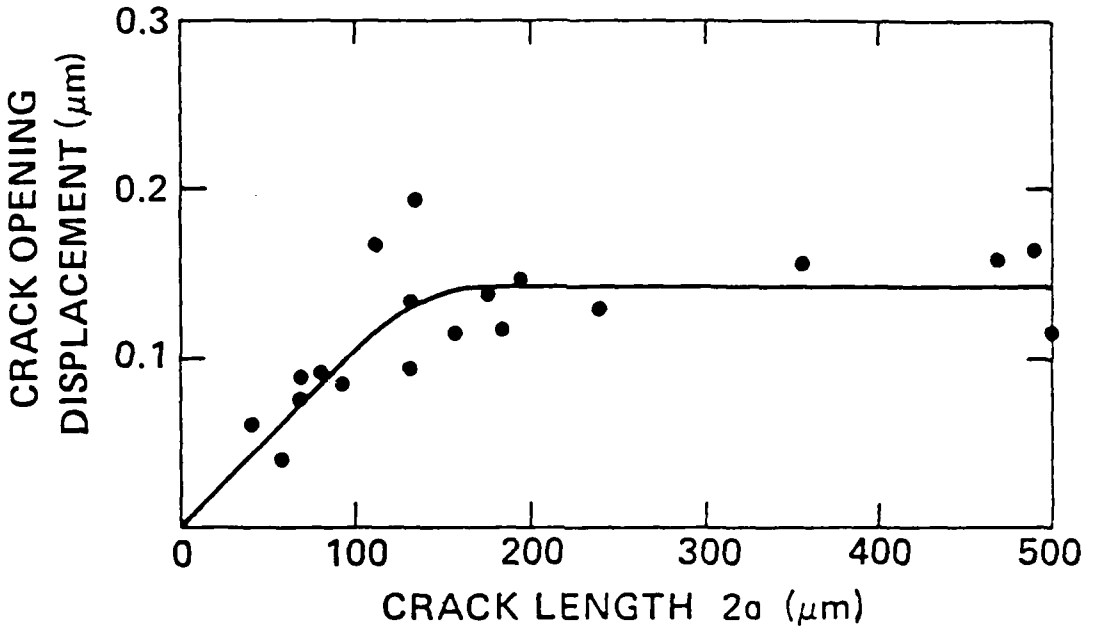

XBL 828-6267

27. Variation of crack mouth opening displacement (at zero load), with crack length a, of small surface cracks in 6Al-2Sn-4Zn-6Mo titanium alloy (σ_0 = 1140 MPa, primary α grain size ≈ 4 μm, β grain size ≈ 12 μm), showing a reduction in crack closure with decreasing crack size (after Ref. 48).

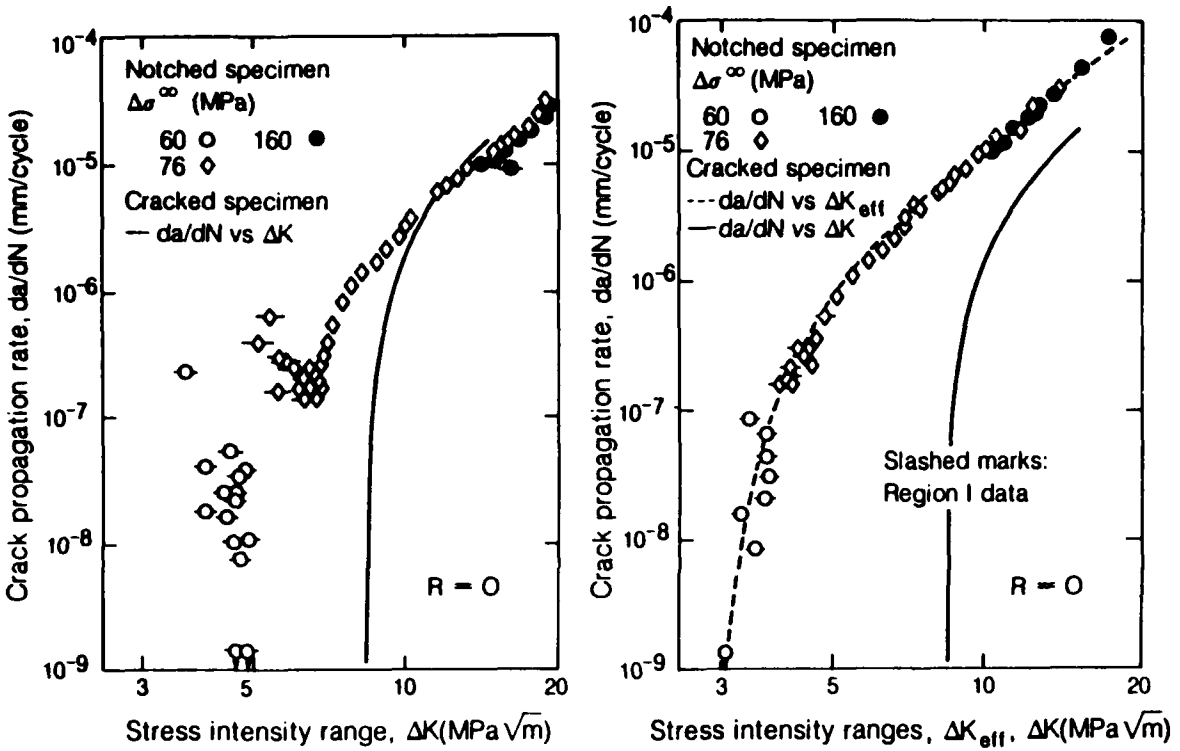

XBL 835-917

28. Variation of crack propagation rate with a) nominal and b) effective stress intensity range values, ΔK and ΔK_{eff}, respectively, in a 0.17% C structural JIM SM416 mild steel (σ_0 = 194 MPa). Note in Fig. b) that the anomalous (sub-threshold) behavior of short cracks is brought into direct correspondence with conventional long crack data when crack closure is accounted for (after Ref. 61).

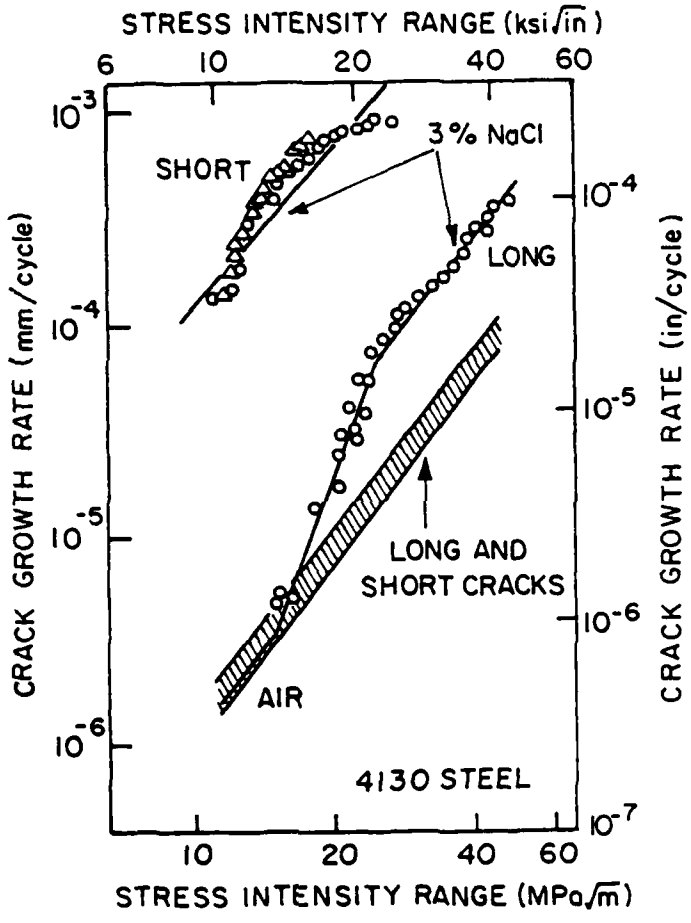

XBL 828-10820

29. Variation of fatigue crack propagation rates (da/dN) as a function of ΔK for long ($a \sim 50$ mm) and physically-short (a = 0.1-0.8 mm) cracks in AISI 4130 steel (σ_0 = 1300 MPa) tested in moist air and aqueous 3% NaCl solution (after Ref. 53).

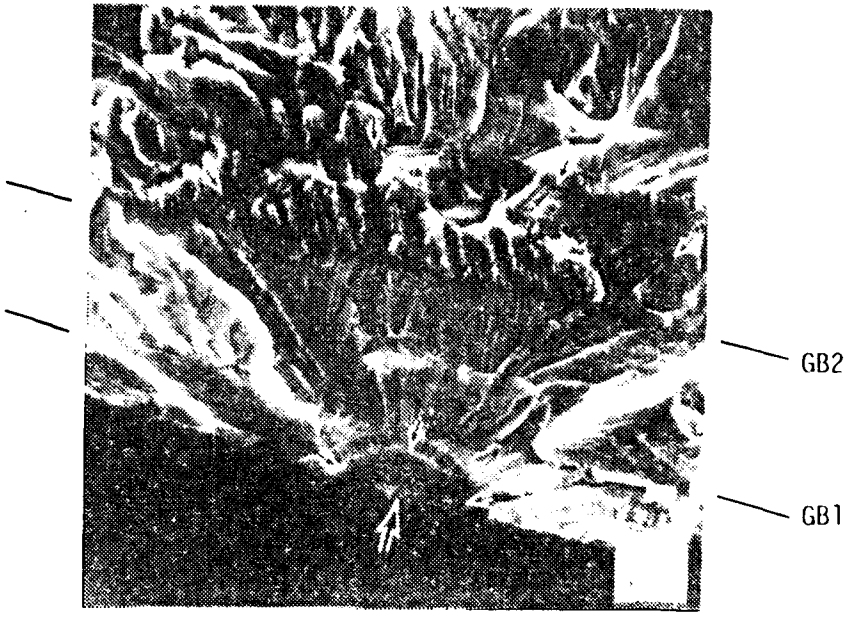

30. Micrograph showing the changes in the direction of crack advance when the crack-tip encounters grain boundaries in 7075-T6 aluminum alloy (after Ref. 71).

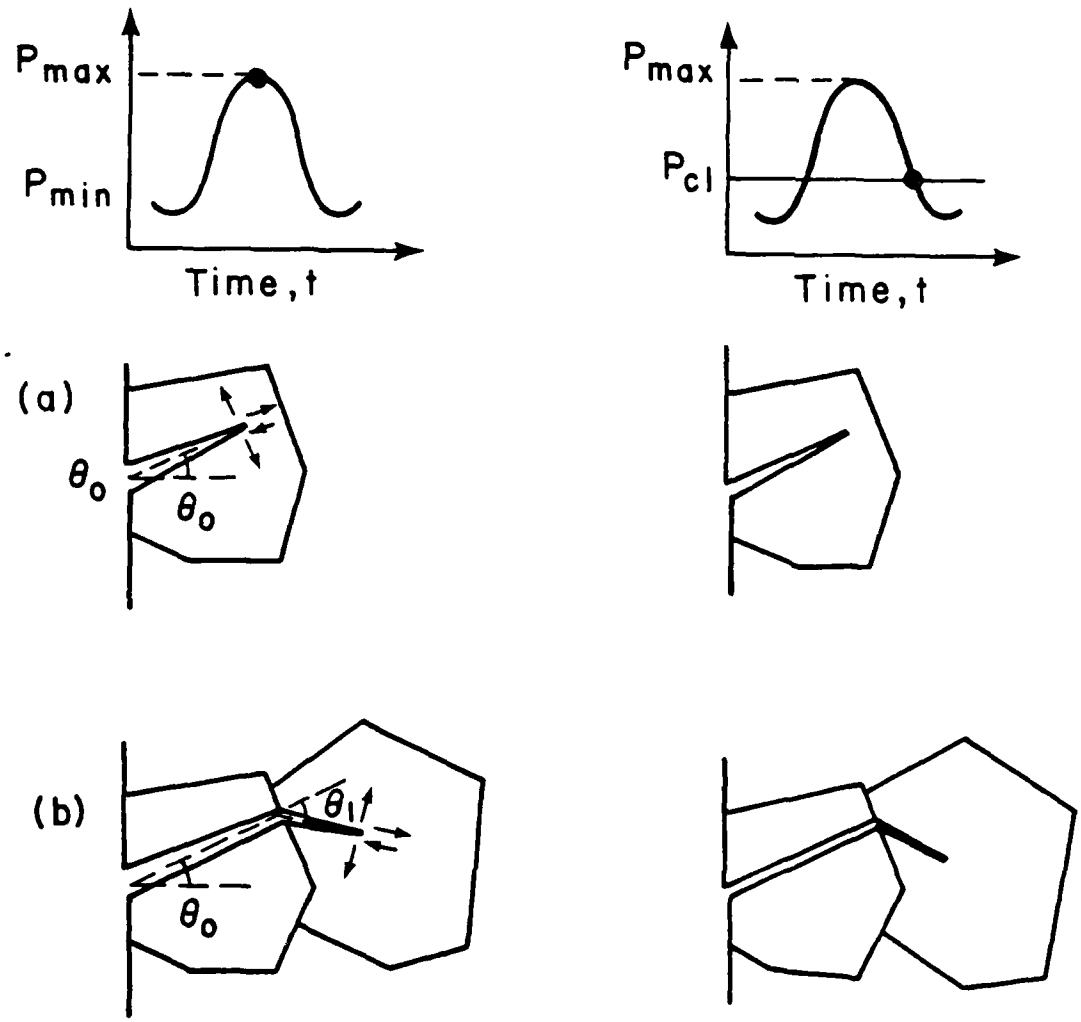

XBL 8212-7376

31. Schematic illustration of the growth and deflection of microstructurally-short fatigue cracks and the resultant crack tip displacements and closure. θ_o is the short crack initiation angle and θ_1 the angle of deflection at the first grain boundary (after Ref. 81).

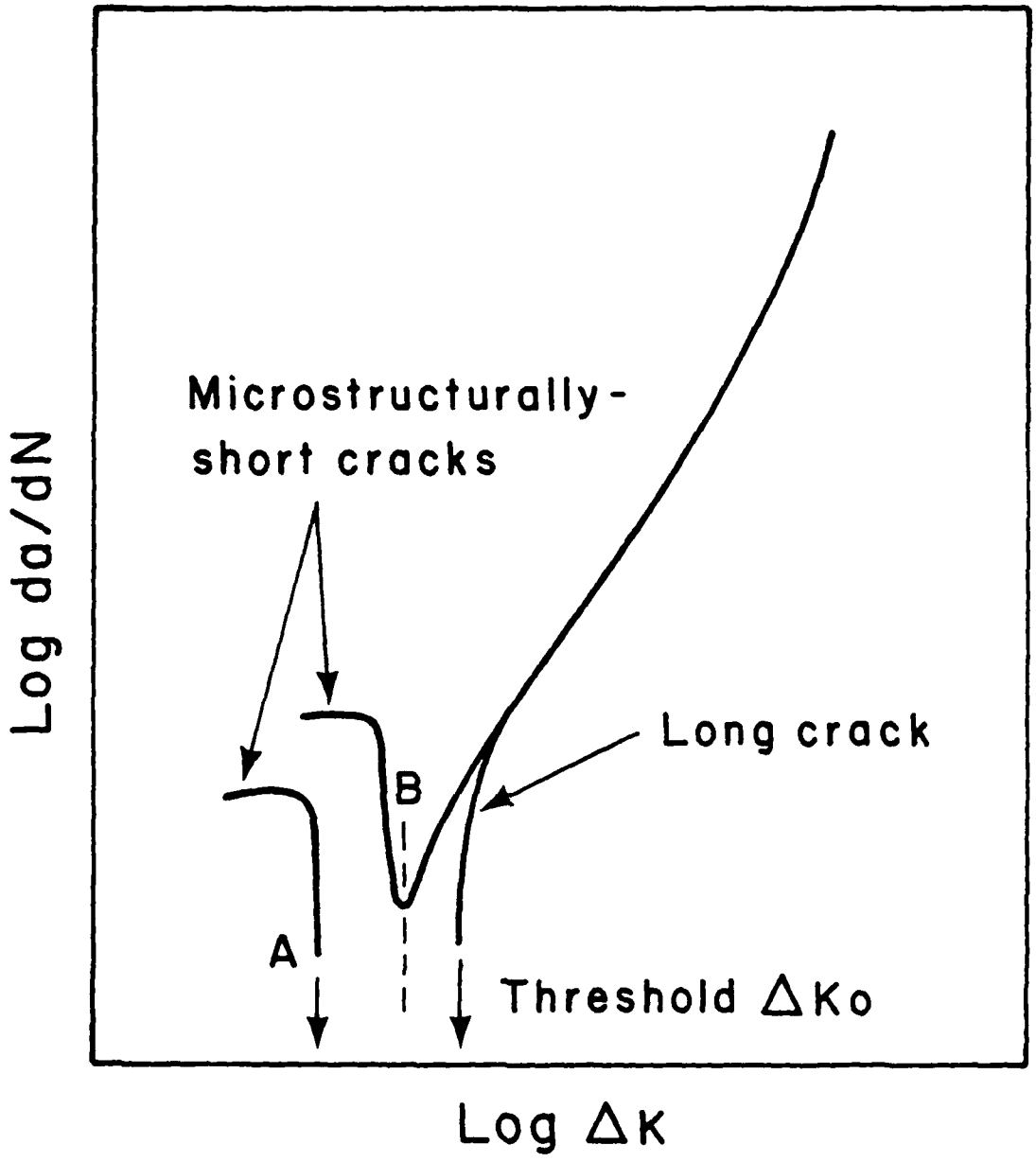

XBL 8212-7374

32. Schematic illustration showing the typical variation of fatigue crack growth rates (da/dN) as a function of ΔK for both long and microstructurally-short fatigue cracks. Note how short cracks grow at a progressively decreasing rate below the long crack threshold ΔK_o before arresting or merging with the long crack data.

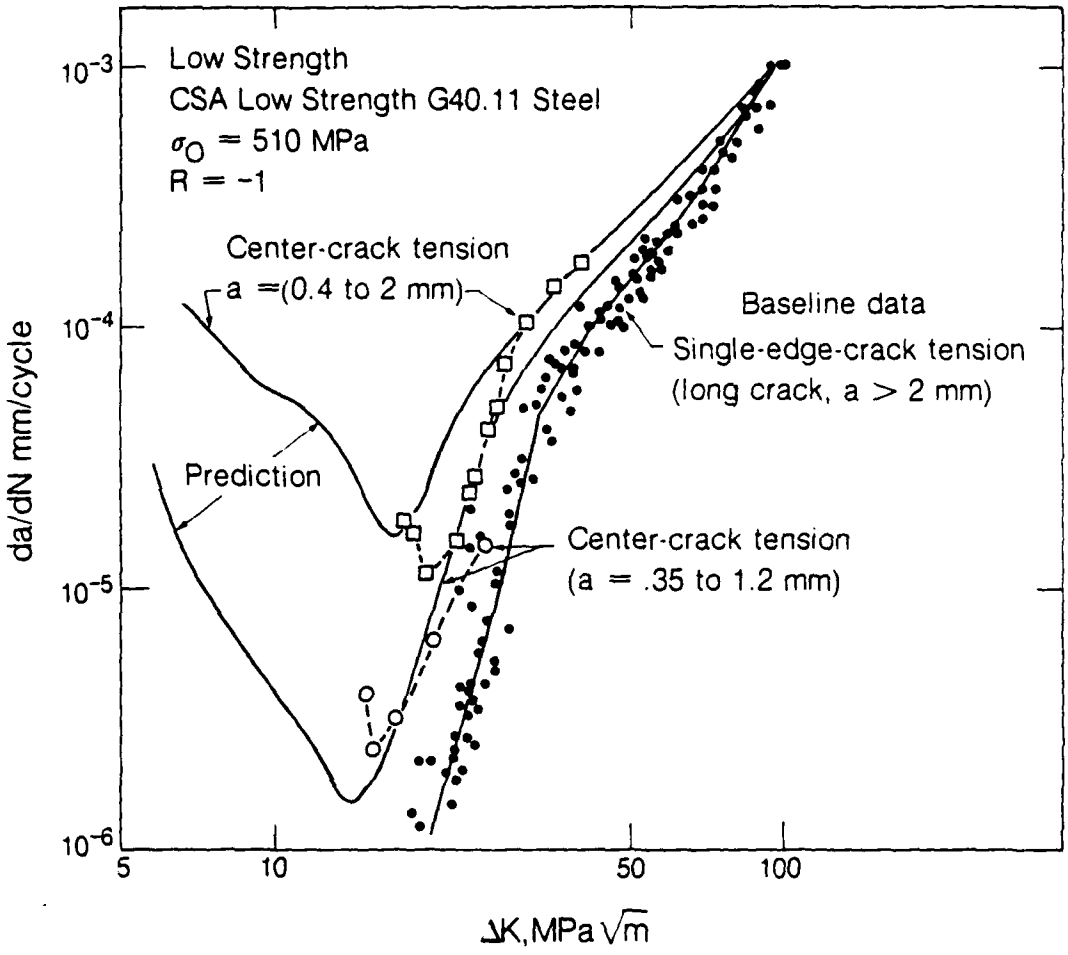

XBL835-914

33. Comparison of experimental results and numerical predictions of crack propagation rates for small cracks in center-cracked tensile specimens of low strength structural (CSA G40.11) steel (σ_o = 510 MPa) subjected to high stress levels (after Ref. 135).

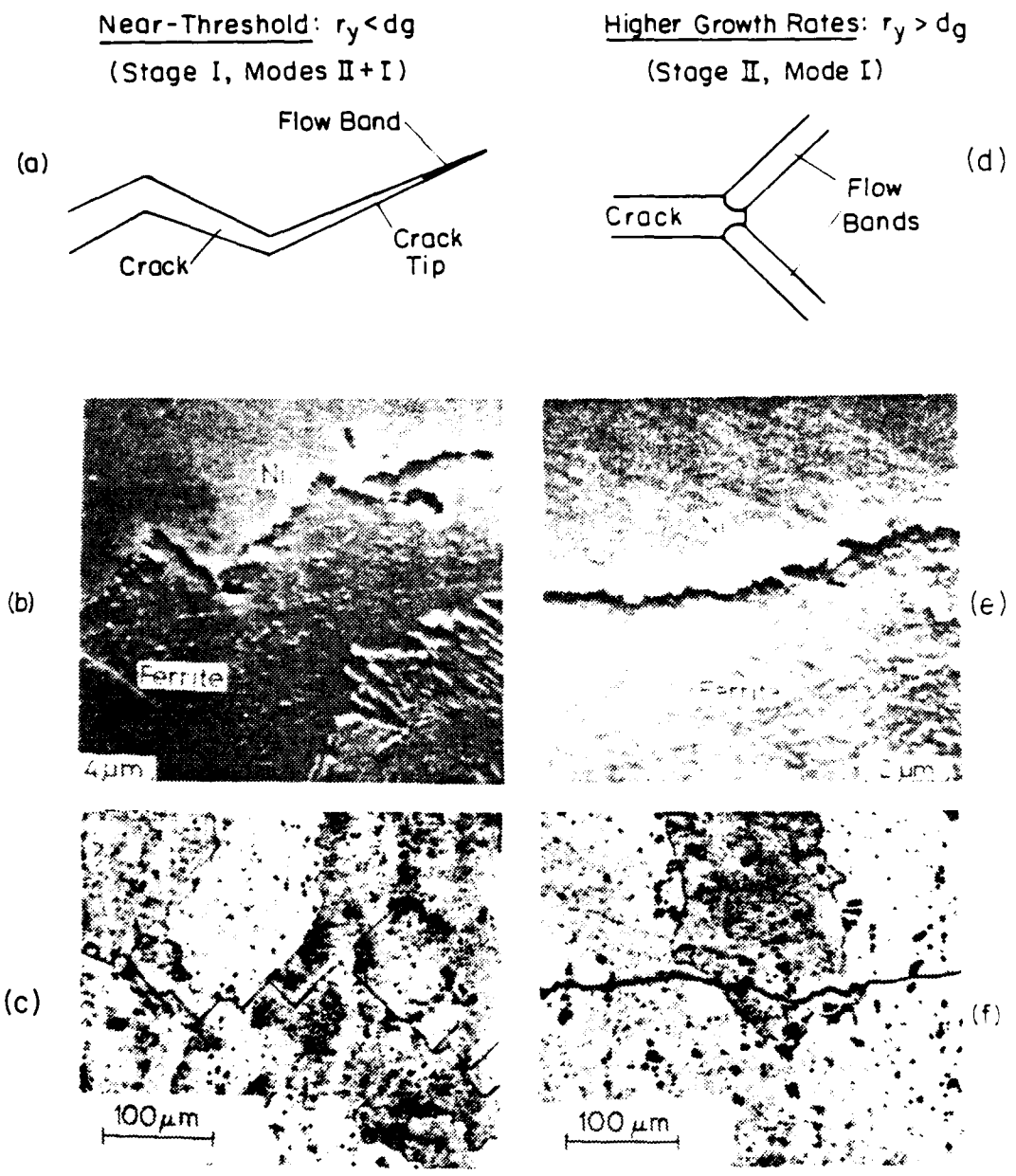

34. Crack opening profiles and resulting long crack path morphologies for (a), (b), (c) near-threshold (Stage I) and (d), (e), (f) nigher growth rate (Stage II) fatigue crack propagation. (b) and (e) are nickel-plated fracture sections in 1018 steel (after Ref. 118), and (c) and (f) are metallographic sections in 7075-T6 aluminum alloy (after Louwaard, 1977, quoted in Ref. 10); (after Ref. 120).

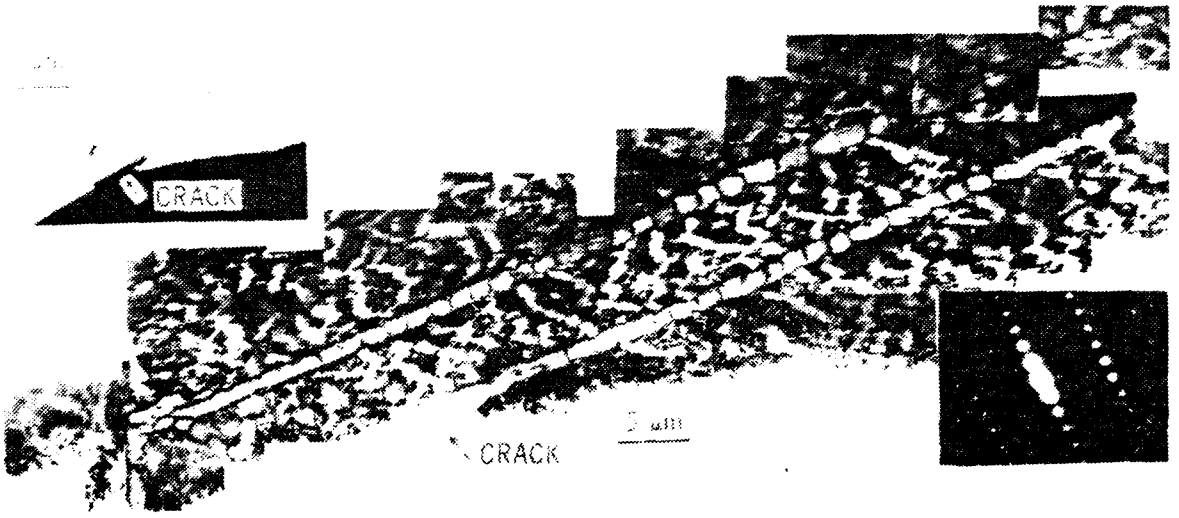

35. Transmission electron micrograph of Stage I micro-cracks propagating within persistent slip bands (PSB's) showing ladder-like dislocation substructures in fatigued polycrystalline high purity copper. Inserts show optical micrographs of the cracks and electron diffraction patterns corresponding to the transmission electron micrographs (after Ref. 148).

ENVIRONMENTAL EFFECTS NOVEL TO THE PROPAGATION OF SHORT FATIGUE CRACKS

R. P. Gangloff

Exxon Research and Engineering Co., Annandale, NJ 08801

and

R. O. Ritchie .

Department of Materials Science and Mineral Engineering
University of California, Berkeley, CA 94720

March 1984

Report No. UCB/RP/84/A1018

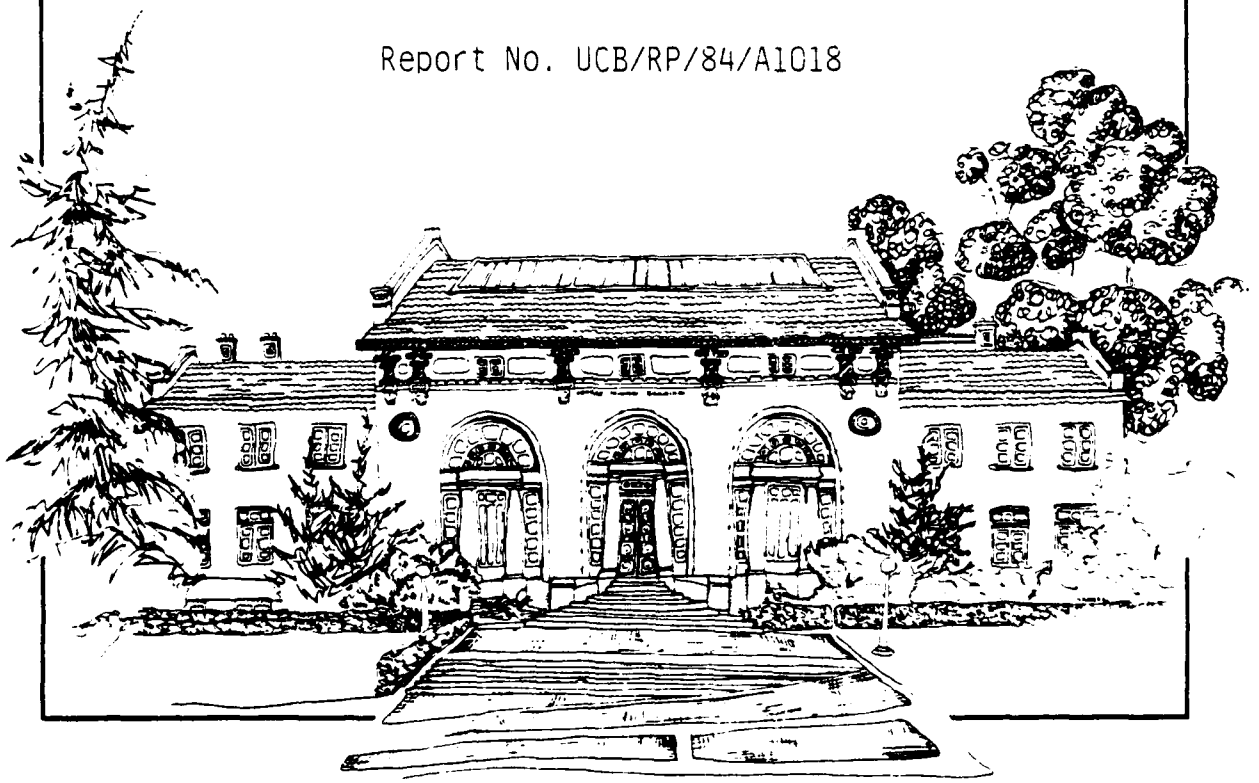

Report No. UCB/RP/84/A1018

ENVIRONMENTAL EFFECTS NOVEL TO THE PROPAGATION OF SHORT FATIGUE CRACKS

R. P. Gangloff

Exxon Research and Engineering Co., Annandale, NJ 08801

and

R. O. Ritchie

Department of Materials Science and Mineral Engineering
University of California, Berkeley, CA 94720

March 1984

IUTAM/ICF/ICM Conference on "Fundamentals of Deformation and Fracture"
Published in the Proceedings of the Eshelby Memorial Symposium,
University of Sheffield, April 1984,
B. A. Bilby and K. J. Miller, eds., Cambridge University Press, 1984

ENVIRONMENTAL EFFECTS NOVEL TO THE PROPAGATION OF SHORT FATIGUE CRACKS

R. P. Gangloff

Exxon Research and Engineering Co., Annandale, NJ 08801, U.S.A.

R. O. Ritchie

University of California, Berkeley, CA 94720, U.S.A.

ABSTRACT

Crack size and opening morphology dominate the mechanical and chemical driving forces for fatigue propagation in embrittling environments. Similitude based on a crack tip field parameter is compromised, particularly for small cracks (< 5 mm) which grow up to several orders of magnitude faster than projected and below apparent threshold conditions. Environment sensitive mechanical and chemical mechanisms which govern the growth of small cracks are reviewed. For the former the retarding effect of crack closure; originating from wake plasticity, surface roughness, deflection, corrosion debris or fluid pressure; increases with increasing crack size particularly within the near threshold regime. Data for high strength steel in H_2 demonstrate the importance of such mechanisms, however, precise models of crack size dependencies and systematic closure measurements are lacking. Considering the chemical driving force, the embrittling activity of the occluded crack differs from that of the bulk environment, and is geometry dependent. The deleterious influence of small crack size is demonstrated experimentally for steels in aqueous chloride solutions, and related quantitatively to crack opening shape and size effects on diffusion, convective mixing and electrochemical reaction. Small crack size promotes hydrogen embrittlement due to enhanced hydrolytic acidification and reduced oxygen inhibition. Chemical crack size effects are material and environment specific; criteria defining limiting crack sizes and opening shapes for K or J-based similitude do not exist.

1. INTRODUCTION

Fracture mechanics analyses of subcritical crack propagation are based on the fundamental notion that a characterizing parameter such as stress intensity (K) or the J integral describes remote loading and geometry effects on crack tip stress and strain distributions, and hence the kinetics of slow growth.(1-3) By similitude, cracks extend at equal rates when subjected to equal mechanical driving forces. Fracture mechanics scaling of laboratory data to predict component life is established, only in part, for fatigue and statically loaded cracks in benign and embrittling environments.(4-8) Recent investigations indicate that stress intensity-based similitude must be modified to account for plasticity,(9) crack motion,(10) closure,(11) deflection,(12) crack size,(13) and environment.(14)

Extensive data demonstrate that short cracks grow faster than projected and below apparent threshold conditions compared to long crack (25-50 mm) kinetics at constant stress intensity.(11,13,15-30) Typically for benign environments, the limiting crack size for deviations from K-based similitude increases from 10 μm for high strength alloys to about 1 mm for low strength materials, as reviewed from a mechanical perspective.(11,13,15-17,31)

In active environments rates of fatigue crack propagation are controlled by interrelated mechanical and chemical driving forces.(32,33) Critically, each driving force is crack size, shape and applied stress sensitive. The theses of this review are that small crack size influences uniquely the mass transport and reaction components of the chemical driving force, and that environmental modifications of the mechanical driving force are novel within the short crack regime. Mechanical and chemical factors which lead to breakdowns in similitude for small fatigue cracks, and which are traceable to environmental effects, are characterized separately.

Data establish the importance and complexity of small crack-embrittling environment interactions. Threshold stress versus crack size results in Fig. 1 indicate threshold stress intensity range (ΔK_o) control for long cracks, and constant stress or endurance limit control for very short cracks in 13Cr steel at two stress ratios (R).(20) While similar size dependencies are observed for moist air and liquid water, crack growth deviates from ΔK_o control at larger limiting crack sizes for the later environment. Embrittlement, evidenced by reduced stress, is promoted for decreased crack size and lower R. Geometry sensitive chemical and mechanical closure effects contribute to the trends depicted in Fig. 1. The potential for small crack chemical contributions to corrosion fatigue, independent of mechanical effects, is illustrated in Fig. 2.(21,24) Cracking in vacuum and moist air is defined

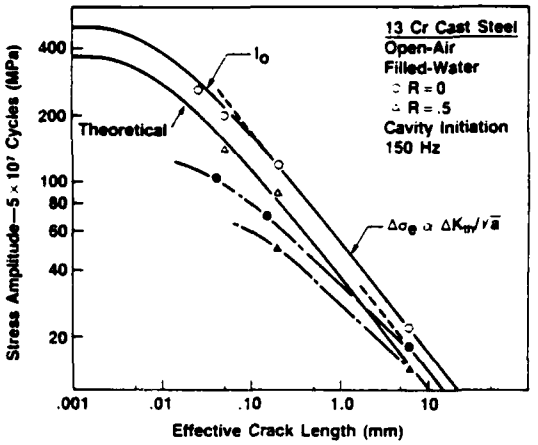

FIG. 1. Variation of fatigue threshold stress with crack length for cast 13Cr steel in air and water at two stress ratios. Note ΔK_o control for long cracks and endurance stress control for short cracks. After Usami and Shida (1979).

uniquely by ΔK, independent of crack size and applied stress. In contrast small cracks in aqueous NaCl grow up to 300 times faster than long cracks at constant ΔK. A multiplicity of da/dN-ΔK relations is observed; chemical embrittlement is enhanced for decreased crack size or reduced stress, and correlates with crack opening shape.(14) Data in Fig. 3 demonstrate the role of crack closure independent of chemical effects.(34-38) Based on long crack

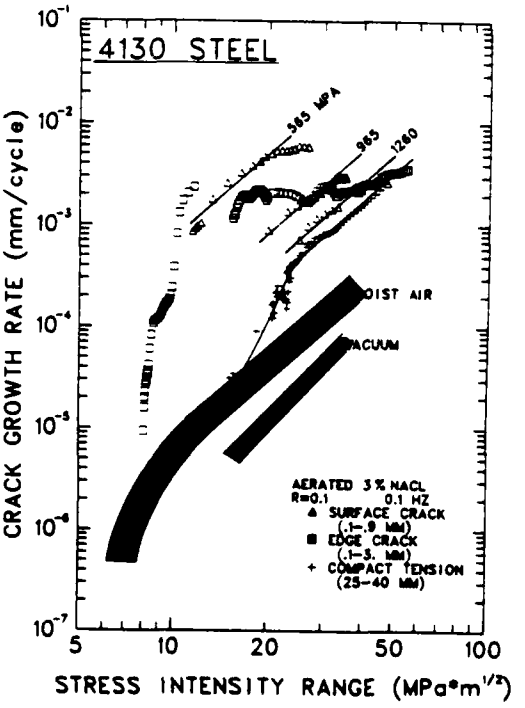

FIG. 2. Crack growth rate versus stress intensity range data for variably sized cracks in high strength (1330 MPa) 4130 steel. Note the accelerated growth of physically short cracks only in aqueous NaCl, and the stress dependence of small crack corrosion fatigue ($\Delta\sigma$ values are listed for surface cracks). After Gangloff (1984).

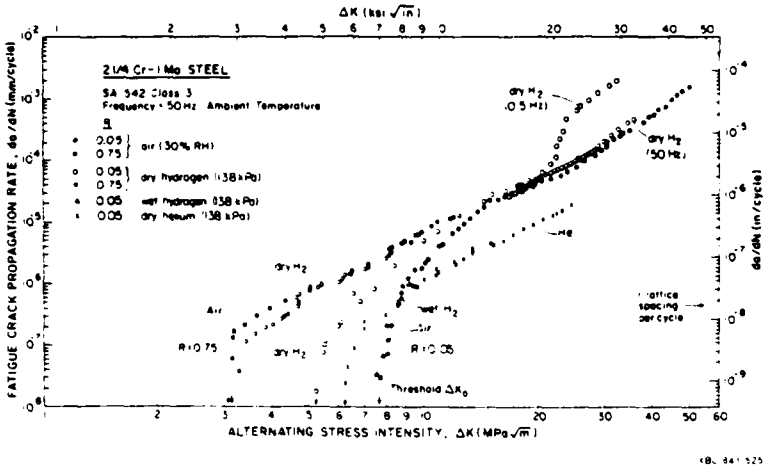

FIG. 3. Influence of load ratio and environment on fatigue propagation of long (~ 50 mm) cracks in low strength bainitic 2 1/4Cr-1Mo steel (σ_o = 500 MPa) in moist air, dry helium and hydrogen gases at R = 0.05 and 0.75. Note the contrasting effect of environment at near-threshold and higher growth rates. After Suresh and Ritchie (1982).

measurements and applied stress intensity, hydrogen embrittlement predominates for high ΔK low frequency conditions, whereas closure dominates crack growth at high frequencies in the near-threshold regime. Reduced rates of growth correlate with low R and moist environments which promote corrosion debris and crack surface contact. Faster growth rates are observed for high R and environments such as He and H_2 which maintain clean crack surfaces.

Environment-assisted growth of small fatigue cracks; nucleated from corrosion pits, weld defects, scratches, porosity or inclusions; is an important failure mode often dominating total life.(39-44) In an example of a pipeline carrying H_2S contaminated oil,(39) 85% of an 87 year (predicted) fatigue life is associated with the growth of a 0.5 mm starting flaw to 1.0 mm. Accelerated short crack growth (e.g., Fig. 2) could reduce total life by 50 to 100 fold. To date, however, most life prediction analyses have scaled long crack data, without accounting for short crack-environment interactions.(45,46)

2. SMALL CRACK-ENVIRONMENT INTERACTIONS: MECHANICAL DRIVING FORCE

2.1 CONCEPT

Of the factors contributing to crack size similitude problems through effects on the mechanical driving force, local

plasticity, crack deflection and crack closure are of major importance as illustrated in Fig. 4.(11,13,15-20) Each of these processes can be modified strongly by an embrittling environment, for example through the role of adsorbed hydrogen in affecting dislocation behavior, or the enhancement of crack closure through crack surface corrosion products or roughness. We examine the influence of environment on the processes affecting the mechanical driving force, and highlight effects unique to small cracks.

2.2 ACTIVE CRACK TIP PLASTICITY

A primary reason for crack size effects is the inappropriate characterization of crack tip fields. Inaccuracies result from the use of linear elastic fracture mechanics to describe crack growth behavior in the presence of extensive local plasticity, i.e., where crack length (a) is comparable with the extent of the active plastic zone ahead of the crack tip, $r_y \sim (1/2\pi)(K_I/\sigma_o)^2$, or where the crack is embedded within the strain field of a notch (Fig. 4a). Plasticity effects may dominate at crack sizes below a limiting length ℓ_o, given by $1/\pi(\Delta K_o/\Delta\sigma_e)^2$, where ΔK_o is the long crack threshold and $\Delta\sigma_e$ is the smooth bar fatigue limit.(25,47)

The extent of local plasticity is often influenced by environment.(48) There is clear experimental evidence that dissolved hydrogen can affect the flow stress of materials.(48,49) In high purity iron softening is observed at temperatures above 200 K, whereas hardening is seen at lower temperatures. In steels

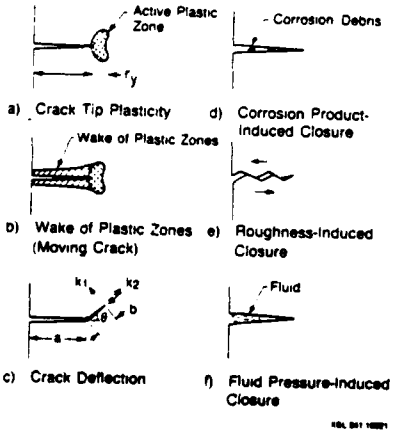

FIG. 4. Schematic illustrations of mechanisms for breakdowns in similitude relevant to small fatigue cracks in embrittling environments.

conversely, softening has been associated with single slip deformation and hardening with multiple slip, and the environmental influence declines with increasing alloy strength. The mechanisms for hydrogen effects on plasticity are imprecise.(48) Hydrogen segregation to dislocation cores enhances double kink nucleation on screw dislocations which facilitates movement. (The effect on edge dislocations may be exactly the reverse.) Softening may also result from the formation of voids induced by high fugacity hydrogen (i.e., during charging). Hardening is related to hydrogen atmospheres on dislocations or increased, hydrogen-stabilized vacancy concentrations, factors which may impede dislocation motion.

With respect to fatigue crack growth, in situ measurements in 7075-T651 aluminum alloys indicate decreased crack tip plasticity, in the form of reduced crack tip fracture strains, in water vapor compared to dry nitrogen and due to the embrittling effect of hydrogen.(50) Conversely, recent studies of aluminum show fatigue cracks to remain sharp when exposed to inert atmospheres, due to a Mode II + I opening, yet to become blunt in moist air where purely Mode I opening occurs.(28) The contributions of crack tip shape, closure, deflection and chemical embrittlement are not fully understood.

While a fundamental mechanism for environment-crack tip deformation interactions is not available, it is clear that environmental effects on plasticity and crack opening morphologies are crucial for the small crack regime.(28) To alleviate the problem of local plasticity, the use of non-linear elastic fracture mechanics, specifically involving the ΔJ parameter, has been suggested.(9,17,25) Data for short surface cracks in elastic-plastic low cycle fatigue samples correlated with conventional long crack results, through the use of ΔJ in place of ΔK as the generalized crack driving force.(12,25) In balance, however, this approach is imprecise for small cracks in elastically loaded material. The use of J is questionable for crack growth, since it is strictly defined for monotonic, increasing, proportional loading.(2,3) Environmental effects on material flow properties must be defined, and the resultant influence on small crack driving force quantified.

2.3 CRACK TIP WAKE PLASTICITY

In addition to active plasticity ahead of the crack, it is necessary to consider the enclave of prior plastic zone left behind the crack tip, particularly when crack size approaches the scale of local plasticity (Fig. 4b). Recent asymptotic analyses of monotonically loaded, Mode I non-stationary cracks indicate that the crack tip strain singularity weakens as the crack moves.(10) Specifically in the limit as $r \to 0$, the plastic strain distribution, $\gamma_p(r)$, is given in terms of an effective plastic zone size (r_y'),

Poisson's ratio (ν) and constant (m) as:

$$\gamma_p = \frac{m}{\sigma_o}\frac{dJ}{da} + \frac{1.88(2-\nu)\sigma_o}{E}\,\ell n\,\left(\frac{r'_y}{r}\right) \qquad (1)$$

Thus, due to wake plasticity behind the growing crack, crack tip strains decay as $\ell n(1/r)$, rather than as $1/\sqrt{r}$ or $1/r$ for a stationary crack in a linear elastic or perfectly plastic solid. This implies that at a fixed K_I or J, the plastic strains ahead of a stationary crack exceed those ahead of a slowly moving crack with its trailing wake of plasticity. More importantly since short cracks sized below r_y have by definition a limited wake, larger plastic strains must occur ahead of a moving short crack compared to the equivalent long crack at the same K_I or J. Recent in situ crack tip deformation measurements on growing fatigue cracks in 7075 aluminum alloy clearly show this to be the case. The strain distribution ahead of a long crack at low ΔK conforms to a $\ell n(1/r)$ singularity,(51) and corresponding crack tip strains and opening displacements for small cracks, 30 to 200 μm in length, are significantly higher.(18)

The effect of wake plastic zone on the mechanical crack driving force and the significance to the crack size similitude question is influenced by chemical factors since environment can affect plasticity. There is, however, no characterizing parameter currently available which considers wake plasticity effects as a function of material flow properties, and which describes driving force independent of crack size.

2.4 CRACK DEFLECTION

Crack deflection contributes to a lack of similitude by causing the near tip driving force to differ from the globally computed K_I or J (Fig. 4c).(15) In general Mode I crack growth data are correlated in terms of K_I or J assuming a linear crack oriented perpendicular to the maximum tensile stresses. Crack paths can, however, deflect out-of-plane due to metallurgical and environmental interactions such that the local driving force at the crack tip is reduced.(12) For an elastic crack deflected through an angle Θ and subjected to tensile and shear loads, the local Mode I and Mode II stress intensity factors, k_1 and k_2, are given in terms of the nominal stress intensities, K_I and K_{II}, and angular functions $a_{ij}(\Theta)$, as: (52)

$$k_1 = a_{11}(\Theta)\,K_I + a_{12}(\Theta)\,K_{II} \quad ,$$
$$k_2 = a_{21}(\Theta)\,K_I + a_{22}(\Theta)\,K_{II} \quad . \qquad (2)$$

For a simply kinked elastic crack, deflection through $\Theta = 45°$ yields $k_1 \approx 0.8K_I$ and $k_2 \approx 0.3K_I$. The 45° crack path deflection induces a significant Mode II shear component at the crack tip and reduces the effective driving force by roughly 15%.(12)

Fatigue crack deflection is promoted by microstructure in duplex structures,(12,53) and at lower ΔK levels where crack growth may be crystallographic, particularly for coarse planar slip materials.(54,55) The effect can be striking for microstructurally-small cracks where prolonged retardation periods or arrest are observed as such cracks encounter and reorient at grain boundaries.(12,26) The crack size dependence upon the mechanics of crack deflection (e.g., Eq. (2)) remains unsolved.

Environmental factors which induce a specific crack path morphology can have a major influence on the mechanical crack driving force through crack deflection. The branching of stress corrosion cracks under specific material/environment/crack velocity conditions,(56) the faceted or crystallographic nature of the fracture plane in certain materials during corrosion fatigue ("brittle" striations in aluminum alloys,(57)) and most importantly the development of intergranular facets and secondary cracks due to hydrogen embrittlement or active path corrosion (4,27,48,57) are examples of environment induced deflection.

The effect of crack deflection is not limited to modifying the local stress intensity for a stationary crack. Under cyclic loading, crack deflection induces irregular fracture surfaces and Mode II crack tip displacements. Such factors promote the development of crack closure, to a degree dependent upon crack length, thus further enhancing the discrepancy between local and global mechanical crack driving forces.

2.5 FATIGUE CRACK CLOSURE

Crack closure, or fracture surface contact, during cyclic loading is a major factor contributing to crack size similitude effects. At lower load ratios (below typically $R = 0.5$) where contact occurs at positive loads (i.e., the closure stress intensity, K_{cl}) during the cycle, the consequence of closure is to reduce the nominal driving force ($\Delta K = K_{max} - K_{min}$) to an effective value, $\Delta K_{eff} = K_{max} - K_{cl}$, where K_{max} and K_{min} are the maximum and minimum applied stress intensities. Crack growth rates decrease in response to the reduced driving force, but often correlate with ΔK_{eff}. Crack closure can result solely from cyclic plasticity,(58) or may be developed through several alternate mechanisms as illustrated in Fig. 4.(53) Closure processes include crack surface corrosion product formation, irregular fracture surface morphologies coupled with inelastic shear displacements, and fluid-induced pressure inside the crack. Whereas plasticity-induced

closure is significant at higher ΔK levels approaching plane stress, higher levels of closure may be developed at lower ΔK levels approaching ΔK_o (plane strain) through the mechanisms depicted in Fig. 4.

All closure phenomena contribute to crack size similitude breakdown through modifications of the near-tip mechanical driving force and to a degree dependent upon crack size. Geometry is crucial because closure must act in the wake of the crack tip. Since short cracks have a restricted wake, growth rate retardations by crack closure mechanisms are limited. At equivalent nominal ΔK levels, short cracks may propagate faster than long cracks due to a higher effective stress intensity. This effect will diminish as closure develops with increasing crack length. Although there is a growing body of experimental evidence to support this notion,(11,19,59,60) with the exception of the fluid pressure-induced closure mechanism, few analytical models exist which incorporate the crack size dependence of closure. Furthermore, indirect, geometry dependent chemical effects on corrosion products and roughness characteristics have not been examined.

CLOSURE INDUCED BY CYCLIC PLASTICITY: Elastic constraint of material surrounding the plastic zone in the wake of the crack front affects material elements plastically deformed at the crack tip, and leads to interference between mating fracture surfaces. Although analyses showing the crack size dependence of closure are not available, recent experimental and numerical studies indicate that the effect of closure diminishes at small crack sizes.(11,19,59-61) Unpublished results by Heubaum and Fine on Van 80 steel (R_B 94) cycled in moist air show this particularly clearly, as reproduced in Fig. 5. High precision closure measurements, using a 0.05 μm sensitivity

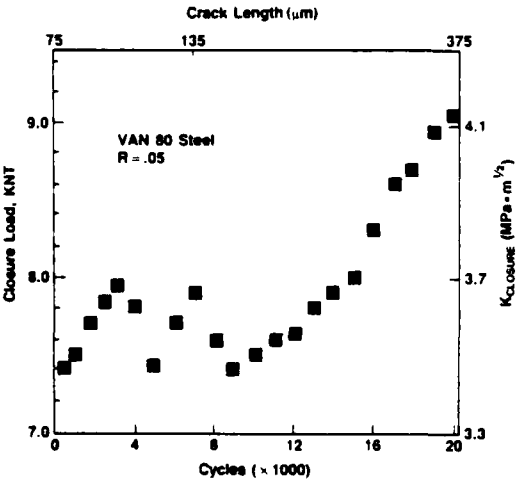

FIG. 5. Experimental evidence for increasing crack closure with increasing small crack size, based on compliance measurements for Van 80 steel cycled in moist air; R = 0.05, K_{max} = 9 to 20 MPa√m. After Heubaum and Fine (1984).

compliance gauge, establish that closure stress intensity (K_{cl}) increases by almost 20% for crack extension from 75 to 375 μm. Although small crack growth rates exceed those for long cracks based on constant ΔK, a unique growth rate-driving force law was reported for ΔK_{eff}.

CLOSURE INDUCED BY CORROSION PRODUCTS: Closure induced by corrosion products(33,53,62-65) is relevant to environmentally influenced crack growth when the size-scale of such debris approaches crack tip opening displacements (v) (Fig. 4d). The mechanism is most potent at low R and at near-threshold stress intensity ranges, especially in lower strength materials where fretting processes during the opening and closing of the crack enhance oxidation and excess deposit formation. The closure mechanism was demonstrated as significant for oxide films formed on alloy steel crack surfaces exposed to moist gases,(53,62-64) and for calcareous deposits produced on structural steel fatigue crack surfaces through electrochemical reactions with seawater.(33,66)

Corrosion product induced closure is modeled approximately in terms of the thickness of excess film (d) and the location of the maximum thickness from the crack tip (2ℓ) to yield:(67)

$$K_{cl} = \frac{d\,E}{4\sqrt{(\pi\ell)}\,(1 - \nu^2)} \quad , \tag{3}$$

For air formed oxide, measured values of d (0.01 to 0.2 μm) and 2ℓ (5μm) correspond to a closure K of about 1.5 MPa$\sqrt{m}$. Significant levels of K_{cl} tend to offset the embrittling influence of an aggressive environment which might otherwise accelerate crack growth. In material and environment systems where susceptibility to embrittlement is small, crack growth rates based on ΔK may appear slower in seemingly more corrosive environments (Fig. 3). To date, no analytical representation of the crack size dependence of reaction product closure has been derived. Apart from size effects on the mechanics of closure, the thickness and composition of reaction products are determined by mass transport and electrochemical reaction, processes which are crack geometry sensitive as developed in ensuing sections.

CLOSURE INDUCED BY FLUID PRESSURE: Environment may influence crack closure through the hydrodynamic wedging effect of fluids inside the crack during cyclic loading (Fig. 4f).(37,39,59) Fluids may induce an internal pressure relatable to a stress intensity (K^*_{max}) which opposes the opening and principally the closing of the crack, and which reduces the effective stress intensity range at the tip to $\Delta K_{eff} = K_{max} - K_{min} - K^*_{max}$. This mechanism results in frequency and viscosity sensitive fatigue crack growth rates in inert fluids. Trends in behavior with these variables are difficult to predict since higher viscosity fluids, which induce higher fluid pressures,

are kinetically limited in their ability to fully ingress into the crack.(59)

Experimental and theoretical analyses of fluid pressure closure provide estimates of K_{cl} as a function of frequency, viscosity and crack size.(38,59) Internal fluid pressure p(x) is distributed along a crack of depth, a, and average opening width, $\langle h \rangle$, according to:

$$p(x) = 6\eta\rho \frac{\dot{h}_{max}}{h^3_{max}} a^2 \ln(1 - x/a), \quad \text{for } d/a = 1$$

$$\text{or} \quad p(x) = 6\eta\rho \frac{\langle \dot{h} \rangle}{\langle h \rangle^3} x(x - d), \quad \text{for } d/a < 1, \tag{4}$$

where ρ is fluid density and η is kinematic viscosity. The extent of fluid penetration (d) during a fatigue load cycle is time dependent and estimated based on capillary flow to be:

$$d^2(t) \approx \frac{\gamma \cos\beta}{3\eta\rho} \int_0^t \langle h \rangle dt, \tag{5}$$

where β is the wetting angle and γ is surface tension. This analysis suggests that the magnitude of closure typically saturates at K_{cl}/K_{max} values approaching 0.5, based on fluid viscosities between 5 and 60,000 cS and growth rates between 10^{-6} and 10^{-3} mm/cycle, indicating that the mechanism is less potent than oxide or roughness-induced closure.(59)

Equations 4 and 5 predict that fluid pressure, and hence the degree of closure, are related to crack size and are diminished at smaller crack lengths. Predictions of closure stress intensity (K^*_{max}) due to fluid pressure, generated by oils of viscosities varying from 5 to 60,000 cS, are shown in Fig. 6 for a 2 1/4Cr-1Mo steel cycled at R = 0.05 and 50 Hz. K^*_{max} decreases as crack length approaches zero, and to a degree dependent upon viscosity. At a fixed nominal ΔK, the smaller crack experiences a higher effective driving force, and hence propagates at a faster speed.

CLOSURE INDUCED BY FRACTURE SURFACE ROUGHNESS: Environmental factors can influence the extent of crack closure through an effect on fracture morphology (Fig. 4e). Irregular fracture surfaces; produced by microbranching, intergranular separation or crystallographic cleavage, together with local mixed mode crack tip displacements; promote roughness induced closure during unloading.(34,35,64,68,69) K_{cl} is developed through premature contact of pronounced asperities. For example, in high strength steels where near-threshold growth rates are often lower in

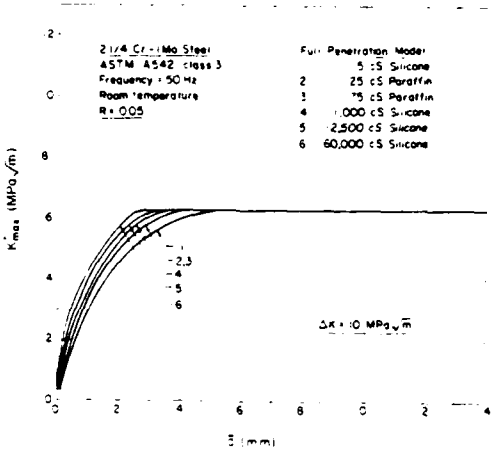

FIG. 6. Evidence for decreased K_{cl} at small crack lengths based on predictions of fluid-induced closure forces for crack propagation in silicone and paraffin oils. K^*_{max} is the stress intensity resulting from fluid pressure and is equivalent to K_{cl}. After Tzou, Hseuh, Evans and Ritchie (1984).

potentially embrittling gaseous hydrogen environments compared to moist air, the intergranular nature of hydrogen-induced fracture surfaces promotes fretting corrosion debris and asperity contact during cyclic loading, leading to closure of varying degrees in each environment.(36,60)

Roughness induced closure is modeled in terms of the extent of surface roughness, or the ratio of asperity height to width (γ), and the ratio of Mode II to Mode I crack tip displacements (μ):(68)

$$\frac{K_{cl}}{K_{max}} = \sqrt{\left(\frac{2\gamma\mu}{1+2\gamma\mu}\right)}. \qquad (6)$$

K_{cl} is significant at low R and for crack tip displacements comparable with asperity size.(68,69) Crack size may influence both the degree of fracture surface roughness through a chemical mechanism and the level of K_{cl} based on crack mechanics. The latter geometry effect has not been analyzed to date, while the former mechanism is considered in Section 3.

2.6 HYDROGEN ASSISTED GROWTH OF SMALL CRACKS IN STEEL

A novel small fatigue crack-environment interaction, traceable to the combined effects of mechanical closure and chemical transport, is summarized in Fig. 7 for 4340 steel (σ_0 = 1030 MPa) stressed in either gaseous hydrogen or helium. At low R (Fig. 7a) 0.1 to 1 mm edge cracks grow five times faster than long (25-50 mm) cracks in compact tension specimens at constant ΔK and in H_2. Cracking in He is well defined by ΔK independent of c ack size for this class of steels (e.g., Fig. 2 and Refs. 13,24,27).

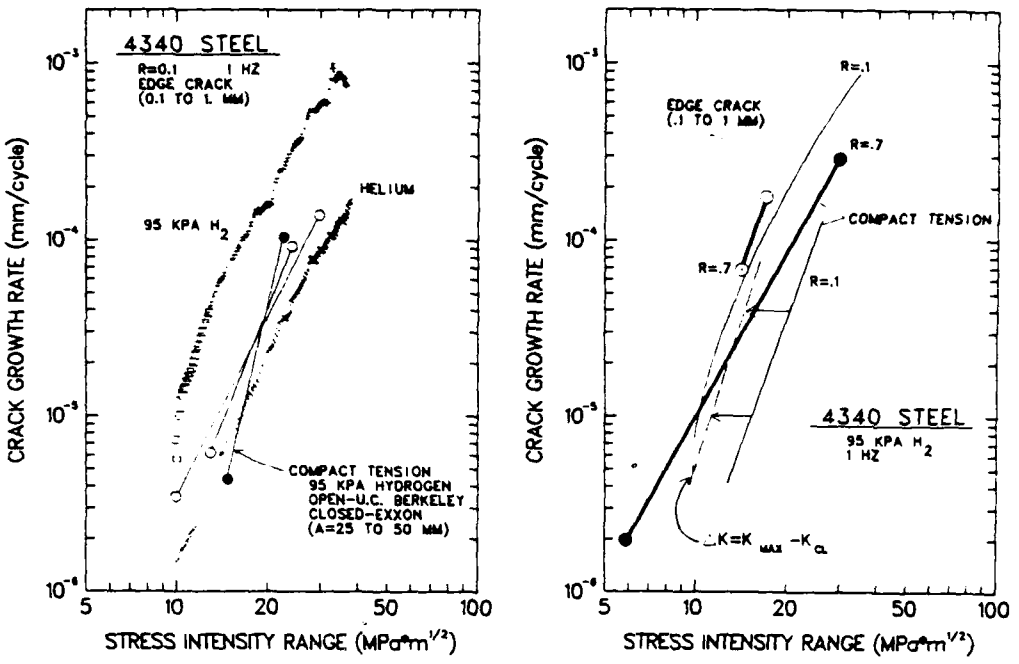

(a) (b)

FIG. 7. The effect of crack size on fatigue growth kinetics for 4340 steel (σ_0 = 1030 MPa) exposed to purified (95 kPa) H_2. (a) 0.1 to 1 mm edge and 25 to 50 mm compact tension cracks at R = 0.1. Note the accelerated growth of small cracks. (b) Edge and surface cracks for R = 0.7. Note the similar growth rates for long and short cracks at high R and the role of closure for long cracks at low R.

The breakdown in similitude for small cracks is also observed for higher strength (σ_0 = 1360 MPa) 4130 steel in H_2.(70) At the high R value where closure is minimized, growth rates for the long crack approach short crack speeds for H_2 (Fig. 7b). In contrast short crack growth rates in H_2 are equivalent at R = 0.1 and 0.7. When low R, long crack results are adjusted for closure based on ΔK_{eff} computed from compliance estimates of K_{cl}, the differences between long and short crack speeds become small as shown by the dashed line in Fig. 7b. Equivalent growth rates are observed for cycling from K_{min} to K_{max} and from K_{cl} to K_{max}, demonstrating the absence of damage for changing stress intensity below K_{cl}.

The crack size effect summarized in Fig. 7 is reasonably explained based on closure. Since crack geometry effects are

accounted for by applied ΔK for high strength alloys in inert environments, the origin of the closure variations must be environmental. Precise micromechanisms for such behavior are uncertain, but the results are consistent with a rougher intergranular fracture surface in hydrogen which both promotes crack deflection and roughness induced closure. This view is speculative. Crack closure was not estimated for short cracks, and no quantitative model exists to explain the crack size dependence of K_{cl} for given roughness. Additionally, roughness differences were not quantified for the cracks represented in Fig. 7.(69) Cracks produced in H_2 were only partially intergranular. Finally, the chemical driving force for embrittlement may be crack size sensitive, and contribute to or dominate mechanical closure.

3. SMALL CRACK-ENVIRONMENT INTERACTIONS: CHEMICAL DRIVING FORCE

3.1 CONCEPT

Crack size and opening shape effects on the chemical driving force for brittle crack growth compromise the stress intensity similitude concept for both static and cyclic stressing. It is unreasonable to assume apriori that a mechanics based crack tip field parameter will describe a chemical driving force. Local crack chemistry controls environment assisted subcritical cracking, and differs from that of the bulk due to enrichment (or depletion) of embrittling (or inhibiting) constituents.(71) The chemistry and embrittling activity of the occluded crack environment is geometry sensitive because of crack size and shape effects on mass transport by diffusion and convection, electrochemical potential and on reaction kinetics.(72-78)

Experiment and transport-reaction modeling are required to define the crack size range where geometry effects on crack chemistry are significant for a given material and environment. Chemical crack size effects are particularly relevant for small cracks because of: (a) the proximity of the crack tip to the bulk environment and applied potential,(73,76) (b) the crack size dependence of convective pumping,(78,79) (c) the large crack surface area to occluded solution volume ratio,(14,24) (d) the likelihood of tortuous crystallographic cracking influencing transport,(54) and (e) the sensitivity to localized environment enhanced plasticity.(26,28) Geometry effects may remain constant with increasing crack size beyond a saturation point,(29,57) consistent with demonstrations of ΔK similitude for aqueous environments.(4-7,50,80)

Chemical crack size effects are predicted for a wide range of embrittling environments. (24,72,73,76,77,81,82) Experimental

confirmations are, however, lacking because of the difficulties associated with isolating chemical and mechanical effects on similitude, and with monitoring the growth of small cracks.

3.2 GASEOUS ENVIRONMENTS

THEORETICAL MODELING: Gaseous environment enhanced fatigue crack propagation rates are controlled by the slow step in the sequence including gas transport, adsorption, diffusion, and chemical embrittlement.(29,32,72) For free molecular flow, collisions between gas molecules and crack walls dominate transport and impede the arrival rate of reactive species at the crack tip.(71,81) Local gas pressure is reduced below the bulk level, and embrittlement is decreased provided that gas transport is rate limiting.

Gas transport to the tip is crack size and opening shape sensitive. Impeded flow occurs when molecular mean free path (λ) exceeds crack opening displacement (ν), with impedance beginning for ν below about 100 λ.(72) Mean free path equals 0.1 μm for H_2, N_2, O_2 and H_2O at 300 K and 200 kPa pressure, and varies inversely with pressure and the square of molecular diameter. Considering an edge crack loaded to K = 10 MPa$\sqrt{m}$, crack mouth opening varies from 2 μm for a depth of 0.1 mm to 18 μm at a depth of 15 mm. For the 100 λ interaction criterion, impeded flow should occur over the entire length of the short crack, but over a much longer length for the deep crack. Crack geometry effects are more likely for lower gas pressure (*e.g.* λ = 20 μm at 5 kPa), for rough crack surfaces and for large molecules (λ = 2 mm for Cd at 5 kPa) relevant to solid metal embrittlement.(82)

Flow impedance (I) is approximated by:(72)

$$I = \left(\phi_1 \int_{a^*}^{a} dx/\nu_{max}^2\right)^{-1} = \phi_2 \sigma^2 a/\log \nu_{max}^* \qquad (7)$$

for a crack of length a along x, of mouth opening, ν, at a stress, σ, the constants ϕ_1 and ϕ_2 and molecular flow starting at a*. Impedance decreases as I increases from 0 to 1, and is time dependent during each stress cycle, $\sigma(t)$. The integral is solved in equation 7 for near tip displacements ($\alpha K\sqrt{(a - x)}$); alternate solutions are obtainable for the complete crack. While approximate, this analysis demonstrates that crack tip pressure and hence embrittling activity depends on stress, crack shape and size. K^2 (or $\sigma^2 a$) in equation 7 results from the assumed form of $\nu(x)$ between a* and a, and is not relatable to a mechanical driving force. ΔK-based similitude is predicted for those long crack cases where changes in log ν^* due to increasing a, have only a mild effect on I, and for those gases where subsequent steps in the reaction sequence are fast compared to transport.(83) Alternately, within the short

crack regime and at constant K, increasing a results in decreasing I and increasing impedance until crack length equals a*. A multiplicity of growth rates would be projected, and ΔK-based similtude compromised.

EXPERIMENTAL CONFIRMATIONS: Experimental evidence of unique small crack-gas environment interactions is limited, since studies of embrittlement have not focused on either small crack growth kinetics or similitude. Typically, ΔK and crack size vary simultaneously, complicating interpretation. Wei and coworkers reported that constant ΔK loading produced constant crack growth rates independent of crack size for long (> 25mm) cracks in an aluminum alloy in water vapor, supporting similitude.(32) Systemmatic studies of this sort must be extended to variable crack size and shape.

Anomalously rapid growth kinetics for small cracks growing in moist air are not relatable to chemical influences because experiments were not conducted in an inert environment to isolate mechanical effects.(11,13,15-17,31). Lankford demonstrated rapid growth rates for small cracks in an aluminum alloy exposed to moist air at constant ΔK.(28) A larger crack size effect was reported for pure N_2, indicating that water vapor transport and reaction did not dominate the crack size-environment interaction.(28) Holder demonstrated that small fatigue cracks in steel grew at anomalously fast rates at low ΔK compared to extrapolated long crack kinetics for moist air, but not in an inert reference environment.(23) Impeded molecular flow, shielding the long crack tip from embrittling H_2O molecules, was invoked. Experiments were, however, limited and flow impedance was not modeled.

Geometry sensitive gas transport may contribute to the effect of crack size on hydrogen assisted fatigue crack propagation rates, Fig. 7a. 1 to 100 λ equals 0.1 to 10 μm for H_2 at 300 K and 100 kPa. Crack mouth opening displacement at maximum load varies from 0.1 to 7 μm for the small crack geometries and from 40 to 200 μm for the compact tension conditions indicated in Fig. 7a. Larger flow impedances (Equation 7) are expected for the long crack. This simple analysis does not consider surface roughness enhanced molecule-wall collisions, and mass transport due to convection or surface diffusion. If flow impedance caused the chemical crack size effect at low R, then growth rates should be crack size independent at high R where the long crack tip is open and accessible to the bulk environment. A stress ratio effect is observed only for the long crack, (Fig. 7b). Gas transport control is not, however, unambiguously identified because data are equally well explained based on crack closure. Determination of the effect of hydrogen pressure on the magnitude of the crack size effect at constant ΔK would differentiate between impeded gas transport, proportional to $P_{H_2}^{-1}$, and crack closure, independent of P_{H_2}.

3.3 AQUEOUS ENVIRONMENTS

STATIC LOADING: DATA AND THEORY Small crack-environment interactions during static loading provide a basis for understanding more complex chemical crack size effects in fatigue. Superposition concepts relate the environmental effect for each loading mode.(84)

Experimental evidence for chemical crack size effects on stress corrosion cracking is virtually nonexistent. Static load growth rate data, presented in Fig. 8a for 0.1 to 2 mm deep elliptical surface and through thickness edge cracks in 4130 steel (σ_0 = 1330 MPa) exposed to 3% NaCl, show Stage I, K-independent (Stage II) kinetics for replicate specimens. Critically, small cracks grow at faster plateau rates and at stress intensities well

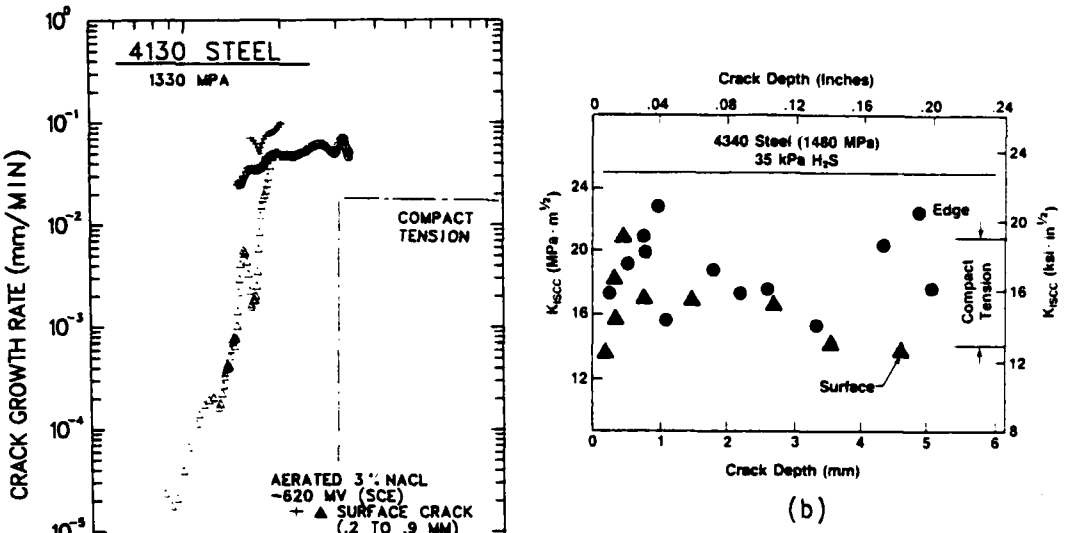

FIG. 8. Crack size effects on static load embrittlement of high strength steels. (a) Growth rate - K data for 0.1 to 2.0 mm deep cracks in 4130 steel (σ_0 = 1330 MPa) exposed to aqueous NaCl. Note the rapid rates of growth for small cracks; after Gangloff (1984). (b) Threshold stress intensity versus crack size for surface and edge flawed specimens of 4340 steel (σ_0 = 1480 MPa) exposed to gaseous H_2S. Note the crack size independence of K_{ISCC} supporting similitude; after Clark (1976).

below the threshold (K_{ISCC}), compared to literature data for long (> 20 mm) cracks in similar steels at constant strength.(85) Shahinian and Judy (7) report constant K_{ISCC} for 3.6 to 10 mm deep elliptical surface flaws and deep cracks in cantelever beam specimens for two strength levels (σ_o = 890 and 1410 MPa) of 4340 steel in 3.5% NaCl.

The crack size effect portrayed in Fig. 8a is traceable to geometry effects on the electrochemical processes which contribute to embrittlement. Cracks at either size scale would not grow in an inert environment at the K levels examined, and crack closure and corrosion product wedging are not relevant. Crack size has no influence on K_{ISCC} for gaseous H_2S embrittlement of a similar steel (Fig. 8b).(85) While embrittlement in aqueous NaCl and gaseous H_2S is attributable to hydrogen, crack geometry only influences solution transport and electrochemical reactions, and hence the level of embrittling hydrogen developed, for the former environment. Specifically, acidic conditions and embrittling hydrogen are produced in the occluded crack exposed to saltwater based on iron and chrome dissolution, water hydrolysis to produce H^+ and cathodic hydrogen and oxygen reductions.(65,86,87) Turnbull and coworkers modeled the geometry dependence of crack potential, pH, dissolved O_2, and cation concentrations leading to hydrogen production; and based on charge and concentration driven diffusional supply of the relevant electrochemical reactions.(55,73,74,89) The material, crack geometry and K conditions of Fig. 8a were analyzed to yield the results listed in Table I. Crack tip acidification (pH), the current density for H^+ reduction (i_H) and the concentration of embrittling hydrogen adsorbed into the metal near the crack tip (C_H) increase significantly with decreasing crack size. Hydrogen reduction is promoted for small cracks through an indirect influence of a reduction in dissolution product concentration by enhanced diffusion. Model predictions are qualitatively consistent with crack growth rate data in Fig. 8a because K_{ISCC} decreases with increasing C_H.

TABLE I

MODEL PREDICTIONS OF LOCALIZED CRACK CHEMISTRY

		CRACK TIP CHEMISTRY*		
		pH	Potential (mV-SCE)	i_H A/cm^2 ($\propto C_H^2$)
CRACK SIZE	0.25 mm Deep 0.5 μm Wide	4.1	-638	5×10^{-7}
	38 mm Deep 250 μm Wide	8.0	-664	3×10^{-8}

*E_{CORR} = -600mV-SCE Bulk pH = 6.0
K = 10 MPa√m

Model predictions and growth rate data for alternate stress corrosion cracking systems have not been compared to establish the importance of crack size. Doig and Flewitt(76) and Turnbull(73,79) predict that crack propagation rates controlled by anodic dissolution increase with decreasing crack size as shown in Fig. 9 for low alloy steel in a boiling caustic solution. Changing crack size between 0.1 and 2 mm significantly influences crack growth rate, while the effect saturates for larger crack sizes. Applied stress intensity is constant, but growth rate changes with crack size due to a chemical influence. Small cracks are sensitive to embrittlement because of relatively small potential differences between tip and surface, and because of enhanced elimination of dissolution products. Both phenomena promote rates of dissolution.

Smyrl and Newman(88) predict that diffusion supplies a propagating stress corrosion crack tip only for depths less than a_c, given by the ratio of diffusivity (D) to crack speed. For $a > a_c$, crack growth is length dependent at constant applied K, while short cracks propagate at faster rates which are not diffusion limited. For example, a_c equals 1 mm for typical values of D (10^{-3} mm^2/sec) and crack speed (10^{-3}mm/sec., Figure 8). Charnock and Taunt(89) demonstrated that solute penetration by diffusion into the occluded crack solution is proportional to $\sqrt{v}$ for a slowly moving crack with chemically reactive crack walls. Environment transport to the crack tip is enhanced for stress and geometry factors which increase crack opening.

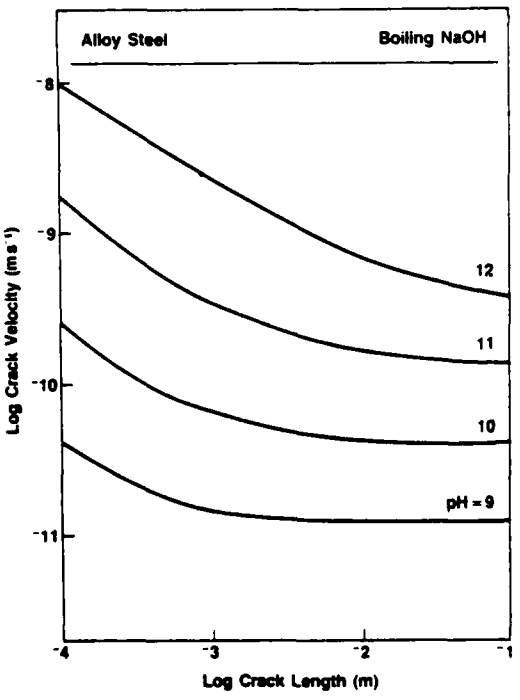

FIG. 9. Predicted effect of crack size on static load growth rates controlled by crack tip anodic dissolution for low alloy steel in boiling NaOH at constant crack opening. After Doig and Flewitt (1983).

CYCLIC LOADING: EXPERIMENTAL RESULTS Small fatigue crack-environment interactions have been investigated only for low alloy steels exposed to aqueous chloride solutions, a system relevant to many applications including offshore structures.(33,65,80,90,91) Specific data are summarized in Table II, where comparisons between short and long crack growth kinetics indicate marked compromises in similitude.

Important trends are apparent based on the data contained in Table II.

i) Small corrosion fatigue cracks always grow faster (between 1.2 and 300 times) than projected based on long crack kinetics at low to moderate ΔK and R values. Crack size influences corrosion fatigue growth rates comparably to well recognized variables.(80)

ii) The size regime for small crack-environment interactions is below about 3 mm. Results are, however, insufficient to exclude a size effect for deeper cracks.

iii) The magnitude of the small crack effect decreases with increasing a at constant $\Delta\sigma$ (increasing ΔK), with increasing $\Delta\sigma$ at constant a and with increasing R. Crack opening shape, approximated by mouth displacement, correlates a, $\Delta\sigma$, ΔK and R effects.(14,24) Stress effects are not universally observed.(29,30)

TABLE II
SMALL FATIGUE CRACK—ENVIRONMENT INTERACTION FOR STEELS IN WATER

Material	σ_y (MPa)	Environment	Crack Sizes (mm)	Rate Defined By ΔK?	$\frac{da/dN_{Short}}{da/dN_{Long}}$ @ ΔK Constant	'Short' Crack Regime (mm)	Mechanical Effect Considered	Comments	Ref
AISI 4130 (.3C-.9Cr-.2Ni)	1330	3% NaCl	.1 to 40	Yes-Air No-NaCl	1.2 to 300	1 to > 2.5	Yes	Small crack growth retarded by increased σ_{MAX}, described by V	21 24
HY-130 (.1C-.5Cr-5Ni)	—	3% NaCl	4 to 2.5	Yes-Air No-NaCl	1.0 to 2.5	4 to 1.0	Yes	ΔK described cracking at a > 1-3 mm; σ_{MAX} not important	29
HY-130	930	3% NaCl	1 to 40	Yes-Air No-NaCl	4.0	.1 to > 1.0	Yes	σ_{MAX} not important	30
HY-130	950	Seawater	> 5	Yes	1.0	—	Yes	Limited Data.	92
13Cr (.03C-12.8Cr-5Ni)	770	Water	?	No	4.0 @ R = 0 High @ R = 8		No	High frequency, near-ΔK_0 data Size effect intensified at high R $\Delta\sigma_{ov}(a)$ in Fig 1	20
Q1N (.17C-1.2Cr-2.4Ni)	825	Seawater	5-8	No	1.0 to 4.0	5 to 2.0	No	Crack size effect eliminated at $\Delta K > 30$ MPa·m$^{\frac{1}{2}}$ and R = 5 K, σ a interactions, reference environment not considered	22
BS-4360 (.18-1.17 Mn)	370	Seawater	1-7	Yes-Air No-Seawater	1.0 to 3.0	1.0-3.0	Yes	Crack size effect eliminated for air cathodic polarization	90
ENS (.3C-.67Mn)	300	Seawater	> 5	No	1.0 to 3.0	5 to 2.0	No	Limited Data	92

iv) The magnitude of the small crack effect decreases with decreasing yield strength, however, a systematic study has not been performed. This trend is consistent with a general decline in both environment sensitivity and the effects of R, frequency and environment activity with decreasing strength.(80,85)

v) The mechanism for the crack size effect is chemical for high strength steels, based on measured crack growth rates in benign environments and on the unlikely occurrence of mechanical effects on similitude for a > 0.1 mm. Mechanical effects may contribute to the rapid growth of short cracks in low strength steels. Studies in an inert environment have not been conducted to separate chemical and mechanical effects for such steels.

vi) Compliance measurements have not been reported for small cracks in embrittling environments. Environment enhanced plasticity, corrosion product and roughness induced closure contributions to retarded cracking cannot be assessed.

vii) The effects of cyclic frequency, electrochemical potential and bulk solution composition on the kinetics of small corrosion fatigue cracks have not been investigated extensively.(14,90)

viii) Small crack corrosion fatigue studies are impeded by problems in crack monitoring,(27) by the low frequencies and ΔK levels of interest,(90) by the possibility of net section yielding (9,25) and by small differences in growth rates, which are none-the-less relevant to long term component integrity.(90,92)

CYCLIC LOADING: THEORETICAL ANALYSES Early explanations for the rapid growth of small corrosion fatigue cracks were based on enhanced environment access to the crack tip.(22,23,54,90) The proximity concept is, however, overly simplistic. Recent results for 4130 steel demonstrate that small crack growth rates decrease with increasing stress and with decreasing crack size for very small cracks; embrittlement decreases as crack opening increases. (14,21,24) Tortuous, Stage I fatigue cracking is often not observed for aqueous environments. The proximity concept implies diffusional flow, however, precise transport mechanisms are not specified. Turnbull(57) demonstrates that mass transport is not necessarily impeded by increased crack depth because of the increasingly important contribution of convection. Finally, the proximity concept does not specify the chemical mechanism for brittle crack

extension. Impeded transport of an inhibiting species to the crack tip will, for example, result in enhanced crack propagation.

Modeling is required to define the effects of crack geometry on the chemical driving force for embrittlement. Mass transport by diffusion and convection determines crack chemistry,(57) which dictates transient reactions with straining crack surfaces,(29) which, in turn, control brittle crack advance. A detailed theory does not exist.(71) Elements of the problem are, however, developed from a hydrogen embrittlement perspective, and are relevant to corrosion fatigue by dissolution and film rupture. For steel in an aqueous solution, hydrogen is produced by hydrolysis within the occluded, pulsating crack.(86,93) The time and cycle dependent corrosion fatigue components to the total crack growth rate, da/dN_{CF}, are defined by (14,29,32,65):

$$\frac{da}{dN_{CF}} = \phi C_H(\sigma,a,t)\ \Delta K^2, \qquad (8)$$

where ϕ is a constant. The chemical driving force is represented by the concentration of adsorbed hydrogen (C_H) which is crack size, stress and time dependent. The mechanical driving force is accounted for by ΔK^2.

If convective mixing is ignored, then modeling of the static crack provides a description of $C_H(\sigma,a,t)$,(57,73,79) with enhanced acidification and hydrogen discharge predicted for decreased crack size (Table I). Since hydrogen embrittlement is probable for the conditions represented in Table II, (65,86,93) this result provides a reasonable explanation for the rapid growth of small corrosion fatigue cracks. For 4130 steel the crack size effect on corrosion fatigue, Fig. 2, is predicted in part based on linear superposition of stress corrosion growth rates for "short" and "long" cracks (Fig. 8a) combined with growth rates for a benign environment.(24) This comparison adds credence to the applicability of the static crack model for hydrogen production.

Crack size dependent convection effects cannot, however, be ignored.(57,74,75,77,78) Considering hydrolysis, no model exists to describe convection effects on electrode potential, pH and metal ion concentrations within a pulsating crack. The importance of crack geometry dependent convection is illustrated by analyses of dissolved O_2 supply and reduction within a crack. Static cracks are presumed to be fully oxygen depleted due to cathodic reduction dominating diffusional supply; O_2 does not affect C_H.(73,74) Convection provides an additional source of oxygen which consumes protonic hydrogen during each load cycle. C_H and da/dN_{CF} are reduced for decreased acidification traceable to "oxygen inhibition".

Perfect mixing analysis of O_2 supply and reaction demonstrates that depletion, and by inference the effect of O_2 on corrosion fatigue, are reduction rate, cyclic frequency, crack size and opening shape dependent. Taunt and Charnock(77) analyzed solute supply and reaction within a crack as a function of load cycles for a variety of rate expressions. Turnbull(74) focused a similar analysis on O_2 depleted at a rate proportional to instantaneous concentration. Each model demonstrates that ΔK similitude is compromised. These approaches were modified(14) to predict the concentration of dissolved $O_2(C_0)$ within small cracks for square wave fatigue loading in aqueous chloride at a frequency of $1/\tau$ and O_2 reduction at a rate given by αC_0. The result is:

$$C_0 = C_B (1 - R) \exp\left(\frac{-\alpha A_c \tau a^*}{2V_{max}}\right) \qquad (9)$$

where C_B = bulk solution oxygen concentration, A_c = crack surface area, V_{max} = crack solution volume at K_{max}, and a^* = geometric constant. For a wedge crack, the ratio of A_c to V_{max} equals $4/\nu_{max}$. As such C_0 depends exponentially on $-1/\nu_{max}$, a parameter which is crack depth sensitive at constant ΔK. (Typically, $\nu_{max} \alpha (\alpha_{max} a) \alpha (K_{ma} \sqrt{a})$.) Physically, depletion is controlled by the ratio of active crack surface area available for reaction, a^*A_c, to the occluded solution volume, V_{max}, which supplies reactant. Small cracks are distinguished by a large surface to occluded solution volume ratio, and hence by extremely low values of C_0 compared to long cracks at constant ΔK. Equation 9 is plotted in Fig. 10 as a function of edge crack depth for constant ΔK, frequency and reaction rate conditions. C_0/C_B is on the order of 10^{-40} for 0.1 mm deep cracks, and rises rapidly to values between 10^{-4} and 10^{-2} for cracks deeper than 5 mm.(14)

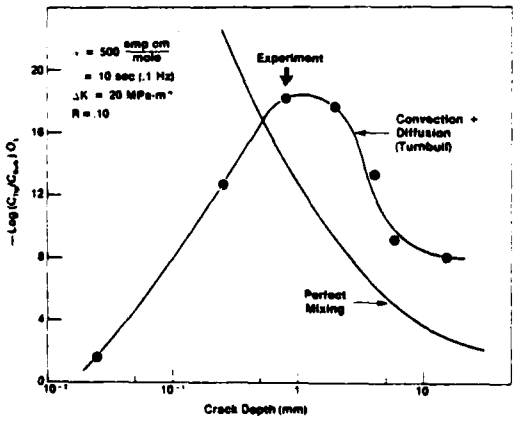

FIG. 10. Analytical predictions of the effect of edge crack length on dissolved oxygen content at constant ΔK. Modeling includes O_2 depletion by cathodic reduction and O_2 supply by either perfect convective mixing (Gangloff, 1984) or diffusion and laminar convection (Turnbull, 1983).

The unique chemical character of small cracks is confirmed by relating perfect mixing to brittle corrosion fatigue. Specifically, the hydrogen ion concentration remaining at the end of a square wave load cycle is calculated based on O_2 reduction to consume H^+ and produce OH^-. O_2 modified acidification is related to C_H and corrosion fatigue crack growth rate through equation 8 to yield either:(16)

$$\text{LOG}\,\frac{da}{dN_{CF}} = \phi + \alpha\tau(a^*/\nu_{max}) \qquad (10)$$

at constant ΔK, or the normalized equation listed and plotted in Fig. 11. (Rates are normalized by an absolute brittle crack growth rate (da/dN_{CF-ABS}) independent of O_2 inhibition to account for the mechanical influence of ΔK^2.) The extent of O_2 inhibition increases as the normalized growth rate parameter decreases from 1.0 to 0. Physically, increased crack length results in increased crack solution volume to active surface area, increased O_2 reduction persisting to longer times during loading, decreased hydrogen production and hence in reduced rates of brittle corrosion fatigue.

The perfect mixing analysis of O_2 inhibition is consistent with experimental results. The logarithm of corrosion fatigue crack growth rate for 4130 steel in saltwater (Fig. 2) varies linearly with reciprocal maximum crack mouth opening as shown in Fig. 11 and predicted by equation 10. The O_2 reduction rate constant inferred from least squares slope analysis is of the correct order. Similar good agreement is observed at constant ΔK without normalization.(14) Considering Fig. 11, compact tension cracking produces small changes in ν_{max} (squares) compared to the results for 0.5 to 3 mm deep edge and surface cracks. The retarding influences

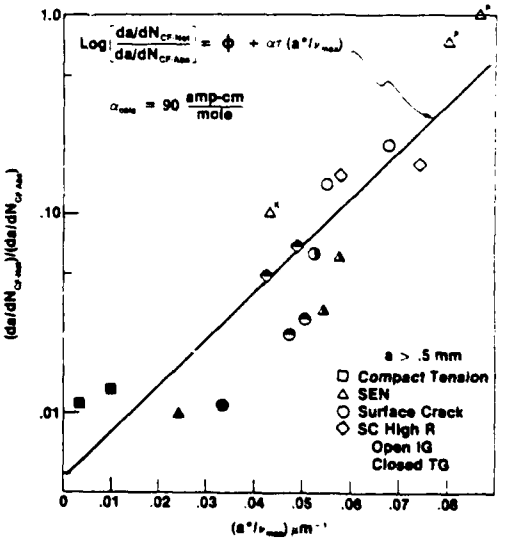

FIG. 11. Experimental data and analytical prediction for the effect of crack shape, given by reciprocal crack mouth opening at maximum load, on corrosion fatigue crack growth rate for 4130 steel in 3% NaCl. Fracture mechanics similitude predicts a horizontal line at 1.0. After Gangloff (1984).

of increased stress, produced by increased R, increased $\Delta\sigma$ or instantaneous stress increases; and of increased crack size are accounted for by maximum crack opening shape. A brittle fracture mode transition occurs with decreasing da/dN_{CF} and correlates with $(\nu_{max})^{-1}$ indicative of a chemical crack size effect. Intergranular cracking (open symbols) at small ν_{max} is replaced progressively by brittle transgranular fracture (filled symbols) at increased ν_{max}. Many of the trends represented for lower strength steels in Table II are consistent with maximum crack mouth opening displacement control and perhaps O_2 inhibition. Small cracks grow at the fastest rates when sized below 1 mm and when stressed at low ΔK and R. Cracking is retarded by increased a, ΔK or R, or equivalently, by increased crack mouth opening.

While the breakdown in ΔK similitude and the correlation between da/dN_{CF} and crack opening are well established in Fig. 11, the O_2 inhibition model is speculative. Acidification differences may contribute to crack size effects, Table I. Experiments with deoxygenated solutions are inconclusive for 4130 steel,(14) relevant values of α are uncertain and may exceed 15 amp·m/mole,(74,75,79) and perfect mixing may provide an inaccurate description of mass transport. Turnbull argues that mass transport within a slowly cycled (< 1 Hz) corrosion fatigue crack is viscous-laminar.(57) Turbulence is expected and perfect mixing is relevant only when crack surface contact occurs. For viscous flow, a transition crack size (a_T) is defined:

$$a_T = \frac{\sqrt{(D/f)}}{1 - R^{(.5 \text{ to } 1.0)}} , \qquad (11)$$

where f is cyclic frequency and the exponent depends on precise crack shape. Diffusion dominates mass transport for cracks sized below a_T, while deeper cracks are supplied predominantly by convection. a_T equals between 0.1 and 0.2 mm for oxygen dissolved in water and a loading frequency of 0.1 Hz.

Crack size, ΔK, frequency, R and chemical reaction rate influence crack chemistry, as illustrated by analysis of diffusional/laminar convectional O_2 supply and cathodic reduction.(57,75,79) A typical prediction is presented in Fig. 10 and compared to the perfect mixing approximation for the same conditions. Note that perfect mixing provides an upper bound on dissolved O_2 within the crack. At very small crack depths, O_2 is enriched significantly due to diffusion. As crack size increases, O_2 diffusion decreases and convection increases. C_0 is minimized, and further increases in crack depth result in increased dissolved O_2 due to convection. The comparison between crack growth rate data and perfect mixing theory, Fig. 11, is for small cracks sized above 0.5 mm to avoid the complicating effects of diffusion. Crack growth rates at constant ΔK for 4130 steel in saltwater exhibit a maximum

AD-A142 609 FATIGUE BEHAVIOR OF LONG AND SHORT CRACKS IN WROUGHT AND POWDER ALUMINUM..(U) CALIFORNIA UNIV BERKELEY DEPT OF MATERIALS SCIENCE AND MINERA.. R O RITCHIE MAY 84 3/3

UNCLASSIFIED UCB/RP/84/A1021 AFOSR-TR-84-0509 F/G 11/6 NL

END
DATE FILMED
8-84
DTIC

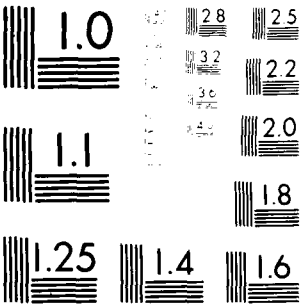

at a = 0.8 mm, and decline with increasing and decreasing crack size.(14) The complex effect of crack size on crack chemistry illustrated in Figure 10 may be general. The minimum value of C_0 represents that crack depth where transport of either a bulk specie to the tip or a crack tip reaction product to the bulk is most effectively impeded. Modeling further indicates that, for the long crack convection dominated regime, concentration increases with decreasing O_2 reduction rate and increasing ΔK, R and frequency. Variable effects on the location of the maximum in Figure 10 have not been analyzed in detail. Experimental evidence for crack size effects of the type predicted in Fig. 10 is lacking.

4. SUMMARY

When analyzing the growth of small fatigue cracks in embrittling gaseous and aqueous environments, ΔK or ΔJ based similitude concepts must be examined. Data confirm that small crack geometry effects are not wholly accounted for by a crack tip field parameter. Crack size and opening shape must be considered as variables, and crack closure phenomena characterized experimentally. Unfortunately, it is not possible to provide general criteria which define limiting crack size and shape for ΔK similitude from an environmental perspective. Crack size effects are material and environment specific, and may vary with alloy strength, cyclic frequency, temperature, applied potential or gas pressure. Theoretical analyses of the mechanical and chemical origins of the driving force for brittle crack growth clearly establish the potential for novel small crack-environment interactions. Refined analyses are required, however, to fully define crack geometry effects. Experimental tools exist to assess the importance of crack size effects for specific corrosion fatigue applications.

Understanding of small crack effects is limited for technologically important, low strength alloys in gas, water, chloride or caustic environments, and for both static and cyclic loading. Deleterious chemical crack size effects are documented for high strength steel in aqueous chloride and gaseous hydrogen, and mechanistic understanding is forthcoming. Complicating plasticity and wake, roughness and corrosion debris induced closure effects are unlikely. In contrast research is required for low strength structural steels. Crack size effects are suggested experimentally and hydrogen is known to embrittle such alloys, albeit less severely compared to high strength steels. Environment enhanced plasticity and closure mechanisms are particularly relevant for lower strength alloys. As such, the range of interactions considered in this review may impact corrosion fatigue and produce complex crack size effects. For alternate environments, the potential exists for crack geometry effects on localized chemistry. For example, the chloride conditions described in previous sections were unbuffered and at the free corrosion potential. Transport of buffering species, as

encountered in seawater or inhibited solutions, and the response of crack tip potential and electrochemical reactions to applied potential, as encountered in cathodic protection, are likely to be crack geometry sensitive. Crack geometry effects related to anodic dissolution and film rupture are largely undefined. The research challenge exists to isolate, measure and model such geometry sensitive processes.

ACKNOWLEDGEMENTS

This work was supported by the Corporate Research Science Laboratories of the Exxon Research and Engineering Company (for R.P.G.), and under Grant No. AFOSR-82-0181 from the U.S. Air Force Office of Scientific Research (for R.O.R.).

REFERENCES

(1) Williams, M. L. (1957). Journal of Applied Mechanics, Trans. ASME, 24, 104-109.
(2) Hutchinson, J. R. (1968). J. Mech. Phys. Solids, 16, 13-31.
(3) Rice, J. R. & Rosengren, G. F. (1968). J. Mech. Phys. Solids, 16, pp. 1-12.
(4) McEvily, A. J. & Wei, R. P. (1973). Corrosion Fatigue: Chemistry Mechanics and Microstructure, eds. O. Deveraux, A. J. McEvily and R. W. Staehle, pp. 381-395, Houston: NACE.
(5) Brown, B. F. (1968). Met. Rev., No. 129, 171-183.
(6) Novak, S. R. & Rolfe, S. T. (1970). Corrosion, 26, 121-130.
(7) Shahinian, P. & Judy, Jr., R. W. (1976). Stress Corrosion: New Approaches, ASTM STP 610, ed. H. L. Craig, Jr., pp. 128-142, Philadelphia: ASTM.
(8) Hertzberg, R. W. (1983). Deformation and Fracture Mechanics of Engineering Materials, pp. 519-618, New York: John Wiley and Sons.
(9) Dowling, N. E. (1977). Cyclic Stress-Strain and Plastic Deformation Aspects of Fatigue Crack Growth, ASTM STP 637, pp. 97-121, Philadelphia: ASTM.
(10) Rice, J. R., et al. (1980). Fracture Mechanics, 12th Conf., ASTM STP 700, pp. 189-221, Philadelphia: ASTM.
(11) Suresh, S., & Ritchie, R. O. (1984). Int. Metals Reviews, 25, in press.
(12) Suresh, S. (1983). Metall. Trans. A, 14A, 2375-2385.
(13) Hudak, S. J. (1981). J. Eng. Matls. Technol., Trans. ASME, Ser. H, 103, 26-35.
(14) Gangloff, R. P. (1984). Embrittlement by the Localized Crack Environment, ed. R. P. Gangloff, Warrendale, PA: TMS-AIME, in press.
(15) Ritchie, R. O., & Suresh, S. (1983). Mater. Sci. Eng., 57, 127-130.
(16) Miller, K. J. (1982). Fat. Eng. Matls. Struc., 5, 223-232.

(17) Leis, B. N., et al. (1983). Air Force Wright Aeronautical Labs, Report No AFWAL-TR-83-4019, Wright-Patterson AFB, Ohio.
(18) Lankford, J. & Davidson, D. L. (1984). Fatigue Crack Growth Threshold: Concepts, eds. D. L. Davidson and S. Suresh, Warrendale, PA: TMS-AIME,in press.
(19) Tanaka, K. & Nakai, Y. (1983). Fat. Eng. Matls. Struc., 5, 315-327.
(20) Usami, S. & Shida, S. (1979). Fat. Eng. Matls. Struc., 1, 471-481.
(21) Gangloff, R. P. (1981). Res. Mech. Let., 1, 299-306.
(22) Jones, B. F. (1982). J. Matl. Sci., 17, 499-507.
(23) Holder, R. (1977). Proc. Conf. on Influence of Environment on Fatigue, pp. 37-41, London: Instit. Mech. Engr.
(24) Gangloff, R. P. (1984). Metall. Trans. A, submitted for publication.
(25) El Haddad, M. H., et al. (1980). Int. J. Fract., 16, 15-30.
(26) Lankford, J. (1982). Fat. Eng. Matls. Struc., 5, 233-248.
(27) Gangloff, R. P. (1982). Advances in Crack Length Measurement, ed. C. J. Beevers, pp. 175-221, London: EMAS.
(28) Lankford, J. (1983). Fat. Eng. Matls. Struc., 6, 5-31.
(29) Wei, R. P., et al. (1984). Embrittlement by the Localized Crack Environment, ed. R. P. Gangloff, Warrendale, PA: TMS-AIME, in press.
(30) Hudak, S. J. & Gangloff, R. P. (1984). unpublished research.
(31) Miller, K. J. (1984). Proc. This Conference, Cambridge: Cambridge University Press.
(32) Wei, R. P. & Simmons, G. W. (1981). Int. J. Frac., 17, 235-247.
(33) Scott, P. M. (1984). Corrosion Fatigue Mechanics, Metallurgy, Electrochemistry and Engineering, ASTM STP, Philadelphia, PA: ASTM, in press.
(34) Walker, N. & Beevers, C. J. (1979). Fat. Eng. Matls. Struc., 1, 135-148.
(35) Minakawa, K. & McEvily, A. J. (1981). Scripta Metall., 15, 633-636.
(36) Toplosky, J. & Ritchie, R. O. (1981). Scripta Metall., 15, 905-908.
(37) Endo, K. et al. (1972). Bull. JSME, 25, 439-445.
(38) Tzou, J.-L., et al. (1984). Acta Met, submitted for publication.
(39) Vosikovsky, O. & Cooke, R. J. (1978). Int. J. Pres. Ves. & Piping, 5, 113-129.
(40) Kesten, M. & Windgasser, K.-F. (1981). Hydrogen Effects in Metals, eds. I. M. Bernstein and A. W. Thompson, pp. 1017-1025, Warrendale, PA: TMS-AIME.
(41) Maddox, S. J. (1974). Weld. Res. Suppl., 53, 4015-4095.
(42) Chauhan, P. & Roberts, B. W. (1979). Metall. Matl. Tech., 131-136.
(43) Bennett, J. A. & Mindlin, H. (1973). J. Test. Eval., 1, 152-161.
(44) Jack, A. R. & Paterson, A. N. (1977). Proc. Inst. Mech. Engr. Conf. Fat., paper C107/77, pp. 75-83, London: IMECHE.
(45) Muller, M. (1982). Metall. Trans. A, 13A, 648-655.

(46) Hoeppner, D. W. (1979). Fatigue Mechanisms, ASTM STP 675, ed. J. T. Fong, pp. 841-870, Philadelphia: ASTM.
(47) Kitagawa, H. & Takahasi, S. (1976). Proc. 2nd Intl. Conf. on Mech. Beh. Matls., pp. 627-663, Metals Park, Ohio: ASM.
(48) Lynch, S. (1983). Advances in the Mechanics and Physics of Surfaces, eds. R. M. Latanision and T. E. Fischer, pp. 265-364, New York: Harwood Academic Publishers.
(49) Hirth, J. P. (1980). Metall. Trans. A, 11A, 861-874.
(50) Davidson, D. L. & Lankford, J. (1983). Fat. Eng. Matls. Struc., 6, 241-256.
(51) Lankford, J. (1983). Mechanical Behavior of Materials - IV, eds. J. Carlsson and N. G. Ohlson, 1, pp. 3-29, Oxford: Pergamon Press.
(52) Bilby, B. A., et al. (1977). Fracture (ICF-4), ed. D. M. R. Taplin, 3, pp. 197-212, Waterloo, Canada: Univ. of Waterloo Press.
(53) Suresh, S. & Ritchie, R. O. (1984). Fatigue Crack Growth Threshold: Concepts, eds. D. L. Davidson and S. Suresh, Warrendale, PA:TMS-AIME, in press.
(54) Tomkins, B. (1977). Proc. Conf. on Influence of Environment on Fatigue, pp.111-115, London: IMECHE.
(55) Forsyth, P. J. E. (1962). Crack Propagation, p. 76, Cranfield College of Aeronautics: Cranfield Press.
(56) Tu, L. K. L. & Seth, B. B. (1978). J. Test Eval., 6, 66-74.
(57) Stubbington, C. A. (1963). Metallurgica, 68, 109-121.
(58) Elber, W. (1971) Damage Tolerance in Aircraft Structures, ASTM STP 486, pp. 230-242, Philadelphia, PA: ASTM.
(59) Tzou, J.-L., et al. (1984). Acta Met., submitted for publication.
(60) Morris, W. L., et al. (1981). Eng. Fract. Mech., 18, 871-977.
(61) Newman, J. C. (1983). Behavior of Short Cracks in Airframe Components, vol. CP 328, pp. 7.1-7.16, Advisory Group for Aeronautical Research and Development.
(62) Ritchie, R. O., et al. (1980). J. Eng. Matls. Tech., Trans. ASME, Ser. H, 102, 293-299.
(63) Stewart, A. T. (1980). Eng. Fract. Mech., 13, 463-478.
(64) Suresh, S., et al. (1981). Metall. Trans. A, 12A, 1435-1443.
(65) Scott, P. M., et al. (1983). Corros. Sci., 23, 559-575.
(66) Hartt, W. H., & Rajpathak, S. S. (1983). "Formation of Calcareous Deposits Within Simulated Fatigue Cracks in Seawater," Corrosion/83, Paper No. 62, Houston: NACE.
(67) Suresh, S., et al. (1982). Fatigue Thresholds, eds. J. Backlund, A. Blom and C. J. Beevers, 1, pp. 391-408, Warley, U.K: EMAS.
(68) Suresh, S. & Ritchie, R. O. (1982). Metall. Trans. A, 13A, 1627-1631.
(69) Esaklul, K. A., et al. (1983). Scripta Met., 17, 1073-1078.
(70) Gangloff, R. P. (1984). unpublished research.
(71) Embrittlement by the Localized Crack Environment (1984). ed. R. P. Gangloff, Warrendale, PA: TMS-AIME, in press.
(72) Lawn, B. R. (1977). Mat. Sci., 13, 277-283.

(73) Turnbull, A. & Thomas, J. G. N. (1982). J. Electrochem. Soc., 129, 1412-1422.
(74) Turnbull, A. (1980). Br. Corros. J., 15, 162-171.
(75) Turnbull, A. (1982). Corros. Sci., 22, 877-893.
(76) Doig, P. & Flewitt, P. E. J. (1983). Metall. Trans. A, 14A, 978-983.
(77) Taunt, R. J. & Charnock, W. (1978). Matl. Sci. Engr., 35, 219-228.
(78) Hartt, W. H., et al. (1978). Corrosion Fatigue Technology, ASTM STP 642, eds. H. C. Craig, Jr., T. W. Crooker, and D. W. Hoeppner, pp. 5-18, Philadelphia: ASTM.
(79) Turnbull, A. (1983). National Physical Laboratory Report No. NPL DMA (D) 363, England.
(80) Jaske, C. E., et al. (1981). MCIC Report 81-42, Columbus, Ohio: Battelle.
(81) Snowdon, K. V. (1963). J. Appl. Phys., 34, 3150-1.
(82) Gangloff, R. P. (1984). Liquid and Solid Metal Induced Embrittlement, ed. M. H. Kamdar, Warrendale, PA: TMS-AIME, in press.
(83) Bradshaw, F. J. (1967). Scripta Met., 1, 41-43.
(84) Wei, R. P. & Gao, Ming (1983). Scripta Met., 17, 959-962.
(85) Carter, C. S. (1977). Stress Corrosion Cracking and Corrosion Fatigue of Medium and High Strength Steel, Boeing Co. Report, Seattle, Washington.
(86) Brown, B. F. (1976). Stress Corrosion Cracking and Hydrogen Embrittlement of Iron Based Alloys, eds. J. Hockmann, J. Slater, R. D. McCright and R. W. Staehle, pp. 747-750, Houston: NACE.
(87) Sandoz, G., et al. (1970). Corros. Sci., 10, 839-845.
(88) Smyrl, W. H. & Newman, J. (1974). J. Electrochem. Soc., 121, 1000-1007.
(89) Charnock, W. & Taunt, R. J. (1978). Metall. Trans. A, 9A, 880-881.
(90) Bardal, E., et al. (1978). Proc. Conf. European Offshore Steel Research, pp. 415-436, London: Welding Institute.
(91) Cotton, H. C. (1979). Proc. Inst. Mech. Engrs., 193, 193-206.
(92) Jones, B. F. (1984). Embrittlement by the Localized Crack Environment, ed. R. P. Gangloff, Warrendale, PA: TMS-AIME, in press.
(93) Barsom, J. M. (1971). Int. J. Frac. Mech., 7, 164-182.

ON THE LOCATION OF CRACK CLOSURE AND THE THRESHOLD CONDITION FOR FATIGUE CRACK GROWTH

E. Zaiken and R. O. Ritchie

Department of Materials Science and Mineral Engineering
University of California, Berkeley, California 94720

April 1984

Report No. UCB/RP/84/A1019

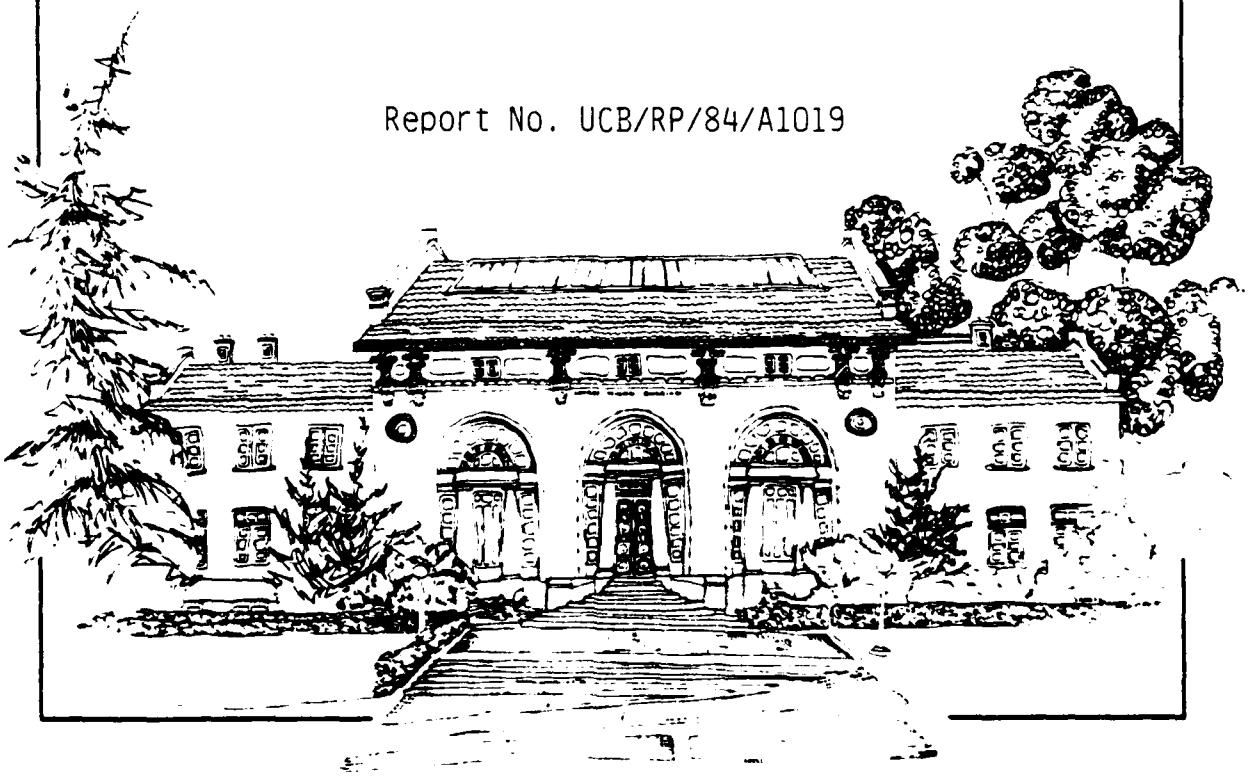

Report No. UCB/RP/84/A1019

ON THE LOCATION OF CRACK CLOSURE AND THE THRESHOLD CONDITION FOR FATIGUE CRACK GROWTH

E. Zaiken and R. O. Ritchie

Department of Materials Science and Mineral Engineering
University of California, Berkeley, CA 94720

April 1984

Submitted to Scripta Metallurgica

ON THE LOCATION OF CRACK CLOSURE AND THE THRESHOLD CONDITION FOR FATIGUE CRACK GROWTH

E. Zaiken and R. O. Ritchie
Department of Materials Science and Mineral Engineering
University of California, Berkeley, California 94720

Introduction

Recent studies on the propagation of fatigue cracks at ultralow growth rates (i.e., typically approaching lattice dimensions per cycle) have suggested that the existence of a fatigue threshold, representing a stress intensity range ΔK_{TH} below which cracks appear dormant, is intimately associated with the development of crack closure in the wake of the crack tip (e.g., 1-13). Observations that short cracks (small compared to microstructural size-scales or the extent of local plasticity) can propagate below this threshold (13-15), are consistent with this notion since by definition short cracks possess a limited wake and are thus less likely to be influenced by closure to the same degree as long cracks (e.g., 13,15).

Such closure, which results from interference between mating fracture surfaces, acts to reduce the local driving force from the nominal level, based on global measurements of applied loads and crack size, e.g., $\Delta K = K_{max} - K_{min}$, to some effective near-tip level, e.g., $\Delta K_{eff} = K_{max} - K_{cl}$, where K_{cl} is the stress intensity at first contact of the crack surfaces during unloading (16). The origin of such closure has been related to several mechanisms (12), including cyclic plasticity (16), the wedging action of insoluble corrosion products (2-4) or irregular fracture surface morphologies coupled with inelastic crack tip shear displacements (5-7), fluid-induced pressure inside the crack (17,18) and metallurgical phase transformations (12).

Despite a good phenominalogical description of closure, the significance of where the actual fracture surface contact develops in relation to the crack tip is still poorly understood. Recent studies (10) in powder metallurgy X-7090-T6 aluminum alloys, where material left in the wake of a crack at threshold was removed by electro-discharge machining, indicated that closure well behind the crack tip was relatively unimportant compared to near-tip closure (i.e., within 1 mm of the tip), which was considered to contribute most to the development of a threshold level. In another study (19) in nickel-based superalloys (Waspaloy), however, where a single 0.31 mm diameter hole was drilled a short distance (within 0.31 mm) behind the tip of a threshold crack, the degree of closure was reported to be not significantly affected.

The aim of the current note is to substantiate whether near-tip crack closure is most responsible for the development of a threshold by specifically monitoring the closure stress intensity, K_{cl}, during the progressive (on load) removal of material in the wake of an arrested crack at ΔK_{TH}.

Experimental Procedures

Tests were performed on commercial, ingot metallurgy 7150 alloy plate, of composition (wt%) Al-1.16Zn-2.16Mg-2.10Cu-0.07Si-0.11Fe-0.13Zr-0.02Ti, in the peak-aged (T6) condition (i.e., solution treated, quenched, stretched 2%, and aged at 121°C for 100 hr). Room temperature mechanical properties are shown in Table 1.

Fatigue crack growth rates were monitored, using D.C. electrical potential techniques, on 6.4 mm thick compact C(T) test-pieces machined in the T-L orientation. Using conventional manual load-shedding to approach the threshold (20), tests were performed under load control at 50 Hz (sine wave) with a load ratio ($R = K_{min}/K_{max}$) of 0.1 in controlled room air (22°C, 45% relative humidity).

TABLE 1

Room Temperature Uniaxial Tensile Properties of 7150-T6

0.2% Offset Yield Strength	U.T.S.	Elong. on 32 mm Gauge	Redn. in Area	Work Hardening Exponent (n)
(MPa)	(MPa)	(%)	(%)	
404	480	6.0	10.3	0.046

Macroscopic crack closure measurements were made with the back-face strain technique using two strain gauges to record strain both parallel and perpendicular to the loading axis. Mean closure loads, deduced from the point during the fatigue cycle at which the resulting elastic compliance curves, of load versus relative strain, deviated from linearity, were utilized to compute stress intensities at closure, K_{cl} (21).

Results and Discussion

The variation in fatigue crack propagation rates with stress intensity range ΔK, for 7150-T6 aluminum alloy over the range 10^{-8} to 10^{-3} mm/cycle, is shown in Fig. 1 from the load shedding data at $R = 0.1$, and indicates a long crack threshold of $\Delta K_{TH} \approx 2.6$ MPa$\sqrt{m}$. Corresponding closure measurements, presented in Fig. 2 as the ratio of closure to maximum stress intensity, K_{cl}/K_{max}, as a function of ΔK, show a progressively increasing influence of closure as the threshold is approached, with $K_{cl}/K_{max} \rightarrow 1$ as $\Delta K \rightarrow \Delta K_{TH}$.

To determine the location of the closure most significant to the development of this threshold, material in the wake of the crack tip was progressively removed, in steps of roughly 1 mm, from cracks arrested at ΔK_{TH}, whilst the specimen was maintained at mean load. Material was removed to within 0.5 mm of the tip using a fine jeweler's saw on cracks typically of a total length (including notch) of the order of 25 mm. The width of the saw cut was approximately 0.3 mm. At each stage of the removal, with the remaining fatigue crack varying from an initial 8 mm to 0.5 mm, closure measurements were made to determine K_{cl} using a threshold loading cycle. The results, in terms of the ratio K_{cl}/K_{max} as a function of the remaining fatigue crack length, $\tilde{a}$, are shown in Fig. 3 and indicate the distribution of closure along the crack length. It is apparent that, although the extent of closure is fairly evenly distributed over the majority of the crack length, more than 40% of the closure is developed within a region 0.5 mm of the crack tip. For example, at ΔK_{TH}, the arrested fatigue crack, of length $\tilde{a} \approx 8$ mm, has a closure stress intensity of $K_{cl} \approx 2.5$ MPa$\sqrt{m}$ ($\Delta K_{eff} \approx 0.4$ MPa$\sqrt{m}$) at the nominal threshold of $\Delta K_{TH} = 2.6$ MPa$\sqrt{m}$ ($R = 0.1$). After removal of 7.5 mm of wake, however, K_{cl} is reduced to 1.1 MPa$\sqrt{m}$ ($\Delta K_{eff} \approx 1.8$ MPa$\sqrt{m}$) such that the remaining closure is confined within the very near tip region.

The effect of this removal of closure can be best appreciated by immediate re-cycling of the previously arrested crack following wake removal ($\tilde{a} = 0.5$ mm) under the same constant $\Delta K = \Delta K_{TH}$ conditions, i.e., similar to experiments in ref. 10. Even though nominal ΔK levels do not exceed the threshold, crack growth re-commences consistent with the local increase in ΔK_{eff} (Fig. 1). In essence, the crack behaves as an effective "short" crack. As shown in Fig. 4, after an initial acceleration subsequent growth rates reach a plateau, but do not completely re-arrest. This is presumably due to experimental difficulties in maintaining constant ΔK cycling precisely at the threshold level of 2.6 MPa$\sqrt{m}$, in a region where growth rates are extremely dependent upon ΔK (Fig. 1).

Parallel studies on mechanisms of fatigue crack growth in this alloy suggest that such crack closure can originate from several sources (22). Oxide-induced closure, however, does not appear to be a major factor as Auger studies on broken fracture surfaces reveal only uniformly thin oxide films, small compared to crack tip opening displacements (i.e., less than 50 Å thick even close to ΔK_{TH}). Due to the irregular nature of the crack path, however, roughness-induced crack closure would seem to provide a more potent contribution, although this effect is less pronounced than in underaged structures where the greater planarity of slip promotes greater crack deflection and hence more closure (22-24).

Concluding Remarks

The present experiments on ingot aluminum alloys provide further confirmation that the development of a threshold for the growth of "long" fatigue cracks is primarily associated with a reduction in local crack driving force due to crack closure in the wake of the crack tip. Moreover, based on studies of the change in K_{cl} during progressive removal of the wake at threshold levels, it appears that, although such closure is fairly evenly distributed over most of the crack length, more than 40% of the closure is confined to the near-tip region; in the present case within 0.5 mm of the crack tip.

Acknowledgements

The work was supported by the Air Force Office of Scientific Research under Grant No. AFOSR 82-0181. Thanks are due to Dr. Alan H. Rosenstein for helpful discussions, the ALCOA Foundation for additional support and ALCOA for provision of material.

References

1. P. C. Paris, R. J. Bucci, E. T. Wessel, W. G. Clark and T. R. Mayer: ASTM Spec. Tech. Publ. 513, p. 141 (1972).
2. R. O. Ritchie, S. Suresh and C. M. Moss: J. Eng. Matls. Tech., 102, 293 (1980).
3. A. T. Stewart: Eng. Fract. Mech., 13, 463 (1980).
4. S. Suresh, G. F. Zamiski and R. O. Ritchie: Met. Trans. A, 12A, 1435 (1981).
5. N. Walker and C. J. Beevers: Fat. Eng. Mat. Struct., 1, 135 (1979).
6. K. Minakawa and A. J. McEvily: Scripta Met., 15, 937 (1981).
7. S. Suresh and R. O. Ritchie: Met. Trans. A, 13A, 1627 (1982).
8. P. K. Liaw, T. R. Leax, R. S. Williams and M. G. Peck: Met. Trans. A, 13A, 1607 (1982).
9. M. Zedalis, L. Filler and M. E. Fine: Scripta Met., 16, 471 (1982).
10. K. Minakawa, J. C. Newman and A. J. McEvily: Fat. Eng. Mat. Struct., 6, 359 (1983).
11. W. W. Gerberich, W. Yu and K. Esaklul: Met. Trans. A, 15A (1984), in press.
12. S. Suresh and R. O. Ritchie: in Fatigue Crack Growth Threshold: Concepts, D. L. Davidson and S. Suresh, eds., TMS-AIME, Warrendale, PA (1984), in press.
13. S. Suresh and R. O. Ritchie: Int. Met. Rev., 25 (1984), in press.
14. J. Lankford: Fat. Eng. Mat. Struct., 5, 223 (1982).
15. J. L. Breat, F. Mudry and A. Pineau: Fat. Eng. Mat. Struct., 6, 349 (1983).
16. W. Elber: ASTM Spec. Tech. Publ. 486, p. 230 (1981).
17. K. Endo, T. Okada, K. Komai and M. Kiyota: Bull. JSME, 15, 1316 (1972).
18. J. L. Tzou, S. Suresh and R. O. Ritchie: Acta Met. (1984), in review.
19. T. V. Duggan: in Fatigue Thresholds, J. Backlund, A. Blom and C. J. Beevers, eds., EMAS Ltd., Warley, U.K., vol. 2, p. 809 (1982).
20. R. O. Ritchie: Int. Met. Rev., 20, 205 (1979).
21. V. B. Dutta, S. Suresh and R. O. Ritchie: Met. Trans. A, 15A (1984), in press.
22. E. Zaiken and R. O. Ritchie: Mater. Sci. Eng. 1984, in review.
23. S. Suresh, A. K. Vasudévan and P. E. Bretz: Met. Trans. A, 15A, 369 (1984).
24. R. D. Carter, E. W. Lee, E. A. Starke and C. J. Beevers: Met. Trans. A, 15A, 555 (1984).

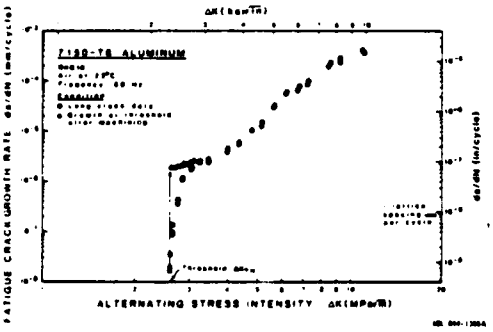

FIG. 1

Variation in fatigue crack propagation rates (da/dN) with stress intensity range (ΔK) for 7150-T6 aluminum alloy in room air at a load ratio of 0.10. Open triangles refer to the behavior of the previously arrested crack at the threshold ΔK_{TH} immediately following removal of the wake to within 0.5 mm of the crack tip.

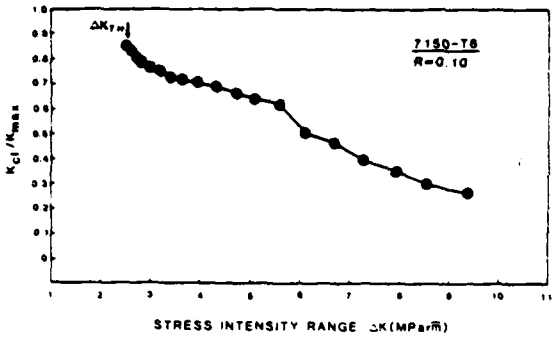

FIG. 2

Experimental closure measurements using the back-face strain technique showing the ratio of closure to maximum stress intensity, K_{cl}/K_{max}, as a function of the alternating stress intensity, ΔK, relevant for the load shedding data shown in Fig. 1.

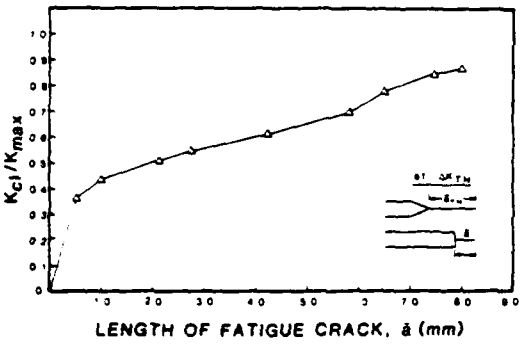

FIG. 3

Variation in crack closure, measured in terms of K_{cl}/K_{max}, for an arrested fatigue crack at ΔK_{TH} (R = 0.1, as a function of remaining fatigue crack length, ã, during progressive machining away of material in the wake of the crack tip.

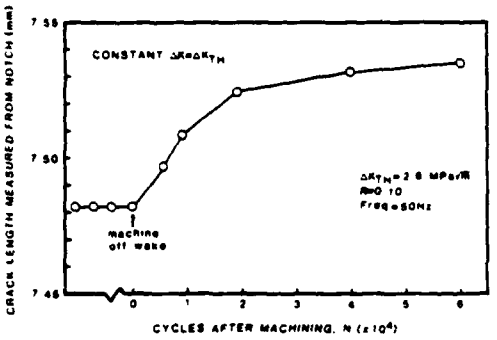

FIG. 4

Fatigue crack growth behavior, in terms of crack length versus number of cycles, in 7150-T6 aluminum at the threshold ΔK_{TH} (R = 0.1), before and after removal of the material in the wake of the crack tip (remaining ã = 0.5 mm). Effect is also shown in terms of da/dN vs. ΔK by the open triangles in Fig. 1.

END 8 84

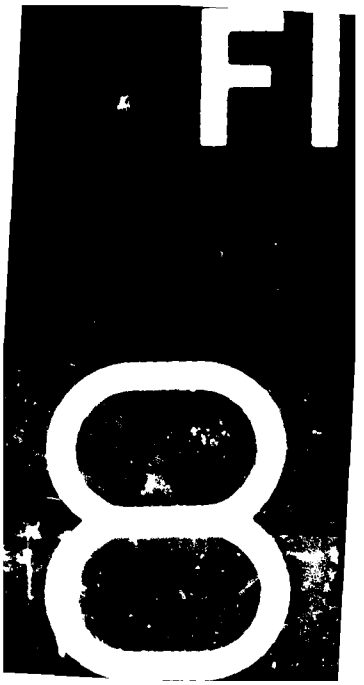
FI
8